



國立中央大學天文研究所
鹿林天文台年報

2014

No.12

國立中央大學天文研究所 編

目錄

研究論文

Dust environment and dynamical history of a sample of short-period comets II. 81P/Wild 2 and 103P/Hartley 2, F. J. Pozuelos, F. Moreno, F. Aceituno, et al., A&A 571, A64 (2014).....	4
THE TAIWANESE-AMERICAN OCCULTATION SURVEY PROJECT STELLAR VARIABILITY. III. DETECTION OF 58 NEW VARIABLE STARS, R. Ishioka, S.-Y. Wang, Z.-W. Zhang, et al., The Astronomical Journal, 147:70 (16pp), 2014 April.....	16
SYNCHROTRON SELF-VERSE COMPTON RADIATION FROM REVERSE SHOCK ON GRB 120326A, Yuji Urata, Kuiyun Huang, Satoko Takahashi, et al., The Astrophysical Journal, 789:146 (8pp), 2014 July 10.....	32
CCD photometry of distant active comets 228P/LINEAR, C/2006 S3 (LONEOS) and 29P/Schwassmann-Wachmann 1, J. C. Shi, Y. H. Ma and J. Q. Zheng, MNRAS 441, 739–744 (2014)	40
Are There Any Ultra-Long Period Cepheids in M31? , Chien-Hsiu Lee, Chow-Choong Ngeow and PTF Collaboration, The Tenth Pacific Rim Conference on Stellar Astrophysics, ASP Conference Series, Vol. 482.....	46
Detection of large color variation in the potentially hazardous asteroid (297274) 1996 SK, Chien-Hsien Lin, Wing-Huen Ip, Zhong-Yi Lin, Fumi Yoshida and Yu-Chi Cheng, RAA 2014 Vol. 14 No. 3, 311–318.....	50
Ground-based photometry for 42 Kepler-field RR Lyrae stars, Young-Beom Jeon, Chow-Choong Ngeow and James M. Nemec, Precision Asteroseismology Proceedings IAU Symposium No. 301, 2013.....	58
On the Activity of Comets, Ma, Yuehua; Shi, Jianchun, 40th COSPAR Scientific Assembly. Held 2-10 August 2014, in Moscow, Russia, Abstract B0.4-41-14.	60

工作報告

鹿林天文台觀測時數統計(2003-2014), 林宏欽、蕭翔耀、林啟生.....	62
AO系統測試報告, 張永欣.....	64
中大鹿林天文台, 林宏欽, 天文館期刊 第六十三期.....	69
那一夜, 鹿林的星空 我們的心空, 陳心平、廖乙馨、許苡蕾、蔡欣儒、許雅婷、王蕾婷、沈庭、陳麒瑞, 天文館期刊 第六十三期.....	74

臺灣流星觀測網介紹 (Taiwan Elegant Meteor and TLE Network), 楊義清, 天文館期刊 第六十六期.....	79
流星現象基礎原理, 吳秉勳, 天文館期刊 第六十六期.....	81
鎏金歲月-流星體與母體軌道相關性研究, 林士超、倪嘉晟、彭宣儒、廖彥朋, 天文館期 刊 第六十六期.....	86
Active brightness variation and polarization behavior of Uxor type young star GM Cep, Po-Chieh Huang, Chang-Yao Chen, Chia-Ling Hu, et al.,	94

新聞報導

新聞報導.....	96
-----------	----

研究論文

Dust environment and dynamical history of a sample of short-period comets

II. 81P/Wild 2 and 103P/Hartley 2

F. J. Pozuelos^{1,3}, F. Moreno¹, F. Aceituno¹, V. Casanova¹, A. Sota¹, J. J. López-Moreno¹, J. Castellano², E. Reina², A. Climent², A. Fernández², A. San Segundo², B. Häusler², C. González², D. Rodriguez², E. Bryssinck², E. Cortés², F. A. Rodriguez², F. Baldris², F. García², F. Gómez², F. Limón², F. Tifner², G. Muler², I. Almendros², J. A. de los Reyes², J. A. Henríquez², J. A. Moreno², J. Báez², J. Bel², J. Camarasa², J. Curto², J. F. Hernández², J. J. González², J. J. Martín², J. L. Salto², J. Lopesino², J. M. Bosch², J. M. Ruiz², J. R. Vidal², J. Ruiz², J. Sánchez², J. Temprano², J. M. Aymami², L. Lahuerta², L. Montoro², M. Campas², M. A. García², O. Canales², R. Benavides², R. Dymock², R. García², R. Ligustri², R. Naves², S. Lahuerta², and S. Pastor²

¹ Instituto de Astrofísica de Andalucía (CSIC), Glorieta de la Astronomía s/n, 18008 Granada, Spain
e-mail: pozuelos@iaa.es

² Amateur Association Cometas-Obs, Spain

³ Universidad de Granada-Phd Program in Physics and Mathematics (FisyMat), 18071 Granada, Spain

Received 3 June 2014 / Accepted 5 August 2014

ABSTRACT

Aims. This paper is a continuation of the first paper in this series, where we presented an extended study of the dust environment of a sample of short-period comets and their dynamical history. On this occasion, we focus on comets 81P/Wild 2 and 103P/Hartley 2, which are of special interest as targets of the spacecraft missions Stardust and EPOXI.

Methods. As in the previous study, we used two sets of observational data: a set of images, acquired at Sierra Nevada and Lulin observatories, and the A/ρ data as a function of the heliocentric distance provided by the amateur astronomical association *Cometas-Obs*. The dust environment of comets (dust loss rate, ejection velocities, and size distribution of the particles) was derived from our Monte Carlo dust tail code. To determine their dynamical history we used the numerical integrator Mercury 6.2 to ascertain the time spent by these objects in the Jupiter family Comet region.

Results. From the dust analysis, we conclude that both 81P/Wild 2 and 103P/Hartley 2 are dusty comets, with an annual dust production rate of $2.8 \times 10^9 \text{ kg yr}^{-1}$ and $(0.4\text{--}1.5) \times 10^9 \text{ kg yr}^{-1}$, respectively. From the dynamical analysis, we determined their time spent in the Jupiter family Comet region as $\sim 40 \text{ yr}$ in the case of 81P/Wild 2 and $\sim 1000 \text{ yr}$ for comet 103P/Hartley 2. These results imply that 81P/Wild 2 is the youngest and the most active comet of the eleven short-period comets studied so far, which tends to favor the correlation between the time spent in JFCs region and the comet activity previously discussed.

Key words. methods: observational – methods: numerical – comets: individual: 81P/Wild 2 – comets: individual: 103P/Hartley 2 – comets: general

1. Introduction

Cometary science has been revolutionized by in situ missions over the last several decades. It will continue to develop and transform with the arrival of Rosetta Spacecraft at Comet 67P/Churyumov-Gerasimenko. Unfortunately, only a few comets have been studied by spacecraft missions. In this paper we focus on comets 81P/Wild 2 and 103P/Hartley 2. Both comets have been the subject of extensive studies in past years and were the targets of the Stardust and EPOXI missions.

Comet nucleus 81P/Wild 2 (hereafter 81P) has been determined as a triaxial ellipsoid having radii of $(1.65 \times 2.00 \times 2.75) \pm 0.05 \text{ km}$ by Duxbury et al. (2004). The surface shows an ancient terrain composed of cohesive porous materials, probably as a consequence of a mixture of fine dust and volatiles when the comet was formed. It also shows the presence of large-impact craters, implying that the cohesive nature of the surface is old, since it was present before the comet entered the inner part of the solar system (Brownlee et al. 2004). Sekanina (2003) established

its current orbit as a consequence of a close encounter with Jupiter in 1974, when its perihelion and aphelion distances decreased from 5.0 to 1.5 AU and from 24.7 to 5.2 AU respectively. Comet 103P/Hartley 2 (hereafter 103P), has a small nucleus with a bilobed shape and a diameter in the range of 0.69 to 2.33 km (A'Hearn et al. 2011). It is considered to be a hyperactive comet, with large-grain production with velocities of several to tens of meters per second (Harmon et al. 2011; Kelley et al. 2013; Boissier et al. 2014). Its orbit period is 6.47 yr, with current perihelion and aphelion distances of $q = 1.05 \text{ AU}$ and $Q = 5.88 \text{ AU}$.

In this paper we study these comets in the same way as in Pozuelos et al. (2014, hereafter Paper I). Thus, we use our Monte Carlo dust tail code (e.g., Moreno 2009), which allows us to obtain the dust parameters: i.e., dust loss rate, ejection velocities and the size distribution of particles, and the emission pattern. For anisotropic emission, we introduce active area regions, along with the rotational parameters of the nucleus: rotation period and orientation of the spin axis defined by the angles

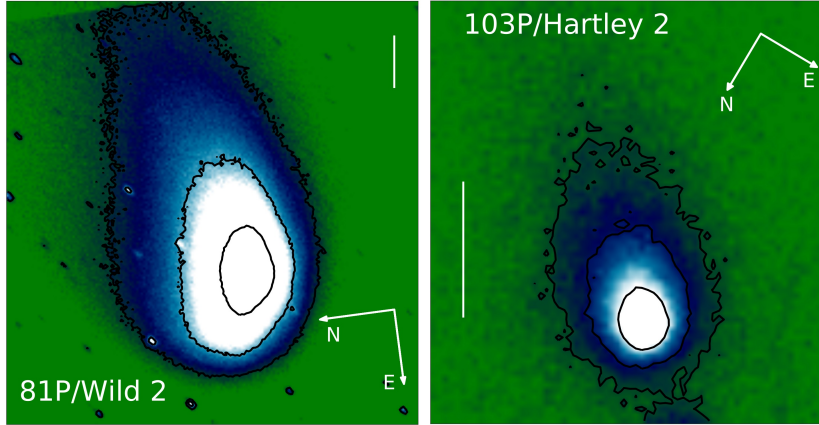


Fig. 1. Representative images of the observations obtained using a CCD camera at 1.52 m telescope at the Observatorio de Sierra Nevada in Granada, Spain. Right panel corresponds to 81P/Wild 2 on April 9, 2010. Isophote levels in solar disk units (SDU) are: 0.25×10^{-13} , 0.77×10^{-13} , 2.20×10^{-13} . Left panel corresponds with comet 103P/Hartley 2 on August 4, 2010. Isophote levels are: 0.20×10^{-13} , 0.40×10^{-13} , 1.10×10^{-13} . In both cases the directions of celestial north and east are given. The vertical bars correspond to 2×10^4 km in the sky.

I (obliquity) and ϕ (argument of the subsolar meridian at perihelion) (e.g., Sekanina 1981). In the second part of our study we analyze the dynamical history of these comets. To perform this task we use the numerical integrator developed by Chambers (1999), which has been used before by other authors, such as Hsieh et al. (2012a,b) and Lacerda (2013). From this analysis we studied the last 15 Myr of these comets, and we obtained the time spent by them in the region of the Jupiter family Comets (JFCs). Both dust environment and dynamical studies allowed us to determine how active these comets are as a function of the time spent as JFCs. We based our studies on two different kinds of observational data: direct imaging in Johnson R filter from ground-based telescopes, most of them obtained at the 1.52-m Sierra Nevada Observatory (Spain), and some of them at the 1-m telescope of Lulin Observatory (Taiwan) (Lin et al. 2012). The second block of observational data corresponds to $Af\rho$ measurements provided by the amateur astronomical association *Cometas-Obs*. These observations almost completely cover the orbital path when the comets are active.

The observations and the data reduction are explained in Sect. 2; the model is described in Sect. 3 ; the dust analysis, and comparison with others currently available are given in Sect. 4; the dynamical study appears in Sect. 5; and finally the summary and conclusions are given in Sect. 6.

2. Observations and data reduction

Most of the images of 81P and 103P were taken at the 1.52 m telescope at the Sierra Nevada Observatory (OSN) in Granada, Spain. We used a 1024×1024 pixel CCD camera with a R Johnson filter. For comet 81P, we also used observations acquired at the 1 m telescope at Lulin Observatory in Taiwan, using a 1340×1300 pixel CCD with an Ash R broadband filter. Table 1 shows the log of the observations. Additional details for the observations at Lulin Observatory are given in Lin et al. (2012) and the references therein. Several images of the comets were taken in order to improve the signal-to-noise ratio. A median stack was obtained from available images. The individual images from each night were bias-subtracted and flat-fielded using standard techniques. To perform the flux calibration, we used the USNO-B1.0 star catalog (Monet et al. 2003), so that each image we acquired was calibrated to mag arcsec^{-2} and then converted to solar disk units (SDU). We rotated each image to the

(N, M) system (Finson & Probstein 1968), where M is the projected Sun-comet radius vector, and N is perpendicular to M in the opposite half plane with respect to the nucleus velocity vector. The images were finally rebinned so that the physical dimensions were small enough to be analyzed with our Monte Carlo dust tail code. Representative reduced images of 81P and 103P are displayed in Fig. 1.

The second block of our observational data are the $Af\rho$ (A'Hearn et al. 1984) measurements carried out by the amateur astronomical association *Cometas-Obs*¹. These observations cover most of the orbital arc where the comets are active. They are given as a function of the heliocentric distance and are always referred to as an aperture of $\rho = 10^4$ km projected on the sky at each observation date. The calibration was made using the star catalogs CMC-14 and USNO A2.0. To make a direct comparison, we computed the $Af\rho$ with $\rho = 10^4$ km from the OSN and Lulin image observations (see Table 1).

It is important to note that some of the observational data correspond to times where the phase angle is close to zero degree. We corrected for the backscattering enhancement (Kolokolova et al. 2004) by the expression:

$$Af\rho' = 10^{\frac{-\beta(30-\alpha)}{2.5}} \times Af\rho, \quad (1)$$

where β is the linear phase coefficient, for which we assumed $\beta = 0.03 \text{ mag deg}^{-1}$, based on the studies by Meech & Jewitt (1987) for several comets. The correction is applied when $\alpha \leq 30^\circ$. More details are given in Sect. 3 of Paper I. This backscattering effect becomes especially important for comet 81P. In Fig. 2 we observe a clear increase in $Af\rho$ for small phase angles and see how these data are corrected after application of Eq. (1). Despite this clear correlation between $Af\rho$ and α , there are authors who attributed this enhancement to an outburst experienced by the comet after perihelion passage. We discuss this in Sect. 4.

3. Monte Carlo dust tail model

As in Paper I, to fit the observational data described in the previous section, we used our Monte Carlo dust tail code (see e.g., Moreno 2009). This code allowed us to generate synthetic images that can be directly compared with the observations, from which we can derive the synthetic $Af\rho$ curves.

¹ See <http://www.astrosurf.com/cometas-obs/>

Table 1. Log of the observations.

Comet	Observation date	r_h ¹ (AU)	Δ (AU)	Resolution (km pixel ⁻¹)	Phase angle (°)	Position angle (°)	$Af\rho$ ($\rho = 10^4$ km) ² (cm)	Telescope
81P/Wild 2	(a) 2010 Jan. 16.81	-1.639	1.080	808.4	35.4	292.6	566 ± 113	Lulin
	(b) 2010 Apr. 9.06	1.660	0.674	899.5	10.1	262.3	351 ± 70	OSN
	(c) 2010 Apr. 21.06	1.695	0.694	926.2	4.7	208.7	272 ± 54	OSN
	(d) 2010 May 15.96	1.789	0.822	1097.2	14.0	125.2	236 ± 47	OSN
	(e) 2010 Jun. 3.93	1.875	0.992	1323.9	21.0	116.7	258 ± 51	OSN
	(f) 2010 Jul. 6.89	2.046	1.404	1873.7	26.8	110.3	139 ± 27	OSN
	(g) 2010 Aug. 21.85	2.302	2.119	2827.9	25.9	103.7	148 ± 29	OSN
103P/Hartley 2	(a) 2010 Jul. 12.14	-1.744	0.916	641.2	29.0	228.5	9 ± 1	OSN
	(b) 2010 Aug. 4.11	-1.541	0.666	444.4	29.4	210.7	16 ± 3	OSN
	(c) 2010 Sept. 6.04	-1.274	0.352	469.7	35.4	179.6	24 ± 4	OSN
	(d) 2010 Nov. 3.16	1.061	0.150	400.3	58.7	282.4	65 ± 13	OSN

Notes. ⁽¹⁾ Negative values correspond to pre-perihelion, positive values to post-perihelion dates. ⁽²⁾ The $Af\rho$ values for phase angle $\leq 30^\circ$ have been corrected according to the Eq. (2) (see text).

This code was successfully used in previous works to determine the dust properties of some short-period comets such as 29P/Schwassmann-Wachmann 1 and 22P/Kopff (Moreno 2009; Moreno et al. 2012), as well as some Main-belt comets: P/2010 R2 (La Sagra), P/2012 T1 (PANSTARRS), and P/2013 P5 (PANSTARRS; Moreno et al. 2011, 2013, 2014). This code is also called the Granada model in Fulle et al. (2010) where the authors describe the dust environment of the Rosetta target 67P/Churyumov-Gerasimenko. The model computes the trajectory of a large number of particles when they are ejected from the nucleus surface and are submitted to the solar gravity and radiation pressure force, describing a Keplerian orbit around the Sun. Considered to be spherically shaped, the particles are characterized by the β parameter, which is the ratio of the radiation pressure force to the gravity force. For those particles $\beta = C_{\text{pr}} Q_{\text{pr}} / (\rho_d d)$, where $C_{\text{pr}} = 1.19 \times 10^{-3}$ kg m⁻², Q_{pr} is the radiation pressure coefficient, ρ the particle density, assumed as $\rho = 1000$ kg m⁻³, and d the particle diameter.

To compute the geometric albedo p_v and Q_{pr} , we used the Mie theory to describe the interaction of the electromagnetic field with spherical particles, assuming a refractive index of $m = 1.88 + 0.71i$ that is typical of carbonaceous spheres at red wavelengths (Edoh 1983). This gives $p_v = 0.04$ for $r \geq 1 \mu\text{m}$ at most of the phase angles, and $Q_{\text{pr}} \sim 1$ (Burns et al. 1979).

In the model, the trajectories and positions of the particles in the N, M plane and their contribution to the tail brightness are computed. The free parameters dust loss rate, ejection velocities, size distribution of the particles, and the dust ejection pattern, which can be either isotropic or anisotropic. In cases where an anisotropic outgassing is obtained, the emission is parametrized by a rotating nucleus with active areas on the surface. The rotation state is parametrized by two angles: the obliquity I of the orbit plane to the equator and the argument ϕ of the sub-solar meridian at perihelion (Sekanina 1981). The size distribution of the particles is defined by the maximum and minimum sizes $r_{\text{max}}, r_{\text{min}}$, and the index δ of the power law function $n(r) \propto r^\delta$, which describes the size distribution. For simplicity r_{min} has been set to $1 \mu\text{m}$ in all calculations. For large sets of comets, δ has been concluded to be in the range of -4.2 and -3.0 (e.g., Jockers 1997). The terminal velocity is parametrized as $v(t, \beta) = v_1(t) \times \beta^\gamma$ where $v_1(t)$ is determined during the modeling process, and the index γ is a constant assumed as $\gamma = 1/2$, which is the value commonly accepted for hydrodynamical drag from sublimating ices (e.g., Moreno et al. 2011; Licandro et al. 2013).

Owing to the large number of parameters that are used in the model, the solution is not unique and it is possible to find an alternative set of parameters to fit the observational data. However, the range of possible solutions is considerably reduced when the available observations cover most of the orbital arc of the comets. For this reason, we combined direct imaging observations and a large number of $Af\rho$ measurements given by different observers in different locations, such as those provided by the association *Cometas-Obs*.

4. Dust analysis

In Paper I, we determined three categories according to the amount of dust emitted: (i) weakly active: 115P, 157P and Rinner with an annual production rate of $T_d \leq 1 \times 10^8$ kg yr⁻¹; (ii) moderately active: 30P, 123P, and 185P where the annual production rate is $T_d = 1 - 3 \times 10^8$ kg yr⁻¹; and (iii) highly active: 78P, 22P, and 118P with an annual production rate of $T_d \geq 8 \times 10^8$ kg yr⁻¹. For three of those targets, an anisotropic ejection pattern was obtained: 30P, 115P, and 157P. The general method used to fit the observations and obtain the dust parameters is a trial-and-error procedure, starting with the simplest scenario, where we consider an isotropic ejection outgassing model, with $r_{\text{min}} = 1 \mu\text{m}$, $r_{\text{max}} = 1 \text{ cm}$, $\delta = -3.5$, and both $v_1(t)$ and dM/dt monotonically symmetric evolution with respect to perihelion. Once we reproduced the tail intensity in the optocenter, we started to vary the parameters and their dependence on the heliocentric distance to obtain the best possible fit. When the observations cannot be reproduced by isotropic emission, we set active areas on the surfaces, i.e., an anisotropic emission pattern, and repeat different combinations of the dust parameters until an acceptable result is obtained.

4.1. 81P/Wild 2

The comet 81P has an effective nucleus of $R_N = 2.00$ km (Sekanina et al. 2004) and a bulk density of $\rho = 600$ kg m⁻³ reported by Davidsson & Gutierrez (2004). Our observational data for comet 81P are six direct images post-perihelion passage at OSN 1.52 m telescope and ~ 300 $Af\rho$ measurements by *Cometas-Obs*, which cover from ~ -2.15 to ~ 2.45 AU. In addition, we benefited from observations carried out in the 1 m Lulin telescope by Z.-Y. Lin. From these observations we selected one pre-perihelion image (January 16.81, 2010) and

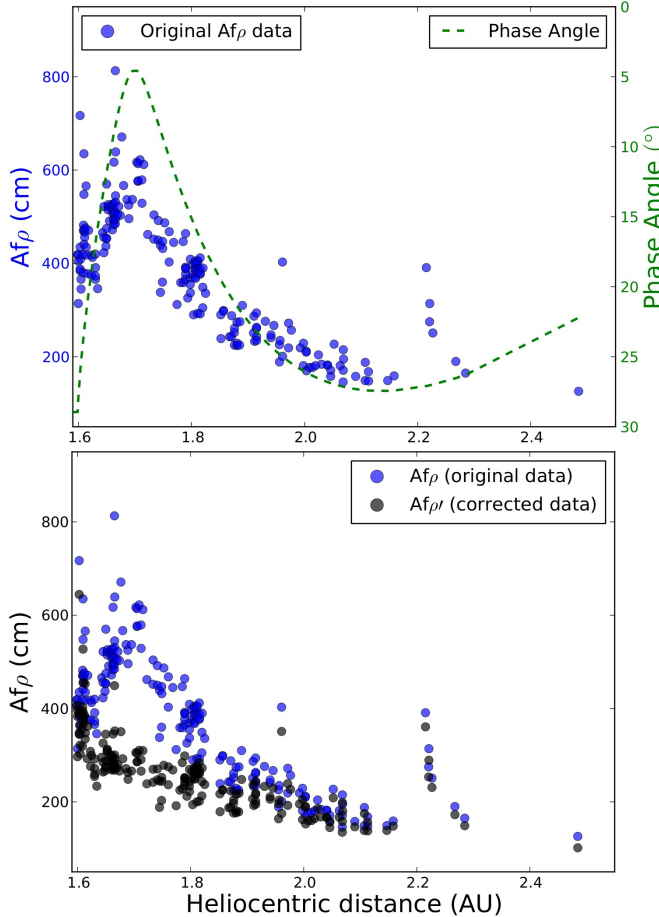


Fig. 2. 81P/Wild 2 $Af\rho$ measurements by *Cometas-Obs*. *Upper panel*: original data and phase angle as a function of heliocentric distance. *Lower panel*: original $Af\rho$ data and corrected $Af\rho$ data by Eq. (1) (see text).

5 $Af\rho$ measurements pre- and post-perihelion (see Table 1). The complete set of $Af\rho$ data as a function of the heliocentric distance is shown in Fig. 4, where all the data have been corrected from backscattering enhancement using Eq. (1).

We observed two enhancements in the measurements that were not related to low α values. We considered them as small outbursts suffered by the comet. The first one occurred on October 29 (2009), when the comet was at $r_h \sim 1.949$ AU inbound, where the maximum value of $Af\rho$ was ~ 782 cm. To our knowledge, this outburst has not been reported previously. In our dust characterization we concluded that the event duration was ~ 40 h, and the comet emitted $m_{\text{ob},I} \sim 9.2 \times 10^8$ kg of dust, reaching a peak dust production rate of 1190 kg s^{-1} , returning to normal activity on November 13. However we only have a limited number of sample observations for this period, so this result must be read with caution. The second outburst was first identified by Bertini et al. (2012). This second event took place post-perihelion, August 5 (2010), at ~ 2.215 AU outbound, with a maximum value of $Af\rho \sim 380$ cm. Our dust analysis estimated this event as three times less intense than the first one, $m_{\text{ob},II} \sim 3.0 \times 10^8$ kg with a duration of ~ 55 h and a peak dust production rate of 450 kg s^{-1} . During both outbursts, I and II, the maximum particle size was 3 cm.

Overall, without taking the outburst events into account, we concluded that the comet reached its maximum level of activity at $r_h \sim 1.64$ AU inbound, that is ~ 40 days before perihelion,

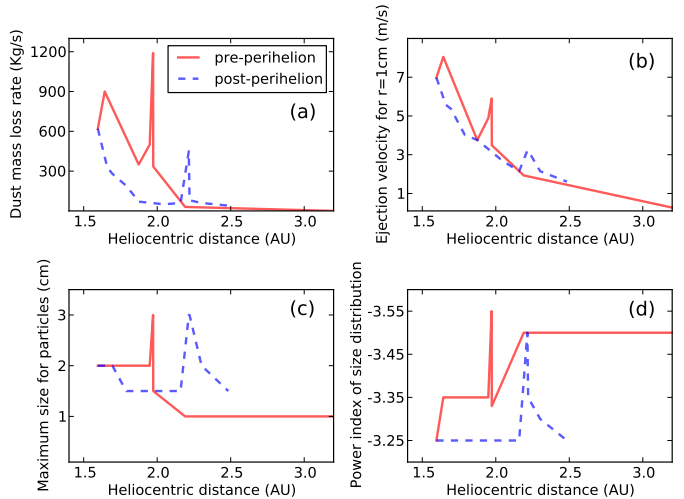


Fig. 3. Best-fit modeled parameters to the dust environment of 81P/Wild 2 $Af\rho$ data and images (Figs. 4 and 5). All parameters are given as a function of the heliocentric distance. From *top to bottom* and *left to right* the panels are a) dust production rate [kg s^{-1}]; b) ejection velocities of 1-cm particles [m s^{-1}]; c) maximum size of particles [cm]; d) power index of the size distribution, δ . The solid red line corresponds to pre-perihelion and the dashed blue line to post-perihelion.

with a dust production rate of 900 kg s^{-1} . The comet emission pattern is found to be anisotropic at 35%, with active areas located on the surface between $+45^\circ$ to -30° . From the anisotropic model we derived the rotational angles as $I = (50 \pm 5)^\circ$ and $\phi = (300 \pm 20)^\circ$. Figure 3 we display the evolution of the dust parameters as a function of heliocentric distance, and in Figs. 4 and 5 we present the comparison of the model with the observational data, which are remarkably similar. From the dust analysis, we determined that the total dust production rate of 81P was $1.1 \times 10^{10} \text{ kg}$ during the 3.8 yr covered by the study, that is, an annual dust production rate of $T_d = 2.8 \times 10^9 \text{ kg yr}^{-1}$ and an average dust mass lost rate of 87.5 kg s^{-1} . The contribution to the annual interplanetary dust replacement, established by Grun et al. (1985) as $2.9 \times 10^{11} \text{ kg yr}^{-1}$, is $\sim 0.96\%$.

4.2. 103P/Hartley 2

The observational data of comet 103P consist of four direct images obtained at the 1.52 m OSN telescope, three pre-perihelion and one post-perihelion (see Table 1), and ~ 430 $Af\rho$ measurements carried out by *Cometas-Obs*, covering pre- and post-perihelion branches in the orbit, from ~ 2.00 to ~ 2.60 AU. The observations have been corrected by Eq. (1) for the data having $\alpha \leq 30^\circ$ as in the case of 81P, but in this case there is not a strong dependence between α and any enhancements in the measurements. This comet has been subjected to an extensive study as a consequence of its encounter with the Deep Impact spacecraft in the framework of the EPOXI mission (see e.g., A'Hearn et al. 2011; Meech et al. 2011). For most of those studies it was considered as a hyperactive comet with an emission of large particles (see e.g., Harmon et al. 2011; Kelley et al. 2013; Boissier et al. 2014). The mean radius (radius of a sphere of equivalent volume) is calculated by Thomas et al. (2013b) as 0.580 ± 0.018 km, but the bulk density is not determined well, since it is in the range of $\rho = 140\text{--}520 \text{ kg m}^{-3}$ (A'Hearn et al. 2011; Richardson & Bowling 2014; Thomas et al. 2013b). Consequently, the escape velocity of particles is in the range of $v_{\text{esc}} = 3.6\text{--}6.9 \text{ cm s}^{-1}$.

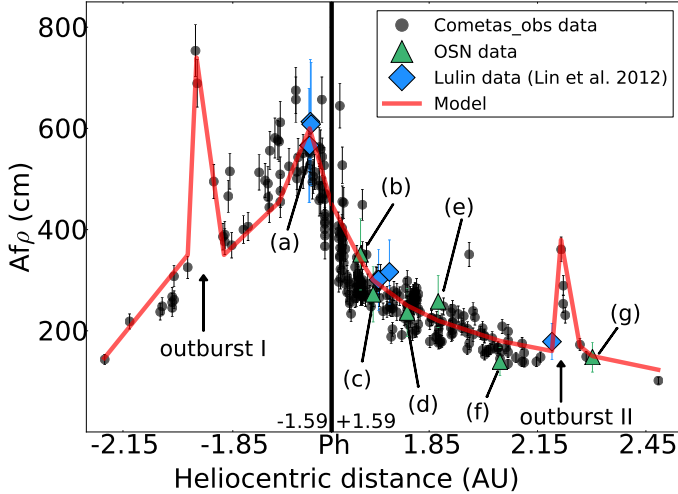


Fig. 4. Comparison of observed and modeled $Af\rho$ data as a function of heliocentric distance. Parameter $Af\rho$ versus heliocentric distance. The $Af\rho$ measurements have been corrected using Eq. (1). Black dots: $Af\rho$ data from *Cometas-Obs*. Green triangles: $Af\rho$ data derived from OSN images. Blue diamonds: $Af\rho$ data from Lulin observatory images. The observations labeled (a) to (g) correspond to the $Af\rho$ derived from images (a) to (g) in Fig. 5. The outbursts I (inbound) and II (outbound) described in the text are marked with arrows. All the $Af\rho$ values refer to $\rho = 10^4$ km.

Thus, for our purposes, we assume the maximum value of the bulk density as $\rho = 520 \text{ kg m}^{-3}$, which corresponds to the upper limit of escape velocity. To perform the dust characterization we introduce two models, which agree with the observations. The first one is based on previous knowledge, i.e., large particle emission and high dust production rate (hyperactivity). The second one tries to reproduce the observations without the emission of large particles and with moderate dust production rate.

Model I or hyperactive model. In this case we consider the results derived from the EPOXI mission and other authors, such as [Harmon et al. \(2011\)](#), where a large size of particles were obtained, with sizes in the range of ~ 20 cm and larger. To try to reproduce these results, we fixed the maximum size of particles to $r = 20$ cm around perihelion, where the comet reaches its maximum dust production rate. This model has a gentle increase in the dust parameters toward perihelion, where a strong increase occurs, peaking at ~ 1.20 AU post-perihelion. This behavior is also seen in the $Af\rho$ measurements (Fig. 8). The maximum dust production rate is found to be 600 kg s^{-1} , and the ejection velocity of 1-cm size particles reaches $\sim 14 \text{ m s}^{-1}$. The total dust mass ejected during the 3.79 yr span in this study is $5.9 \times 10^9 \text{ kg}$, so the annual dust production rate is $T_d = 1.5 \times 10^9 \text{ kg yr}^{-1}$. This model represents an annual contribution of 0.51% to interplanetary dust. Figure 6 we show the evolution of the dust parameters as a function of the heliocentric distance, and in Figs. 8 and 9 we show the comparison between the available observations and the model.

Model II or standard model. In this case, the maximum particle size was not forced to 20 cm, but is a free parameter that can have any possible value. It reaches 3 cm at perihelion. As in *Model I* the peak of the dust parameter occurs after perihelion at ~ 1.20 AU, where the dust production rate is 160 kg s^{-1} , and the ejection velocity for 1 cm particles is $\sim 7 \text{ m s}^{-1}$. In this case the total dust emitted by the comet was $1.7 \times 10^9 \text{ kg}$, and the annual dust production rate was $T_d = 4.5 \times 10^8 \text{ kg yr}^{-1}$. The contribution to the interplanetary dust per year represents 0.15% of the total. The evolution along the heliocentric distance of the

dust parameters is displayed in Fig. 7, and the comparison of the observations to the model are shown in Figs. 8 and 10.

In both cases, *Models I and II*, the emissions have been found to be isotropic.

4.3. Discussion

The dust characterization of 81P shows the peak of activity around ~ 40 days pre-perihelion. In previous studies of this comet during the perihelion passages in 1990, 1997, and 2004, the comet showed the peak of activity a few weeks pre-perihelion due to a seasonal effect. [Sekanina \(2003\)](#) studied this behavior when the comet activity reached its maximum value three weeks before perihelion with a post-perihelion fading. To explain this behavior, the author proposed that the spin axis is not quite normal to the orbital plane. In addition, [Farnham & Schleicher \(2005\)](#) attribute this conduct to a strong seasonal effect with at least one source region moving from summer to winter speedily. Analogous results of this behavior have also been obtained in independent studies by other authors (e.g., [Hanner & Hayward 2003](#); [Hadamacik & Levasseur-Regourd 2009](#)).

In the analysis carried out by [Bertini et al. \(2012\)](#), the authors identified an enhancement of $Af\rho$ measurements ~ 60 days post-perihelion. The authors also noticed that during that period there was a minimum phase angle, and they corrected the effect by reducing all $A(\alpha)f\rho$ values to $\alpha = 0^\circ$, and using $A(0)f\rho$ as reference. After the authors applied the correction, the enhancement on $Af\rho$ measurements was still evident, which led them to consider it as an outburst event. In our case, *Cometas-Obs* also reported this enhancement in the $Af\rho$ measurements, but in contrast to [Bertini et al. \(2012\)](#), the enhancement completely disappeared after correction (using Eq. (1), see Fig. 2), so we concluded that the comet started to fade after the pre-perihelion peak.

During the Stardust flyby on 2 January 2004 (at $r_h = 1.855$ AU post-perihelion), [Green et al. \(2004\)](#) used the Dust Flux Monitor Instrument (DFMI) to obtain a cumulative mass distribution index ξ (where the number of particles of mass m or larger is given by the power law $N(m) \propto m^{-\xi}$) in the coma ranges from 0.3 to 1.1, where $\xi = 0.75 \pm 0.05$ was found to be the best fit for the data. From this cumulative mass distribution index we can conclude that the power index of the differential size distribution is $\delta = -3\xi - 1$. Thus, δ is in the range of -1.9 to -4.3 , with the best match to the data being $\delta = -3.25 \pm 1.25$. This value perfectly agrees with the one derived from our model at the same heliocentric distance.

The rotational parameters derived from the model agree with the ones proposed by [Sekanina et al. \(2004\)](#), who concluded that $I = 55^\circ$ and $\phi = 150^\circ$. The equivalent solution for ϕ is $180^\circ + \phi = 330^\circ$, [Sekanina \(1981\)](#), which is close of our value. [Belton et al. \(2013a\)](#) established a relationship between mini-outbursts suffered by the comet 9P/Temple 1 and pits (large population of quasi-circular depression) on the surface of the comet, reported by the encounter of Stardust-NExT spacecraft and Deep Impact mission (see e.g., [Veverka et al. 2013](#); [A'Hearn et al. 2005](#); [Thomas et al. 2013a](#)). The authors argue that $\sim 96\%$ of these features were due to mini-outbursts, while $\sim 4\%$ had their origin in other processes, such as collisions with asteroidal material and cryo-volcanism. From this relationship, the authors propose that the pits observed on the surface of 81P are also due to outburst events. In our model, we have identified two outbursts, one inbound and the other outbound, both more intense than the mini-outbursts studied by [Belton et al. \(2013a\)](#), which were in the range of $6\text{--}30 \times 10^4 \text{ kg}$. However, [Brownlee et al. \(2004\)](#),

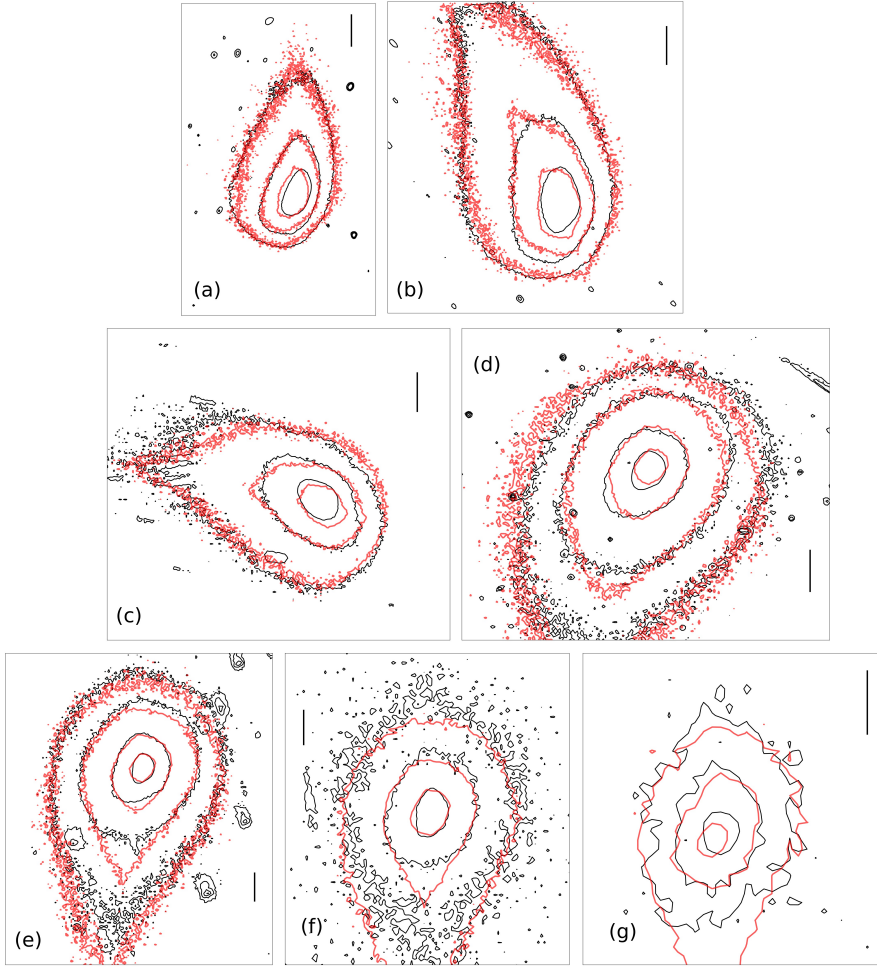


Fig. 5. Isophote field comparison between observations and model. The black contours correspond to the observations and the red ones to the model. The dates and the SDU levels are **a**) Jan. 16.81, 2010. Levels are 0.80×10^{-13} , 2.00×10^{-13} , and 5.00×10^{-13} SDU; **b**) Apr. 9.06, 2010. Levels are 0.25×10^{-13} , 0.77×10^{-13} , and 2.20×10^{-13} SDU; **c**) Apr. 21.06, 2010. Levels are 0.25×10^{-13} , 0.77×10^{-13} , and 2.20×10^{-13} SDU; **d**) May 15.96, 2010. Levels are 0.10×10^{-13} , 0.25×10^{-13} , 0.77×10^{-13} , and 2.20×10^{-13} SDU; **e**) Jun. 3.93, 2010. Levels are 0.10×10^{-13} , 0.25×10^{-13} , 0.77×10^{-13} , and 2.20×10^{-13} SDU; **f**) Jul. 6.89, 2010. Levels are 0.08×10^{-13} , 0.25×10^{-13} , and 0.77×10^{-13} SDU; **g**) Aug. 21.85, 2010. Levels are 0.25×10^{-13} , 0.77×10^{-13} , and 2.20×10^{-13} SDU. See log of the observations in Table 1.

Kirk et al. (2005) and Basilevsky & Keller (2006, 2007) considered the origin of pits in the context of impact phenomena. Therefore, the relationship between outbursts and pits are not clear in the case of 81P, and more studies would be desirable to determine how often the outbursts occur in this comet, and if they are the cause of pits on the surface.

The comet 81P has been found to be the most active one in the whole sample of short-period comets studied in Paper I and in this paper, with an annual dust production rate of $T_d = 2.8 \times 10^9 \text{ kg yr}^{-1}$.

Our study of the 103P offers two solutions to fitting the observation: *Model I*, where the comet is found to be hyperactive, and *Model II* where we proposed a standard dust behavior. In *Model I* we imposed large size particles (up to $r_{\max} = 20 \text{ cm}$) and we concluded that the annual dust production rate is $T_d = 1.5 \times 10^9 \text{ kg yr}^{-1}$, with a dust production rate of 300–550 kg s $^{-1}$ during perihelion and Deep Impact spacecraft closest approach. In contrast, in *Model II* our solution also agrees with the observations but with a maximum particle size of $r_{\max} = 3 \text{ cm}$, where the annual dust production rate is $T_d = 4.5 \times 10^8 \text{ kg yr}^{-1}$. During the perihelion and Deep Impact encounter, the dust mass loss rate was in the range of 120–140 kg s $^{-1}$. Thus, the range of the dust production rate obtained by our study is 120–550 kg s $^{-1}$ during perihelion passage and spacecraft encounter. Harmon et al. (2011) established a value of 300 kg s $^{-1}$ roughly in the same period, while Boissier et al. (2014) inferred a much wider range of 830–2700 kg s $^{-1}$ based on their two models under various assumptions, such as the dust composition, size distribution,

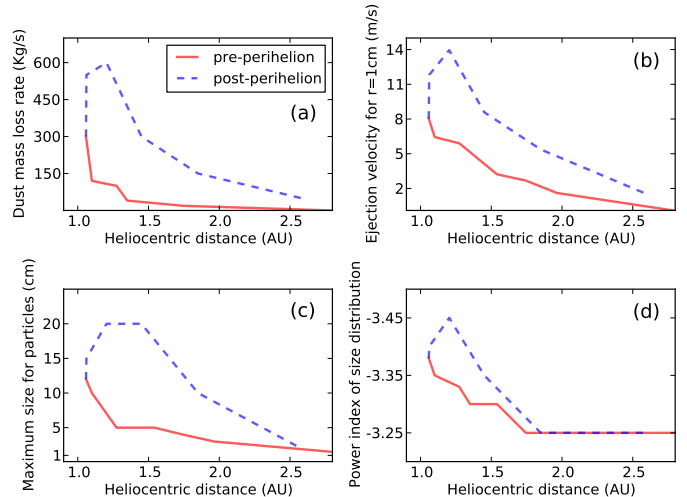


Fig. 6. As Fig. 3 but for comet 103P/Hartley 2. Corresponding to *Model I*. This model fits the observations displayed in Figs. 9 and 8, where it is represented by the red line.

and grain velocities. The authors attributed the uncertainty of their values to the uncertainties in the size distribution cut-off and kinematics. The total dust emitted by 103P for the whole orbit during 2010 perihelion passage, has been found to be in the range of $1\text{--}4 \times 10^9 \text{ kg}$ in previous studies (see e.g.,

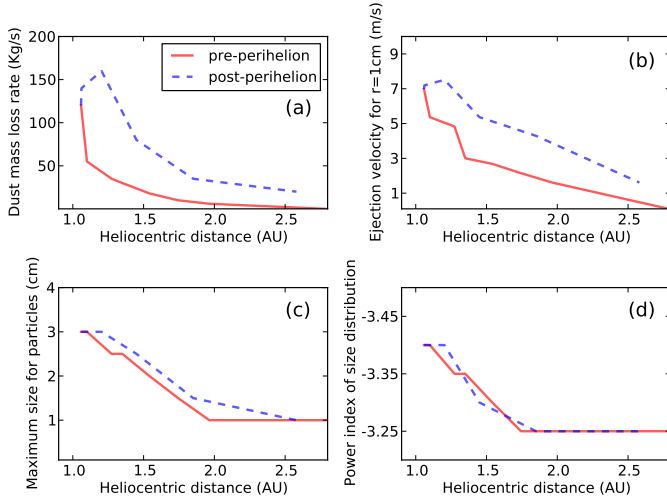


Fig. 7. As in Fig. 3 but for comet 103P/Hartley 2. Corresponding to *Model II*. This model fits the observations displayed in Figs. 10 and 8 where it is represented by the blue line.

Lisse et al. 2009; Bauer et al. 2011; Thomas et al. 2013b; Knight & Schleicher 2013). These values agree with the range of $1.7\text{--}5.9 \times 10^9$ kg derived from our models, which cover most of the time in which the comet is active.

The very complex rotational state of the nucleus was studied in detail in Belton et al. (2013b). In Belton (2013) the authors described the active areas migration over the lobes of the nucleus following the Sun; thus, the strong activity shown by this comet is correlated with the rotation of the nucleus. Two faint dust jets seem to have had their origin in those active areas (see e.g., Lara et al. 2011; Mueller et al. 2013; Tozzi et al. 2013). Thanks to this correlation between active areas and rotation of the nucleus, the comet has an isotropic pattern of time-averaged outgassing from its nuclear surface. This fact led Groussin et al. (2004), Lisse et al. (2009), and Knight & Schleicher (2013) to report the comet as a highly active nucleus with $\sim 100\%$ of the surface area active. These results agree with the isotropic dust emission pattern derived from our *Models I* and *II*.

Another important point is the nature of the large chunks, observed during the EPOXI flyby and inferred from radar observations (see e.g., A'Hearn et al. 2011; Harmon et al. 2011), and the real size of them. Knight & Schleicher (2013) deduced that those chunks are large dust grains (up to 20 cm) because of the lack of interaction between the radiation pressure and the dust jets observed. However, Kelley et al. (2013) propose two models: (1) the icy case, where the particles have an albedo of 0.67, $\rho = 0.1 \text{ g cm}^{-3}$, and the size of particles are in the range of 1–20 cm; (2) the dusty case, with an albedo of 0.049, $\rho = 0.3 \text{ g cm}^{-3}$, and the particle sizes in the range of 10–210 cm. The authors concluded that the icy model is more likely. However, these models may not reflect the true nature of the particles, although they did produce useful information on the limits of particle size and the fact that a coma of both icy and dusty particles is possible.

To explain the relatively short life times of those large chunks, Tozzi et al. (2013) established that they need to have some impurities such as silicates embedded in them, and inferred the presence of grains which might have lot of organics. Finally, Boissier et al. (2014) present two models based on crystalline/amorphous (of ratio of 1) silicate particles with a grain density of $\rho = 0.5 \text{ g cm}^{-3}$, where the maximum size of the

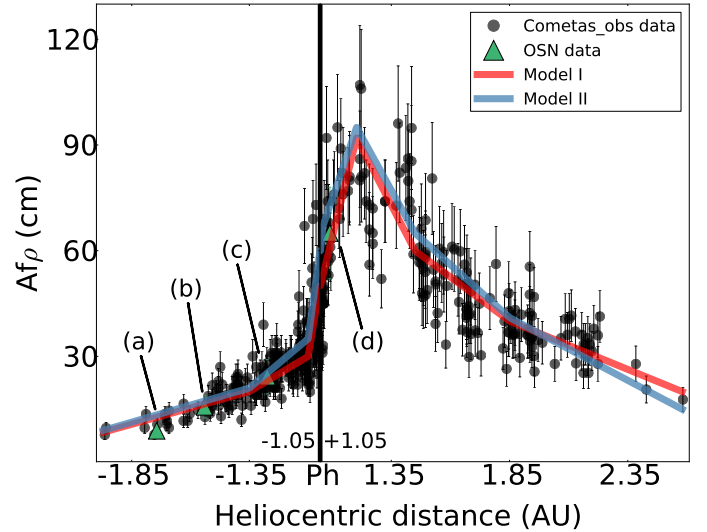


Fig. 8. Comparison between observational data and the models proposed for the comet 103P/Hartley 2. $Af\rho$ measurements have been corrected using Eq. (1). Black dots are the data from *Cometas-Obs*, and green triangles marked from (a) to (d) are the observations at OSN telescope. The red line corresponds to *Model I* or *Hyperactive model*, which fits the observations in Fig. 9. The blue line is the *Model II* or *Standard model*, and its fits with observations can be checked in Fig. 10. All the $Af\rho$ values are referred to $\rho = 10^4 \text{ km}$.

particles was obtained depending on the escaping gas: (1) $a_{\max} = 1 \text{ m}$, to H_2O ; (2) $a_{\max} = 2.4 \text{ m}$, to CO_2 . Therefore, the true nature and the size of the large chunks observed are not completely accurate and are still under study. The presence of the large particles in the coma of this comet was already inferred in Epifani et al. (2001) during the observations of 1 January 1998 using the ISOCAM. The authors deduced that the dust production rate at perihelion ranged from 10 kg s^{-1} to 100 kg s^{-1} . The peak of the dust production rate and the ejection velocities of the particles occurred two weeks after perihelion, with a rapid decrease just before it. However, the authors attributed this behavior to the instability of the model outputs around perihelion, showing unrealistically large variations in the power index of the size distribution. The best fitting power law was found to be $\delta = -3.2 \pm 0.1$ by the authors. In the 2010 perihelion passage, the power index of the size distribution derived from our models take values from -3.45 to -3.25 , which are bit higher than the values assumed/derived by other authors, such as Bauer et al. (2011) of -4.0 , Kelley et al. (2013) in the range of -6.6 to -4.7 , and Boissier et al. (2014) of -3.5 .

It is important to note that in general, when the power index is $-3 < \delta < -4$, the dust mass depends on the largest particles, while the brightness in the tail depends on the smallest grains, so that it is always difficult to determine the large particle population in the tail (Fulle 2004). For this reason, the mass found in the models should be considered as lower limits of the total dust emitted (see Paper I). In the case of 103P, *Model I* is closer to a real solution than *Model II*, which represents a lower limit in the dust production.

As a result of the particle velocities obtained in Paper I, the characterization of 22P/Kopff in Moreno et al. (2012), the result presented by Fulle et al. (2010) to comet 67P/Churyumov-Gerasimenko, and this study, we found a definite relationship between the ejection velocities and the heliocentric distance. For example, for $r = 1 \text{ cm}$ particles, we found a power law given by $v = A \times r_h^{-B}$, where A and B parameters were given

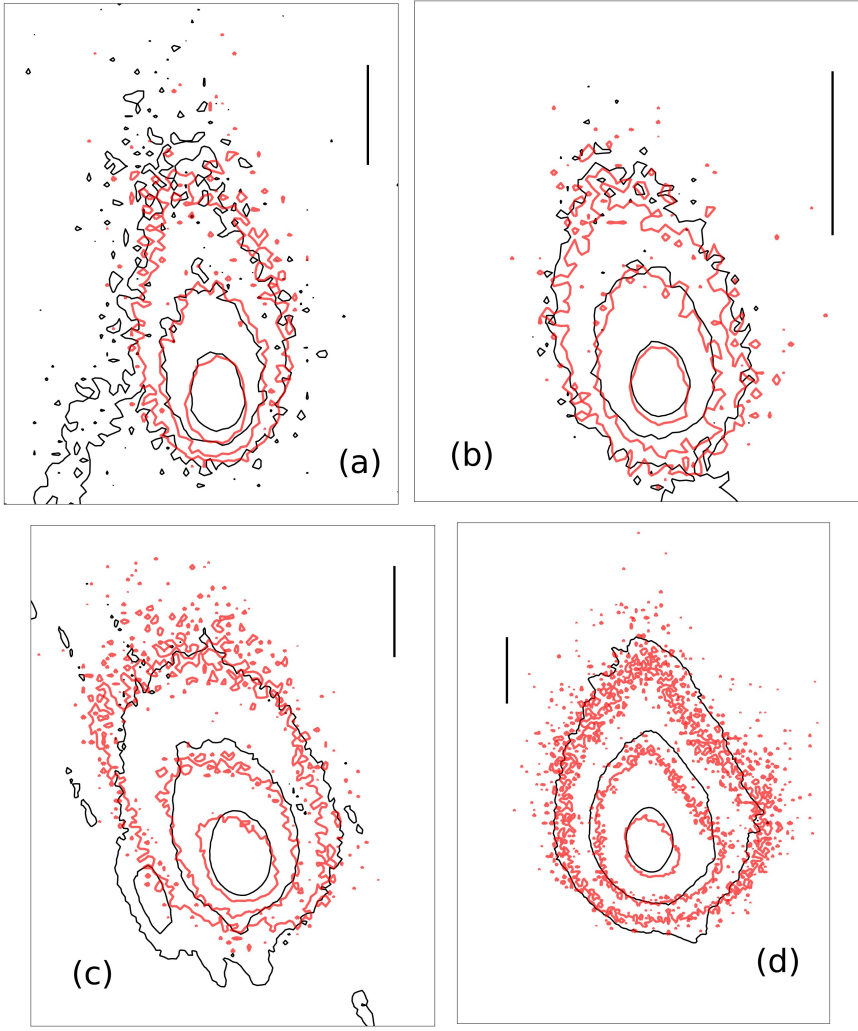


Fig. 9. Isophote field comparison between observations and *Model I* or *Hyperactive model*. The black contours correspond to the observations and the red ones to the model. The dates and the SDU levels are **a)** Jul. 12.14, 2010. Levels are 0.30×10^{-14} , 0.55×10^{-14} , and 1.20×10^{-14} SDU; **b)** Aug. 4.11, 2010. Levels are 0.20×10^{-13} , 0.40×10^{-13} , and 1.10×10^{-13} SDU; **c)** Sep. 6.04, 2010. Levels are 0.15×10^{-13} , 0.40×10^{-13} , and 1.10×10^{-13} SDU; **d)** Nov. 3.16, 2010. Levels are 0.55×10^{-13} , 1.25×10^{-13} , 4.00×10^{-13} SDU. See log of the observations in Table 1.

by $A = 7.067 \text{ m}^{B+1}/\text{s}$ and $B = 1.998$. Thus, the ejection velocity law is roughly inversely proportional to $\sim r_h^2$. This agrees with the results from hydrodynamical inner coma models by Crifo & Rodionov (1997) and disagrees with the r_h^{-1} dependence by Whipple (1951). The result of the fit is displayed in Fig. 11, where in addition to the 11 comets studied between Paper I and this study, we add the ejection velocity of 1 cm particles of the comet 67P/Churyumov-Gerasimenko, obtained by Fulle et al. (2010). In that figure, one can see that 81P at ~ 2.0 AU and 22P at $r_h > 2.5$ AU have deviated from this trend. In the case of 81P, this behavior it is due to the outburst I characterized in Sect. 4.1, and for 22P it comes from the strong dust ejection anisotropies at the large heliocentric distances identified by Moreno et al. (2012).

5. Dynamical history analysis

To obtain the dynamical evolution of the two comets studied in this paper, we followed the same procedure as described in Paper I, which is based on previous studies by Levison & Duncan (1994). We used version 6.2 of Mercury's numerical integrator developed by Chambers (1999). We generated 99 clones having 2σ dispersion in three of the orbital elements: semimajor axis, a , inclination, i , and eccentricity, e , where σ is the uncertainty in the corresponding parameter as given in the JPL Horizons online solar system data². The orbital parameters and

the σ values are given in Table A.1. The 99 clones plus the real object give a total of 100 massless particles to perform the statistical study. The Sun and the eight planets are considered to be massive bodies. To control the close encounters of the massless particles with the massive bodies, we used the hybrid algorithm that combines a symplectic algorithm with a Burlisch-Stoer integrator (see Chambers 1999). The initial time step was eight days, and the clones were removed when their heliocentric distance was > 1000 AU.

We performed backward integrations of 15 Myr. The non-gravitational forces were neglected according to the same arguments posed by Lacerda (2013), where the change rate of the semimajor axis, da/dt , is produced by a non-gravitational acceleration, T , created by single sublimation jet tangential to the comet's orbit and affecting its motion during the life time of sublimation, t_{sub} :

$$\frac{da}{dt} = \frac{2Va^2T}{GM_\odot} \quad (2)$$

$$T = \frac{dM_d}{dt} \times \frac{v_d}{m_{\text{nuc}}} \quad (3)$$

$$t_{\text{sub}} = m_{\text{nuc}} \times \left(\frac{dM_d}{dt} \right)^{-1}. \quad (4)$$

Therefore, the total deviation of the semimajor axis D would be

$$D = \frac{da}{dt} \times t_{\text{sub}}. \quad (5)$$

² See ssd.jpl.nasa.gov/?horizons

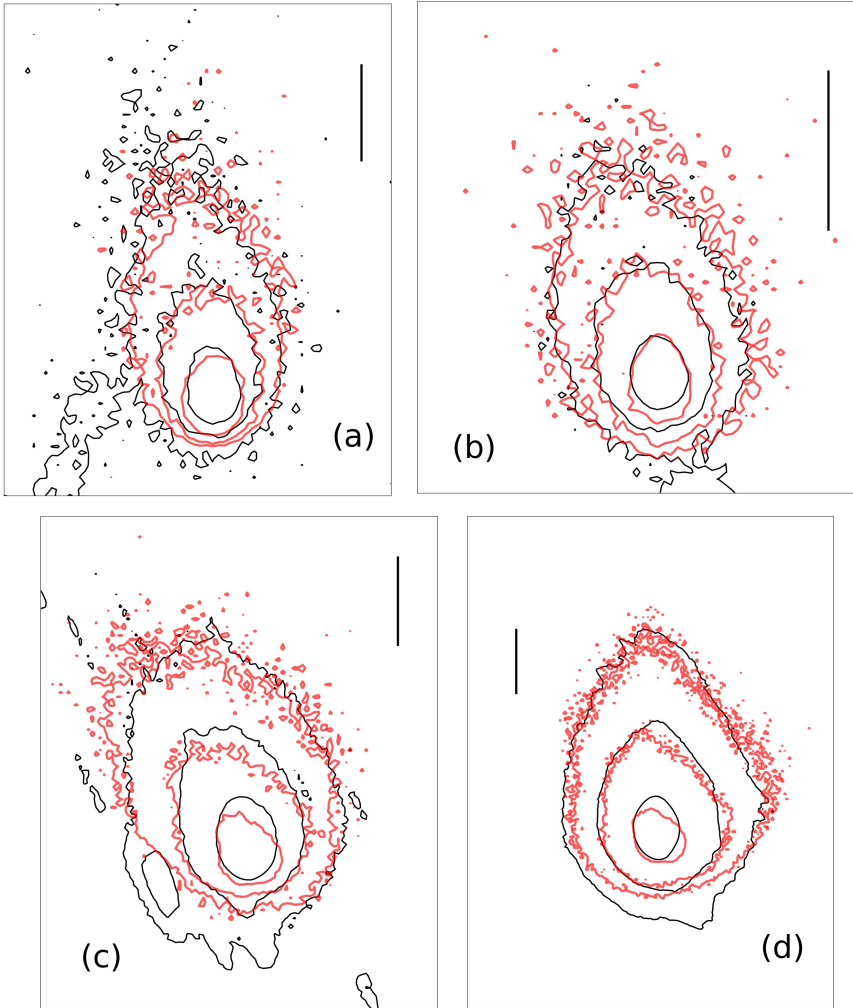


Fig. 10. As in Fig. 9 but for *Model II* or standard model.

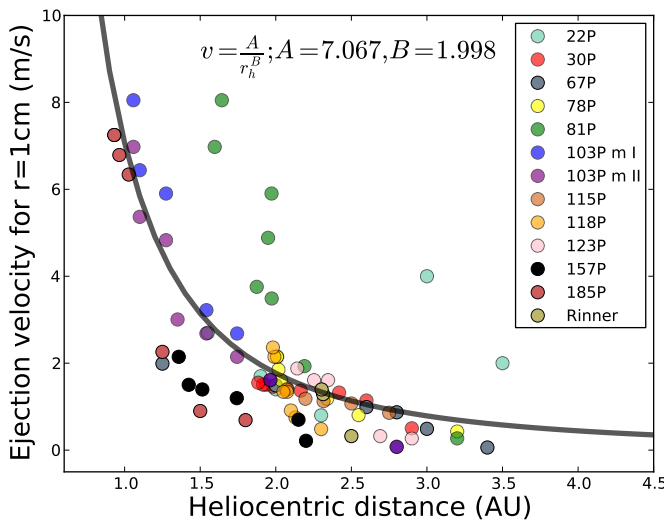


Fig. 11. Ejection velocities of 1 cm particles versus the heliocentric distance for all comets in the sample plus the result obtained by Fulle et al. (2010) in the study of comet 67P/Churyumov-Gerasimenko. The complete set of comets are: 22P/Kopff, 30P/Reinmuth 1, 67P/Churyumov-Gerasimenko, 78P/Gehrels 2, 81P/Wild 2, 103P/Hartley 2 (*Model I* and *Model II*), 115P/Maury, 118P/Shoemaker-Levy 4, 123P/West-Hartley, 157P/Tritton, 185P/Petriew, and P/2011 W2 (Rinner). The color code is given in the legend. The solid black line is the best fit found for that distribution: $v = A \times r_h^{-B}$, with $A = 7.067 \text{ m}^{B+1}/\text{s}$ and $B = 1.998$.

In these equations, dM_d/dt is the dust mass loss rate, V the orbital velocity, a the semimajor axis, G the gravitational constant, M_\odot the Sun mass, v_d is the dust velocity, and m_{nuc} the mass of the nucleus. In Paper I, we estimated the highest deviation of the semimajor axis for the complete sample of comets as $D = 0.32$ AU. We found $D_{81P} = 0.24$ AU, $D_{103P \text{ Model I}} = 0.24$ AU, and $D_{103P \text{ Model II}} = 0.21$ AU. These values are in the same range as those found in Paper I and in Lacerda (2013). For further details we refer the readers to Sect. 5 of Paper I.

5.1. Discussion

In Paper I, we concluded that after the 15 Myr backward integration, just 12 of the initial 900 massless particles survived, which means $\sim 98.7\%$ were ejected from the solar system and $\sim 1.3\%$ remained in it. This result agrees with Levison & Duncan (1994), where the authors concluded that $\sim 1.5\%$ endured in the solar system after integration. Thus, in Paper I, eleven of the twelve remaining particles were in Transneptunian region, while one was in Centaur region (see Fig. 10 in Paper I). In this study, just 3 three clones of the initial 200 particles remained in the solar system after the 15 Myr integration, which is $\sim 1.5\%$. These clones were 81P/clon34 and 81P/clon94, which are in Transneptunian region, and 103P/clon57 in Centaur region. Therefore, this result agrees with the one obtained in Paper I, and with Levison & Duncan (1994).

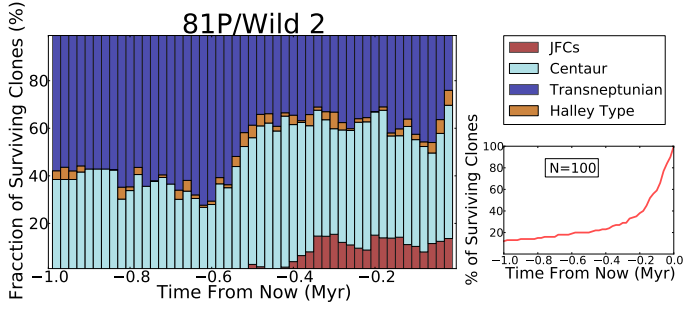


Fig. 12. 81P/Wild 2 backward in time orbital evolution during 1 Myr. *Left panel:* fraction of surviving clones (%) versus time from now (Myr). The colors represent the regions visited by the test particles (red: Jupiter family region; cyan: Centaur; blue: Transneptunian; yellow: Halley type). The resolution is 2×10^4 yr. *Right bottom panel:* the % of surviving clones versus time from now (Myr), where $N = 100$ is the number of the initial test massless particles.

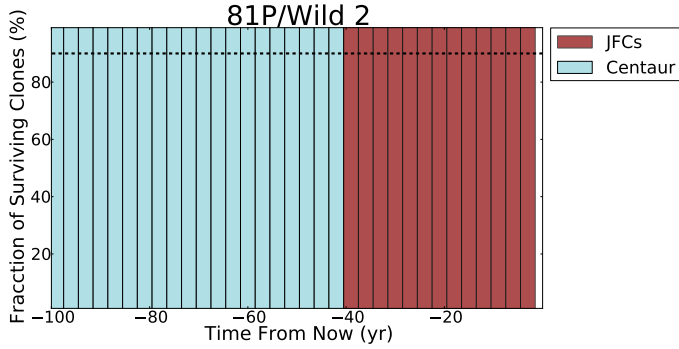


Fig. 13. 81P/wild 2 last 100 yr. fraction of surviving clones (%) versus time from now (yr). The colors represent the regions visited by the test particles (red: Jupiter family region; cyan: Centaur). The dashed line marks the bars with a confidence level equal or larger than 90% of the clones in the Jupiter family region. The resolution is 3 yr, and the number of the initial test particles is $N = 100$.

After the analysis of the 15 Myr integration in Paper I, to obtain a general view of the regions visited by comets, we focused on the first 1 Myr of backward integration in the orbital evolution, where $\sim 20\%$ of the massless particles still remained in the solar system. We inferred that all of them have a Centaur and Transneptunian past, while the Halley Type region was the most unlikely source for those comets, as expected. This is consistent for the other comets, 81P and 103P, under study in this paper (see Figs. 12 and B.1).

After that, to obtain the time spent by each comet in the JFCs region, we displayed the last 5000 yr using a 100 yr temporal resolution. We found that all targets were relatively young in the JFCs region, with ages between $100 < t < 4000$ years. The youngest comets of the sample were 22P/Kopff (~ 100 yr), 78P/Gehrels 2 (~ 500 yr), and 118P/Shoemaker-Levy 4 (~ 600 yr). On the other hand, the oldest comet was 123P with $\sim 3 \times 10^3$ yr. In this study, following the same steps, we have inferred that 81P is ~ 40 yr, while 103P is ~ 1000 yr (see Figs. 13 and B.2). The result for 81P agrees with the current knowledge about it: Sekanina & Yeomans (1985) described a very close encounter with Jupiter in 1974, and, as result of that approach, the comet was inserted in the inner regions of the solar system.

Finally, in Paper I we related the annual dust production rate for each comet (T_d) within the time spent in the JFCs region. We concluded that the most active comets in our sample were also

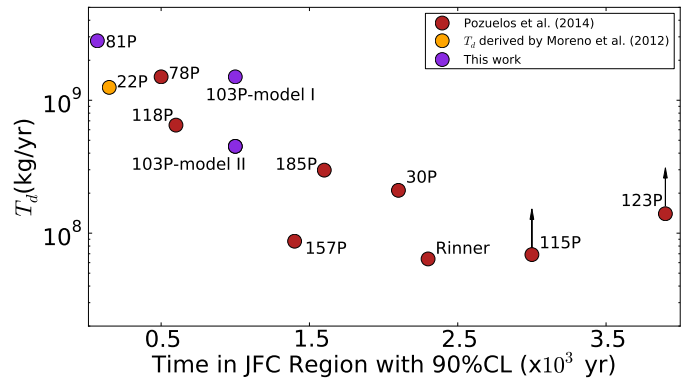


Fig. 14. Annual dust production rate of our targets obtained in the dust analysis (see Sect. 4) versus the time in the JFCs region with a 90% C.L. derived from dynamical studies (see Sect. 5). Red circles are the results derived from Pozuelos et al. (2014); yellow circle is the comet 22P/Kopff, where dust analysis was carried out in Moreno et al. (2012); violet circles are the results of the comets 81P/Wild 2 and 103P/Hartley 2, studied in this work. The comets with arrows mean the T_d given for them are lower limits (see text in Paper I).

the youngest ones, i.e., 22P, 78P, and 118P. Here we added the results obtained for 81P and 103P. We found that 81P is both the youngest and the most active comet in the whole sample. This result is displayed in Fig. 14, where the 11 comets under study are shown.

6. Summary and conclusions

To increase the number of comets analyzed in Paper I, in this work we extended the study to comets 81P/Wild 2 and 103P/Hartley 2, which are of special interest as targets of the spacecraft missions Stardust and EPOXI. We presented optical images of those comets and $Af\rho$ values as a function of the heliocentric distance provided by the amateur astronomical association *Cometas-Obs*. To fit the observational data, we used our Monte Carlo dust tail code (see e.g., Moreno 2009), from which we derived the dust parameters as a function of the heliocentric distance: dust loss rate, ejection velocities of particles, the size distribution, and the overall emission pattern.

The main results are as follows.

- Comet 81P/Wild 2 was found to be the most active in the whole sample of eleven comets, with an annual dust production rate of $T_d = 2.8 \times 10^9$ kg yr $^{-1}$. Its emission pattern was established as anisotropic with active areas located from 45° to -30° on the surface. The rotational parameters, I and ϕ , were found to be $I = (55 \pm 5)^\circ$ and $\phi = (300 \pm 20)^\circ$. In addition, we found two small outbursts suffered by the comet, one inbound and one outbound, where the total dust emitted was $m_{ob,I} \sim 9.2 \times 10^8$ kg and $m_{ob,II} \sim 3.0 \times 10^8$ kg, respectively.
- In the case of the comet 103P/Hartley 2, we proposed two models: *Model I* or the *hyperactive model*, where according to previous knowledge of this comet (see e.g., A'Hearn et al. 2011; Meech et al. 2011; Harmon et al. 2011), we forced the maximum size of particles to be in the range of $r_{max} = 20$ cm. The dust production rate of this model was obtained as $T_d = 1.7 \times 10^9$ kg yr $^{-1}$. *Model II* or the *standard model* was carried out without the restriction in the maximum size of the particles. In that case, the result in the annual dust production rate was $T_d = 4.5 \times 10^8$ kg yr $^{-1}$. The ejection of comet 103P, in both models, was found to be isotropic.

- For both comets, the power index of the size distribution, δ , was found to be in the range $-4 < \delta - 3 <$. In this range, the brightness and mass are decoupled, so the mass depends on the largest ejected grains, while the brightness depends on the micrometer-size grains. For this reason, the dust production rate in our models should be regarded as lower limits. In the case of 103P, the presence of large chunks from the EPOXI mission and radar observations were found in the tail. While the true nature of these chunks is still under study, the size of them is estimated as ~ 20 cm. Thus, in our study, *Model I* seems to be more realistic than *Model II*, which should be considered as a lower limit for this comet.
- We concluded that the best match to the dust ejection velocity law is $v \propto r_h^{-1.998}$ which agrees with $v \propto r_h^{-2}$ obtained by Crifo & Rodionov (1997) from hydrodynamical models of the inner cometary comae, for intermediate-sized particles.

The second block of our study concerned determination of the dynamical evolution of the targets over the past 15 Myr. We used the numerical integrator developed by Chambers (1999). As in Paper I, the statistical study for each comet was implemented using 100 test massless particles: 1 real particle plus 99 clones with 2σ dispersion in the orbital parameters a , e , and i . In these integrations, the Sun and the eight planets were considered to be massive bodies, and close encounters between them and test particles were permitted. Therefore, from the initial 200 massless particles, we removed those that were beyond 1000 AU at any time during the integration. The main results were:

- The analysis showed that $\sim 1.5\%$ of the massless particles remained in the solar system after the 15 Myr integration, and the most likely sources of them were the Centaur and Transneptunian regions. This result agrees with Paper I and with the studies of Levison & Duncan (1994).
- We were able to deduce, with 90% confidence level, how long these targets spent as members of the JFCs: 81P ~ 40 yr and 103P ~ 1000 yr. Thus, 81P was found to be the youngest target in the whole sample of short-period comets studied between Paper I and this study.

In Fig. 14 we added the results from Paper I and the ones obtained from this work for the comets 81P and 103P. In that figure, we plotted the annual dust production rate [kg yr^{-1}] (see Table 3 in this work, and Table 4 in Paper I) versus the time spent by the comets in the JFCs region with a 90% confidence level obtained in the dynamical analysis. From this figure, we concluded that 81P is both the youngest and the most active comet. Therefore, the relationship between activity and the time spent in JFCs, still seems to be evident. Despite the general trend in our sample of comets, this result should be taken with caution, because two exceptions to this trend were found in Paper I, 157P/Tritton and 123P/West-Hartley. To establish firmer conclusions about the cometary activity and the dynamical evolution, it would be desirable to perform more studies on other short-period comets.

Acknowledgements. We would like to thank Dr. Z.-Y. Lin and Dr. L.M. Lara for sharing the observations of comet 81P/Wild 2 carried out in Lulin Observatory (Taiwan) with us. We would also like to thank the entire Amateur Astronomical Association *Cometas-Obs* for always looking for comets. We would also like to thank Dr. Chambers for his help using his numerical integrator. We are grateful to the anonymous referee for comments and suggestions to improve this paper. This work was supported by contracts AYA2012-3961-CO2-01 and FQM-4555 (Proyecto de Excelencia, Junta de Andalucía).

Comet	Emission pattern ¹	Active areas location (°)	Size distribution r_{\min}, r_{\max} (cm)	Size distribution $\delta_{\min}, \delta_{\max}$	Obliguity (°)	Argument of subsolar meridian at perihelion (°)
81P/Wild 2	Ani (35%)	-30 to +45	$10^{-4}, 3$	-3.55, -3.25	50	300
103P/Hartley 2 (<i>Model I</i>)	Iso	-	$10^{-4}, 20$	-3.45, -3.25	-	-
103P/Hartley 2 (<i>Model II</i>)	Iso	-	$10^{-4}, 3$	-3.40, -3.25	-	-

Table 2. Dust properties summary of the targets under study I.

Comet	Peak dust loss rate (kg s^{-1})	Peak ejection velocity of 1-cm grains (m s^{-1})	Total dust mass ejected (kg)	Total dust mass ejected per year (kg/yr)	Averaged dust mass loss rate (kg s^{-1})	Contribution to the interplanetary dust (%) ¹
81P/Wild 2	900	8.0	1.1×10^{10}	2.8×10^9	87.5	0.96
103P/Hartley 2 (<i>Model I</i>)	600	13.9	5.9×10^9	1.5×10^8	46.8	0.51
103P/Hartley 2 (<i>Model II</i>)	160	7.5	1.7×10^9	4.5×10^8	14.1	0.15

Notes. ⁽¹⁾ Iso = Isotropic ejection; Ani = Anisotropic ejection.

Table 3. Dust properties summary of the targets under study II.

Notes. ⁽¹⁾ Annual contribution to the interplanetary dust replacement (Grun et al. 1985).

Table A.1. Orbital parameters of the short-period comets under study.

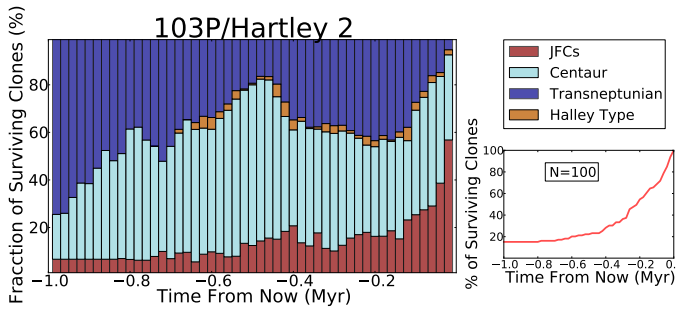
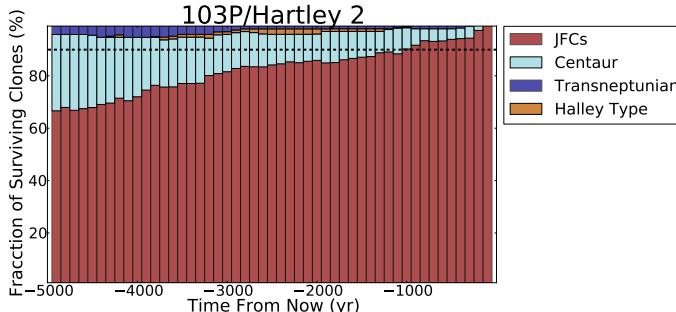
Comet	$e \pm \sigma$	$a \pm \sigma$ (AU)	$i \pm \sigma$ (°)	node (°)	peri (°)	M (°)
81P	0.53735432	3.45011496	3.238287			
JPL K103/7	$\pm 5e-8$	$\pm 4e-8$	$\pm 2e-6$	136.10661	41.69284	171.41550
103P	0.695145	3.47276	13.61716			
JPL 183	$\pm 1e-6$	$\pm 1e-5$	$\pm 2e-5$	219.76266	118.19548	353.71670

Appendix A: Orbital parameters of comets**81P/Wild 2 and 103P/Hartley 2**

In Table A.1 we show the orbital elements of the comets used during the dynamical studies in Sect. 5. They are extracted from JPL Horizons online solar system data³.

Appendix B: Dynamical analysis of comet 103P/Hartley 2

In Figs. B.1 and B.2, we show the dynamical analysis of the comet 103P/Hartley 2 described in Sect. 5. We present the fraction of the surviving clones versus time from now on different time scales. In both cases, the colored bars correspond to different regions visited by test particles: red to Jupiter family; cyan to Centaur; yellow to Haley type; blue to Transneptunian. The number of the initial test particles is $N = 100$.

**Fig. B.1.** As in Fig. 12, but for comet 103P/Hartley 2.**Fig. B.2.** As in Fig. 13, but for the comet 103P/Hartley 2. The total plotted time is 5×10^3 yr, with a resolution of 100 yr.**References**

- A'Hearn, M. F., Schleicher, D. G., Millis, R. L., Feldman, P. D., & Thompson, D. T. 1984, AJ, 89, 579
A'Hearn, M. F., Belton, M. J. S., Delamere, W. A., et al. 2005, Science, 310, 258
A'Hearn, M. F., Belton, M. J. S., Delamere, W. A., et al. 2011, Science, 332, 1396
Basilevsky, A. T., & Keller, H. U. 2006, Planet. Space Sci., 54, 808
Basilevsky, A. T., & Keller, H. U. 2007, Sol. Syst. Res., 41, 109
Bauer, J. M., Walker, R. G., Mainzer, A. K., et al. 2011, ApJ, 738, 171
Belton, M. J. S. 2013, Icarus, 222, 653
Belton, M. J. S., Thomas, P., Carcich, B., et al. 2013a, Icarus, 222, 477
Belton, M. J. S., Thomas, P., Li, J.-Y., et al. 2013b, Icarus, 222, 595
Bertini, I., Barbieri, C., Ho, T.-M., et al. 2012, A&A, 541, A159
Boissier, J., Bockelée-Morvan, D., Biver, N., et al. 2014, Icarus, 228, 197
Brownlee, D. E., Horz, F., Newburn, R. L., et al. 2004, Science, 304, 1764
Burns, J. A., Lamy, P. L., & Soter, S. 1979, Icarus, 40, 1
Chambers, J. E. 1999, MNRAS, 304, 793
Crifo, J. F., & Rodionov, A. V. 1997, Icarus, 127, 319
Davidsson, B. J. R., & Gutierrez, P. J. 2004, in BAAS, 36, 1118
Duxbury, T. C., Newburn, R. L., & Brownlee, D. E. 2004, J. Geophys. Res. (Planets), 109, 12
Edoh, O. 1983, Univ. Arizona, USA
Epifani, E., Colangeli, L., Fulle, M., et al. 2001, Icarus, 149, 339
Farnham, T. L., & Schleicher, D. G. 2005, Icarus, 173, 533
Finson, M. J., & Probstein, R. F. 1968, ApJ, 154, 327
Fulle, M. 2004, in Motion of cometary dust, eds. M. C. Festou, H. U. Keller, & H. A. Weaver (University of Arizona Press), 565
Fulle, M., Colangeli, L., Agarwal, J., et al. 2010, A&A, 522, A63
Green, S. F., McDonnell, J. A. M., McBride, N., et al. 2004, J. Geophys. Res. (Planets), 109, 12
Groussin, O., Lamy, P., Jorda, L., & Toth, I. 2004, A&A, 419, 375
Grun, E., Zook, H. A., Fechtig, H., & Giese, R. H. 1985, Icarus, 62, 244
Hadamik, E., & Levasseur-Regourd, A. C. 2009, Planet. Space Sci., 57, 1118
Hanner, M. S., & Hayward, T. L. 2003, Icarus, 161, 164
Harmon, J. K., Nolan, M. C., Howell, E. S., Giorgini, J. D., & Taylor, P. A. 2011, ApJ, 734, L2
Hsieh, H. H., Yang, B., & Haghighipour, N. 2012a, ApJ, 744, 9
Hsieh, H. H., Yang, B., Haghighipour, N., et al. 2012b, AJ, 143, 104
Jockers, K. 1997, Earth Moon and Planets, 79, 221
Kelley, M. S., Lindler, D. J., Bodewits, D., et al. 2013, Icarus, 222, 634
Kirk, R. L., Duxbury, T. C., Hötz, F., et al. 2005, in 36th Annual Lunar and Planet. Sci. Conf., eds. S. Mackwell, & E. Stansbery, 2244
Knight, M. M., & Schleicher, D. G. 2013, Icarus, 222, 691
Kolokolova, L., Hanner, M. S., Levasseur-Regourd, A.-C., & Gustafson, B. Å. S. 2004, in Physical properties of cometary dust from light scattering and thermal emission, ed. G. W. Kronk, 577
Lacerda, P. 2013, MNRAS, 428, 1818
Lara, L. M., Lin, Z.-Y., & Meech, K. 2011, A&A, 532, A87
Levison, H. F., & Duncan, M. J. 1994, Icarus, 108, 18
Licandro, J., Moreno, F., de León, J., et al. 2013, A&A, 550, A17
Lin, Z.-Y., Lara, L. M., Vincent, J. B., & Ip, W.-H. 2012, A&A, 537, A101
Lisse, C. M., Fernandez, Y. R., Reach, W. T., et al. 2009, PASP, 121, 968
Meech, K. J., & Jewitt, D. C. 1987, A&A, 187, 585
Meech, K. J., A'Hearn, M. F., Adams, J. A., et al. 2011, ApJ, 734, L1
Monet, D. G., Levine, S. E., Canzian, B., et al. 2003, AJ, 125, 984
Moreno, F. 2009, ApJS, 183, 33
Moreno, F., Lara, L. M., Licandro, J., et al. 2011, ApJ, 738, L16
Moreno, F., Pozuelos, F., Aceituno, F., et al. 2012, ApJ, 752, 136
Moreno, F., Cabrera-Lavers, A., Vaduvescu, O., Licandro, J., & Pozuelos, F. 2013, ApJ, 770, L30
Moreno, F., Licandro, J., Álvarez-Iglesias, C., Cabrera-Lavers, A., & Pozuelos, F. 2014, ApJ, 781, 118
Mueller, B. E. A., Samarasinha, N. H., Farnham, T. L., & A'Hearn, M. F. 2013, Icarus, 222, 799
Pozuelos, F. J., Moreno, F., Aceituno, F., et al. 2014, A&A, 568, A3
Richardson, J. E., & Bowling, T. J. 2014, Icarus, 234, 53
Sekanina, Z. 1981, Ann. Rev. Earth Planetary Sci., 9, 113
Sekanina, Z. 2003, J. Geophys. Res. (Planets), 108, 8112
Sekanina, Z., & Yeomans, D. K. 1985, AJ, 90, 2335
Sekanina, Z., Brownlee, D. E., Economou, T. E., Tuzzolino, A. J., & Green, S. F. 2004, Science, 304, 1769
Thomas, P., A'Hearn, M., Belton, M. J. S., et al. 2013a, Icarus, 222, 453
Thomas, P. C., A'Hearn, M. F., Veverka, J., et al. 2013b, Icarus, 222, 550
Tozzi, G. P., Epifani, E. M., Hainaut, O. R., et al. 2013, Icarus, 222, 766
Veverka, J., Klaasen, K., A'Hearn, M., et al. 2013, Icarus, 222, 424
Whipple, F. L. 1951, ApJ, 113, 464

³ See ssd.jpl.nasa.gov/?horizons

THE TAIWANESE–AMERICAN OCCULTATION SURVEY PROJECT STELLAR VARIABILITY. III. DETECTION OF 58 NEW VARIABLE STARS

R. ISHIOKA¹, S.-Y. WANG¹, Z.-W. ZHANG¹, M. J. LEHNER^{1,2,3}, C. ALCOCK³, T. AXELROD⁴, F. B. BIANCO⁵, Y.-I. BYUN⁶, W. P. CHEN⁷, K. H. COOK¹, D.-W. KIM⁸, S.-K. KING¹, T. LEE¹, S. L. MARSHALL¹,

P. PROTOPAPAS^{3,9}, J. A. RICE¹⁰, M. E. SCHWAMB¹, J.-H. WANG¹, C.-Y. WEN¹, AND C.-C. NGEOW⁷

¹ Institute of Astronomy and Astrophysics, Academia Sinica, 11F of Astronomy-Mathematics Building, National Taiwan University, No. 1, Sec. 4, Roosevelt Road, Taipei 10617, Taiwan; ishioka@asia.sinica.edu.tw

² Department of Physics and Astronomy, University of Pennsylvania, 209 South 33rd Street, Philadelphia, PA 19104, USA

³ Harvard-Smithsonian Center for Astrophysics, 60 Garden Street, Cambridge, MA 02138, USA

⁴ Steward Observatory, 933 North Cherry Avenue, Room N204, Tucson, AZ 85721, USA

⁵ Center for Cosmology and Particle Physics, New York University, 4 Washington Place, New York, NY 10003, USA

⁶ Department of Astronomy and University Observatory, Yonsei University, 134 Shinchon, Seoul 120-749, Korea

⁷ Institute of Astronomy, National Central University, No. 300, Jhongda Road, Jhongli City, Taoyuan County 320, Taiwan

⁸ Max Planck Institute for Astronomy, Königstuhl 17, D-69117 Heidelberg, Germany

⁹ Initiative in Innovative Computing, Harvard University, 60 Oxford Street, Cambridge, MA 02138, USA

¹⁰ Department of Statistics, University of California Berkeley, 367 Evans Hall, Berkeley, CA 94720, USA

Received 2013 August 5; accepted 2013 December 23; published 2014 February 24

ABSTRACT

The Taiwanese–American Occultation Survey project is designed for the detection of stellar occultations by small-size Kuiper Belt Objects, and it has monitored selected fields along the ecliptic plane by using four telescopes with a 3 deg^2 field of view on the sky since 2005. We have analyzed data accumulated during 2005–2012 to detect variable stars. Sixteen fields with observations of more than 100 epochs were examined. We recovered 85 variables among a total of 158 known variable stars in these 16 fields. Most of the unrecovered variables are located in the fields observed less frequently. We also detected 58 variable stars which are not listed in the International Variable Star Index of the American Association of Variable Star Observers. These variable stars are classified as 3 RR Lyrae, 4 Cepheid, 1 δ Scuti, 5 Mira, 15 semi-regular, and 27 eclipsing binaries based on the periodicity and the profile of the light curves.

Key words: stars: variables: Cepheids – stars: variables: delta Scuti – stars: variables: general

Online-only material: color figures, machine-readable and VO tables

1. INTRODUCTION

Variable stars are important tools for studying not only stellar structure and evolution, but also galactic astronomy. Stars such as Cepheid and RR Lyrae are used as standard candles to measure distances, and supernovae can be used to estimate star formation rates as well as distance indicators. Because of the importance of variability in the universe, several large-scale surveys, such as the All Sky Automated Survey (ASAS; Pojmanski et al. 2005), the Northern Sky Variability Survey (NSVS; Woźniak et al. 2004), the Catalina Real-Time Transient Survey (Drake et al. 2009), and the Panoramic Survey Telescope and Rapid Response System (Kaiser et al. 2010), are dedicated to explore the variable sky in recent years, and they have discovered many variable sources. Also, many surveys whose primary purposes are specified to other scientific goals such as gravitational lensing events, gamma-ray burst detection, and celestial censuses of the universe, have also discovered numerous variable stars as byproducts, such as the Optical Gravitational Lensing Experiment (OGLE; Cieślinski et al. 2003; Wray et al. 2004), the Massive Compact Halo Object (Alcock et al. 1995, 1998), the Robotic Optical Transient Search Experiment (ROTSE; Akerlof et al. 2000; Yeşilyaprak et al. 2012), and the Sloan Digital Sky Survey (SDSS; Sesar et al. 2007). The large-scale deep surveys have provided a more complete census of variable stars. Meanwhile, the bright variable stars discovered in shallower surveys, such as ASAS and NSVS help us obtain more detailed information on stellar variability.

The Taiwanese–American Occultation Survey (TAOS) is a project whose aim is to search for stellar occultation by Kuiper Belt Objects (KBOs) at a distance of Neptune’s orbit or beyond (Alcock et al. 2003; Lehner et al. 2009; Zhang et al. 2013). For that purpose, TAOS telescopes have monitored thousands of bright stars with a wide field of view since 2005. The data set, accumulated for a period of 7 yr, contains information on the variability of bright stars in the TAOS fields.

This is the third paper of the series of the TAOS stellar variability studies, following the detection of low-amplitude δ Scuti stars (Kim et al. 2010) and the detection of 15 variable stars in TAOS field 151 (Mondal et al. 2010). We report the detection of 58 new variable stars in 16 TAOS fields which have been observed most frequently among 167 TAOS fields in addition to the previously examined field 151.

2. OBSERVATIONS AND DATA REDUCTION

The TAOS telescope system consists of four 50 cm telescopes, each equipped with a $2 \text{ k} \times 2 \text{ k}$ CCD camera, yielding a field of view of about 3 deg^2 , with the plate scale of about $3 \text{ arcsec pixel}^{-1}$. All TAOS telescopes observe the same field simultaneously during an observing run for KBO event search. Each run begins with a set of “stare-mode” images, which are standard images with exposure times of 1 s, followed by 90 minutes of observations collected in “zipper-mode” observation, which is a special CCD readout mode to yield a time resolution of 5 Hz in photometry. A complete run ends with another set of stare-mode images after the zipper-mode

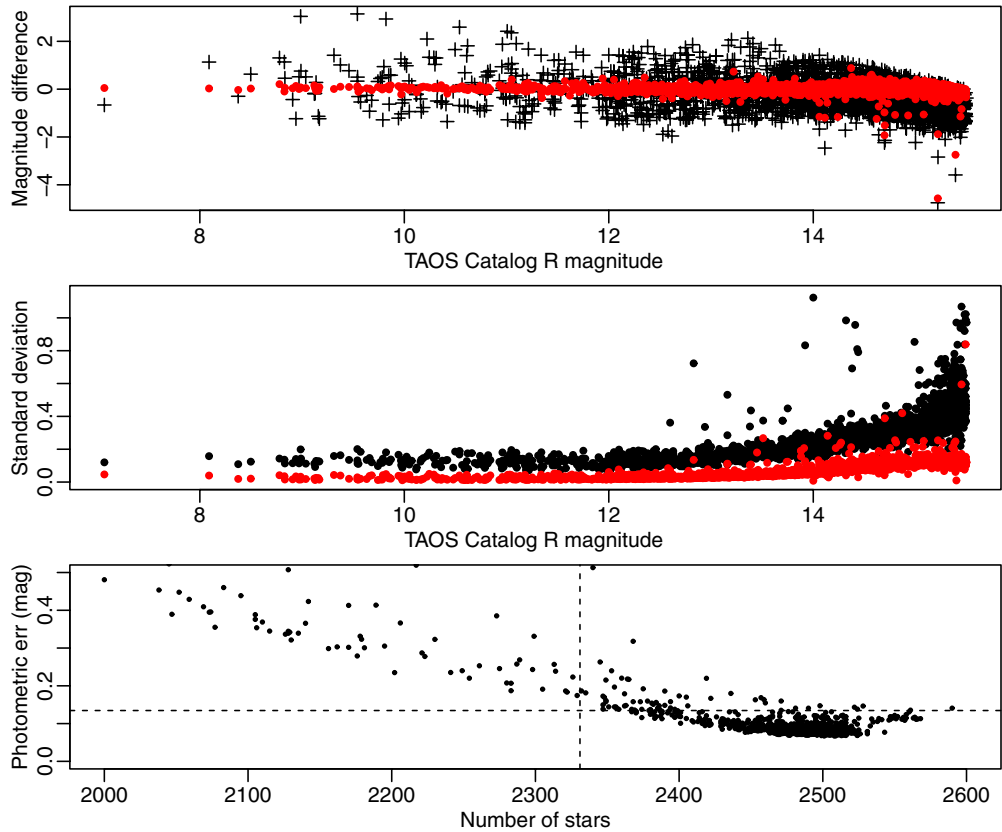


Figure 1. Top panel: TAOS catalog R magnitude vs. calibrated magnitude on two different nights. The vertical axis represents the difference between observed and cataloged magnitudes. Black crosses and red points indicate two different nights. Standard deviations against the linear fittings are 0.72 and 0.19 for respective nights. Middle panel: catalog magnitudes vs. standard deviations of the light curves of 2752 stars in Field 060. Black and red points correspond to before and after removing poor images, respectively. Bottom panel: number of detected stars vs. photometric error. The photometric error is defined as the median value of the absolute difference between the catalog and calibrated magnitudes of stars in 1251 epochs of images of Field 060 with telescope B. Dashed lines represent the thresholds and images located in the lower right part of the panel meet the criteria.

(A color version of this figure is available in the online journal.)

Table 1
Log of Observations

Field ^a	Field Center (J2000)		Number of Epochs (Good/All) ^b				Nstar ^c	Threshold ^d		
	R.A. (h m s)	Decl. (d m s)	Total	Tel A	Tel B	Tel C	Tel D	Nstar	Err	
F043	+02 55 54.00	+15 03 30.00	138/191	72/155	112/176	73/119	80/105	914	821–826	0.13–0.16
F049	+04 06 24.70	+18 35 20.00	158/217	85/158	134/197	23/128	50/102	1461	1255–1277	0.16–0.21
F054	+07 58 50.70	+22 04 40.00	737/933	288/712	610/870	370/634	356/437	2284	1902–1929	0.12–0.17
F060	+04 48 00.00	+20 46 20.00	993/1251	451/917	846/1181	489/813	408/558	2718	2260–2331	0.11–0.15
F061	+09 16 43.30	+19 39 00.00	271/353	164/263	225/328	31/193	163/207	1203	1020–1027	0.13–0.18
F074	+11 00 11.30	+08 33 00.00	358/393	209/290	286/371	182/228	189/248	917	739–752	0.16–0.20
F081	+14 57 06.00	−15 06 00.00	203/298	96/257	176/287	0/144	129/187	1635	1407–1444	0.14–0.20
F095	+14 00 00.00	−11 12 00.00	120/156	88/133	98/145	25/80	78/99	1143	1018–1034	0.18–0.24
F133	+00 30 00.00	+01 03 59.00	352/411	168/339	293/390	154/230	187/238	830	678–690	0.12–0.22
F146	+16 55 22.70	+03 24 20.00	190/321	143/292	165/315	0/109	109/221	3162	2684–2819	0.17–0.42
F005	+21 30 00.00	−16 00 00.00	94/158	52/127	79/157	32/55	56/116	1574	1420–1437	0.16–0.23
F088	+11 30 22.00	+04 38 10.00	86/117	51/100	77/115	3/43	52/75	688	590–597	0.16–0.22
F099	+16 00 06.00	−19 02 20.00	77/115	40/110	61/109	0/47	42/67	2949	2497–2562	0.16–0.22
F135	+20 32 08.00	+00 24 50.00	46/107	31/96	40/106	4/14	32/87	3522	3420–3561	0.29–0.39
F158	+18 53 44.00	−17 23 00.00	65/102	44/94	60/100	21/37	39/67	19795	18943–20336	0.15–0.24
F167	+17 14 49.30	−18 14 30.00	94/136	47/125	76/129	8/52	59/83	14319	12921–14051	0.15–0.23

Notes.

^a TAOS field number.

^b Number of epochs of observations after/before removing poor images. Total: combined all telescopes, and Tel A–D: each telescope.

^c Number of stars detected in more than 40 epochs of images.

^d Criteria used to select good images. Nstar is the threshold of the number of detected stars. Err is the threshold of the photometric errors. Values are minimum and maximum numbers of four telescopes.

Table 2
Typical Photometric Error for Each Telescope

	Mag = 9	Mag = 10	Mag = 11	Mag = 12	Mag = 13	Mag = 14	Mag = 15
Tel A	0.03 ± 0.01	0.03 ± 0.01	0.03 ± 0.01	0.04 ± 0.01	0.06 ± 0.01	0.11 ± 0.02	0.20 ± 0.02
Tel B	0.03 ± 0.01	0.03 ± 0.01	0.03 ± 0.01	0.04 ± 0.01	0.05 ± 0.01	0.10 ± 0.01	0.18 ± 0.02
Tel C	0.02 ± 0.01	0.02 ± 0.01	0.02 ± 0.01	0.03 ± 0.01	0.05 ± 0.01	0.11 ± 0.02	0.21 ± 0.03
Tel D	0.02 ± 0.01	0.02 ± 0.01	0.02 ± 0.01	0.03 ± 0.01	0.04 ± 0.01	0.08 ± 0.02	0.16 ± 0.02

Table 3
Limiting TAOS R Magnitude

Field	Tel A	Tel B	Tel C	Tel D	Comb.	Field	Tel A	Tel B	Tel C	Tel D	Comb.
F005	14.70	14.91	14.76	14.90	14.95	F088	14.80	14.64	14.52	14.98	14.73
F043	15.03	14.96	15.02	15.17	15.12	F095	14.75	14.76	14.58	14.76	14.84
F049	14.90	14.95	14.75	14.76	14.69	F099	14.75	14.81	NA	14.91	14.81
F054	15.01	15.01	14.90	15.15	14.89	F133	14.70	14.45	14.62	14.90	14.86
F060	15.06	15.11	14.97	15.11	15.06	F135	14.55	14.75	14.60	14.56	14.69
F061	14.95	14.88	14.85	15.15	15.06	F146	14.66	14.91	NA	14.90	14.80
F074	14.80	14.81	14.56	14.96	14.95	F158	14.75	14.85	14.80	14.80	14.95
F081	14.85	15.01	NA	15.12	15.02	F167	14.75	14.85	14.65	14.84	14.85

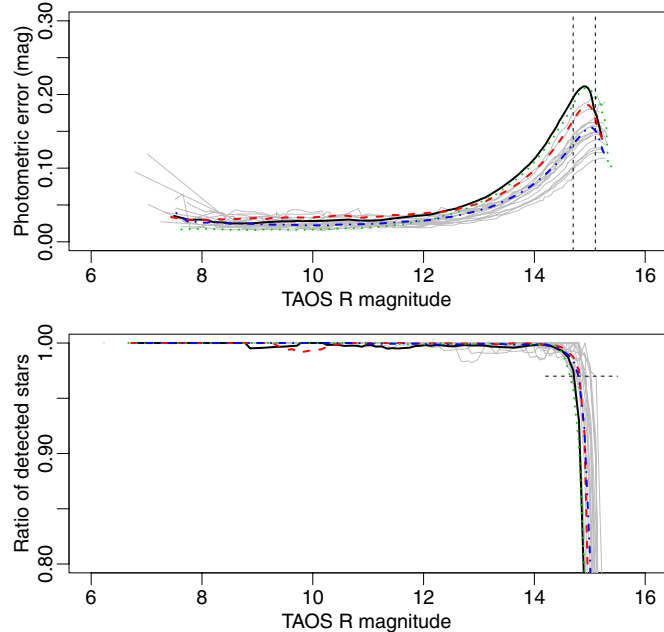


Figure 2. Upper panel: TAOS R magnitude vs. photometric error determined by the median photometric error values for stars observed by each telescope (thick lines: black—Tel. A, red—Tel. B, green—Tel. C, and blue—Tel. D) and in different fields (gray lines). Dashed vertical lines represent the limiting magnitudes of 14.7 and 15.1 for Field 135 and 43, respectively. Lower panel: TAOS R magnitude vs. ratio of stars detected in more than 95% of frames for each field (gray lines) and with different telescopes (thick lines: black—Tel. A, red—Tel. B, green—Tel. C, and blue—Tel. D). A short dashed horizontal line shows the 97% threshold to determine the limiting magnitude.

(A color version of this figure is available in the online journal.)

observing is finished (see Lehner et al. 2009, for more details). The purpose of the stare-mode observation is to provide required information for the photometric analysis pipeline of the zipper-mode data. Across the sky, 167 TAOS fields were selected along the ecliptic plane to have a higher star density but to avoid stars brighter than eighth magnitude. Some fields have been observed more frequently than others. For frequently observed fields, the accumulated stare-mode data can be used for variable star studies. Among the 167 fields, 16 fields with more than 100 epochs of observations were selected for variable star detection

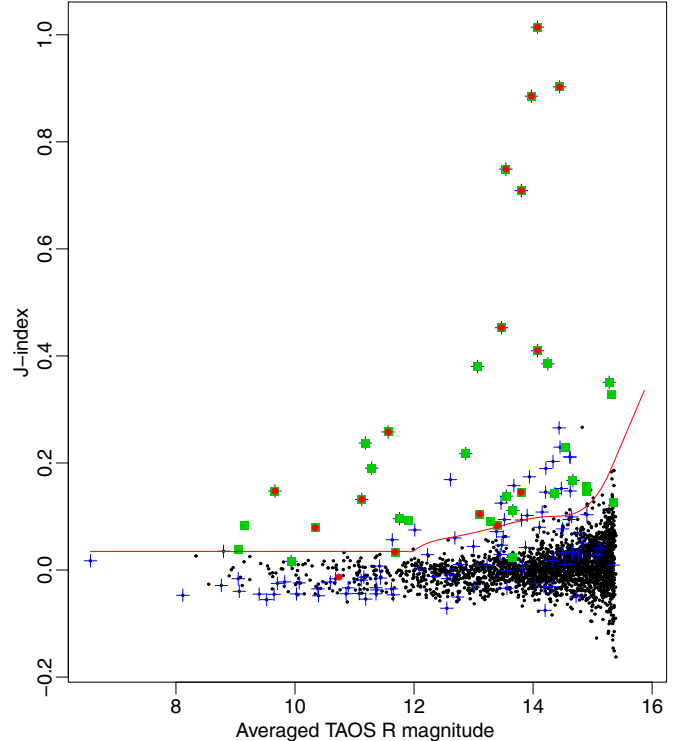


Figure 3. Magnitude vs. J -index diagram for Field 060 derived from a pair of telescope B light curves and combined light curves of the other three telescopes. The red line indicates the threshold to select candidates. Blue crosses, green squares, and red points indicate SD-selected candidates, J -selected candidates, and variables, respectively.

(A color version of this figure is available in the online journal.)

in this study. Table 1 shows the field IDs and pointing centers of these fields.

Photometry was done for stars with TAOS catalog R magnitudes brighter than 15.5 by the TAOS photometry pipeline (Zhang et al. 2009). The TAOS catalog was compiled from Tycho2, UCAC3, CMC14, Two Micron All Sky Survey (2MASS), GSC2.3, and SDSS7. In the TAOS catalog, the astrometry was based on UCAC3, and the R magnitude was based on GSC2.3 F magnitude. For the stars are not in GSC2.3 but are shown in

Table 4
Numbers of Candidates and Variable Stars

Field	Epochs ^a	Stars ^b	Candidates ^c	Number of Detected VSs			Number of Known VSs	
				Total	New	Known	Candidates ^c	All
F054	737	2284	30	10	6	4	4	6
F060	993	2718	39	15	12	3	3	4
Subtotal		5002	69(1.4%) ^d	25(36%) ^e	18(72%) ^f	7(70%) ^g	7(70%) ^g	10
F043	138	914	13	5	0	5	6	7
F049	158	1461	27	6	0	6	7	8
F061	271	1203	20	6	1	5	6	6
F074	358	917	21	3	2	1	1	1
F081	203	1635	26	13	7	6	7	7
F095	120	1143	29	1	0	1	2	2
F133	352	830	6	1	0	1	1	1
F146	190	3162	24	8	3	5	6	6
Subtotal		11,265	166(1.5%) ^d	43(26%) ^e	13(30%) ^f	30(79%) ^g	36(95%) ^g	38
F005	94	1574	27	6	3	3	3	4
F088	86	688	14	1	0	1	1	2
F099	77	2949	24	3	1	2	5	5
F135	46	3522	57	4	0	4	9	11
F158	65	19,795	254	22	13	9	20	23
F167	94	14,319	205	39	10	29	52	65
Subtotal		42,847	591(1.4%) ^d	75(13%) ^e	27(36%) ^f	48(44%) ^g	90(82%) ^g	110
Total		59,114	816(1.4%) ^d	143(18%) ^e	58(41%) ^f	85(54%) ^g	133(84%) ^g	158

Notes.^a Number of epoch with good images.^b Number of stars detected in more than 40 epochs of images.^c Number of stars of known variables selected as candidates.^d Percentages of candidates against stars.^e Percentages of detected variables against candidates.^f Percentages of newly detected variables against all detected variables.^g Percentages of known variables detected and selected as candidates against all of the known variables.

other catalogs, so a linear transformation was used to convert the different photometric systems to GSC2.3 *F* magnitude.

2.1. Data Selection

Since not all TAOS data were collected under photometric conditions, only the stare images with good photometric quality were used in this study. The accuracy of the photometry greatly depends on the sky condition and the magnitudes of stars. The relation between observed and cataloged magnitudes of stars in Field 060 for photometric and non-photometric nights are shown in the top panel of Figure 1 as an example. This shows the large variation of data quality in TAOS observations.

We selected images with good photometric quality based on the number of detected stars (N_{star}) and photometric error (Err) of each of the images. The photometric error was defined by the median value of the differences between observed and cataloged magnitudes of detected stars in each image. The threshold of N_{star} for each field is set to be 90% of the maximum number of detectable stars for the field. After removing the poor images which did not meet the threshold of N_{star} , the threshold of the Err for each field is set to be 1.5σ above the median value of the Err of remaining images. The middle panel shows the standard deviations (SDs) of light curves of 2752 stars¹¹ in Field 060 before and after removing poor quality images which did not meet the thresholds. The bottom panel in Figure 1 shows N_{star} versus Err diagram for all 1251 epochs of images of Field 060.

Only the images at the lower right quadrant are good images. Table 1 shows the numbers of epochs for each field used in this analysis, along with the numbers of stars detected in more than 40 epochs and the values of the thresholds to select images with good photometric quality.

Among 14,967 images obtained with four telescopes for 16 fields, 6156 images are removed as poor images. The ratio of the rejected images over the total images is 0.4, however, percentages of rejected images are greatly different between telescopes and fields with the range from 18% for Field 54 with telescope A to 100% for Fields 81, 146, and 99 with telescope C, as listed in Table 1. Telescopes B and D with total rejection ratios of ~ 0.3 provided better photometric quality than telescopes A and C with ratios of ~ 0.5 .

After removing the poor images, we estimated the typical photometric error of different magnitude stars and the limiting magnitude of each telescope in each field. The typical photometric error for each magnitude was estimated from median values of SD of the light curves for stars in the respective magnitude bin. The bins were set using a moving window with a 0.1 mag step and a width changing from 1 mag to 0.2 mag. The window width is adjusted so that the number of stars is similar in each bin. The typical photometric error for stars brighter than 12 mag is nearly constant (around 0.02–0.03 mag). The error gradually increases for fainter stars and is 0.15–0.20 mag for stars around 15 mag. Table 2 lists the typical photometric error for different magnitude stars of each telescope derived by combining the data from all 16 fields. The upper panel of Figure 2 shows the typical

¹¹ Stars detected in two or more epochs after removing poor quality images.

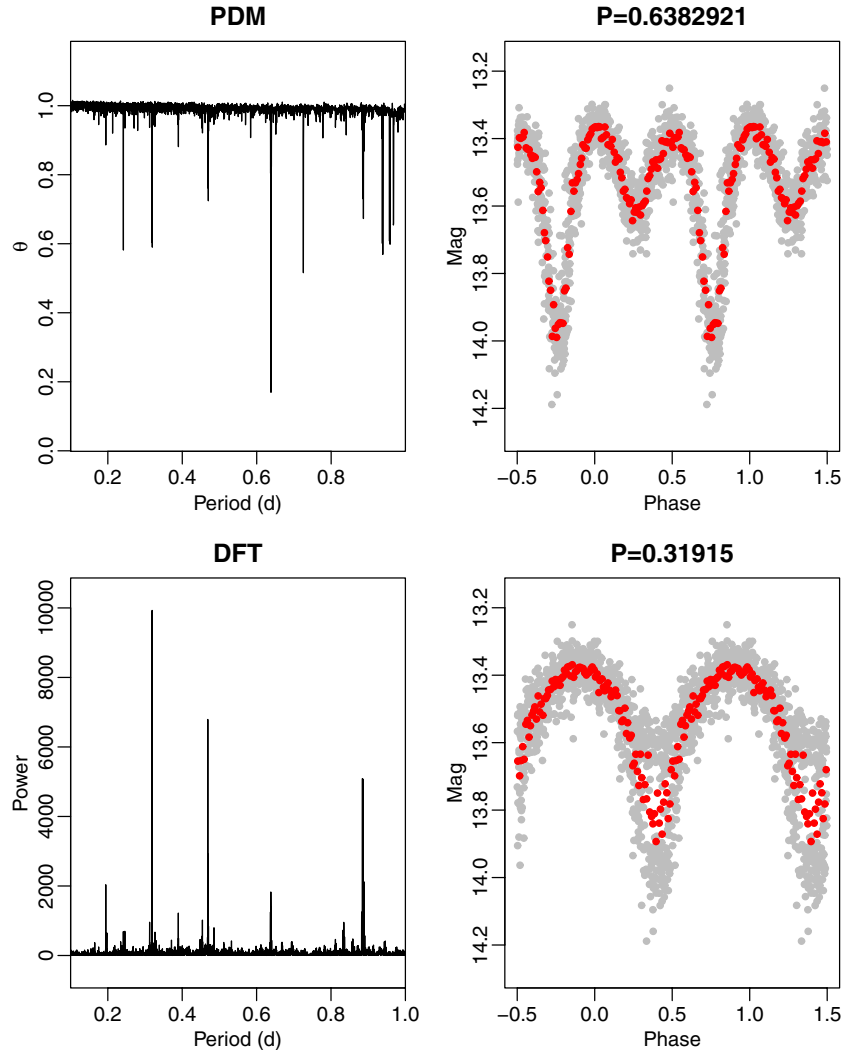


Figure 4. Comparison of the results of the period analysis derived from the PDM method (upper) and DFT method (lower). Left panels show the period–theta diagrams. Right panels show phase-folded light curves. Gray and black points represent phased and phase-averaged light curves, respectively. The strongest signal of the spectrogram from the DFT method is at a half period of that derived from the PDM method.

(A color version of this figure is available in the online journal.)

Table 5
List of Known Variable Stars in 16 TAOS Fields

TAOS ID	Object ID		Catalog					TAOS		
	USNO-B1.0	Star Name	Vmag (mag)	Period (days)	Amp (mag)	Type	N ^a	P _{DFT} ^b (days)	P _{PDM} ^b (days)	Amp ^c (mag)
005.00009	0738-0814213	ASAS J212837–1609.0	9.89	18.167191	0.06	MISC	94	NA	NA	0.06
005.00396	0743-0843803	ASAS J213301–1541.8	12.97	0.082903	0.45	BCEP/DSCT	94	0.076540	0.08290296	0.4
005.00688	0743-0842507	NSVS 17219709	14.21	0.543961	0.88	RRAB	94	0.544095	0.5441166	0.85
005.01435	0743-0842018	SEKBO 102605.334	14.90	0.651650	0.7	RRAB	84	0.6528	0.6527767	0.5
043.00001	1046-0029951	NSV 15603	7.55	7.64	0.09	NA	138			<0.1
043.00005	1046-0030524	ASAS J025652+1436.6	8.70	56.996444	0.3	MISC	138	57.4	57.67	0.3
043.00027	1053-0031020	BR Ari	10.36	60.51	0.12	RS	138	72.8192	76.7	0.1
043.00051	1056-0039561	ASAS J025521+1539.4	11.00	33.998	0.21	RS/ESD	138	33.61	33.84	0.15
043.00097	1056-0040215	ASAS J025822+1540.3	11.53	0.6424174	0.54	RRAB	138	0.642422	0.6424209	0.5
043.00275	1050-0030082	ASAS J025239+1504.3	13.21	0.5921955	0.77	RRAB	138	0.59221	0.5921378	0.8

Notes.

^a Number of epoch.

^b Period derived from period analysis. NA means the object was not detected as a variable candidate. Blank means no detection of meaningful period.

^c When there is no TAOS period, the amplitude was derived using the catalog period.

(This table is available in its entirety in machine-readable and Virtual Observatory (VO) forms in the online journal. A portion is shown here for guidance regarding its form and content.)

Table 6
List of Previously Uncataloged Variable Stars in 16 TAOS Fields

TAOS ID	USNO B1.0	R.A. decl. (J2000)	Rmag (mag)	N ^a	P _{DFT} ^a (days)	P _{PDM} ^a (days)	Amp (mag)	Type
005.00921	0746-0813891	323.1635 -15.32215	14.24	94	0.319876	0.3198652	0.7	RR/OC
005.00955	0747-0803979	323.0227 -15.24368	14.28	94	0.81275	0.8127761	0.6	OC
005.01788	0744-0835997	322.456 -15.55384	15.24	93	146.1	144.9	1.5	Pul
054.00125	1114-0164679	119.4484 21.41544	11.149	737	1.4377000	2.875253	0.1	D
054.00435	1119-0172489	119.6793 21.94714	12.85	737	0.579488	1.1607276	0.1	OC
054.00780	1116-0171489	120.4895 21.69124	13.61	737	0.221623	0.4432462	0.6	SD
054.00850	1117-0174408	119.5247 21.7437	13.74	737	0.3349867	0.5015099	0.7	SD
054.00916	1116-0171086	120.0515 21.65149	13.84	737	0.1919673	0.3839438	0.3	OC
054.01481	1127-0182109	119.1762 22.7095	14.51	736	0.1585343	0.3170605	0.3	OC/RR
060.00072	1103-0056893	72.23601 20.35759	10.321	993	0.088421	0.08121988	0.08	Dsct
060.00177	1108-0058270	71.9698 20.88583	11.48	993	30.9375	30.9646316	0.15	sPul
060.00217	1111-0059960	71.98213 21.11767	11.85	993	9.528166	9.525339	0.05	sPul
060.00567	1109-0058272	71.63566 20.98915	13.06	992	0.6852657	1.37050885	0.2	SD/D
060.00764	1112-0063905	72.57811 21.24817	13.45	993	0.31915	0.6382921	0.8	SD
060.01019	1112-0061624	71.38461 21.25024	13.88	993	0.316524	0.6330263	1.0	SD
060.01029	1106-0057084	71.84878 20.69625	13.89	992	0.42078	0.8414859	0.3	SD
060.01041	1111-0060463	72.27741 21.13705	13.91	993	0.2864	0.5728208	0.8	SD
060.01202	1105-0057706	71.82675 20.57948	14.06	993	0.37801	0.5482275	0.5	SD
060.01274	1108-0058098	71.85808 20.82781	14.14	993	0.1619275	0.3238403	0.3	OC
060.01276	1109-0059167	72.20344 20.91905	14.14	993	0.56089	0.7179834	1.2	SD
060.01402	1102-0058053	72.605 20.29844	14.26	993	NA	NA	1.2	L
061.00059	094-0169752	139.11 19.42362	10.731	271	13.94081	13.93424	0.2	sPul
074.00482	0993-0203912	165.0271 9.353473	13.99	358	0.15389	0.3077757	0.9	OC/SD
074.00745	0990-0201678	165.1016 9.003732	14.65	344	0.164840	0.3296808	0.9	OC
081.00149	0742-0306311	223.6492 -15.74792	11.745	203	12.114496	24.240000	0.2	sPul
081.00176	0746-0298147	223.6174 -15.33418	12.000	203	0.3211346	0.3211347	0.2	RR/ELV/SD
081.00549	0744-0305168	224.6273 -15.56192	13.48	203	0.326064	0.4914476	0.5	OC
081.00940	0750-0296700	224.9408 -14.9714	14.31	203	0.8968033	0.8967631	1.0	RR
081.01046	0742-0307291	224.3807 -15.76408	14.5	203	0.3092092	0.3092088	0.5	RR/OC
081.01141	0754-0295316	224.6334 -14.55273	14.65	203	0.4250575	0.2980352	0.7	RR/OC
081.01361	0749-0294838	224.8522 -15.02932	14.9	203	0.2262797	0.3688668	0.7	OC/SD
099.01571	0711-0315802	239.1581 -18.8471	14.27	77	0.891406	0.8913761	1.2	RR
146.00892	0929-0363399	253.9785 2.905618	13.5	190	0.38848	0.5591467	0.4	OC
146.01273	0931-0317033	253.3615 3.115102	13.95	190	0.258539	0.4106175	0.5	OC
146.02326	0931-0319136	254.319 3.199092	14.75	190	2.45306	4.906567	1.0	SD
158.00443	0733-0714833	282.6194 -16.61553	11.18	65	268	NA	3.5	M
158.02632	0726-0983803	283.7697 -17.30579	12.91	65	116	117	1.2	Pul
158.03010	0727-0968975	282.7519 -17.21255	13.04	65	204	206	1.6	Pul
158.03355	0729-0943936	284.0212 -17.02446	13.14	65	0.215452	0.3543472	1.3	SD
158.03980	0728-0954550	282.7732 -17.16336	13.33	65	109.6	110.7	2.5	SR
158.05344	0725-0972933	282.8104 -17.47347	13.63	65	206.0	211.9	4.0	M
158.09398	0720-0976942	282.7024 -17.96888	14.23	63	124	NA	3.0	M
158.13567	0723-1005240	283.9894 -17.66208	14.648	65	440	NA	4.0	M
158.15838	S3033323113189 ^b	284.1404 -17.04979	14.820	65	NA	NA	2.0	L
158.16292	0733-0714737	282.6152 -16.61804	14.85	64	268	520	2.5	Pul
158.19884	0728-0962875	283.1613 -17.11101	15.08	65	160	NA	2.3	Pul
158.25535	0727-0998000	284.2059 -17.27155	15.37	56	197.65	189.5	3.2	M
158.26931	0728-0954528	282.7720 -17.16582	15.44	60	220.7	223.5	2.2	Pul
167.01061	0720-0489483	258.2018 -17.91735	12.44	94	54.5	55.5	1.2	Pul
167.01256	0715-0381754	258.9583 -18.47618	12.58	94	80	80	0.8	Pul
167.01546	0721-0513564	259.408 -17.86621	12.76	94	309	307	1.3	Pul
167.02306	0724-0501771	258.1829 -17.58355	13.15	94	143	143	1.5	Pul
167.02540	0724-0511622	259.2946 -17.53316	13.24	94	720	NA	1.2	L
167.03494	0715-0375925	258.4826 -18.46945	13.57	94	0.233304	0.3781340	0.45	OC
167.05343	0714-0382994	259.1773 -18.53733	14.02	94	124.3	128.6	2.0	Pul
167.06867	0719-0490902	258.9099 -18.07264	14.293	94	0.795055	0.7950784	0.6	RR
167.06874	0713-0372495	258.0081 -18.64727	14.298	94	0.194626	0.2455117	0.8	OC
167.12874	0712-0373746	258.7981 -18.47818	15	94	0.56082	0.4174338	1.0	OC/SD

Notes.^a N: number of observed epochs. P_{DFT} and P_{PDM}: period derived from DFT and PDM analysis.^b GSC2.2.1.

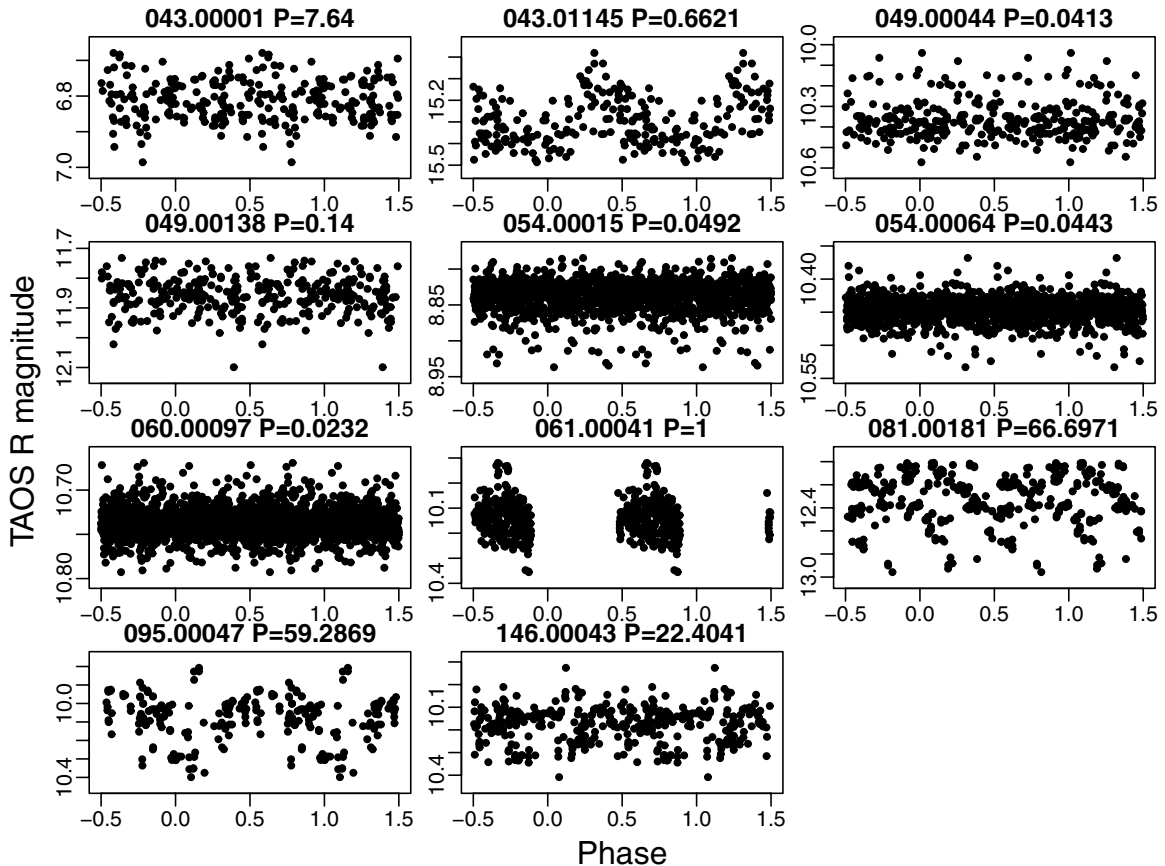


Figure 5. Phase-folded light curves of 11 unrecovered known variable stars with cataloged periods in fields with more than 100 good epochs.

photometric error as a function of magnitude. The thick lines are the errors of each telescope, and the thin gray lines are the errors for each field. The photometric error is larger for mag 7 and 8 stars because of the limited number of very bright stars and the occasional saturation. Some of the fields have much higher errors than others, because the thresholds to select “good” images are set for each field, respectively, as listed in Table 1.

The limiting magnitude was defined by magnitude where the star detection ratio is less than 97% in the corresponding magnitude bin. The bins were set using a moving window with a width of 0.1 mag and a 0.05 mag step over the range of 14–15.5 mag. The limiting magnitude for each field ranges from 14.7 mag for Field 135 to 15.1 mag for Field 43. The lower panel of Figure 2 shows the detection ratio as a function of magnitude. The fluctuations between 10 mag and 14 mag are due to stars near the edges of the frames, which were sometimes omitted from the photometry. The thick lines are the ratios for each telescope, and the thin gray lines are the ratios for each field. Table 3 lists limiting magnitudes for each telescope for each field.

Among these fields, several stars in Field 054 were observed with the Tenagra Telescope to confirm their variability. Also, Field 060 was independently analyzed by Ngeow et al. (2010).

3. PERIOD ANALYSIS AND RESULTS

3.1. Candidate Variables

We used J -indices (Stetson 1996), which is derived from the I -index (Welch & Stetson 1993), as the criteria to select

candidates of variable stars. We used $1/\sigma$ as the weights to calculate the index, where σ is the error in the magnitude. For each star, four or fewer light curves were generated synchronously from different telescopes. For each individual light curve, a J -index was calculated by pairing the light curve with a light curve generated by combining the light curves of the two or three other telescopes. Thus, for each star, we have three or four J -indices in most cases, depending on the number of telescopes that are used to collect data on that star. We set limits of 0.1σ or 5σ above the median J value for stars brighter than 12 mag, and 3σ above the median J value in a 0.3 mag bin for stars fainter than 12 mag. Stars were selected as candidates if two or more J indices are identified as candidates. The SDs of light curves were also tested as the selection criteria, but in the end, we determined that this was not a good method to use, given that many light curves exhibit large variances due to moon phase and image distortion from telescope tracking errors.

Figure 3 shows a magnitude versus J -index diagram for telescope B in field 60. The red line indicates the threshold to select candidates. Blue crosses, green squares, and red points indicate SD-selected candidate, J -selected candidate, known and newly detected variable stars, respectively. As the figure shows, many of SD-selected candidates have small J -indices. Furthermore some J -selected candidates and variable stars are not selected as candidates, thus only the J -indices are used for the candidate’s selection. There are some J -selected candidates below the red line, which are selected from J -index values of other light curve pairs. Table 4 shows the number of variable star candidates along with the numbers of epochs and stars for each field.

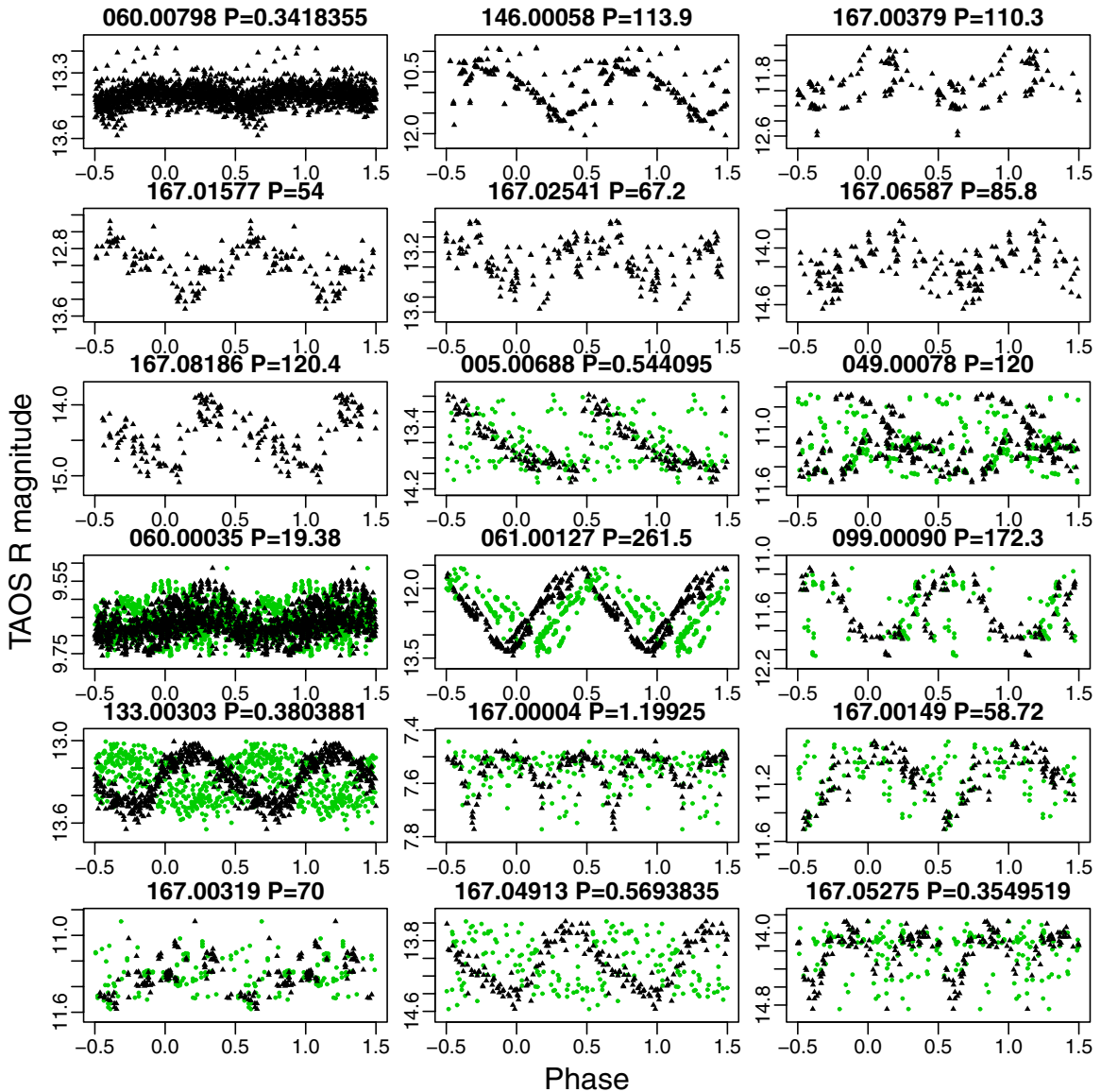


Figure 6. Phase-folded light curves of 18 known variable stars recovered from TAOS data with periods newly determined or improved by our analysis. Green and black points represent light curves folded by cataloged period and TAOS period, respectively.

(A color version of this figure is available in the online journal.)

3.2. Period Analysis

Both the Period Dispersion Minimization (PDM; Stellingwerf 1978) and the discrete Fourier transform (DFT; Deeming 1975) methods were used to search for periodicities of candidate variables. The PDM method computes the variance of phase-folded light curves against trial periods to find a period which minimizes the variance. The DFT method computes the Fourier power over an ensemble of frequencies and finds significant periodicities even for unevenly sampled data. PDM has an advantage over the Fourier methods when the light curves are non-sinusoidal. When a periodogram shows signals stronger than 10σ above the background noise, we checked the periodogram and phase-folded light curve of the star by eyes. We obtained consistent results from two methods for most of the single-peaked pulsating stars, though the DFT method tends to give us aliases for eclipsing binaries. Figure 4 shows an example of the results of the period analysis for an eclipsing binary

derived from a PDM method and a DFT method. In such case, only the PDM method gives us the right period.

3.3. Previously Known Variables

We searched the International Variable Star Index (VSX) of the American Association of Variable Star Observers (AAVSO) for known variable stars in our fields on VizieR Search Page.¹² The VSX database is populated with the General Catalog of Variable Stars (GCVS; Kholopov et al. 1998) including the New catalog of suspected variable stars (NSV catalog; Kukarkin et al. 1982), and the published catalogs from sky surveys, NSVS (Woźniak et al. 2004), ASAS-III (Pojmanski et al. 2005), OGLE-II (Woźniak et al. 2002), ROTSE-I (Akerlof et al. 2000), and variables reported in the Information Bulletin on Variable Stars. We found in total 158 variable stars from the VSX database matched with the TAOS star catalogs for the 16 fields.

¹² <http://vizier.u-strasbg.fr/viz-bin/VizieR?-source=B%2Fvsx>

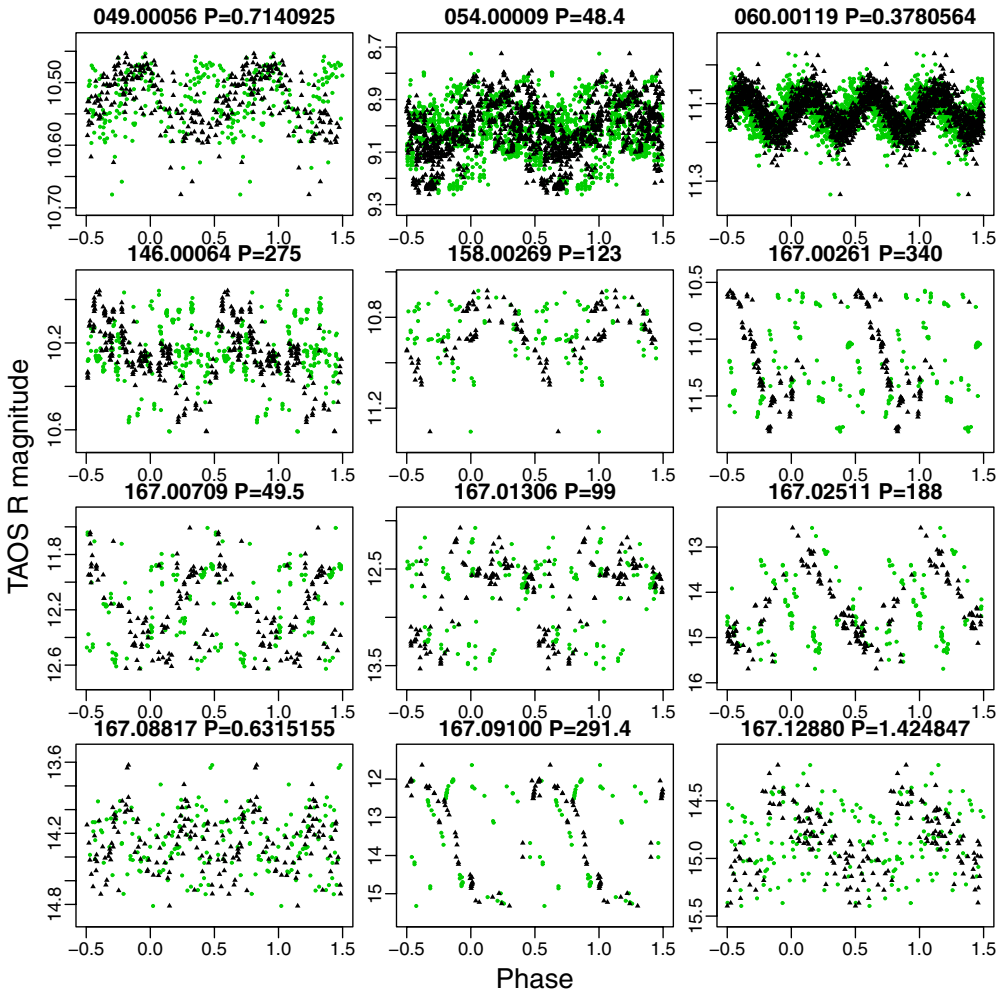


Figure 7. Phase-folded light curves of 12 known variable stars recovered from TAOS data, whose periods by our analysis are different from catalogued ones. Green and black points represent light curves folded by catalogued period and TAOS period, respectively.

(A color version of this figure is available in the online journal.)

Table 5 lists the period derived from TAOS data for the known variables along with catalogued magnitude, period, amplitude and type. Numbers of known variables, known variables selected as candidates, and recovered from our analysis in each field are summarized in Columns 7–9 of Table 4 with detection rates.

A total of 48 known variables are listed in TAOS master catalog of the ten fields with more than 100 epochs of good observations. An additional nine variable stars in the TAOS catalog have no photometric data since they are located at the edge of the fields. Among the 48 stars with enough observation points, we recovered 37 of them. Among the remaining 11 stars, five stars are not identified as candidates. The other six stars are identified as candidates, but we did not detect any strong periodicity in the light curves for these stars.

Figure 5 shows phase-folded light curves of the 11 unrecovered stars. Of the five stars not identified as candidates, TAOS 054.00015, TAOS 054.00064, and TAOS 060.00097 are δ Sct stars with amplitudes between 0.003 and 0.007 mag, which are much smaller than the accuracy of our photometry. TAOS 043.01145 is an RRAB star with brightness close to the detection limit. This object did not meet the criteria to be a candidate variable, because its J -index was calculated for only a single pair of light curves. Its period, however, was recovered by our

period analysis with both methods. TAOS 049.00138 is a flare star; whose phase-folded TAOS light curve with its known period did not show a clear profile.

Among the six stars which were identified as candidates but for which we did not obtain likely periods, TAOS 049.00044 is a δ Sct star with small amplitude of 0.009 mag. TAOS 061.00041 is an ASAS variable with a classification of MISC. Its catalogued period of 1.0 day should be a false periodicity. The other four stars, TAOS 043.00001, TAOS 081.00181, TAOS 095.00047, and TAOS 146.00043, are variables with classifications of MISC or SR and their phase-folded TAOS light curves with known periods did not show clear profiles.

The recovery rate of known variables in the 6 fields with less than 100 epoch good observations is worse than that of the more observed 10 fields due to an insufficient number of data points. Most of the unrecovered variable stars are either semi-regular variable stars with long periods or without period determination, or their brightnesses are close to our detection limit. For a few cases, we could not find the same flux change listed in the catalog. For example, TAOS 005.00009 and 088.00014 are ASAS variable stars with amplitudes of 0.06 and 0.07 mag, respectively. Though the accuracy of our photometry is better than 0.06 mag, the phase-folded light curves with the known periods do not show clear features.

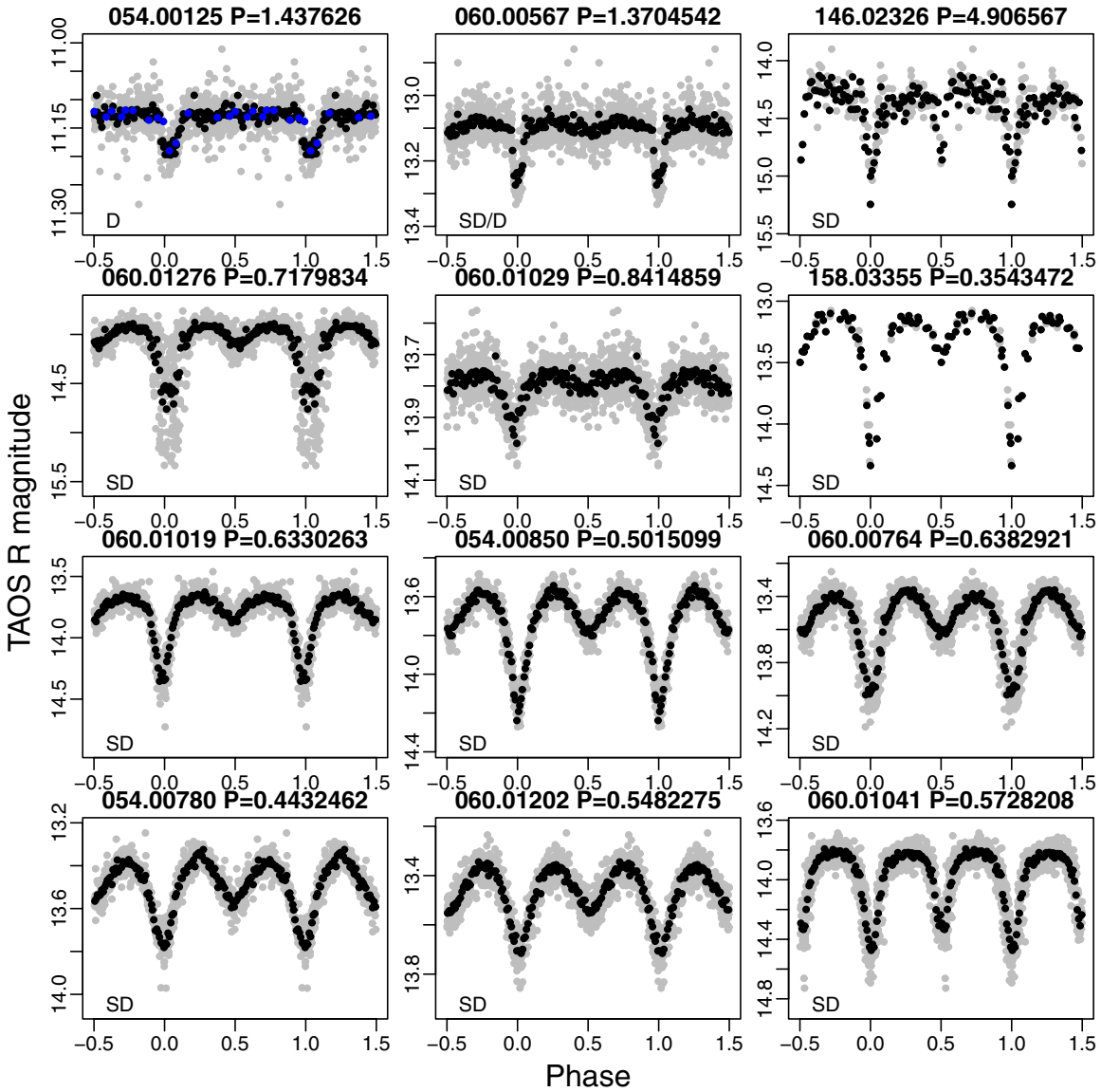


Figure 8. Phase-folded light curves of 12 newly discovered eclipsing variable stars. Gray and black points represent phased and phase-averaged light curves, respectively. Blue points are observations by Tenagra Telescope.
(A color version of this figure is available in the online journal.)

In total, we recovered 85 variable stars from 158 known variables. Among them, we detected uncataloged periods for seven stars (TAOS 060.00798, TAOS 146.00058, TAOS 167.00379, TAOS 167.01577, TAOS 167.02541, TAOS 167.06578, and TAOS 167.08186). TAOS 060.00798 is a flare star with three reported recurrences of flare events within a month by Kim et al. (2009). The other six stars are semi-regulars or long-period variables (LPVs). We obtained more precise periods for 11 stars (TAOS 005.00688, TAOS 049.00078, TAOS 060.00035, TAOS 061.00127, TAOS 099.00090, TAOS 133.00303, TAOS 167.00004, TAOS 167.00149, TAOS 167.00319, TAOS 167.04913, and TAOS 167.05275). We also detected different periods from catalogued ones for 12 stars (TAOS 049.00056, TAOS 054.00009, TAOS 060.00119, TAOS 146.00064, TAOS 158.00269, TAOS 167.00261, TAOS 167.00709, TAOS 167.01306, TAOS 167.02511, TAOS 167.08817, TAOS 167.09100, and TAOS 167.12880). Figures 6 and 7 show the phase-folded light curves of known variable

stars recovered from TAOS data by our analysis with new or improved periods.

3.4. Newly Detected Variables

Among 616 uncataloged candidates in the 16 TAOS fields, we found 55 variable stars with determined periods, and three variable stars without periodicity. The selected candidates which are not variable stars show variable flux mainly because they showed either a 1 day period due to a changing distortion of images related to telescope pointing, or a monthly period due to moon phase. Other candidates did not show significant periods due to insufficient numbers of data points or the phase-folded light curves did not show meaningful profiles. Table 6 lists the detected 58 variable stars with their TAOS IDs, USNO B1.0 catalog IDs, coordinates, R magnitudes, numbers of epochs, periods derived from DFT and PDM methods, amplitudes of variability, and the variable classifications based on the shape of light curves, periods, and amplitudes.

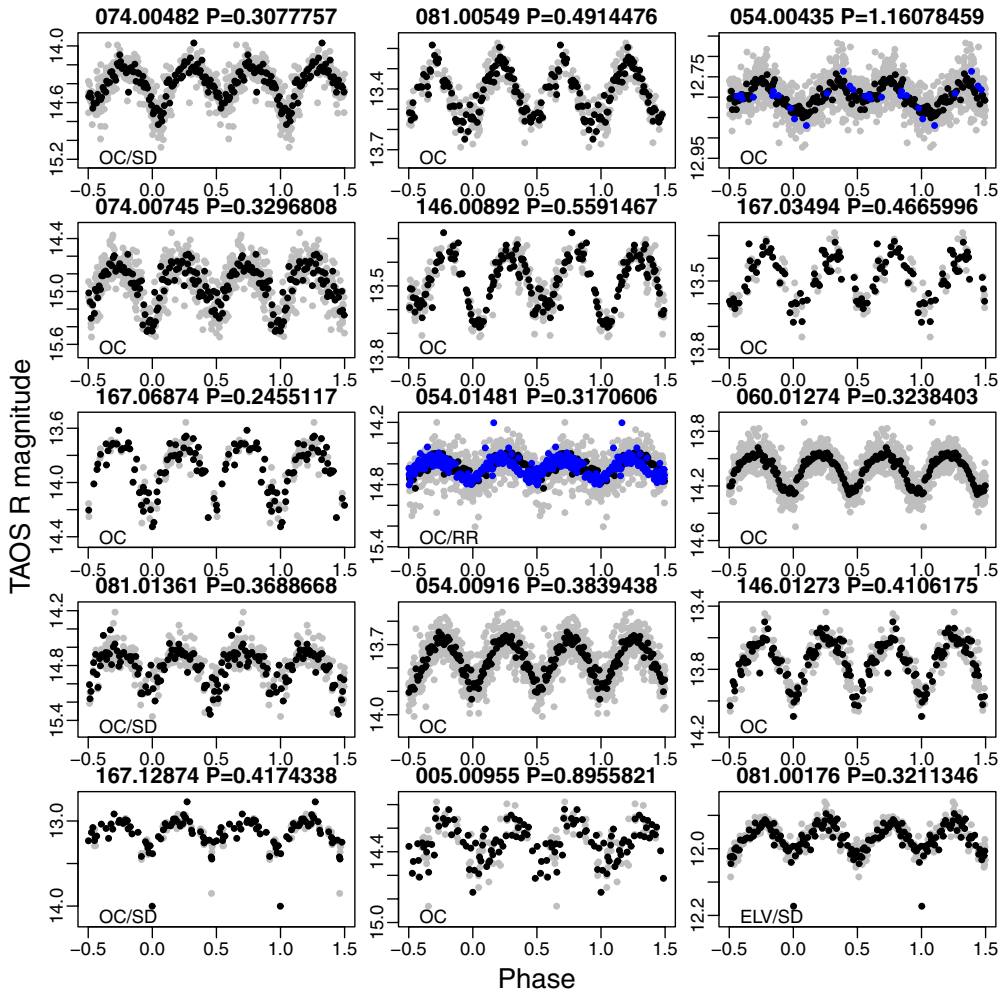


Figure 9. Phase-folded light curves of 15 newly discovered eclipsing variable stars. Gray and black points represent phased and phase-averaged light curves, respectively. Blue points are observations by Tenagra Telescope.

(A color version of this figure is available in the online journal.)

3.4.1. Eclipsing Binaries

The largest group of the uncatalogued variables consists of 27 eclipsing binaries. Among them, only four stars have periods longer than 1 day. Others are systems with periods less than 1 day. We classified one star as a detached binary, 11 stars as semi-detached binaries, 13 stars as overcontact binaries, and one star as an ellipsoidal variable based on their orbital periods and light curve shapes. Detached binaries (D) are traditionally referred to as Algol-type systems, whose light curves are characterized near constant brightness outside of eclipse, and unequal primary and secondary minima. Semi-detached binaries (SD) are represented by Beta Lyrae-type systems (EB), whose light curves are smooth with the primary eclipse much deeper than the secondary minimum. Their periods are usually longer than 0.4 days. W UMa systems are typical representatives of contact binaries (OC), which generally consist of main-sequence stars of nearly the same spectral type, mostly from around middle F to early G. The W UMa systems typically have periods between 0.25 and 1.2 days. Ellipsoidal variations are caused by the significant distortion of stellar surfaces. The phased light curves of the newly detected eclipsing variable stars are shown in Figures 8 and 9. Because of the limitation on the photometry accuracy of TAOS data, the ingress and egress points of the eclipses and out-of-eclipse regions are not pronounced, and

some of stars classified as SD might be OC binaries, and vice versa.

3.4.2. Short- and Intermediate-period Pulsating Stars (δ Sct, RR Lyr, and Cepheid)

We classified 11 stars as short- and intermediate-period pulsating stars with periods shorter than 100 days. Among them, one is a δ Scuti, three are RRab variables, nine are RRc or other short-period pulsating stars (though five of them might be W UMa binaries with twice the periods), and four are possible Cepheids. δ Scuti, RR Lyr, and Cepheids are pulsating stars located in the instability strip of the Hertzsprung–Russell (H–R) diagram. δ Scuti stars are main-sequence or sub-giant stars with spectral types ranging of A2 to F2 in the lower part of the strip. Their period and amplitude ranges are 0.02–0.3 days and 0.0003–0.9 mag. RR Lyr stars are horizontal branch giant stars with spectral types of A–F, and they have period and amplitude ranges of 0.2–1.1 days and 0.2–2 mag. There are three subclasses, RRab, RRc, and RRd. Cepheids are supergiants pulsating with periods between one and 100 days and amplitudes of 0.1–2 mag. Figure 10 shows the phased light curves of the 11 short-period pulsating stars. In some cases, we might classify an overcontact binary to be RR Lyr, or vice versa. Figure 11 shows phased light curves of the 5 variables with dubious classifications.

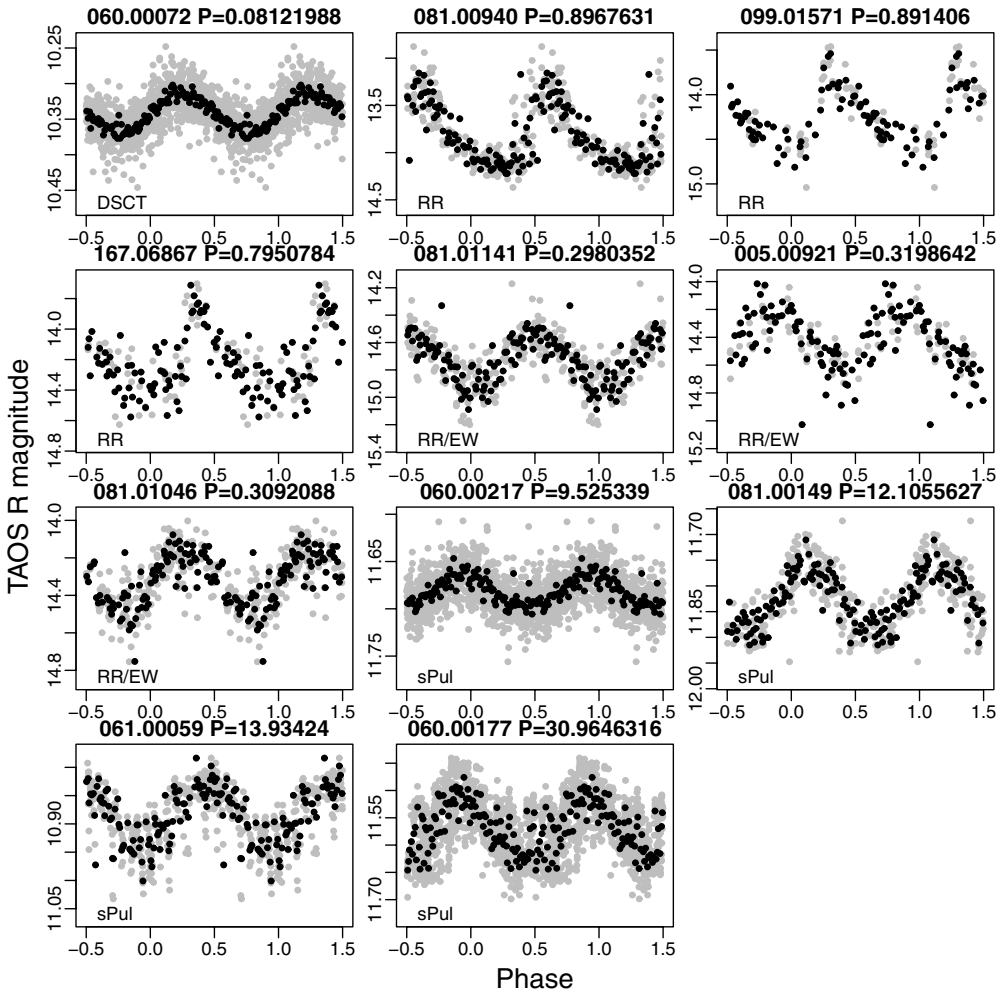


Figure 10. Phase-folded light curves of 11 newly discovered short- and intermediate-period pulsating variable stars. Gray and black points represent phased and phase-averaged light curves, respectively.

3.4.3. Long-period Variables (Mira, SR, and L)

The remaining 20 new variable stars are LPV stars. Among them, five are Mira stars and the others are semi-regular variable stars or stars for which we did not find likely periods. Mira stars are large amplitude variable stars (more than 2 mag) with long periods between 100 and 1000 days. They are located on the asymptotic giant branch of the H-R diagram. Semi-regular variables are red giants or supergiants with long periods that can range from 30 to 1000 days and amplitudes between 0.1 and 2 mag. Figures 12 and 13 show the phased light curves of the 17 long-period pulsating stars and the light curves of three LPVs, respectively.

3.5. Color–Color Diagrams

Figure 14 shows color–color diagrams of known and newly detected TAOS variable stars along with the loci of dwarfs and giants taken from Bessell & Brett (1988) and Johnson (1966) for reference. Optical colors are derived from Tycho $BT-VT$ and SDSS $B-V$ for $B-V$, TychoV – TAOSR and SDSS $V-R$ for $V-R$, and TychoB – TAOSR, GSC $Bj-R$, and SDSS $B-R$ for $B-R$. SDSS BVR are calculated from SDSS $ugri$ using the transformation equations in Lupton (2005). Infrared colors are derived from 2MASS J , H , and K . Blue and red points represent LPVs and short-period pulsating stars, respectively. Green points represent eclipsing binaries. Filled

points are newly detected variable stars, and open points are known objects. The location and classification of each previously uncataloged variable are consistent with those of known variables in the color–color diagram. Locations of LPVs and short-period variables are well separated in the color diagram, while short-period pulsating stars (Cepheid, RR Lyrae, and δ Scuti) and eclipsing binaries are overlapped. Some stars are off the main group due to uncertainty in 2MASS JHK photometry or photometry at different epochs.

3.6. Detection Rates

We divided the 16 fields into three groups depending on the frequency of observations. The most frequently observed fields are Fields 54 and 60 with more than 700 epoch observations. Eight fields are moderately observed with 120–358 epoch observations. The other six fields are with fewer than 100 epoch observations.

As listed in Table 4, the rates of stars selected as candidate variables are almost the same (1.4%–1.5%) for all of the three groups, although the rates of individual fields scatter are between 0.7% and 2.5%. On the other hand, the ratios of the stars identified as variables against the selected candidates decrease from 36% to 13% as the frequency of observations decreases.

The recovery rate of a known variable star for the least observed group is significantly lower than those of the other

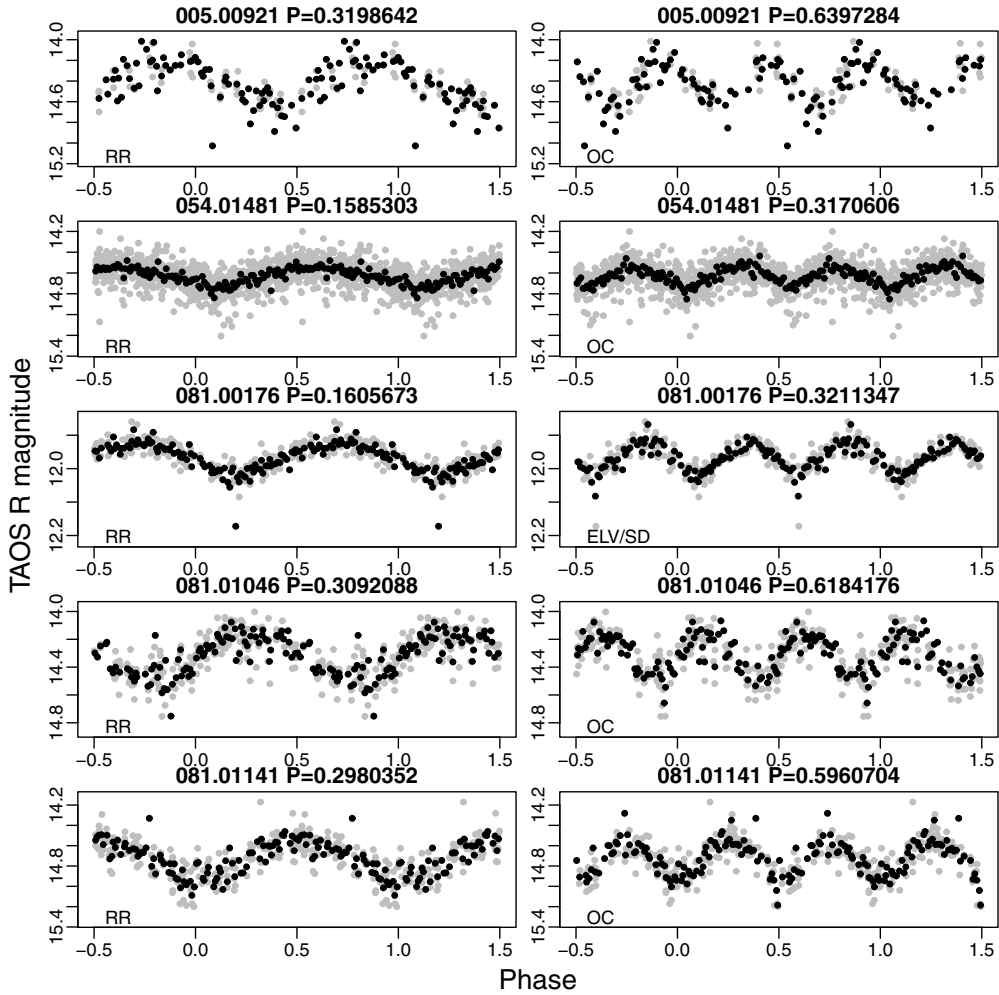


Figure 11. Phase-folded light curves of five variables with dubious classifications. Gray and black points represent phased and phase-averaged light curves, respectively.

groups. There is, however, no significant difference between the recovery rates of known variable stars for the two better observed groups; 70% for fields 54 and 60 and 79% for fields with 120–358 epochs. This is mainly due to the photometric accuracy of the TAOS data. For example, three unrecovered variables in fields 54 and 60 are δ Sct stars with small amplitudes of 0.003–0.007 mag.

The ratio of newly detected variables over the known recovered variables for the most observed group (72%) is significantly higher than others. On the other hands, the ratios for the other two groups are 30% for the group with 120–358 epochs and 36% for the group with less than 100 epochs. They are similar in spite of far fewer observations for the later group. Among 27 newly detected variables in the least observed group, 23 variables are detected in the very crowded fields 158 and 167 located in the galactic plane. This may be due to better spatial resolution of TAOS than ASAS, which is one of the main sources of bright variables.

3.7. Comparison with the ASAS Survey

Among several large-scale surveys of variable stars, the data of ASAS is most similar to the TAOS data. The numbers of observations for stars are distributed between 46 and 1716 with a median value of 221, and the limiting magnitude is about 15 mag. The photometric error of TAOS data is better than that

of ASAS data for stars brighter than 14 mag and comparable for stars fainter than 14 mag.

The ratio of eclipsing binaries among newly discovered variables is 27/58, which is much higher than the ratio of 20/158 for known variables. It is also high in comparison with other surveys. For example, the rate of eclipsing binaries is about 1/5 in ASAS Variable Stars in the Southern Hemisphere (Pojmanski et al. 2006) and 1/4 in GCVS (Samus et al. 2009). The cause of the higher rate in our result is that there were 14 eclipsing binaries among 18 new variables in Fields 54 and 60. The frequent observations for the two fields enabled the detection of narrow eclipses and the distinction between eclipsing binaries and RR or DSCT stars. If we exclude the 18 variables, the ratio of eclipsing binaries becomes 13/54, which is consistent with the ratios of GCVS or ASAS variables. Among 14 new eclipsing binaries in the two fields, 13 stars are fainter than 13 mag, which is close to the detection limit of ASAS variables. Only 4155 stars among 50,122 ASAS variables are fainter than 13 mag.

Eight of the 16 fields analyzed in this paper are relatively close to the galactic plane ($|b| < 30$), and the other eight fields are located at higher galactic latitudes ($|b| > 30$). The ratios of eclipsing binaries, RR Lyrae and δ Sct stars, and LPV stars detected by our analysis at lower and higher latitudes are 29/11, 22/19, and 56/6, respectively. Despite the small size of our sample, they are consistent with the ratios of ASAS variables, which are 7841/3258, 2753/1908, and 19,980/3285,

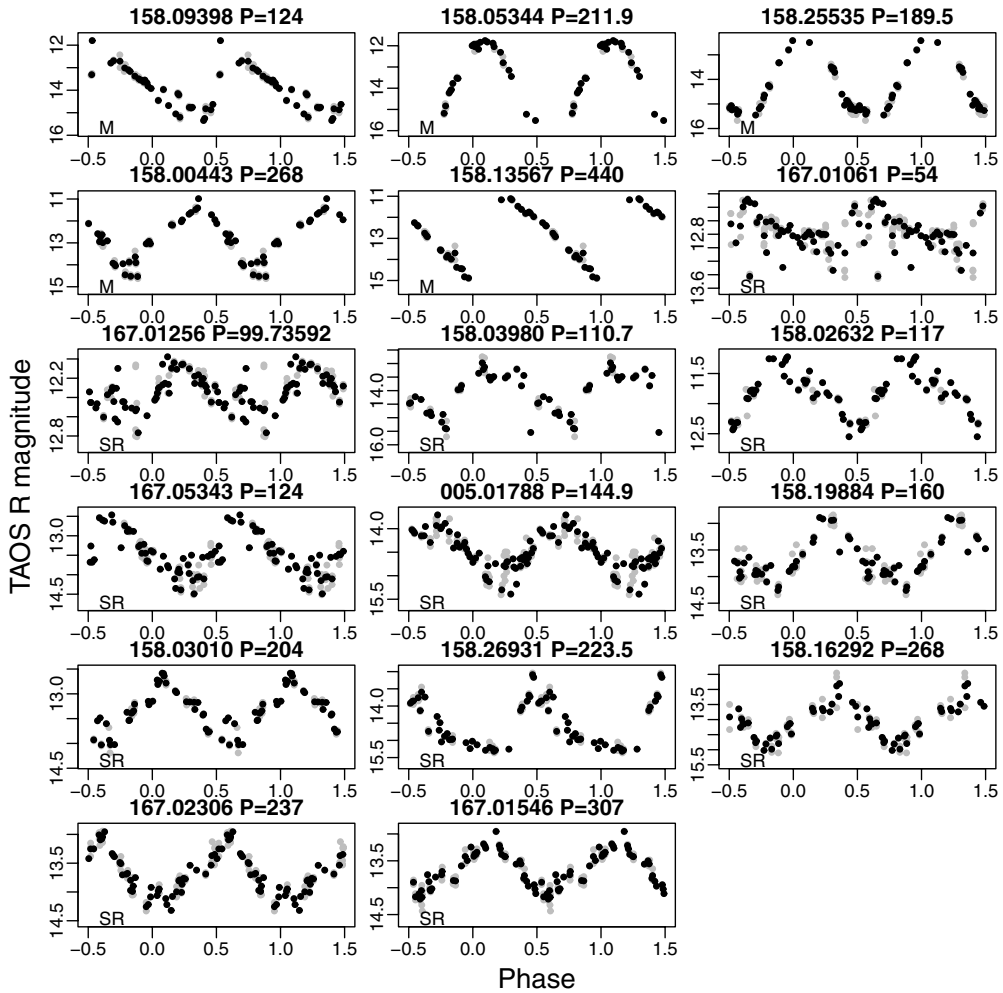


Figure 12. Phase-folded light curves of 17 newly discovered long-period pulsating variable stars. Gray and black points represent phased and phase-averaged light curves, respectively.

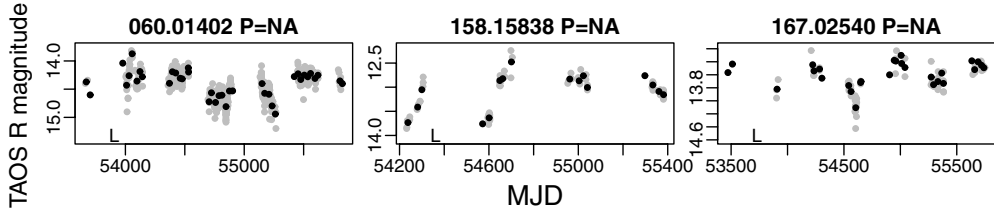


Figure 13. Phase-folded light curves of three LPVs without periods detected. Gray and black points represent phased and phase-averaged light curves, respectively.

respectively. The higher ratio of our LPVs is due to the 12 LPVs detected in Field 158, which is one of the least observed fields. The sparse observation over a long period is the cause of preferentially detection of LPVs.

4. SUMMARY

With 59,114 stars in the 16 TAOS fields, 816 variable star candidates were selected. We detected 58 previously uncataloged variable stars among the candidates. Among the 158 known variable stars in these fields, 133 stars were selected as candidates and 85 of them were recovered by our analysis with determined periods. We determined new or improved periods for 23 of 85 detected known variables. The light curves, periods, amplitudes, and classification, if available, of previously uncataloged variable stars are presented in this paper. About

half of the detected variable stars are eclipsing binaries, and the others are pulsation stars such as Cepheids, RR Lyrae stars, δ Scuti, Mira, semi-regular variables, or other LPVs.

We compared variables detected in TAOS data with variables found by ASAS, which is one of the main sources of bright variables. With better photometry accuracy of TAOS, most of our newly detected variables which are undetected as variables by ASAS are fainter than 13 mag. Because of the better spatial resolution of TAOS than ASAS, we detected 23 new variables in field 158 and 160 which are the most crowded fields among the 16 analyzed fields. Since the fields are two of the least observed fields, LPVs were preferentially detected in these fields. That is the reason for the higher detection ratio of LPVs for lower galactic latitude fields. Excluding these LPVs, our detection ratios of various types and space distributions of variable stars are consistent with those of ASAS variables.

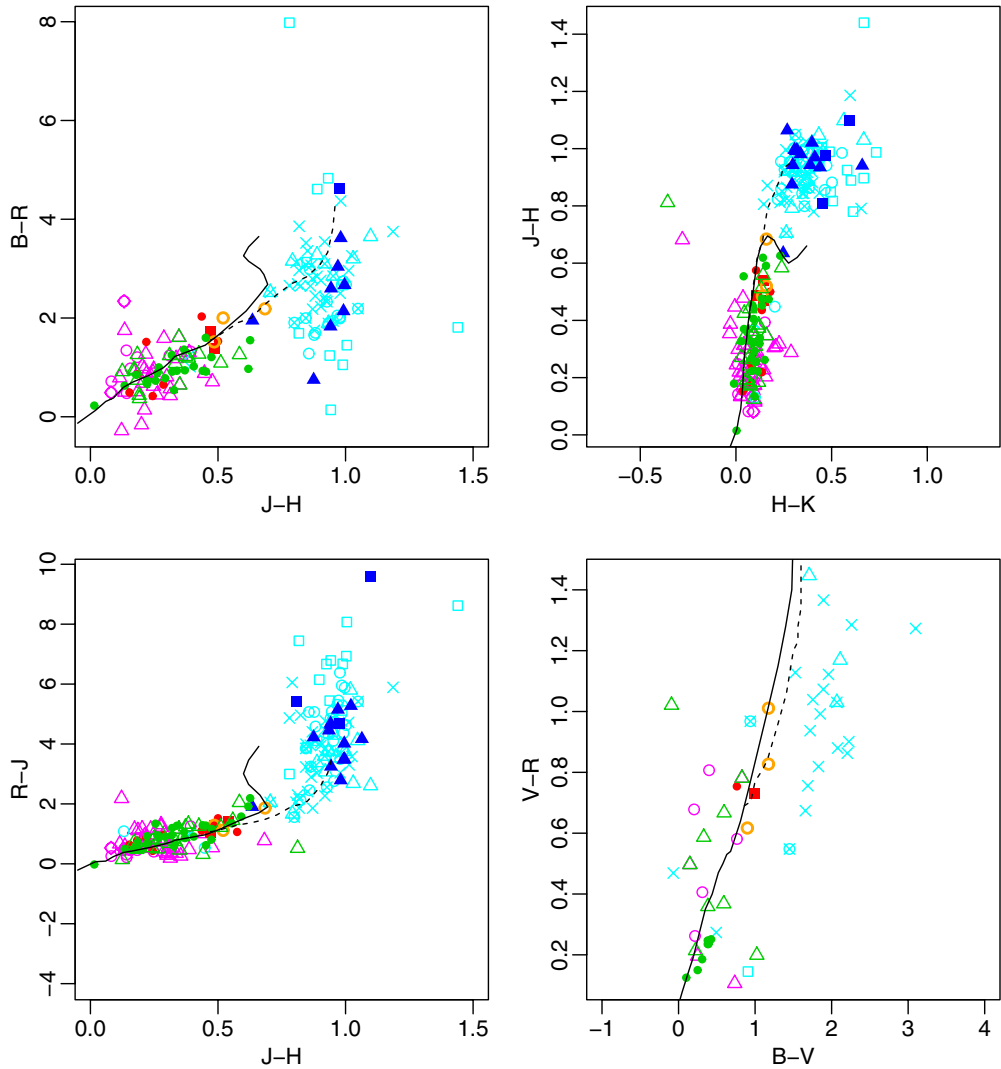


Figure 14. Color-color diagrams of known and recovered variable stars. The loci of dwarfs (solid lines) and giants (dashed lines) are taken from Bessell & Brett (1988) and Johnson (1966). Filled points are newly detected variable stars, and open points are known objects. Blue and red symbols represent long-period variables and short-period pulsating stars, respectively (blue or light blue: circles—SR, triangles—L, squares—M, crosses—MISC; violet: circles—DSCT, triangle—RR, diamonds—CEP; red: points—RR or DTSC, squares—short-period pulsating stars). Green and orange symbols represent eclipsing binaries and RS CVn stars.

(A color version of this figure is available in the online journal.)

Table 7
TAOS Photometry Catalog

TAOS ID	MJD	Median (mag)	TAOS A (mag)	TAOS B (mag)	TAOS C (mag)	TAOS D (mag)	σ_A (mag)	σ_B (mag)	σ_C (mag)	σ_D (mag)
TAOS005.00396	54625.8166956	12.7515	12.752	12.782		12.726	0.033	0.022		0.029
TAOS005.00396	54626.7904381	12.8592	12.835	12.884			0.025	0.016		
TAOS005.00396	54636.7718667	12.8507	12.848			12.853	0.026			0.018
TAOS005.00396	54647.7365192	13.0180	13.046	13.018		12.975	0.019	0.029		0.024
TAOS005.00396	54647.7993311	12.8780	12.915	12.878		12.857	0.030	0.021		0.015

(This table is available in its entirety in machine-readable and Virtual Observatory (VO) forms in the online journal. A portion is shown here for guidance regarding its form and content.)

We will begin a program to monitor the TAOS fields which have not been observed frequently enough to find variable stars, using a few minutes between the last run and twilight on each night. As mentioned above, many variables fainter than 13 mag are likely undetected by ASAS. The TAOS monitoring program will obtain useful data to detect more new variable stars, as well as for the known, though not well-observed, variable stars in

these fields. In addition, we will soon analyze the 7 yr of zipper-mode data in order to search for stellar variability on timescales faster than 90 minutes, such as δ Scuti stars (Kim et al. 2010) and flare stars.

The work at National Central University was supported by the grant NSC 96-2112-M-008-024-MY3. C.C.N. thanks a separate

NSC grant 101-2112-M-008-017-MY3. Y.I.B. acknowledges the support of the National Research Foundation of Korea through grant 2009-0075376. Work at Academia Sinica was supported in part by the thematic research program AS-88-TP-A02. Work at the Harvard College Observatory was supported in part by the National Science Foundation under grant AST-0501681 and by NASA under the auspices of the U.S. Department of Energy by Lawrence Livermore National Laboratory in part under Contract W-7405-Eng-48 and by Stanford Linear Accelerator Center under Contract DE-AC02-76SF00515. Part of this work is supported by a Research Fellowship of the Japan Society for the Promotion of Science for Young Scientists. This research has made use of the International Variable Star Index (VSX) database, operated at AAVSO, Cambridge, Massachusetts, USA, and the SIMBAD database and the VizieR catalog access tool, operated at CDS, Strasbourg, France. We thank the anonymous referee for many comments that improved this paper.

APPENDIX

THE DATA OF VARIABLE STARS

The TAOS photometry of variable stars listed in Tables 5 and 6 is presented in Table 7, available online.

REFERENCES

- Akerlof, C., Amrose, S., Balsano, R., et al. 2000, *AJ*, **119**, 1901
 Alcock, C., Allsman, R. A., Alves, D. R., et al. 1998, *AJ*, **115**, 1921
 Alcock, C., Allsman, R. A., Axelrod, T. S., et al. 1995, *AJ*, **109**, 1653
 Alcock, C., Dave, R., Giannarco, J., et al. 2003, *EM&P*, **92**, 459
 Bessell, M. S., & Brett, J. M. 1988, *PASP*, **100**, 1134
 Cieslinski, D., Diaz, M. P., Mennickent, R. E., & Pietrzynski, G. 2003, *PASP*, **115**, 193
 Deeming, T. J. 1975, *Ap&SS*, **36**, 137
 Drake, A. J., Djorgovski, S. G., Mahabal, A., et al. 2009, *ApJ*, **696**, 870
 Johnson, H. L. 1966, *ARA&A*, **4**, 193
 Kaiser, N., Burgett, W., Chambers, K., et al. 2010, *Proc. SPIE*, **7733**, 77330E
 Kholopov, P. N., Samus, N. N., Frolov, M. S., et al. 1998, Combined General Catalogue of Variable Stars, GCVS, SIMBAD (Moscow: Sternberg Astron. Inst.)
 Kim, D.-W., Protopapas, P., Alcock, C., et al. 2009, ATel, **2035**, 1
 Kim, D.-W., Protopapas, P., Alcock, C., et al. 2010, *AJ*, **139**, 757
 Kukarkin, B. V., & Kholopov, P. N. 1982, New Catalogue of Suspected Variable Stars (Moscow: Nauka)
 Lehner, M. J., Wen, C.-Y., Wang, J.-H., et al. 2009, *PASP*, **121**, 138
 Lupton, R. 2005, in Transformations between SDSS magnitudes and UBVR_cI_c, <http://www.sdss2.org/dr5/algorithms/sdssUBVRITransform.html#Lupton2005>
 Mondal, S., Lin, C. C., Chen, W. P., et al. 2010, *AJ*, **139**, 2026
 Ngeow, C. C., Chang, D., Pan, K., et al. 2010, *BAAS*, **41**, 839
 Pojmanski, G., Maciejewski, G., Pilecki, B., & Szczegiel, D. 2006, *yCat*, **2264**, 0
 Pojmanski, G., Pilecki, B., & Szczegiel, D. 2005, *AcA*, **55**, 275
 Samus, N. N., Durlevich, O. V., et al. 2009, *yCat*, 102025, 0
 Sesar, B., Ivezić, Z., Lupton, R. H., et al. 2007, *AJ*, **134**, 2236
 Stellingwerf, R. F. 1978, *ApJ*, **224**, 953
 Stetson, P. B. 1969, *PASP*, **108**, 851
 Welch, D. L., & Stetson, P. B. 1993, *AJ*, **105**, 1813
 Woźniak, P. R., Udalski, A., Szymanski, M., et al. 2002, *AcA*, **52**, 129
 Woźniak, P. R., Vestrand, W. T., Akerlof, C. W., et al. 2004, *AJ*, **127**, 2436
 Wray, J. J., Eyer, L., & Paczyński, B. 2004, *MNRAS*, **349**, 1059
 Yeşilyaprak, C., Yerli, S. K., Güçsav, B. B., et al. 2012, *NewA*, **17**, 504
 Zhang, Z.-W., Kim, D.-W., Wang, J.-H., et al. 2009, *PASP*, **121**, 1429
 Zhang, Z.-W., Lehner, M. J., Wang, J.-H., et al. 2013, *AJ*, **146**, 14

SYNCHROTRON SELF-VERSE COMPTON RADIATION FROM REVERSE SHOCK ON GRB 120326A

YUJI URATA¹, KUIYUN HUANG^{2,3}, SATOKO TAKAHASHI^{2,4,5}, MYUNGSHIN IM⁶, KAZUTAKA YAMAOKA^{7,8},
MAKOTO TASHIRO⁹, JAE-WOO KIM⁶, MINSUNG JANG⁶, AND SOOJONG PAK¹⁰

¹ Institute of Astronomy, National Central University, Chung-Li 32054, Taiwan; urata@astro.ncu.edu.tw

² Academia Sinica Institute of Astronomy and Astrophysics, Taipei 106, Taiwan

³ Department of Mathematics and Science, National Taiwan Normal University, Lin-kou District, New Taipei City 24449, Taiwan

⁴ Joint ALMA Observatory, Alonso de Cordova 3108, Vitacura, Santiago, Chile

⁵ National Astronomical Observatory of Japan, 2-21-1 Osawa, Mitaka, Tokyo 181-8588, Japan

⁶ Center for the Exploration of the Origin of the Universe, Department of Physics and Astronomy, FPRD, Seoul National University, Shillim-dong, San 56-1, Kwanak-gu, Seoul, Korea

⁷ Solar-Terrestrial Environment Laboratory, Nagoya University, Furo-cho, Chikusa-ku, Nagoya, Aichi 464-8601, Japan

⁸ Division of Particle and Astrophysical Science, Graduate School of Science, Nagoya University, Furo-cho, Chikusa-ku, Nagoya, Aichi 464-8601, Japan

⁹ Department of Physics, Saitama University, Shimo-Okubo, Saitama 338-8570, Japan

¹⁰ School of Space Research, Kyung Hee University, Yongin, Gyeonggi 446-701, Korea

Received 2013 November 27; accepted 2014 May 14; published 2014 June 24

ABSTRACT

We present multi-wavelength observations of a typical long duration GRB 120326A at $z = 1.798$, including rapid observations using a Submillimeter Array (SMA) and a comprehensive monitoring in the X-ray and optical. The SMA observation provided the fastest detection to date among seven submillimeter afterglows at 230 GHz. The prompt spectral analysis, using *Swift* and *Suzaku*, yielded a spectral peak energy of $E_{\text{peak}}^{\text{src}} = 107.8^{+15.3}_{-15.3}$ keV and an equivalent isotropic energy of E_{iso} as $3.18^{+0.40}_{-0.32} \times 10^{52}$ erg. The temporal evolution and spectral properties in the optical were consistent with the standard forward shock synchrotron with jet collimation (6.69 ± 0.16). The forward shock modeling, using a two-dimensional relativistic hydrodynamic jet simulation, was also determined by the reasonable burst explosion and the synchrotron radiation parameters for the optical afterglow. The X-ray light curve showed no apparent jet break and the temporal decay index relation between the X-ray and optical ($\alpha_o - \alpha_X = -1.45 \pm 0.10$) indicated different radiation processes in each of them. Introducing synchrotron self-inverse Compton radiation from reverse shock is a possible solution, and the detection and slow decay of the afterglow in submillimeter supports that this is a plausible idea. The observed temporal evolution and spectral properties, as well as forward shock modeling parameters, enabled us to determine reasonable functions to describe the afterglow properties. Because half of the events share similar properties in the X-ray and optical as the current event, GRB 120326A will be a benchmark with further rapid follow-ups, using submillimeter instruments such as an SMA and the Atacama Large Millimeter/submillimeter Array.

Key words: gamma-ray burst: individual (120326a) – radiation mechanisms: non-thermal

Online-only material: color figures

1. INTRODUCTION

Gamma-ray bursts (GRBs) are among the most powerful explosions in the universe and are observationally characterized by intense short flashes primarily in a high-energy band (so-called prompt emission) and long-lived afterglows observed from X-ray to radio wavelengths. The GRB afterglow is believed to involve a relativistically expanding fireball (e.g., Meszaros & Rees 1997). Interstellar matter (ISM) influences the fireball shell after it has been collected and considerable energy is transferred from the shell to the ISM. The energy transfer is caused by two shocks: a forward shock propagating into the ISM and a reverse shock propagating into the shell. It is also believed that the forward shock produces long-lived afterglows and the reverse shock generates short-lived bright optical flashes (e.g., Akerlof et al. 1999) and/or intense radio afterglows (e.g., Kulkarni et al. 1999).

A number of afterglows have been densely monitored in X-ray and optical bands since the launch of the *Swift* satellite (Gehrels et al. 2004), and a significant number of afterglows showed the different temporal evolutions in X-ray and optical bands. These results indicated that the simple forward shock model cannot explain their behavior altogether and additional processes are required (e.g., Panaiteescu et al. 2006; Huang et al. 2007; Urata et al. 2007; Li et al. 2012).

Inverse Compton scattering and/or reverse shocks may play an important role in solving the problem. Panaiteescu & Vestrand (2011) suggested local inverse Compton scattering to describe the X-ray band's faster decay compared with that of the optical. Kobayashi et al. (2007) introduced a synchrotron self-inverse Compton radiation from a reverse shock to explain the X-ray flare and its early afterglows. Thus, confirming the existence of reverse shocks at particularly longer wavelengths and ascertaining their typical occurrence conditions is critical. Because the expected lifetime of reverse shocks at longer wavelengths is substantially longer than the lifetime of those at optical wavelengths, decoding radiations into forward and reverse shock components is possible. In addition, numerous rapid optical follow-ups are missing the reverse shock components; however, several successful detections at optical wavelengths have been made.

The possible reason for the missing reverse shock component could be that the typical reverse shock synchrotron frequency is far below the optical band. Submillimeter observations are the key elements used to catch reverse shock and to understand the emission mechanism of GRB afterglows. Searching for reverse shock emission in the submillimeter wavelength would test this possibility. These submillimeter observations also provide clean measurements of source intensity, unaffected

by scintillation and extinction. However, no systematic submillimeter observational studies in the early afterglow phase exist. This has remained the case in reverse shock studies for some time. One of the main reasons for this is the absence of dedicated submillimeter telescopes and strategic follow-ups with rapid response which involve employing open-use telescopes for these challenging observations. In addition, it is nearly impossible to have rapid (several hours after the burst) follow-ups with current open-use telescopes which require manual preparation of the observational scripts. In addition to this technical problem, the sensitivities of current submillimeter telescopes, except for the Atacama Large Millimeter/submillimeter Array (ALMA), are not good enough to detect the number of afterglows in the submillimeter band (e.g., de Ugarte Postigo et al. 2012). Hence, rapid careful target selections are required to conduct effective submillimeter follow-up observations using open-use resources.

GRB 120326A was detected and localized using *Swift* (Siegel et al. 2012). The *Suzaku*/Wide-band All-Sky Monitor (*Suzaku*/WAM) and the *Fermi* Gamma-ray Burst Monitor (*Fermi*/GBM) also detected this burst, and quick-look spectral analyses were reported (Iwakiri et al. 2012; Collazzi 2012). The optical afterglow was discovered by Klotz et al. (2012) and observed at the early stage by using several telescopes. The optical afterglow also exhibited remarkable rebrightening (Walker et al. 2012). The afterglow at submillimeter and radio bands was also detected using an Submillimeter Array (SMA; Urata et al. 2012), the Combined Array for Research in Millimeter-wave Astronomy (Perley et al. 2012), and the Expanded Very Large Array (Laskar et al. 2012). The SMA observation provided the fastest afterglow detection (about 4.6×10^4 s after the burst) among seven submillimeter afterglows at 230 GHz, which are mostly detected about 1×10^5 s (~ 1 day) after the bursts. Although numerous follow-ups in various wavelengths have been conducted, submillimeter afterglow monitoring from the earlier phase ($< 1 \times 10^5$ s) is still rare and essential to understand the puzzle of afterglow radiation. The redshift was determined to be $z = 1.798$, according to a series of metal absorption features (Tello et al. 2012). We used $f(t, v) \propto t^\alpha v^\beta$ to express the afterglow properties.

2. OBSERVATIONS

The *Swift* Burst Alert Telescope (*Swift*/BAT) triggered and located GRB 120326A at 01:20:29 (T_0) UT on 2012 March 26. *Swift* immediately slewed to the burst and the X-Ray Telescope (XRT) initiated follow-up observations at 59.5 s after the burst. The X-ray afterglow was identified and localized at R.A. = $18^{\text{h}}15^{\text{m}}36\overset{\text{s}}{.}47$, decl. = $+69^{\circ}15'37\overset{\text{s}}{.}0$, with an uncertainty of $4''.1$. The X-ray afterglow was observed using the XRT until $\sim 5 \times 10^5$ s. UVOT also obtained images by using the White filter starting 67 s after the burst and no counterpart in the band was observed.

The *Suzaku*/WAM also triggered the burst at 01:20:31.9 ($T_0 + 2.9$ s) UT on 2012 March 26. The WAM (Yamaoka et al. 2009) is a lateral shield of the Hard X-ray Detector (Takahashi et al. 2007) on board the *Suzaku* satellite (Mitsuda et al. 2007) and is a powerful GRB spectrometer covering an energy range of 50–5000 keV to determine prompt spectral energy peaks, E_{peak} (e.g., Ohno et al. 2008; Tashiro et al. 2007; Urata et al. 2009). As shown in Figure 1, the prompt X-ray and γ -ray light curves observed using the *Swift*/BAT and *Suzaku*/WAM exhibited a single fast rise and exponential decay structure.

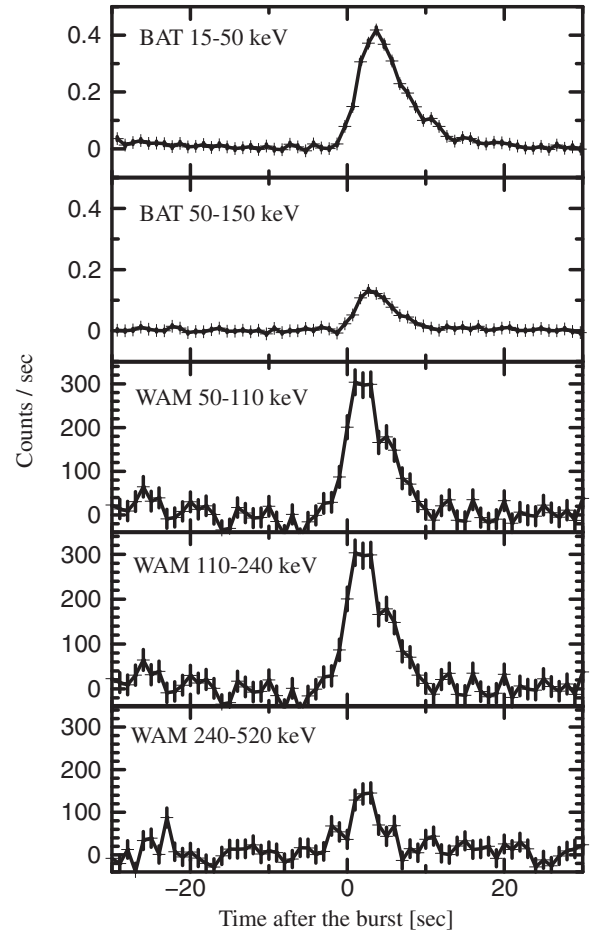


Figure 1. Prompt γ -ray light curves observed by *Swift*/BAT and *Suzaku*/WAM. The trigger time of *Swift*/BAT is used as T_0 .

We performed the optical afterglow observations using the Lulin 1 m telescope (LOT; Huang et al. 2005) and the LOAO robotic 1 m telescope (Han et al. 2005; Lee et al. 2010) within the framework of the EAON (Urata et al. 2003). Four color observations were made with LOT on the night of March 26. The LOAO data were obtained in the *R*-band filter from 2013 March 26 to April 2. The afterglow was also observed with Camera for Quasars in the Early Universe (Park et al. 2012; Kim et al. 2011; Lim et al. 2013) on the 2.1 m Otto-Struve Telescope of the McDonald observatory, Texas, USA. The data were obtained in *g*, *r*, *i*, *z*, and *Y* filters, starting at 2013 March 26, 10:09:22 (UT) and continued until April 2. The logs for both observations are summarized in Table 1.

We also triggered the submillimeter continuum follow-up observations by using the seven 6 m antennas of SMA (Ho et al. 2004). The first continuum observation at 230 GHz (with an 8 GHz bandwidth) was conducted at 10:15:05 on 2012 March 26, about 4.6×10^4 s after the BAT trigger. As Urata et al. (2012) reported, the submillimeter counterpart was observed at the location of the X-ray and optical afterglow. The continuous monitoring using the SMA was also performed at the same frequency setting on March 27, 29, 31, and April 6 and 11. Table 2 summarizes the scientific observations that were conducted for four nights, because of weather conditions and antenna reconfiguration. Figure 2 shows submillimeter light curves of all the GRB afterglows detected at the 230 GHz to date. Among all seven events, we successfully detected the earliest submillimeter afterglow on GRB 120326A. A possible

Table 1
Log of Optical Observations

Instruments	$T-T_0$ (s)	Filter	Exposure (s)	Flux Density (mJy)
CQUEAN	35818	<i>g</i>	120	$(5.031 \pm 1.114) \times 10^{-2}$
CQUEAN	36428	<i>g</i>	120	$(5.843 \pm 0.364) \times 10^{-2}$
LOT	62495	<i>g</i>	300	$(2.751 \pm 0.130) \times 10^{-2}$
LOT	66550	<i>g</i>	300	$(2.781 \pm 0.132) \times 10^{-2}$
CQUEAN	118878	<i>g</i>	120	$(1.549 \pm 0.072) \times 10^{-2}$
CQUEAN	203667	<i>g</i>	120	$(9.670 \pm 1.290) \times 10^{-3}$
CQUEAN	203788	<i>g</i>	120	$(7.200 \pm 1.310) \times 10^{-3}$
CQUEAN	203909	<i>g</i>	120	$(9.820 \pm 1.150) \times 10^{-3}$
CQUEAN	210775	<i>g</i>	120	$(8.840 \pm 2.050) \times 10^{-3}$
CQUEAN	210896	<i>g</i>	120	$(9.580 \pm 2.540) \times 10^{-3}$
CQUEAN	211018	<i>g</i>	120	$(1.460 \pm 0.271) \times 10^{-2}$
CQUEAN	291923	<i>g</i>	120×5	$(5.800 \pm 1.330) \times 10^{-3}$
CQUEAN	382503	<i>g</i>	300×3	$(2.600 \pm 0.320) \times 10^{-3}$
CQUEAN	468068	<i>g</i>	300×3	$(1.550 \pm 0.420) \times 10^{-3}$
LOAO	119527	<i>R</i>	300	$(7.517 \pm 0.848) \times 10^{-2}$
LOAO	119845	<i>R</i>	300	$(6.792 \pm 0.654) \times 10^{-2}$
LOAO	120163	<i>R</i>	300	$(8.395 \pm 0.596) \times 10^{-2}$
LOAO	120532	<i>R</i>	300	$(1.019 \pm 0.055) \times 10^{-1}$
LOAO	120882	<i>R</i>	300	$(1.096 \pm 0.059) \times 10^{-1}$
LOAO	121197	<i>R</i>	300	$(8.395 \pm 0.596) \times 10^{-2}$
LOAO	206539	<i>R</i>	300	$(4.787 \pm 0.579) \times 10^{-2}$
LOAO	206865	<i>R</i>	300	$(4.365 \pm 0.633) \times 10^{-2}$
LOAO	207181	<i>R</i>	300	$(5.105 \pm 0.740) \times 10^{-2}$
LOAO	207498	<i>R</i>	300	$(3.565 \pm 0.373) \times 10^{-2}$
LOAO	301087	<i>R</i>	900	$(2.148 \pm 0.242) \times 10^{-2}$
LOAO	300315	<i>R</i>	900	$(2.128 \pm 0.275) \times 10^{-2}$
LOAO	303167	<i>R</i>	1200	$(2.884 \pm 0.349) \times 10^{-2}$
LOAO	589749	<i>R</i>	2700	$(5.750 \pm 0.880) \times 10^{-3}$
CQUEAN	31732	<i>r</i>	300	$(1.734 \pm 0.022) \times 10^{-1}$
CQUEAN	33129	<i>r</i>	300	$(1.636 \pm 0.008) \times 10^{-1}$
CQUEAN	34399	<i>r</i>	300	$(1.510 \pm 0.027) \times 10^{-1}$
CQUEAN	36739	<i>r</i>	300	$(1.478 \pm 0.010) \times 10^{-1}$
LOT	63503	<i>r</i>	300	$(8.434 \pm 0.177) \times 10^{-2}$
LOT	67564	<i>r</i>	300	$(8.591 \pm 0.165) \times 10^{-2}$
CQUEAN	117385	<i>r</i>	300	$(4.955 \pm 0.036) \times 10^{-2}$
CQUEAN	202218	<i>r</i>	120	$(1.812 \pm 0.207) \times 10^{-2}$
CQUEAN	202340	<i>r</i>	120	$(2.526 \pm 0.175) \times 10^{-2}$
CQUEAN	202461	<i>r</i>	120	$(2.544 \pm 0.141) \times 10^{-2}$
CQUEAN	209219	<i>r</i>	120	$(2.586 \pm 0.236) \times 10^{-2}$
CQUEAN	209633	<i>r</i>	120	$(2.720 \pm 0.116) \times 10^{-2}$
CQUEAN	209754	<i>r</i>	120	$(2.496 \pm 0.119) \times 10^{-2}$
CQUEAN	286528	<i>r</i>	120	$(1.715 \pm 0.075) \times 10^{-2}$
CQUEAN	286650	<i>r</i>	120	$(1.712 \pm 0.067) \times 10^{-2}$
CQUEAN	286771	<i>r</i>	120	$(1.603 \pm 0.065) \times 10^{-2}$
CQUEAN	295768	<i>r</i>	120	$(2.072 \pm 0.291) \times 10^{-2}$
CQUEAN	381506	<i>r</i>	180	$(8.050 \pm 0.380) \times 10^{-3}$
CQUEAN	381688	<i>r</i>	180	$(7.040 \pm 0.390) \times 10^{-3}$
CQUEAN	381869	<i>r</i>	180	$(8.500 \pm 0.380) \times 10^{-3}$
CQUEAN	466726	<i>r</i>	300	$(5.300 \pm 0.710) \times 10^{-3}$
CQUEAN	467028	<i>r</i>	300	$(3.770 \pm 0.670) \times 10^{-3}$
CQUEAN	467329	<i>r</i>	300	$(4.860 \pm 0.550) \times 10^{-3}$
CQUEAN	552707	<i>r</i>	300	$(2.890 \pm 0.270) \times 10^{-3}$
CQUEAN	553009	<i>r</i>	300	$(2.930 \pm 0.290) \times 10^{-3}$
CQUEAN	553310	<i>r</i>	300	$(3.070 \pm 0.300) \times 10^{-3}$
CQUEAN	639867	<i>r</i>	300×6	$(1.970 \pm 0.300) \times 10^{-3}$
CQUEAN	32074	<i>i</i>	300	$(3.621 \pm 0.010) \times 10^{-1}$
CQUEAN	33448	<i>i</i>	300	$(3.701 \pm 0.005) \times 10^{-1}$
CQUEAN	34711	<i>i</i>	300	$(3.803 \pm 0.023) \times 10^{-1}$
CQUEAN	37050	<i>i</i>	300	$(3.311 \pm 0.039) \times 10^{-1}$
LOT	68583	<i>i</i>	300	$(1.964 \pm 0.028) \times 10^{-1}$
LOT	64510	<i>i</i>	300	$(1.982 \pm 0.021) \times 10^{-1}$
CQUEAN	117705	<i>i</i>	300	$(1.257 \pm 0.003) \times 10^{-1}$
CQUEAN	202624	<i>i</i>	120	$(6.634 \pm 0.084) \times 10^{-2}$
CQUEAN	202746	<i>i</i>	120	$(6.164 \pm 0.082) \times 10^{-2}$
CQUEAN	202867	<i>i</i>	120	$(7.226 \pm 0.084) \times 10^{-2}$

Table 1
(Continued)

Instruments	$T-T_0$ (s)	Filter	Exposure (s)	Flux Density (mJy)
CQUEAN	209979	<i>i</i>	120	$(5.834 \pm 0.089) \times 10^{-2}$
CQUEAN	210100	<i>i</i>	120	$(6.346 \pm 0.102) \times 10^{-2}$
CQUEAN	210222	<i>i</i>	120	$(6.188 \pm 0.103) \times 10^{-2}$
CQUEAN	286927	<i>i</i>	120	$(4.194 \pm 0.069) \times 10^{-2}$
CQUEAN	287048	<i>i</i>	120	$(4.292 \pm 0.099) \times 10^{-2}$
CQUEAN	287169	<i>i</i>	120	$(4.360 \pm 0.071) \times 10^{-2}$
CQUEAN	287313	<i>i</i>	120	$(4.186 \pm 0.063) \times 10^{-2}$
CQUEAN	295903	<i>i</i>	120	$(4.150 \pm 0.235) \times 10^{-2}$
CQUEAN	296025	<i>i</i>	120	$(5.662 \pm 0.943) \times 10^{-2}$
CQUEAN	380844	<i>i</i>	180	$(2.118 \pm 0.036) \times 10^{-2}$
CQUEAN	381025	<i>i</i>	180	$(2.092 \pm 0.038) \times 10^{-2}$
CQUEAN	381206	<i>i</i>	180	$(2.278 \pm 0.036) \times 10^{-2}$
CQUEAN	465783	<i>i</i>	300	$(1.256 \pm 0.056) \times 10^{-2}$
CQUEAN	466084	<i>i</i>	300	$(1.178 \pm 0.060) \times 10^{-2}$
CQUEAN	466386	<i>i</i>	300	$(1.390 \pm 0.057) \times 10^{-2}$
CQUEAN	648922	<i>i</i>	300×6	$(4.880 \pm 0.290) \times 10^{-3}$
CQUEAN	32416	<i>z</i>	300	$(9.325 \pm 0.016) \times 10^{-1}$
CQUEAN	33766	<i>z</i>	300	$(9.250 \pm 0.021) \times 10^{-1}$
CQUEAN	35023	<i>z</i>	300	$(9.018 \pm 0.073) \times 10^{-1}$
LOT	65534	<i>z</i>	300	$(5.278 \pm 0.088) \times 10^{-1}$
LOT	69604	<i>z</i>	300	$(4.358 \pm 0.085) \times 10^{-1}$
CQUEAN	118015	<i>z</i>	300	$(3.025 \pm 0.006) \times 10^{-1}$
CQUEAN	203042	<i>z</i>	120	$(1.639 \pm 0.020) \times 10^{-1}$
CQUEAN	203163	<i>z</i>	120	$(1.970 \pm 0.032) \times 10^{-1}$
CQUEAN	203285	<i>z</i>	120	$(1.660 \pm 0.024) \times 10^{-1}$
CQUEAN	210347	<i>z</i>	120	$(1.744 \pm 0.018) \times 10^{-1}$
CQUEAN	210468	<i>z</i>	120	$(1.650 \pm 0.018) \times 10^{-1}$
CQUEAN	210589	<i>z</i>	120	$(1.744 \pm 0.019) \times 10^{-1}$
CQUEAN	287478	<i>z</i>	120	$(1.113 \pm 0.017) \times 10^{-1}$
CQUEAN	287600	<i>z</i>	120	$(1.112 \pm 0.017) \times 10^{-1}$
CQUEAN	287721	<i>z</i>	120	$(1.147 \pm 0.016) \times 10^{-1}$
CQUEAN	380256	<i>z</i>	120	$(5.236 \pm 0.079) \times 10^{-2}$
CQUEAN	380438	<i>z</i>	120	$(5.696 \pm 0.083) \times 10^{-2}$
CQUEAN	380619	<i>z</i>	120	$(5.524 \pm 0.078) \times 10^{-2}$
CQUEAN	464838	<i>z</i>	180	$(2.944 \pm 0.141) \times 10^{-2}$
CQUEAN	465140	<i>z</i>	180	$(2.680 \pm 0.103) \times 10^{-2}$
CQUEAN	465441	<i>z</i>	180	$(2.204 \pm 0.100) \times 10^{-2}$
CQUEAN	554653	<i>z</i>	300	$(1.784 \pm 0.060) \times 10^{-2}$
CQUEAN	554955	<i>z</i>	300	$(2.248 \pm 0.062) \times 10^{-2}$
CQUEAN	555256	<i>z</i>	300	$(2.120 \pm 0.064) \times 10^{-2}$
CQUEAN	32776	<i>Y</i>	300	1.585 ± 0.004
CQUEAN	118338	<i>Y</i>	300	$(5.005 \pm 0.025) \times 10^{-1}$
CQUEAN	205445	<i>Y</i>	120×6	$(3.576 \pm 0.054) \times 10^{-1}$
CQUEAN	288007	<i>Y</i>	120×3	$(2.672 \pm 0.053) \times 10^{-1}$

reason for this successful submillimeter monitoring was the target selection using the quick optical follow-ups.

3. ANALYSIS AND RESULTS

The BAT data were analyzed using the standard BAT analysis software included in HEADAS version 6.12. The time-averaged spectrum (15–150 keV) from $T_0 - 2$ to $T_0 + 11$ s was extracted using `batgrbproduct`. Response matrices were generated by the task `batdrmg`, using the latest spectral redistribution matrices. The WAM spectral and temporal data were extracted using `hxmdkwamlc` and `hxmdkwamspec` in HEADAS version 6.12. The background was estimated using the fitting model described in Sugita et al. (2009). Response matrices were

Table 2
Log of SMA Observations

Instruments	Observing Period (UT)	$T - T_0$ (s)	Band (GHz)	Beam Size	Flux Density (mJy)
SMA	2012 Mar 26 13:00–15:00	45571	230	1''.74 × 1''.14	2.84 ± 0.86
SMA	2012 Mar 26 15:10–17:30	53971	230	1''.69 × 1''.02	3.56 ± 0.75
SMA	2012 Mar 26 18:00–20:15	64171	230	2''.03 × 0''.96	3.36 ± 1.04
SMA	2012 Mar 27 13:25–19:15	138480	230	1''.62 × 1''.11	2.38 ± 0.51
SMA	2012 Mar 29 12:45–18:50	310290	230	0''.62 × 0''.37	1.76 ± 0.50
SMA	2012 Apr 11 15:50–21:10	1377571	230	0''.55 × 0''.42	<1.44 (3 σ)

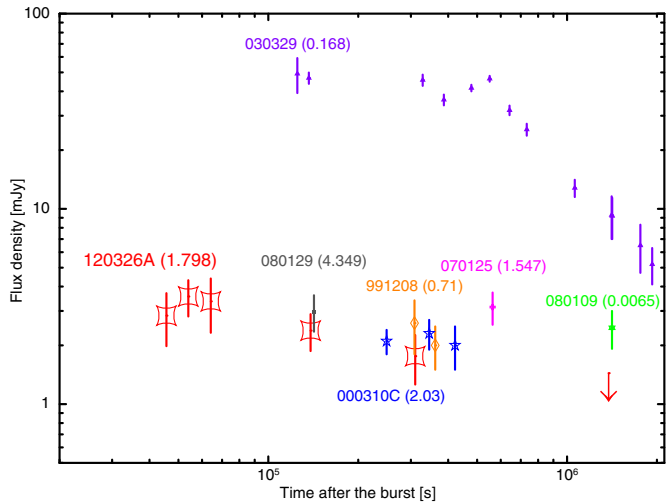


Figure 2. Light curves of all the submillimeter afterglows detected in the 230 GHz band to date. The SMA observation on GRB 120326A provides the earliest submillimeter detection and continuous monitoring. The values noted in brackets are the redshifts of each event. The samples are taken from Galama et al. (2000) for 991208, Berger et al. (2000) for 000310C, Resmi et al. (2005) and Sheth et al. (2003) for 030329, Chandra et al. (2008) for 070125, Gorosabel et al. (2010) for 080109, and Greiner et al. (2009) for 080129.

(A color version of this figure is available in the online journal.)

generated by the WAM response generator as described in Ohno et al. (2008). We used three models for the joint spectral fitting: the power-law model, power law with exponential cutoff model, and the Band function model. As shown in Figure 3, the spectrum was reasonably fitted with the Band function. The fitting yielded a low-energy photon index of $1.17^{+0.53}_{-0.32}$, a high-energy photon index of $2.23^{+0.09}_{-0.11}$, and a $\nu F \nu$ spectrum peak energy in the source frame $E_{\text{peak}}^{\text{src}}$ of $107.8^{+15.2}_{-15.3}$ keV ($\chi^2/\nu = 0.92$ for $\nu = 63$). Both the power law ($\chi^2/\nu = 1.55$ for $\nu = 65$) and power law with exponential cutoff models ($\chi^2/\nu = 1.38$ for $\nu = 67$) were not acceptable, leaving the curvature of the residuals around 30–40 keV at the observer frame (the second and third panels in Figure 3). We also estimated the equivalent isotropic radiated energy in the prompt phase at the 1–10,000 keV band E_{iso} as $3.18^{+0.40}_{-0.32} \times 10^{52}$ erg, assuming cosmological parameters: $H_0 = 71 \text{ km s}^{-1} \text{ Mpc}^{-1}$, $\Omega_m = 0.27$, and $\Omega_\Lambda = 0.73$.

We obtained a reduced *Swift*/XRT light curve with a flux density unit at 10 keV from the U.K. Swift Science Data Center (Evans et al. 2007, 2009). The light curves shown in Figure 4 were suitably fitted using the broken power-law model described in Urata et al. (2009), using the best-fitted parameters of $\alpha_{X1} = 0.19 \pm 0.09$, $\alpha_{X2} = -2.35 \pm 0.15$, and $t_{bX} = (5.29 \pm 0.32) \times 10^4$ s. We also generated the time-

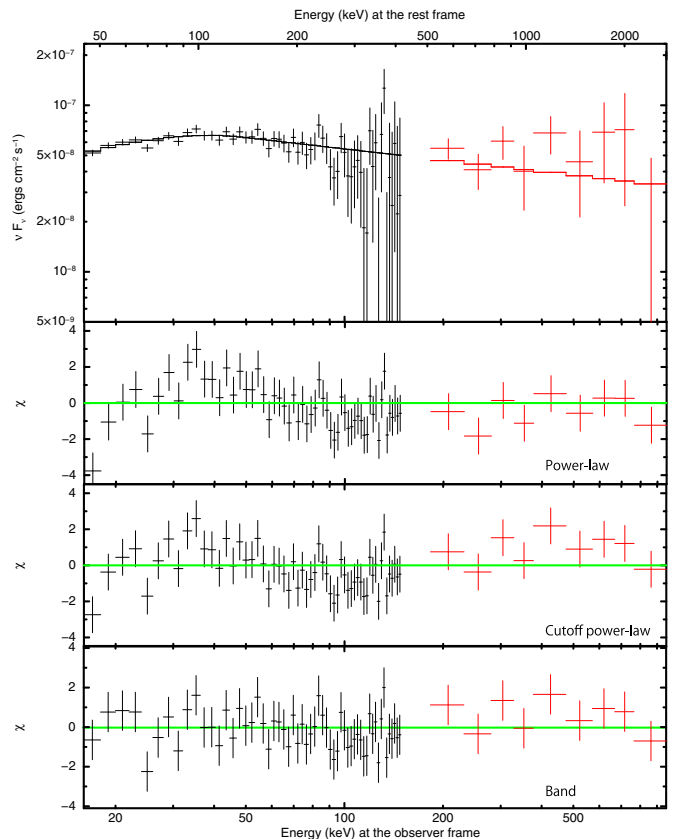


Figure 3. Time-averaged spectrum of the prompt emission, observed using *Swift*/BAT and *Suzaku*/WAM. The BAT and WAM data are shown in black and red, respectively. In the top panel, the solid lines indicate the best-fit Band function model. The lower panels show residuals for fitting with power law (second), power law with exponential cutoff (third), and Band (fourth) models. (A color version of this figure is available in the online journal.)

averaged spectrum at a mean time of 6.47×10^4 s (from 55741 to 73639 s). The spectra were suitably fitted using the power law modified by photo-electric absorptions (Galactic and intrinsic), and the photon index was estimated as $1.95^{+0.18}_{-0.17}$.

A standard routine, including bias subtraction and flat-fielding corrections, was employed to process the optical data by using the IRAF package. The DAOPHOT package was used to perform the aperture photometry of the GRB images. Standard star observation in one night is used to derive magnitudes of reference stars in the vicinity of the GRB afterglow, and these reference stars were used to perform photometry of the afterglow. We also made use of the Pan-STARRS1 3 π catalogs (Magnier et al. 2013; Schlafly et al. 2012; Tonry et al. 2012) to calibrate our g' , r' , i' , z' , and Y -band data. As shown in Figure 4, the light curves in the g' , r' , i' , and z' bands

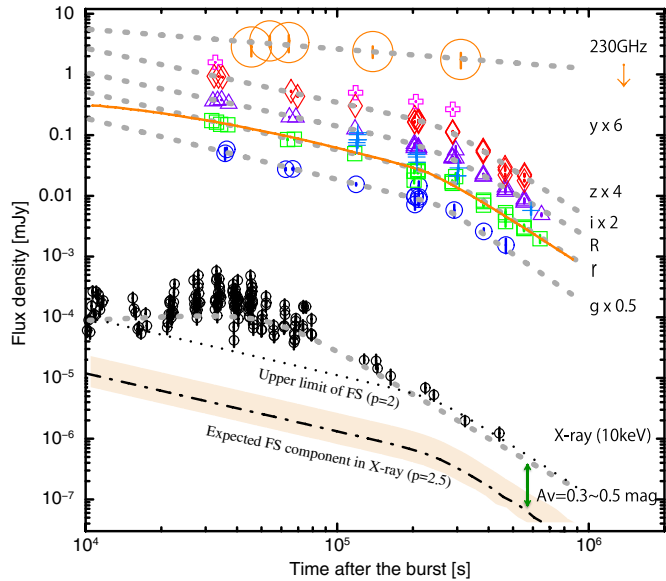


Figure 4. X-ray, optical, and submillimeter light curves of the GRB 120326A afterglow. The gray dotted lines show the best analytical fitted functions described in the text. The orange solid line shows the best modeling function for the r -band light curve obtained with the numerical simulation using boxfit. The black dashed-dotted and dotted lines indicate the shifted optical light curve to the X-ray bands by a factor of $(v_X/v_{\text{opt}})^{-p/2}$ with $p = 2.5$ and $p = 2$, respectively.

(A color version of this figure is available in the online journal.)

indicated the achromatic temporal break at $\sim 2.6 \times 10^5$ s. We successfully fitted the broken power-law model to the g' -, r' -, i' -, and z' -band light curves. Regarding the g' band, we have obtained $\alpha_{g1} = -1.01 \pm 0.06$, $\alpha_{g2} = -2.84 \pm 0.16$, and $t_{bg} = (2.58 \pm 0.15) \times 10^5$ s; regarding the r' band, $\alpha_{r1} = -0.96 \pm 0.01$, $\alpha_{r2} = -2.64 \pm 0.09$, and $t_{br} = (2.58 \pm 0.07) \times 10^5$ s; regarding the i' band, $\alpha_{i1} = -0.88 \pm 0.02$, $\alpha_{i2} = -2.48 \pm 0.05$, and $t_{bi} = (2.51 \pm 0.10) \times 10^5$ s; regarding the z' band, $\alpha_{z1} = -0.89 \pm 0.01$, $\alpha_{z2} = -2.64 \pm 0.10$, and $t_{bz} = (2.63 \pm 0.06) \times 10^5$ s; and regarding the y' band, we fitted the light curve by using the simple power-law model, because the y' -band observations covered only before the temporal break. The light curve was fitted with the model and we obtained $\alpha_y = -0.87 \pm 0.03$. The decay indices before and after the break are ~ -1 and ~ -2 , respectively, which is highly consistent with typical well-observed long GRB optical afterglows. In Figure 5, we plot the spectral flux distribution with the submillimeter and X-ray data. We fitted the optical data alone using a power-law function and obtained $\beta = -1.44 \pm 0.10$, -1.11 ± 0.09 , and -1.18 ± 0.17 at $t = 6.42 \times 10^4$ s, 1.38×10^5 s, and 3.10×10^5 s, respectively. To remove the effects of the Galactic interstellar extinction, we used the reddening map by Schlafly & Finkbeiner (2011).

The raw data of the SMA observations were calibrated using the MIR and MIRIAD packages and images were made with the natural weighting. Regarding the first night of observation, we split the data into three periods to describe the temporal evolution of submillimeter afterglow. Table 2 summarizes each observation period and flux density measurements (upper part). Because of adverse weather conditions during the first 1.08×10^4 s, only the data recorded after 13:00 on March 26 UT were used for the scientific analysis. In the final period, we constrained the 3σ upper limit. With our SMA follow-ups, we successfully monitored the afterglow from 4.32×10^4 to

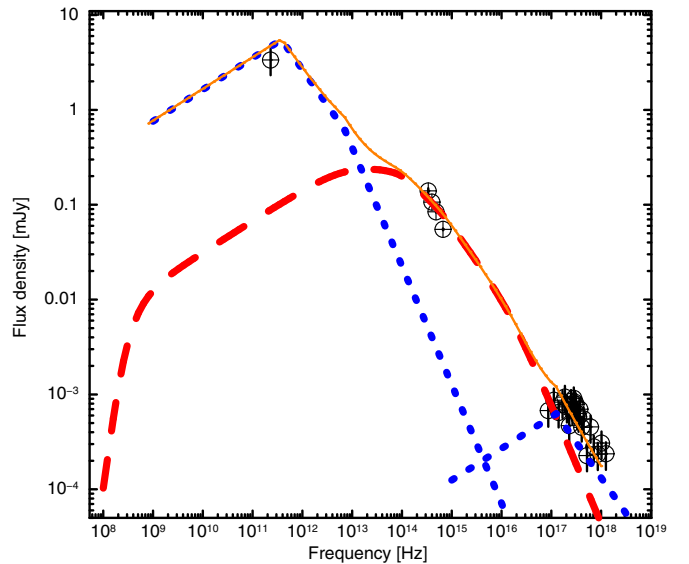


Figure 5. Spectral energy distribution at 6.42×10^4 s after the burst. The red dashed line shows the forward shock synchrotron model spectrum calculated using the boxfit code with the same parameters for the best modeling light curve shown in Figure 4. The blue dotted lines show the reverse shock synchrotron radiation and its self-inverse Compton component calculated based on Kobayashi et al. (2007) using the observed values and model function for the forward shock component.

(A color version of this figure is available in the online journal.)

3.46×10^5 s as shown in Figure 4. The submillimeter afterglow exhibited a flat evolution with slight brightening between the first and second periods. To describe the temporal evolution, we fitted the submillimeter data with the single power-law function and obtained $\alpha_{\text{submillimeter}} = -0.33 \pm 0.08$, which was considerably flatter than those of the X-ray and optical.

4. DISCUSSION

4.1. Prompt Emission and Energetics Relations

The joint fitting of the *Swift*/BAT and *Suzaku*/WAM suitably constrained the spectral parameters of the prompt emission of GRB 120326A that are critical to characterize the event. As shown in Figure 6, the spectral peak energy in the source frame, $E_{\text{peak}}^{\text{src}}$, is one of the lowest events among the sample of the joint *Swift*/BAT–*Suzaku*/WAM analysis. The trend is similar to that of the vFv spectral peak energy at the observer frame $E_{\text{peak}}^{\text{obs}}$ in comparison to a larger set of $E_{\text{peak}}^{\text{obs}}$ values of 479 GRBs drawn from the *Fermi*/GBM catalog (von Kienlin et al. 2014); however, the *Fermi*/GBM measurements do not represent $E_{\text{peak}}^{\text{src}}$ due to the lack of redshift information. By comparing with the *HETE*-2 sample (Sakamoto et al. 2005), GRB 120326A can be categorized as X-ray-rich GRBs. Using the definition with *Swift*/BAT data (Sakamoto et al. 2008), we confirm that GRB 120326A with an ~ 0.74 fluence ratio in the 25–50 keV and 50–100 keV bands falls into the X-ray-rich GRB family.

The abundance of the multi-color optical light curves for estimating the jet break time suggests that GRB 120326A is a favorable target for evaluating $E_{\text{peak}}^{\text{src}}-E_{\text{iso}}$ (Amati et al. 2002) and $E_{\text{peak}}^{\text{src}}-E_{\gamma}$ (Ghirlanda et al. 2007) relations. Here, $E_{\text{peak}}^{\text{src}}-E_{\gamma}$ is the correlation between the intrinsic spectrum peak energy, $E_{\text{peak}}^{\text{src}}$, and the jet collimation-corrected energy in the prompt phase, E_{γ} . The closure relation of the observed optical temporal decay and the spectral indices (e.g., Sari et al. 1999; Zhang &

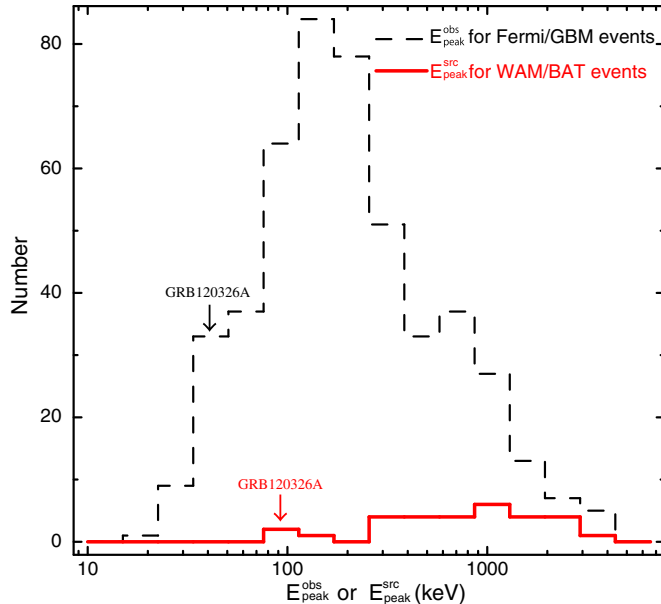


Figure 6. Distribution of $E_{\text{peak}}^{\text{src}}$ for BAT/WAM events and $E_{\text{peak}}^{\text{obs}}$ for *Fermi*/GBM events. GRB 120326A is one of the lowest $E_{\text{peak}}^{\text{src}}$ events among the BAT/WAM sample. $E_{\text{peak}}^{\text{obs}}$ also shows the same trend with large *Fermi*/GBM samples; though the measurements were analyzed without redshift correction. (A color version of this figure is available in the online journal.)

Mészáros 2004) indicates that, of all the $p > 2$ options, the optical results are consistent with both the fast and the slow cooling and both the wind and the ISM medium, as long as $\nu_{m,\text{FS}}$ and $\nu_{c,\text{FS}}$ lie below the optical band. Here, $\nu_{m,\text{FS}}$ and $\nu_{c,\text{FS}}$ are the characteristic synchrotron frequency and the cooling frequency based on the standard forward shock synchrotron model. Thus, the jet opening angle and the jet corrected energy are estimated using t_{br} as 6.69 ± 0.16 and $(2.17 \pm 0.10) \times 10^{50}$ erg by assuming the circumburst density, $n = 1.0 \text{ cm}^{-3}$, and the energy conversion efficiency, $\eta_{\gamma} = 0.2$. To convert the measured jet break time, t_{br} , to the jet opening angle, we used the formulation of Sari et al. (1999) and Frail et al. (2001). As shown in Figure 7, GRB 120326A obeys the $E_{\text{peak}}^{\text{src}}-E_{\text{iso}}$ and $E_{\text{peak}}^{\text{src}}-E_{\gamma}$ relations within a 3σ confidence level. Therefore, GRB 120326A belongs to the typical long duration GRB family, even with a low $E_{\text{peak}}^{\text{src}}$.

4.2. Does the Classical Forward Shock Synchrotron Model Work?

Based on the closure relations, the observed temporal evolution and spectral features of the optical afterglow are consistent with those of the forward shock synchrotron model. The fact that $\nu_{m,\text{FS}}$ and $\nu_{c,\text{FS}}$ both lie below the optical band implies that within the standard synchrotron model, X-ray afterglows lie in the same spectral regime as the optical emission, and that the standard model predicts the same temporal and spectral shape for X-rays as for the optical.

However, the observed X-ray light curve shows a significant deviation from the predicted behavior of the standard model and appears to require an additional component. Using the testing method of the forward shock model and the decay index ($\alpha_0 - \alpha_X$) relation between the optical and X-ray (Urata et al. 2007), we find that GRB 120326A is a clear outlier ($\alpha_0 - \alpha_X = -1.45 \pm 0.10$) and the origin of the X-ray afterglow could differ from that of the optical. For conducting a more rigorous analysis, we selected the normal optical decay phase

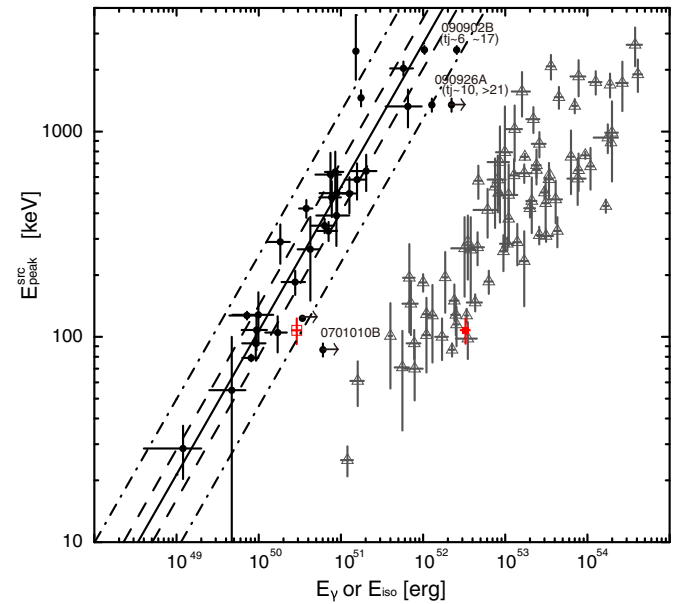


Figure 7. $E_{\text{peak}}^{\text{src}}-E_{\text{iso}}$ relation in Amati et al. (2002; open triangle) and the $E_{\text{peak}}^{\text{src}}-E_{\gamma}$ relation corrected for a homogeneous circumburst medium (filled circle). GRB 120326A marked with red box points obeyed both relations. The solid line indicates the best-fit correlation derived by Ghirlanda et al. (2007). The dashed and dashed-dotted lines indicate the 1σ and 3σ scatter of the correlation, respectively.

(A color version of this figure is available in the online journal.)

as from 3.2×10^4 s to 2.1×10^5 s. The optical light curve in this phase is well-fitted with a simple power-law function with an index of -0.96 ± 0.01 . For the time range, we forced the X-ray light curve to fit with the simple power-law function and obtained the decay index of -1.54 ± 0.14 . Hence, this event remained an outlier ($\alpha_0 - \alpha_X = -0.58 \pm 0.14$) and the X-ray emission could have an extra component such as X-ray flare on the forward shock synchrotron emission.

To check the excess in the X-ray light curve, we shifted the optical light curve to the X-ray band with the factor $(\nu_X / \nu_{\text{opt}})^{-p/2}$ by assuming that the X-ray and optical lie on the same segment of the synchrotron radiation. We used $p = 2.48$ with a 3σ error of 0.15 estimated from the optical observations and the closure relation. As shown in Figure 4, the shifted light curve shows a significant gap with that of the observed X-ray and the gap is smaller after $\sim 3 \times 10^5$ s. One of the main reasons for the gap is no consideration of the intrinsic extinction for the optical component at the burst site, which is due to the lack of spectral coverage in the optical observations. If the main X-ray component after 3×10^5 s originated from the same segment of forward shock synchrotron radiation with the optical (sharing a similar decay index with that of the optical), $A_V = 0.3 \sim 0.5$ mag with the Small Magellanic Cloud extinction curve is required to fill up the smaller gap after 3×10^5 s. The extinction value of $A_V = 0.3 \sim 0.5$ mag is larger compared to the majority of optically bright events ($A_V < 0.25$ mag; Kann et al. 2006, 2010). We also added the shifted optical light curve with $p = 2$ that provides the upper limit of the forward shock synchrotron radiation under the $p > 2$ condition (Figure 4). Although these imply that adjusting p and introducing extinction may be the solution to explain the gap after 3×10^5 s, there remains a significant X-ray excess between 2×10^4 and 3×10^5 s.

The forward shock synchrotron model based on the optical afterglow is also unable to explain the submillimeter emission.

Based on the closure relation, the slow decay observed in the submillimeter light curve requires $\nu_{c,FS} < \nu_{\text{submillimeter}} < \nu_{m,FS}$ (i.e., a fast cooling condition for both ISM and wind types). Hence, $\nu_{c,FS} < \nu_{\text{submillimeter}} < \nu_{m,FS} < \nu_{\text{opt}}$ is required to satisfy the closure relation for the submillimeter and optical afterglows altogether. In addition to the closure relation, the observed flux densities (both in the submillimeter and optical bands) at 6.42×10^4 s and the temporal decay index in the optical bands tightly constrain the range of characterized frequencies as $\nu_{c,FS} < 2.3 \times 10^{11}$ Hz and $\nu_{m,FS} \sim 3 \times 10^{14}$ Hz in order to make the fast cooling condition. With these conditions, we find that even a drastic case (e.g., $\epsilon_B \sim 1$ and $\epsilon_e \sim 1$ with a very high density of $n > \text{several} \times 10^3 \text{ cm}^{-3}$) cannot meet the condition, and that the origin of submillimeter component could also differ from that of the optical. Thus, additional radiation is required to explain X-ray and submillimeter emissions altogether.

4.3. Forward Shock Synchrotron Modeling

To describe the entire spectral energy distribution (SED), we performed modeling for the optical light curves and spectra by using the boxfit code (van Eerten et al. 2012) that involved two-dimensional relativistic hydrodynamical jet simulations to determine the burst explosion and the synchrotron radiation parameters with a homogeneous circumburst medium. Hence, hereafter, we only consider the ISM condition and do not verify whether the ISM or wind condition is favorable. This code also performs data fitting with the downhill simplex method combined with simulated annealing. Based on the observational results, we fixed $\theta_{\text{jet}} = 6.7^\circ$ and a power-law electron spectrum of slope $p = 2.5$. The observing angle was also fixed as $\theta_{\text{obs}} = 0$. By using only the optical data with the code, we determined the optimal modeling parameters to describe the optical light curves as $E = 3.9 \times 10^{52}$ erg, $n = 1.0 \text{ cm}^{-3}$, $\epsilon_B = 1.0 \times 10^{-3}$, and $\epsilon_e = 6.9 \times 10^{-1}$. To adjust the model function, we also set the jet opening angle as a free parameter and then $\theta_{\text{jet}} = 8.1^\circ$ provided favorable agreement ($\chi^2/\nu = 3.9$ for $\nu = 94$) with observing the light curve. The solid line in Figure 4 indicates the best model function for the r' -band light curve, which also agreed well with the analytical model function. This opening angle adjustment is reasonable because $\theta_{\text{jet}} = 6.7^\circ$ was estimated by considering the conical jet. An additional note is that the post-jet-break closure relation is no longer valid under the consideration of the detailed spreading of the jet (van Eerten & MacFadyen 2013). However, we are not concerned about this, since we were able to achieve the good fit with the simulation-based fit models. With the adjusted jet opening angle, GRB 120326A still obeyed the $E_{\text{peak}}^{\text{src}} - E_\gamma$ relation. We also attempted to determine the optimal solution by using optical and submillimeter data with the code. However, no sufficient solution describes the temporal evolutions of submillimeter and optical afterglows at once, which were determined by the χ^2 evaluation with 2.3×10^4 . All of the trials provided reduced χ^2 greater than 13. This is consistent with the forward shock tests described above. We generated the forward shock synchrotron model spectrum by using the boxfit with the best modeling parameters for the light curve. Figure 5 shows the SED at 6.42×10^4 s after the burst. The spectrum in the X-ray and submillimeter exhibited substantial excesses from the best model function and indicated that the afterglow spectrum required additional radiation components. This interpretation is also consistent with the result of the $\alpha o - \alpha_X$ relation and the shifted optical light curve to the X-ray band with factor $(\nu_X/\nu_{\text{opt}})^{-p/2}$.

4.4. Reverse Shock and Synchrotron Self-Compton Radiation

A solution that explains the X-ray excess and the different origin of the submillimeter emission is the introduction of synchrotron self-inverse Compton radiation from reverse shock. This is one of the most feasible methods of dealing with two notable observed properties at once. Assuming that the deceleration time is near the X-ray light curve peak at $t_{BX} \sim 5.2 \times 10^4$ s, the initial Lorentz factor Γ_0 is estimated as ~ 16 , which is consistent with the thin-shell case ($\Gamma_c \sim 365$). Here, Γ_c is the critical Lorentz factor that distinguishes thin shell models, where the reverse shock remains Newtonian, from thick shell models (Sari & Piran 1995; Kobayashi et al. 2007). This lower Γ_0 might be associated with the low $E_{\text{peak}}^{\text{src}}$ property. It might also originate from the cocoon fireball as part of two-component jet in the collapsar framework (e.g., Ramirez-Ruiz et al. 2002). In this case, thermal radiation is expected to arise in the optical light curves (Kashiyama et al. 2013; Nakauchi et al. 2013). However, the observed optical light curves show no excess in the late phase.

Using the estimated parameters described above, we calculated the model function for synchrotron self-inverse Compton radiation from reverse shock under the thin-shell condition described in Kobayashi et al. (2007). For this calculation, we assumed $\epsilon_{B,RS} \sim 5 \times 10^{-3}$, and peak flux densities of reverse and forward shocks as $F_{\text{max},RS} \sim 5.5 \text{ mJy}$ and $F_{\text{max},FS} \sim 0.2 \text{ mJy}$, respectively. Figure 5 shows the calculated spectrum for the reverse shock and inverse Compton components at 6.42×10^4 s with the obtained key parameters of $\nu_{m,RS}^{\text{Sync}} \sim 4 \times 10^{11}$ Hz, $\nu_{c,RS}^{\text{Sync}} \sim 7 \times 10^{12}$ Hz, $\nu_{m,RS}^{\text{IC}} \sim 1 \times 10^{17}$ Hz, and $\nu_{c,RS}^{\text{IC}} \sim 4 \times 10^{19}$ Hz. Although the observed X-ray flux was slightly brighter than the calculated self-inverse Compton component, the total spectrum including forward shock sufficiently described the overall properties of the afterglow. Because $\nu_{\text{obs}} < \nu_{m,RS}^{\text{Sync}}$, the expected decay index of the reverse shock component in the observed submillimeter band was ~ -0.46 , which was consistent with the slow temporal evolution of the submillimeter afterglow ($\alpha_{\text{submillimeter}} = -0.33$). The evolution, which was relatively shallower than expected, also implies the smooth transition of $\nu_{m,RS}^{\text{Sync}}$ in the observing band, unlike the sharp break in Figure 4. This could be consistent with other spectrum breaks such as the non-existence of the sharp cooling break in the afterglow spectrum (e.g., Granot & Sari 2002; van Eerten & Wijers 2009; Curran et al. 2010). The observed X-ray decay ($\alpha_X \sim -2.4$) and spectrum ($\beta_X \sim -0.96$) indices were also basically consistent with the expected values ($\alpha_X \sim -2.8$ and $\beta_X \sim -0.75$) for $\nu_{m,RS}^{\text{IC}} < \nu_{\text{obs}} < \nu_{c,RS}^{\text{IC}}$.

5. SUMMARY

We conducted multi-wavelength observations of a typical long-duration GRB 120326A, including rapid observations using SMA. Our SMA observation successfully made the fastest afterglow detection among seven submillimeter afterglows at 230 GHz and monitored from 4.32×10^4 to 3.46×10^5 s. The submillimeter afterglow showed considerably slower temporal evolution ($\alpha_{\text{submillimeter}} = -0.33 \pm 0.08$) which is not likely to be explained by the forward shock synchrotron model. Based on our dense optical observations, we found that the optical afterglows were well-fitted by the broken power-law model, and the forward shock synchrotron model is feasible to explain the properties. With the boxfit code, we also found the reasonable model function within the forward shock synchrotron model

under the assumption of ISM circumburst medium. Using the simple testing method of the forward shock model with temporal decay indices of optical and X-ray afterglows, we found that the origin of the X-ray afterglow could differ from that of the optical. Our joint spectrum fitting for prompt emission using *Swift*/BAT and *Suzaku*/WAM also characterized the event and found that the current event obeys the $E_{\text{peak}}^{\text{src}} - E_{\text{iso}}$ and $E_{\text{peak}}^{\text{src}} - E_{\gamma}$ relations within a 3σ confidence level.

Based on the detection and the slow decay of the afterglow in submillimeter, we introduced the synchrotron self-inverse Compton radiation from reverse shock and found that this is a plausible method to explain the diversity. This successful modeling could benefit other GRBs. Similar to GRB 120326A, numerous events exhibited no apparent jet breaks in the X-ray band and different temporal evolutions between the X-ray and optical. These observational properties imply that additional components, such as reverse shock and its synchrotron self-inverse Compton radiation, cause different temporal evolution and hide obvious jet breaks in the X-ray. Because of a lack of submillimeter observations for these samples, interpretation from the same picture for these events was difficult. Thus, further rapid follow-ups and continuous monitoring with submillimeter instruments such as SMA and ALMA will enable systematic testing of the reverse shock and self-inverse Compton radiation.

We thank Glen Petitpas for various arrangements on the SMA observations and Shiho Kobayashi for useful comments. We also thank all of staff at the Lulin observatory. This work is partly supported by the Ministry of Education and the National Science Council of Taiwan grants NSC 100-2112-M-008-007-MY3(YU), 99-2112-M-002-002-MY3(KYH). M.I., J.W.K., M.J., and S.J. acknowledge support from the National Research Foundation of Korea (NRF) grant No. 2008-0060544, funded by the Korea government (MSIP). This work made use of data supplied by the UK Swift Science Data Centre at the University of Leicester. This paper includes data taken at the McDonald Observatory of the University of Texas in Austin. The PS1 Surveys have been made possible through contributions of the Institute for Astronomy, the University of Hawaii, the Pan-STARRS Project Office, the Max-Planck Society and its participating institutes, the Max Planck Institute for Astronomy, Heidelberg and the Max Planck Institute for Extraterrestrial Physics, Garching, The Johns Hopkins University, Durham University, the University of Edinburgh, Queen’s University Belfast, the Harvard-Smithsonian Center for Astrophysics, and the Las Cumbres Observatory Global Telescope Network, Incorporated, the National Central University of Taiwan, and the National Aeronautics and Space Administration under grant No. NNX08AR22G, issued through the Planetary Science Division of the NASA Science Mission Directorate.

REFERENCES

- Akerlof, C., Balsano, R., Barthelmy, S., et al. 1999, *Natur*, **398**, 400
 Amati, L., Frontera, F., Tavani, M., et al. 2002, *A&A*, **390**, 81
 Berger, E., Sari, R., Frail, D. A., et al. 2000, *ApJ*, **545**, 56
 Chandra, P., Cenko, S. B., Frail, D. A., et al. 2008, *ApJ*, **683**, 924
 Collazzi, A. C. 2012, GCN, **13145**, 1
 Curran, P. A., Evans, P. A., de Pasquale, M., Page, M. J., & van der Horst, A. J. 2010, *ApJL*, **716**, L135
 de Ugarte Postigo, A., Lundgren, A., Martín, S., et al. 2012, *A&A*, **538**, A44
 Evans, P. A., Beardmore, A. P., Page, K. L., et al. 2007, *A&A*, **469**, 379
 Evans, P. A., Beardmore, A. P., Page, K. L., et al. 2009, *MNRAS*, **397**, 1177
 Frail, D. A., Kulkarni, S. R., Sari, R., et al. 2001, *ApJL*, **562**, L55
 Galama, T. J., Bremer, M., Bertoldi, F., et al. 2000, *ApJL*, **541**, L45
 Granot, J., & Sari, R. 2002, *ApJ*, **568**, 820
 Gehrels, N., Chincarini, G., Giommi, P., et al. 2004, *ApJ*, **611**, 1005
 Ghirlanda, G., Nava, L., Ghisellini, G., & Firmani, G. 2007, *A&A*, **466**, 127
 Gorosabel, J., de Ugarte Postigo, A., Castro-Tirado, A. J., et al. 2010, *A&A*, **522**, A14
 Greiner, J., Krühler, T., McBreen, S., et al. 2009, *ApJ*, **693**, 1912
 Han, W., Mack, P., Lee, C.-U., et al. 2005, *PASJ*, **57**, 821
 Ho, P. T. P., Moran, J. M., & Lo, K. Y. 2004, *ApJL*, **616**, L1
 Huang, K. Y., Urata, Y., Filippenko, A. V., et al. 2005, *ApJL*, **628**, L93
 Huang, K. Y., Urata, Y., Kuo, P. H., et al. 2007, *ApJL*, **654**, L25
 Iwakiri, W., Tashiro, M., Terada, Y., et al. 2012, GCN, **13176**, 1
 Laskar, T., Zauderer, A., & Berger, E. 2012, GCN, **13181**, 1
 Lee, I., Im, M., & Urata, Y. 2010, *JKAS*, **43**, 95
 Li, L., Liang, E.-W., Tang, Q.-W., et al. 2012, *ApJ*, **758**, 27
 Lim, J., Chang, S., Pak, S., et al. 2013, *JKAS*, **46**, 161
 Kann, D. A., Klose, S., & Zeh, A. 2006, *ApJ*, **641**, 993
 Kann, D. A., Klose, S., Zhang, B., et al. 2010, *ApJ*, **720**, 1513
 Kashiyama, K., Nakachi, D., Suwa, Y., Yajima, H., & Nakamura, T. 2013, *ApJ*, **770**, 8
 Kim, E., Park, W.-K., Jeong, H., et al. 2011, *JKAS*, **44**, 115
 Klotz, A., Gendre, B., Boer, M., & Atteia, J. L. 2012, GCN, **13107**, 1
 Kobayashi, S., Zhang, B., Mészáros, P., & Burrows, D. 2007, *ApJ*, **655**, 391
 Kulkarni, S. R., Frail, D. A., Sari, R., et al. 1999, *ApJL*, **522**, L97
 Magnier, E. A., Schlafly, E., Finkbeiner, D., et al. 2013, *ApJS*, **205**, 20
 Meszaros, P., & Rees, M. J. 1997, *ApJ*, **476**, 232
 Mitsuda, K., Bautz, M., Inoue, H., et al. 2007, *PASJ*, **59**, 1
 Nakachi, D., Kashiyama, K., Suwa, Y., & Nakamura, T. 2013, *ApJ*, **778**, 67
 Ohno, M., Fukazawa, Y., Takahashi, T., et al. 2008, *PASJ*, **60**, 361
 Panaitescu, A., Mészáros, P., Burrows, D., et al. 2006, *MNRAS*, **369**, 2059
 Panaitescu, A., & Vestrand, W. T. 2011, *MNRAS*, **414**, 3537
 Park, W.-K., Pak, S., Im, M., et al. 2012, *PASP*, **124**, 839
 Perley, D. A., Alatalo, K., & Horesh, A. 2012, GCN, **13175**, 1
 Ramirez-Ruiz, E., Celotti, A., & Rees, M. J. 2002, *MNRAS*, **337**, 1349
 Resmi, L., Ishwara-Chandra, C. H., Castro-Tirado, A. J., et al. 2005, *A&A*, **440**, 477
 Sakamoto, T., Hullinger, D., Sato, G., et al. 2008, *ApJ*, **679**, 570
 Sakamoto, T., Lamb, D. Q., Kawai, N., et al. 2005, *ApJ*, **629**, 311
 Sari, R., & Piran, T. 1995, *ApJL*, **455**, L143
 Sari, R., Piran, T., & Halpern, J. P. 1999, *ApJL*, **519**, L17
 Schlafly, E. F., & Finkbeiner, D. P. 2011, *ApJ*, **737**, 103
 Schlafly, E. F., Finkbeiner, D. P., Jurić, M., et al. 2012, *ApJ*, **756**, 158
 Sheth, K., Frail, D. A., White, S., et al. 2003, *ApJL*, **595**, L33
 Siegel, M. H., Barthelmy, S. D., Burrows, D. N., et al. 2012, GCN, **13105**, 1
 Sugita, S., Yamaoka, K., Ohno, M., et al. 2009, *PASJ*, **61**, 521
 Takahashi, T., Abe, K., Endo, M., et al. 2007, *PASJ*, **59**, 35
 Tashiro, M. S., Abe, K., Angelini, L., et al. 2007, *PASJ*, **59**, 361
 Tello, J. C., Sanchez-Ramirez, R., Gorosabel, J., et al. 2012, GCN, **13118**, 1
 Toma, K., Ioka, K., & Nakamura, T. 2008, *ApJL*, **673**, L123
 Tonry, J. L., Stubbs, C. W., Lykke, K. R., et al. 2012, *ApJ*, **750**, 99
 Urata, Y., Huang, K., Im, M., et al. 2009, *ApJL*, **706**, L183
 Urata, Y., Huang, K. Y., Takahashi, S., & Petitpas, G. 2012, GCN, **13136**, 1
 Urata, Y., Nishiura, S., Miyata, T., et al. 2003, *ApJL*, **595**, L21
 Urata, Y., Yamazaki, R., Sakamoto, T., et al. 2007, *ApJL*, **668**, L95
 van Eerten, H., & MacFadyen, A. 2013, *ApJ*, **767**, 141
 van Eerten, H., van der Horst, A., & MacFadyen, A. 2012, *ApJ*, **749**, 44
 van Eerten, H. J., & Wijers, R. A. M. J. 2009, *MNRAS*, **394**, 2164
 von Kienlin, A., Meegan, C. A., Paciesas, W. S., et al. 2014, *ApJS*, **211**, 13
 Walker, C., Court, J., Duffy, R., et al. 2012, GCN, **13112**, 1
 Yamaoka, K., Endo, A., Enoto, T., et al. 2009, *PASJ*, **61**, S35
 Zhang, B., & Mészáros, P. 2004, *IJMPA*, **19**, 2385



CCD photometry of distant active comets 228P/LINEAR, C/2006 S3 (LONEOS) and 29P/Schwassmann–Wachmann 1

J. C. Shi,^{1,2}★ Y. H. Ma^{1,2} and J. Q. Zheng³

¹Purple Mountain Observatory, Chinese Academy of Sciences, Nanjing 210008, China

²Key Laboratory of Planetary Sciences, Chinese Academy of Sciences, Nanjing 210008, China

³Tuorla Observatory, FI-21500 Piikkiö, Finland

Accepted 2014 March 25. Received 2014 February 18; in original form 2013 December 18

ABSTRACT

We present photometric investigations of three distant active comets, 228P/LINEAR, C/2006 S3 Lowell Observatory Near-Earth-Object Search (LONEOS) and 29P/Schwassmann–Wachmann 1. The data were obtained with the 1-m optical telescope at Lulin Observatory in Taiwan on 2011 February 5 and 6. These comets were observed at heliocentric distances larger than 3 au, all of them appeared to be active. By cometary morphological and photometric studies, the upper limits of the nuclei radii were derived. Also, the surface brightness profiles, $A\rho$ parameters, mass production rates and the coma colours were measured. Finally, we discussed possible driver of activity in comets.

Key words: techniques: photometric – comets: general.

1 INTRODUCTION

Generally, a comet at a large distance from the Sun is supposed to be inactive due to the low temperature and the absence of gas sublimation leading to coma formation. But it is known from observations that the activity of comets far from the Sun is common (Luu 1993; Lamy et al. 2004; Meech & Svoren 2004; Mazzotta Epifani et al. 2007, 2008, 2009, 2010, 2011; Korsun, Ivanova & Afanasiev 2008; Snodgrass, Lowry & Fitzsimmons 2008; Ivanova, Korsun & Afanasiev 2009; Jewitt 2009). Meech & Hainaut (2001) discussed the importance of observing distant comets in investigating the processes of formation and evolution of planetesimals.

The primary driver of activity in comets close to the Sun is sublimation of water ice and can be explained by the standard model (Whipple 1950). Beyond a heliocentric distance of 3 au, the sublimation rate for water ice decreases significantly. Though activity is lower, water ice sublimation driven activity is still measurable out to 5–6 au (Meech & Jewitt 1986). Beyond this distance, the activity of comets must be explained by other mechanisms. Ivanova et al. (2011) summarized various mechanisms to explain the nucleus activity at large heliocentric distances. These are the sublimation of more volatile admixtures, such as CO and/or CO₂ ice (Houpis & Mendis 1981; Luu 1993); polymerization of HCN (Retig 1992); crystallization of the amorphous water ice (Prialnik 1992; Gronkowski & Smela 1998) and annealing of the amorphous water ice (Meech et al. 2009).

The objects of our observation are comets at heliocentric distances larger than 3 au. By the observations, we aimed to investigate the physical properties and activities of distant comets

228P/LINEAR, C/2006 S3 Lowell Observatory Near-Earth-Object Search (LONEOS) and 29P/Schwassmann–Wachmann 1.

Object 228P/LINEAR is not really a ‘distant’ object, but results for this comet are interesting and the data are relatively scarce. It was first discovered by the LINEAR monitoring telescope on 2001 December 17, and designated P/2001 YX_127 (LINEAR) (Green 2002). The comet was recovered by J. Scotti with the Spacewatch II telescope at Kitt Peak on 2009 October 18, it was very slightly diffuse, with a short but faint tail (Green 2009a). The permanent number 228P has been assigned to comet P/2009 U2 = P/2001 YX_127 on 2009 November 11 (Green 2009b).

Object C/2006 S3 (LONEOS) was discovered on 2006 September 19 at a heliocentric distance of 14.29 au by the LONEOS programme based in Flagstaff, Arizona. It presented a diffuse 10 arcsec coma, which was elongated towards the east, but showed no tail (Green 2006). The comet passed its perihelion on 2012 April 16.

Object 29P/Schwassmann–Wachmann 1 was discovered on 1927 November 15 by Arnold Schwassmann and Arno Arthur Wachmann at the Hamburg Observatory in Bergedorf, Germany. Jewitt (1990) noted that the coma of 29P/Schwassmann–Wachmann 1 never disappeared completely since its discovery. Trigo-Rodriguez et al. (2008, 2010) found a clear periodicity of 50 d based on the outbursts recorded from 2002 to 2010. But it is still impossible to predict the time of outburst.

In this paper, we present the results of data processing, the upper limits of the nuclei radii, the surface brightness profiles, the dust production and mass production rates and the colour index.

2 OBSERVATIONS AND DATA PROCESSING

Our observations were carried out with the 1-m optical telescope at Lulin Observatory in Taiwan. Imaging data were obtained with

* E-mail: jshi@pmo.ac.cn

Table 1. Log of all observations.

Comet	q (au)	UT date	R_h (au)	Δ (au)	$\alpha(^{\circ})$	$N_{\text{exp}} \times \text{filter}$	$t_{\text{exp}}(\text{s})$
228P/LINEAR	3.428	2011-04-05	3.474 ^I	3.321	16.7	9 \times B, 9 \times V, 9 \times R	60
		2011-04-06	3.473 ^I	3.334	16.7	10 \times B, 10 \times V, 10 \times R	60
C/2006 S3 (LONEOS)	5.131	2011-04-05	5.860 ^I	6.167	9.1	7 \times B, 7 \times V, 7 \times R	60
		2011-04-06	5.857 ^I	6.147	9.2	15 \times B, 14 \times V, 14 \times R	60
29P/Schwassmann– Wachmann 1	5.743	2011-04-05	6.253 ^O	5.390	5.0	28 \times B, 28 \times V, 28 \times R	60
		2011-04-06	6.253 ^O	5.398	5.1	19 \times B, 19 \times V, 19 \times R	60

Note. q is the perihelion distance; R_h is the heliocentric distance in au; superscripts ‘I’ and ‘O’ refer to whether the comet is inbound (pre-perihelion) or outbound (post-perihelion); Δ is the geocentric distance in au; α is the solar phase angle in degrees; and t_{exp} is the total exposure time in seconds.

an Alta U42 2k \times 2k CCD camera. The camera had a pixel scale of 0.348 arcsec and a field of view (FOV) of 11.9 \times 11.9 arcmin². Conditions were excellent and both two nights were photometric. The seeing measured in the images on the first night varied between 1.0 and 1.4 arcsec, with an average of 1.1 arcsec. The seeing measured in the images on the second night varied between 1.1 and 1.9 arcsec, with an average of 1.1 arcsec.

The images of comets were collected through Asahi broad-band B , V , R filters and in a sequence of BVR, \dots, BVR . The B filter has the effective wavelength $\lambda_e = 4405$ Å and full width at half-maximum (FWHM) of $\Delta\lambda = 1160$ Å, the V filter has $\lambda_e = 5400$ Å and $\Delta\lambda = 850$ Å, the R filter has $\lambda_e = 6578$ Å and $\Delta\lambda = 1215$ Å. During the observations, the telescope was set to track the sidereal motion, with exposure times chosen so that the apparent motion of the comet would be less than 0.4 arcsec, and would thus remain within the seeing disc. The log of all observations is listed in Table 1.

Standard bias subtraction, flat-field correction and cleaning from cosmic ray tracks were performed on all images. The bias value was obtained from an average of several zero-exposure frames. Flat-fields were constructed from dithered images of the twilight sky. To avoid the contaminating effects of the coma, we chose the region far from the nucleus as background sky statistics which was used for photometry in the IRAF task PHOT. To provide absolute photometric calibration, we observed the Landolt photometric standard stars PG1047, PG1323 and SA104. These stars were taken throughout the night. Using the IRAF package PHOTCAL, Landolt standard star measurements gave the zero-point, extinction coefficient and colour term for each filter for each night. These were then used to calculate the magnitudes of the field stars in each frame. Taking the mean of these values gave us a very accurate measurement of the brightness of our comparison stars. Adding this value to each of the differential comet magnitudes gave us accurate calibrated comet magnitudes.

3 COMET MORPHOLOGY

Despite the large heliocentric distance at the time of observation, comets 228P/Linear, C/2006 S3 (LONEOS) and 29P/Schwassmann–Wachmann 1 were easily identifiable and appeared active in every single exposure. To increase the signal-to-noise ratio for the image analysis, we decided to co-add the B , V and R images in order to obtain three ‘final’ images for each filter. We selected the co-added images of comets observed through R filter on April 6 (the first column of Fig. 1) as one representative image and profile for each comet, since there is no obvious morphological difference between filters and between the two nights of observation. Co-added R -band images of the comets were analysed using a radial normalization method (Birkle & Boehnhardt 1992) to reveal

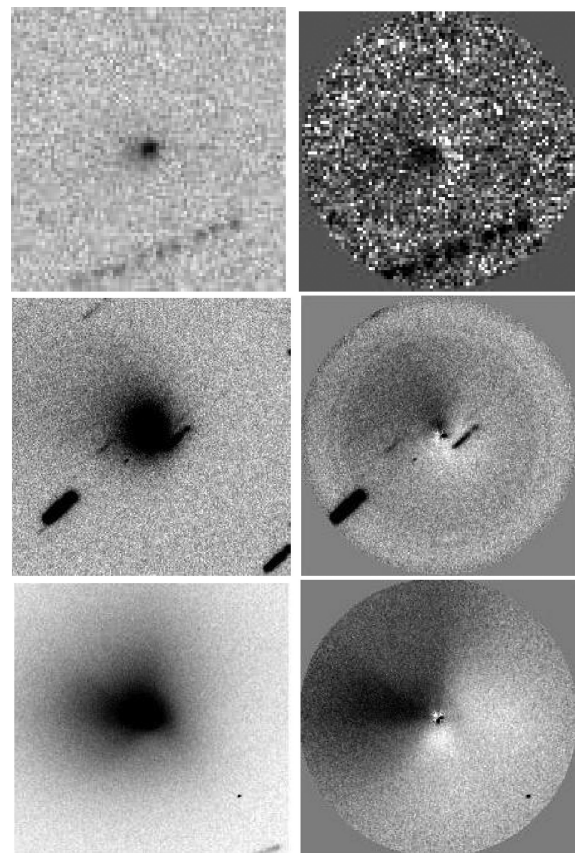


Figure 1. Coma structures of comets 228P/LINEAR (top), C/2006 S3 (LONEOS) (middle) and 29P/Schwassmann–Wachmann 1 (bottom) in the R filter on 2011 April 6. First column shows co-added images, second column shows radial renormalization enhancement of the final images. All images are oriented north-up, east-left. The FOV of 228P/LINEAR is 0.53 \times 0.53 arcmin². The FOVs of C/2006 S3 (LONEOS) and 29P/Schwassmann–Wachmann 1 are 1.29 \times 1.29 arcmin². The scales of the processed images are the same as those of the unprocessed images.

possible structures inside the coma (the second column of Fig. 1). Comet 228P/LINEAR shows a fan-like structure in the south-east quadrant. Comet C/2006 S3 (LONEOS) shows a fan-like structure in the north-east quadrant. For 29P/Schwassmann–Wachmann 1, there is a fan-like structure in the north-east quadrant and three jets emanating from the nucleus and curving right, this is consistent with the nucleus having an anticlockwise rotation as viewed from *Spitzer* (Stansberry et al. 2004).

4 PHOTOMETRY

4.1 Nucleus size

The photometric R magnitude, m_R , can be used to estimate the upper limit of the geometric cross-section of the cometary nucleus, using the expression of Russell (1916) derived for asteroids observed at large phase angle, which, in the case of a spherical object, is given by

$$A_R a_N^2 < 2.24 \times 10^{22} R_h^2 \Delta^2 10^{0.4(m_{\odot} - m_R + \beta\alpha)}, \quad (1)$$

where $A_R = 0.04$ (Lamy et al. 2004) is the geometric albedo, a_N is the radius of the target in (m), R_h is the heliocentric distance in (au), Δ is the geocentric distance in (au), $m_{\odot} = -27.10$ (Holmberg, Flynn & Portinari 2006) is the magnitude of the Sun in the same wavelength band as the observations, α is the phase angle in ($^{\circ}$), $\beta = 0.035$ (Lamy et al. 2004) is the phase coefficient (mag deg^{-1}). An analogous stack that aligns the field stars instead of the comet was used to investigate the best choice of aperture for the photometry. The radius of the photometry aperture is the star's FWHM in these co-added images that aligns the field stars. From the equation (1), we obtain the upper limit of the nucleus radius of comet 228P/LINEAR is $a_N < 4.05$ km and the average R magnitude is $m_R = 20.127 \pm 0.018$; for comet C/2006 S3 (LONEOS), $a_N < 35.75$ km and $m_R = 17.613 \pm 0.008$; for comet 29P/Schwassmann–Wachmann 1, $a_N < 36.25$ km and $m_R = 17.291 \pm 0.008$.

4.2 Surface brightness profiles

The surface brightness profiles of the comets are presented in Fig. 2. Diagonal lines indicate a gradient $m = \frac{d \log B}{d \log \rho}$, where $m = -1$ represents a symmetric steady-state coma model, and $m = -1.5$ represents a solar radiation pressure model. The profiles of comet 228P/LINEAR shows the gradient approaching $m = -1.5$. The profile of comets C/2006 S3 (LONEOS) and 29P/Schwassmann–Wachmann 1 can be divided into two parts, the inner part has a steep brightness gradient, this can be explained as ‘acceleration zone’ (Jewitt & Meech 1987), in which the grains are accelerated to terminal velocity around the nucleus and the grain number density should deviate from the inverse square law. The outer part has the gradient approaching $m = -1.5$.

4.3 $Af\rho$ and mass production rate

The $Af\rho$ value (cm; A'Hearn et al. 1984), is usually used as a proxy for the cometary dust production, and can be estimated using the formalism

$$Af\rho = \frac{4R_h^2 \Delta^2 10^{0.4(m_{\odot} - m_C)}}{\rho}, \quad (2)$$

where A is the average grain albedo, f is the ratio of the cross-section of the dust grains to the total FOV, ρ is the projected radius of the photometric aperture in (cm), m_{\odot} is the solar magnitude in the same band, m_C is the comet integrated magnitude calculated for the aperture of radius ρ . When the cometary coma is in a steady state, $Af\rho$ is an aperture-independent parameter. To determine the radius at which the $Af\rho$ value is begin constant, we calculated the $Af\rho$ parameter for different values of the aperture radius.

The multi-aperture $Af\rho$ values in R band show that the $Af\rho$ values of comet 228P/LINEAR on 2011 April 5 increase suddenly outside 3.2 arcsec, this is caused by nearby stellar contamination. For comet 228P/LINEAR on 2011 April 6 outside 1.7 arcsec and for comet

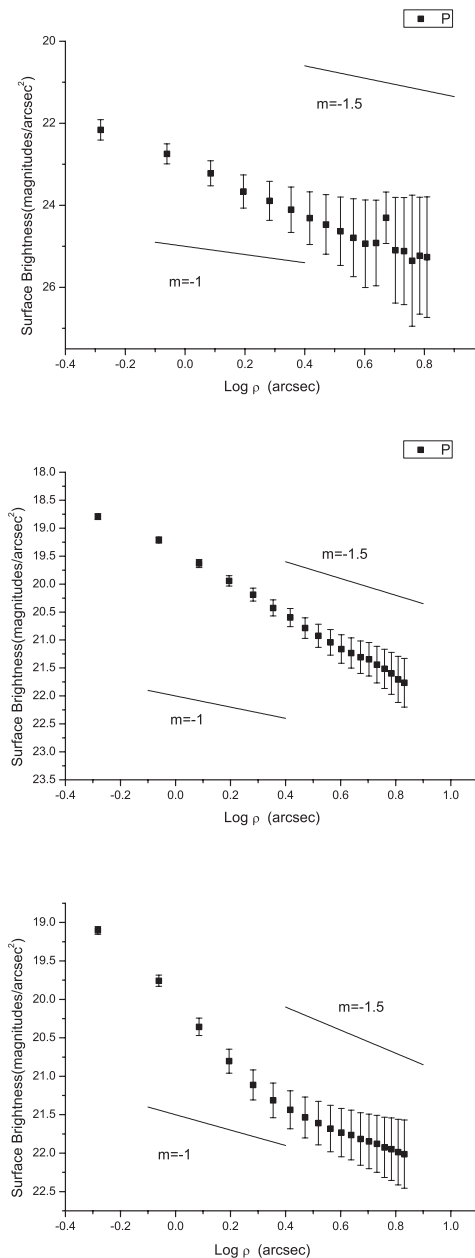


Figure 2. Surface brightness profiles of comets 228P/LINEAR (top), C/2006 S3 (LONEOS) (middle) and 29P/Schwassmann–Wachmann 1 (bottom) in the R filter on 2011 April 6.

C/2006 S3 (LONEOS) on 2011 April 5 and 6 outside 3.13 arcsec, the $Af\rho$ is constant (within the error bars), so depicting a dust environment consistent with a scenario of steady-state emission. But for comet 29P/Schwassmann–Wachmann 1 on both nights, the multi-aperture $Af\rho$ values show that the $Af\rho$ is bulge first then dip, which may indicate a non-steady-state dust emission.

The coma integrated magnitudes, derived for all the filters in a circular aperture of $\rho = 5$ arcsec and the $Af\rho$ values in R band are summarized in Table 2.

Dust production rate can then be used to estimate mass-loss rate Q_{dust} . The formalism is presented by Meech & Weaver (1996)

$$Q_{\text{dust}} = \frac{Af\rho(4a_{\text{dust}}v_{\text{ej}}\sigma)}{3p}, \quad (3)$$

Table 2. Coma magnitude, colours and $Af\rho$ at reference aperture of $\phi = 5$ arcsec.

Comets	ρ (10^5 km)	B band (mag)	V band (mag)	R band (mag)	$B - V$	$V - R$	$Af\rho$ (cm)
228P/LINEAR							
April 5	6.90	19.42 ± 0.03	18.58 ± 0.02	18.26 ± 0.01	0.84 ± 0.04	0.32 ± 0.02	71.4 ± 2.1
April 6	6.93	20.42 ± 0.06	19.64 ± 0.04	18.78 ± 0.02	0.78 ± 0.07	0.83 ± 0.04	44.0 ± 2.3
C/2006 S3 (LONEOS)							
April 5	12.81	17.21 ± 0.01	16.50 ± 0.01	16.06 ± 0.01	0.71 ± 0.01	0.44 ± 0.01	2846.1 ± 54.5
April 6	12.77	17.00 ± 0.01	16.38 ± 0.01	15.97 ± 0.01	0.62 ± 0.01	0.41 ± 0.01	3082.6 ± 43.2
29P/Schwassmann–Wachmann 1							
April 5	11.20	17.16 ± 0.01	16.27 ± 0.01	15.79 ± 0.01	0.89 ± 0.01	0.48 ± 0.01	3617.6 ± 57.4
April 6	11.22	17.03 ± 0.01	16.25 ± 0.01	15.77 ± 0.01	0.78 ± 0.01	0.48 ± 0.01	3713.1 ± 70.6

Note. ρ is linear radius at reference aperture of $\phi = 5$ arcsec and $Af\rho$ is obtained in the R band.

where a_{dust} is a mean dust grains radius, p is the geometric albedo of the dust grains, σ is grain density and v_{ej} is the grain ejection velocity.

Expansion measurements for comet Hale–Bopp in the range $4 \leq r \leq 14$ au infer that the radial outflow speed of dust grains from the nucleus is $v(r) = v_0(r_0/r)^{1/4}$, where $v_0 = 550 \text{ m s}^{-1}$ and $r_0 = 5$ au (Biver et al. 2002). Probstein’s theory (Probstein 1969; Fulle, Cremonese & Bhm 1998) predicts, for spherical grains emitted from a perfectly homogeneous nucleus, a dust velocity is close to 10 per cent of the gas value. Since the Hale–Bopp measurements refer to gas, we adopt a more realistic dust grain ejection velocity $v_{\text{ej}} = v(r)/10$.

The dust size distribution, which a good approximation is obtained by setting a power-law distribution with $q = 3.5$ in a dust grain size range between $a_- = 0.1 \mu\text{m}$ and $a_+ = 1 \text{ cm}$ (Grün et al. 2001). To calculate the dust production rate, we took dust particle radius value of a_{dust} equal to the size of the average dust grain ($a_-a_+)^{1/2} \simeq 30 \mu\text{m}$.

For the dust grain albedo, we assume $p = 0.04$. For the density of the grain material, based on systematic experiments, Niimi et al. (2012) estimated that the average density of the entire sample was $\sigma = 0.49 \pm 0.18 \text{ g cm}^{-3}$, the sample was collected from comet 81P/Wild 2 and returned to Earth by the NASA Stardust mission (Brownlee et al. 2006).

Using equations (2) and (3), we estimated the dust mass production rate of comets. For comet 228P/LINEAR, the mass-loss rate Q_{dust} equals 11.2 kg s^{-1} on 2011 April 5 and 6.9 kg s^{-1} on 2011 April 6, respectively. For comet C/2006 S3 (LONEOS), Q_{dust} equals 345.7 kg s^{-1} on 2011 April 5 and 374.5 kg s^{-1} on 2011 April 6, respectively. For comet 29P/Schwassmann–Wachmann 1, Q_{dust} equals 425.4 kg s^{-1} on 2011 April 5 and 436.6 kg s^{-1} on 2011 April 6, respectively.

The variation of the $Af\rho$ parameter and mass production rate mostly mean the variation of the activity of comets at different epoch. But for comet 228P/LINEAR observed on 2011 April 5 the variation is caused by nearby stellar contamination, we use the data observed on 2011 April 6 only to do analyses hereafter.

4.4 Coma colour

The data obtained during the observations allow us to perform an analysis of the coma colour. Table 2 summarizes the coma B , V , R magnitude and colour at reference aperture of $\phi = 5$ arcsec. The temporal variations of the $B - V$ and $V - R$ colours greater than the photometric uncertainty may be attributed to intrinsic variations

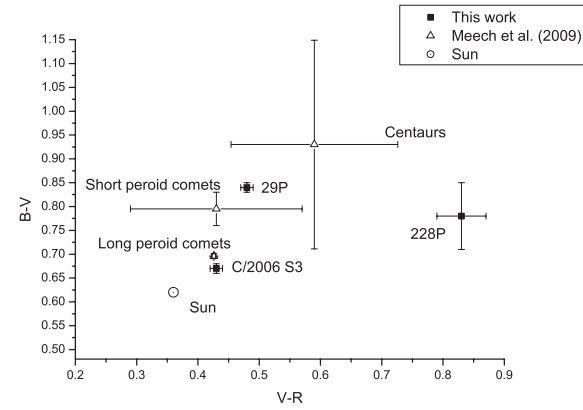


Figure 3. $B - V$ colour plotted against $V - R$ colour for this work (filled square) and other work (triangles). The colour of the Sun is marked (○).

of the coma properties (e.g. composition, dust size distribution) coupled with different observing conditions (Mazzotta Epifani et al. 2011).

Fig. 3 shows broad-band colours $B - V$ versus $V - R$ diagram. The data of this work (filled square) are taken from the average colour indices of Table 2, the solar colour indices (○) used here are $B - V = 0.62$ and $V - R = 0.36$ (Drilling & Landolt 2000), while other data (triangles) are taken from table 6 of Meech et al. (2009). Fig. 3 suggests a trend of increasing ($B - V$) with increasing ($V - R$), implying that the albedo of these nuclei continues to rise through the B , V and R bands. Comparing the coma colour indices we obtained with the solar colour indices, we find that the colours of all three comets are redder than that of the Sun. Comet 228P/Linear is a short-period comet (SP), its colour indices is in the error bars range of average colour indices of SP in $B - V$ but not in $V - R$. Comet C/2006 S3 (LONEOS) is a long-period comet (LP), its colour indices is closer to average colour indices of LP. Comet 29P/ Schwassmann–Wachmann 1 is a Centaur, its colour indices is in the error bars range of average colour indices of Centaur.

5 DISCUSSION

Generally, the values of $Af\rho$ vary within the range between 5 and 5000 cm and are mainly affected by the size of the comet and its distance from the Sun. Comparing the values of $Af\rho$ for all three comets, we find that the activity of comet 228P/LINEAR is much lower than other two comets, which can be explained by the smaller

Table 3. Summary of available broad-band photometry results of comet 29P/Schwassmann–Wachmann 1.

R_h (au)	$Af\rho$ (cm)	Q_{dust} (kg s^{-1})	$B - V$	$V - R$	Number of jets	Reference
6.253 ^O	3665.4	431.0	0.84 ± 0.01	0.48 ± 0.01	3	This work
5.865 ^O	1168					Ivanova et al. (2011)
6.118 ^O	890					Ivanova et al. (2011)
5.865 ^O	7325	365	0.64 ± 0.09	0.54 ± 0.08		Ivanova et al. (2009)
5.967 ^O	4637	182			2–3	Ivanova et al. (2009)
5.919 ^I	16600					Szabo et al. (2002)
5.810 ^I			0.78 ± 0.03	0.50 ± 0.03		Jewitt (2009)
5.886 ^I			0.8	0.502		Hartmann, Cruikshank & DeJewitt (1982)
5.822 ^I		10				Meech et al. (1993)
5.772 ^P		600 ± 300				Jewitt (1990)
5.724 ^P		300 ± 100				Fulle (1992)
5.865 ^O					5–6	Moreno (2009)
6.067 ^O					4–5	Korsun et al. (2008)
6.192 ^O	5000–56 000 ^b					Trigo-Rodriguez et al. (2010)
6.254 ^O	2700–20 000 ^b	22–500				Trigo-Rodriguez et al. (2010)
6.255 ^I	2000–12 500 ^b	16–300				Hosek et al. (2013)
						Hosek et al. (2013)

Note. Superscripts ‘I’ refer to the comet is inbound (pre-perihelion), ‘O’ refer to the comet is outbound (post-perihelion), ‘P’ refer to the comet is at perihelion, ‘^b’ refer to the comet outburst.

size of the comet. Comparing comet C/2006 S3 (LONEOS) with 29P/Schwassmann–Wachmann 1, we find that though the comet 29P/Schwassmann–Wachmann 1 has the same upper limit of the nucleus size and larger distance from the Sun than the comet C/2006 S3 (LONEOS), the activity is higher than C/2006 S3 (LONEOS), which may be indicated the composition difference between two comets.

As there are no publications about comets 228P/LINEAR and C/2006 S3 (LONEOS) at present, we cannot compare the physical properties and activity for these comets with observational data of other observers.

For comet 29P/Schwassmann–Wachmann 1, Meech et al. (1993) summarized the radius of the nucleus lies in the range of 15–44 km as obtained from visual photometry, Stansberry et al. (2004) obtained the nuclear radius is 27 ± 5 km from the analysis of its thermal emission in 2003 November; our value for the upper limit of the nucleus radius lies in this range.

Table 3 summarizes available broad-band photometry results of comet 29P/Schwassmann–Wachmann 1 up to present. From Table 3, we can find that the variation of the $Af\rho$ parameter may be connected with variations in the number of jets. Hosek et al. (2013) obtained that the average quiescent dust production of 29P/Schwassmann–Wachmann 1 is around $Af\rho = 2000$ cm, our value is higher than 2000 cm which indicates the comet is during an outburst phase. Senay & Jewitt (1994) and Crovisier et al. (1995) inferred a CO production rate of $\sim 2000 \text{ kg s}^{-1}$ in comet 29P/Schwassmann–Wachmann 1. The CO production rate exceeds even the larger estimates of dust production, showing that CO is an important driver of activity in comet 29P/Schwassmann–Wachmann 1.

Comet 228P/LINEAR is a Jupiter Family Comet, whose primary driver of activity is sublimation of water ice. Though it was observed at a heliocentric distance of 3.47 au and activity is lower, water ice sublimation driven activity is still possible. For comets C/2006 S3 (LONEOS), it was observed at a heliocentric distance larger than 5 au, water ice sublimation driven activity is impossible, CO sublimation driven activity is a possible mechanism, but we need more observation data to affirm it. Comparing with water ice driven activity, Mazzotta Epifani et al. (2009) concluded

that CO and its associated dust flux are expected to leave the comet nucleus uniformly from all the nucleus surface, its loss rate should be changed very slowly with time after the onset of activity since the source of a CO-driven activity originates from the nucleus interior.

6 CONCLUSIONS

Our observations reveal the activity and physical properties of comet 228P/LINEAR, C/2006 S3 (LONEOS) and 29P/Schwassmann–Wachmann 1 at larger heliocentric distance, including the following:

(i) Comets 228P/Linear, C/2006 S3 (LONEOS) and 29P/Schwassmann–Wachmann 1 were observed to be active at heliocentric distances larger than 3 au.

(ii) The surface brightness profiles of the comets show that all three comets can be explained by a solar radiation pressure model.

(iii) Dust production and mass production rates of three comets were estimated. $Af\rho$ and Q_{dust} of comet 228P/LINEAR were about 44 cm and 6.9 kg s^{-1} , respectively. $Af\rho$ and Q_{dust} of comet C/2006 S3 (LONEOS) were about 2964.4 cm and 360.1 kg s^{-1} , respectively. $Af\rho$ and Q_{dust} of comet 29P/Schwassmann–Wachmann 1 were about 3665.4 cm and 431.0 kg s^{-1} , respectively. The results demonstrate that 228P/LINEAR has a lower activity, while C/2006 S3 (LONEOS) and 29P/Schwassmann–Wachmann 1 have higher activity even at large heliocentric distances.

(iv) The coma colour indices of comet 228P/LINEAR are $B - V = 0.78 \pm 0.07$ and $V - R = 0.83 \pm 0.04$. The average coma colour index of comet C/2006 S3 (LONEOS) are $B - V = 0.67 \pm 0.01$ and $V - R = 0.43 \pm 0.01$. The average coma colour indices of comet 29P/Schwassmann–Wachmann 1 are $B - V = 0.84 \pm 0.01$ and $V - R = 0.48 \pm 0.01$.

(v) For comet 228P/LINEAR, water ice sublimation driven activity is possible. For comet 29P/Schwassmann–Wachmann 1, activity could be explained by the sublimation or the release of CO and/or CO_2 . For comet C/2006 S3 (LONEOS), CO sublimation driven activity is a possible mechanism, but more observation data are needed.

ACKNOWLEDGEMENTS

This work was based on observations obtained at Lulin Observatory whose staff and assistants kindly helped us to finish these observations. We thank David Jewitt for discussions about the manuscript. We acknowledge the support of the National Natural Science Foundation of China (Grant nos. 11003048, and 10933004), CAS Oversea Study & Training Program, Minor Planet Foundation of Purple Mountain Observatory and the exchange program between Finnish Academy (FA) and NSFC.

REFERENCES

- A'Hearn M. F., Schleicher D. G., Feldman P. D., Millis R. L., Thompson D. T., 1984, AJ, 89, 579
- Birkle K., Boehnhardt H., 1992, Earth Moon Planets, 57, 191
- Biver N. et al., 2002, Earth Moon Planets, 90, 5
- Brownlee D. et al., 2006, Science, 314, 1711
- Crovisier J., Biver N., Bockelee-Morvan D., Colom P., Jorda L., Lellouch E., Paubert G., Despois D., 1995, Icarus, 115, 213
- Drilling J. S., Landolt A. U., 2000, in Cox A. N., ed., *Allen's Astrophysical Quantities*. Springer, New York
- Fulle M., 1992, Nature, 359, 42
- Fulle M., Cremonese G., Böhm C., 1998, ApJ, 116, 1470
- Green D. W. E., 2002, IAU Circ., 7828
- Green D. W. E., 2006, IAU Circ., 8752
- Green D. W. E., 2009a, IAU Circ., 9085
- Green D. W. E., 2009b, IAU Circ., 9094
- Gronkowski P., Smela J., 1998, A&A, 338, 761
- Grün E. et al., 2001, A&A, 377, 1098
- Hartmann W. K., Cruikshank D. P., Dejewij J., 1982, Icarus, 52, 377
- Holmberg J., Flynn C., Portinari L., 2006, MNRAS, 367, 449
- Hosek M. W., Jr, Blaauw R. C., Cooke W. J., Suggs R. M., 2013, AJ, 145, 122
- Houpis H. L. F., Mendis D. A., 1981, Moon Planets, 25, 397
- Ivanova A. V., Korsun P. P., Afanasiev V. L., 2009, Sol. Syst. Res., 43, 453
- Ivanova O. V., Skorov Y. V., Korsun P. P., Afanasiev V. L., Blum J., 2011, Icarus, 211, 559
- Jewitt D., 1990, ApJ, 351, 277
- Jewitt D., 2009, ApJ, 137, 4296
- Jewitt D., Meech K. J., 1987, ApJ, 317, 992
- Korsun P. P., Ivanova O. V., Afanasiev V. L., 2008, Icarus, 198, 465
- Lamy P. L., Toth I., Fernandez Y. R., Weaver H. A., 2004, in Festou M. C., Keller H. U., Weaver H. A., eds, *Comets II, The Sizes, Shapes, Albedos, and Colors of Cometary Nuclei*. Univ. Arizona Press, Tucson, AZ, p. 223
- Luu J. X., 1993, PASP, 105, 946
- Mazzotta Epifani E., Palumbo P., Capria M. T., Cremonese G., Fulle M., Colangeli L., 2007, MNRAS, 381, 713
- Mazzotta Epifani E., Palumbo P., Capria M. T., Cremonese G., Fulle M., Colangeli L., 2008, MNRAS, 390, 265
- Mazzotta Epifani E., Palumbo P., Capria M. T., Cremonese G., Fulle M., Colangeli L., 2009, A&A, 502, 355
- Mazzotta Epifani E., Dall'Ora M., di Fabrizio L., Licandro J., Palumbo P., Colangeli L., 2010, A&A, 513, A33
- Mazzotta Epifani E., Dall'Ora M., Perna D., Palumbo P., Colangeli L., 2011, MNRAS, 415, 3097
- Meech K. J., Hainaut O. R., 2001, in Marov M. Y., Rickman H., eds, *Collisional Processes in the Solar System*. Kluwer, Dordrecht, p. 261
- Meech K. J., Jewitt D. C., 1986, Icarus, 66, 561
- Meech K. J., Svoren J., 2004, in Festou M. C., Keller H. U., Weaver H. A., eds, *Comets II, Using Cometary Activity to Trace the Physical and Chemical Evolution of Cometary Nuclei*. Univ. Arizona Press, Tucson, AZ, p. 317
- Meech K. J., Weaver H. A., 1996, Earth Moon Planets, 72, 119
- Meech K. J., Belton M. J. S., Mueller B. E. A., Dicksion M. W., Li H. R., 1993, AJ, 106, 1222
- Meech K. J. et al., 2009, Icarus, 201, 719
- Moreno F., 2009, ApJS, 183, 33
- Niimi R. et al., 2012, ApJ, 744, 18
- Prialnik D., 1992, ApJ, 388, 196
- Probstein R. F., 1969, in Bisshop F. et al., *Problems of Hydrodynamics and Continuum Mechanics*. Soc. Indust. Appl. Math., Philadelphia, PA, p. 568
- Rettig T. W., Tegler S. C., Pasto D. J., Mumma M. J., 1992, ApJ, 398, 293
- Russell H. N., 1916, ApJ, 43, 173
- Senay M. C., Jewitt D. C., 1994, Nature, 371, 229
- Snodgrass C., Lowry S. C., Fitzsimmons A., 2008, MNRAS, 385, 737
- Stansberry J. A. et al., 2004, ApJS, 154, 463
- Szabo Gy. M., Kiss L. L., Sarnecky K., Sziladi K., 2002, A&A, 384, 702
- Trigo-Rodriguez J. M., Garca-Melendo E., Davidsson B. J. R., Snchez A., Rodriguez D., Lacruz J., de Los Reyes J. A., Pastor S., 2008, A&A, 485, 599
- Trigo-Rodriguez J. M., Garca-Hernndez D. A., Snchez A., Lacruz J., Davidsson B. J. R., Rodriguez D., Pastor S., de Los Reyes J. A., 2010, MNRAS, 409, 1682
- Whipple F. L., 1950, ApJ, 111, 375

This paper has been typeset from a \TeX / \LaTeX file prepared by the author.

Are There Any Ultra-Long Period Cepheids in M31?

Chien-Hsiu Lee,^{1,2} Chow-Choong Ngeow,¹ and PTF Collaboration

¹*Graduate Institute of Astronomy, National Central University, Jhongli 32001, Taiwan*

²*University Observatory Munich, Scheinerstrasse 1, 81679 Munich, Germany*

Abstract. Ultra long period Cepheids (ULPCs) are classical Cepheids with period longer than 80 days. These ULPCs followed a different period-luminosity (P-L) relation than their shorter period counterparts, and has the potential to be used as standard candles to determine distances out to 100Mpc. Until today, only about 40 ULPCs have been identified in 10 nearby galaxies, excluding M31. Since M31 is one of the nearest spiral galaxy, which serves as a local benchmark to calibrate the distance scale ladder, the ULPCs found in this galaxy can be used to calibrate the ULPC's P-L relation. We therefore performed a comprehensive search of ULPCs in M31 by using the data from the Palomar Transient Factory (PTF) project. The imaging data from PTF spanned about 3 years, usually with daily sampling when M31 is visible in the sky, makes it an ideal dataset to search for the ULPCs. Eight candidates have been found based on the difference imaging analysis, with three of them are most likely ULPCs. Data based on the follow-up *VI*-band observations from P60 and LOT will be used to confirm ULPC nature of these candidates.

1. Introduction: The Ultra-Long Period Cepheids

Classical Cepheids (hereafter Cepheids) are radially pulsating variable stars with period range from ~ 1 to ~ 100 days. Cepheids obey the famous period-luminosity (P-L) relation (also known as the Leavitt Law). The calibrated P-L relation is considered a standard candle, and it is a crucial rung of the distance scale ladder (that connects local distance indicators to cosmic distance indicators). Cepheid distances to nearby galaxies, via the P-L relation, can be used to calibrate a host of secondary distance indicators and hence determining the Hubble constant for galaxies located within the Hubble flow.

In extra-galactic distance scale work, Cepheids with period (P) longer than ~ 80 days are generally ignored for two reasons. It has been known that these very long period Cepheids showed up as outliers in the P-L plot (for example, see Figure 7 in Freedman 1988). Furthermore, observing strategies for extra-galactic Cepheids using *Hubble Space Telescope* generally focused on Cepheids with periods from 10 to ~ 60 days, and hence Cepheids with $P > 80$ days are ignored. However, Bird et al. (2009) proposed that these very long period Cepheids follow a different P-L relation than their shorter period counterparts, and called them the ultra-long period Cepheids (ULPCs). These ULPCs are not a new class of variables but represent a sub-class of Cepheids, as they also populated the instability strip on the color-magnitude diagram (CMD, see Bird et al. 2009; Fiorentino et al. 2013). The mass for ULPCs was estimated to range

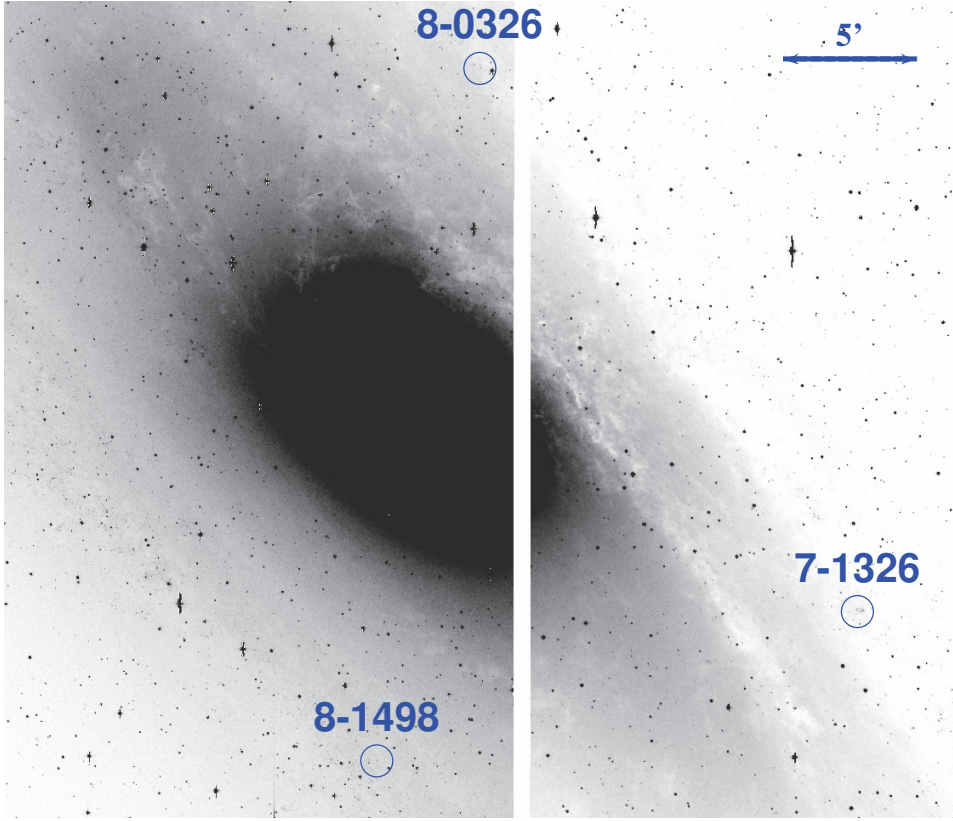


Figure 1. Locations of our 3 most promising ULPC candidates in the R -band PTF images.

from $\sim 15M_{\odot}$ to $\sim 20M_{\odot}$ by using evolutionary tracks from stellar evolution models (Fiorentino et al. 2013). The ULPCs have $M_V \sim -7$ mag. to -9 mag., which are ~ 2 magnitude brighter than the shorter period Cepheids, suggest that they can be used to derive distance to galaxies that are well within the Hubble flow (~ 100 Mpc and beyond) by using next generation 30m-class telescopes, and hence determining the Hubble constant in a single step (Fiorentino et al. 2013) without calibrating the secondary distance indicators.

2. Searching of ULPCs in M31 with PTF

The host galaxies for the current sample of ULPCs, as given in Fiorentino et al. (2012), do not include M31 – the nearest spiral galaxy from us. Past variability surveys of M31 either do not span long enough to find ULPCs or these surveys only cover small patches of M31, hence no ULPCs have been identified in M31 to-date. Since M31 has the potential to be a local anchoring galaxy for the extra-galactic distance scale ladder (see Vilardell et al. 2010, and reference therein), there is a strong motivation to identify ULPCs in M31.

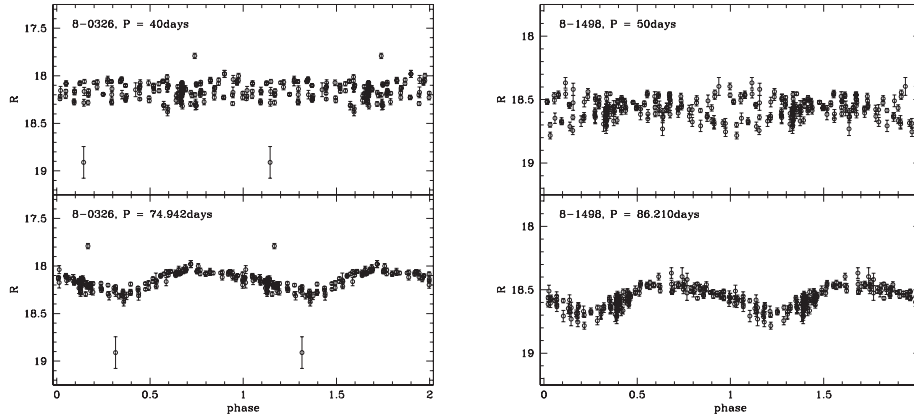


Figure 2. Comparison of the folded light curves with published periods (*top panels*, periods adopted from Magnier et al. 1997) and the periods found by us (*bottom panels*) for the two most promising ULPC candidates in M31.

To search for ULPCs in M31, we use the imaging data taken from Palomar Transient Factory (PTF, Law et al. 2009; Rau et al. 2009). This is because the large field-of-view from PTF data (~ 7 deg-squared), together with (up to) daily observing cadence, make PTF data ideal for searching the ULPCs in M31. We used the *R*-band data taken with P48 Telescope that span from January 2010 to 2012 (total 172 frames) for our purpose. These data have been reduced by the PTF team prior to download. Image subtraction technique and several selection criteria were used to identify ULPC candidates in M31 (Lee et al. 2013). We initially identified 8 ULPC candidates, however further analysis revealed that only 3 of them could be ULPCs and other 5 candidates are most likely belong to long period variable stars (such as Miras, see Lee et al. 2013). Figure 1 shows the location of the 3 most promising ULPC candidates with respect to M31 in the PTF image. Two out of these three candidates have been detected in Magnier et al. (1997), however the time span of their observations was not long enough to correctly determine the periods (see Figure 2).

3. Follow-Up Observations with P60 and LOT

Follow-up time series observations in *V*- and *I*-band are needed to confirm the ULPC nature of these 8 candidates. By adopting the distance and extinction to M31, the *VI*-band photometry for these candidates can be compared to other ULPCs in the *VI*-band P-L relations and CMD. The follow-up observations have been carried out with the P60 Telescope (*f*/8.75) at Palomar Observatory (USA) and the Lulin One-meter Telescope (LOT, *f*/8) at Lulin Observatory (Taiwan) from October 2012 to January 2013. The P60 telescope was equipped with a 2048×2048 CCD with a pixel scale of $0.38''/\text{pixel}$ (Cenko et al. 2006); LOT was equipped with a 1340×1300 CCD, which has a pixel scale of $0.52''/\text{pixel}$ (Kinoshita et al. 2005). Observations with both telescopes were done in queue-mode, at which the pre-scheduled observations were carried out when weather permitted. Figure 3 shows the seeing distributions based on the images taken from these two telescopes. All the imaging data has been processed, with instrumental

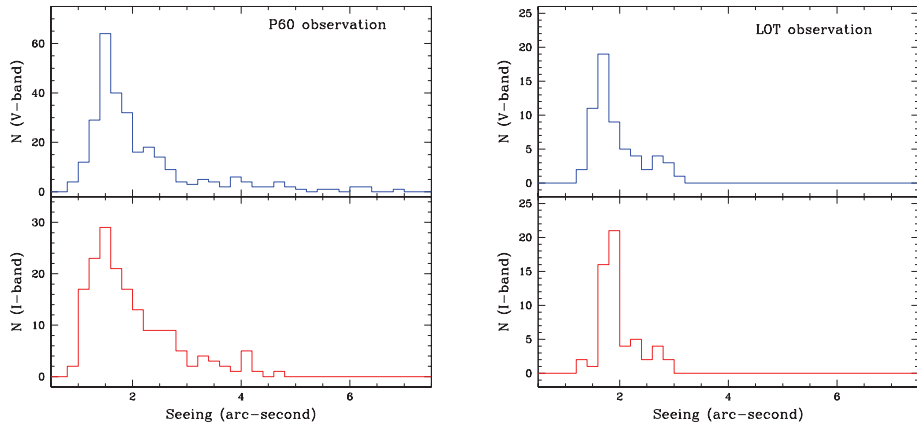


Figure 3. Seeing distributions from the P60 (*left panels*) and LOT (*right panels*) observations.

magnitudes extracted based on PSF photometry. Currently we are working on calibrating the magnitudes using catalogs from Massey et al. (2006), and the final results will be presented elsewhere in near future.

Acknowledgments. We acknowledge the support from NSC grants NSC101-2112-M-008-017-MY3 & NSC101-2119-M-008-007-MY3.

References

- Bird, J. C., Stanek, K. Z., & Prieto, J. L. 2009, ApJ, 695, 874
 Cenko, S. B., Fox, D. B., Moon, D.-S., et al. 2006, PASP, 118, 1396
 Fiorentino, G., Clementini, G., Marconi, M., et al. 2012, Ap&SS, 341, 143
 Fiorentino, G., Annibali, F., Clementini, G., et al. 2013, IAU Symposium, 289, 282
 Freedman, W. L. 1988, ApJ, 326, 691
 Kinoshita, D., Chen, C.-W., Lin, H.-C., et al. 2005, Chinese Journal of Astronomy and Astrophysics, 5, 315
 Law, N. M., Kulkarni, S. R., Dekany, R. G., et al. 2009, PASP, 121, 1395
 Lee, C.-H., Ngeow, C.-C., Yang, T.-C., et al. 2013, Submitted to IEEE Xplore for Icon-Space2013 Conference
 Magnier, E. A., Augusteijn, T., Prins, S., van Paradijs, J., & Lewin, W. H. G. 1997, A&AS, 126, 401
 Massey, P., Olsen, K. A. G., Hodge, P. W., et al. 2006, AJ, 131, 2478
 Rau, A., Kulkarni, S. R., Law, N. M., et al. 2009, PASP, 121, 1334
 Vilardell, F., Ribas, I., Jordi, C., et al. 2010, A&A, 509, A70

Detection of large color variation in the potentially hazardous asteroid (297274) 1996 SK

Chien-Hsien Lin¹, Wing-Huen Ip^{1,2}, Zhong-Yi Lin², Fumi Yoshida³ and Yu-Chi Cheng²

¹ Space Science Institute, Macau University of Science and Technology, Avenida Wai Long, Taipa, Macau; chlin@must.edu.mo

² Institute of Astronomy, National Central University, Zhongli, Taoyuan 32049

³ National Astronomical Observatory, Osawa, Mitaka, Tokyo 181-8588, Japan

Received 2013 April 20; accepted 2013 September 5

Abstract Low-inclination near-earth asteroid (NEA) (297274) 1996 SK, which is also classified as a potentially hazardous asteroid, has a highly eccentric orbit. It was studied by multi-wavelength photometry within the framework of an NEA color survey at Lulin Observatory. Here, we report the finding of large color variation across the surface of (297274) 1996 SK within one asteroidal rotation period of 4.656 ± 0.122 hours and classify it as an S-type asteroid according to its average colors of $B - V = 0.767 \pm 0.033$, $V - R = 0.482 \pm 0.021$, $V - I = 0.801 \pm 0.025$ and the corresponding relative reflectance spectrum. These results might be indicative of differential space weathering or compositional inhomogeneity in the surface materials.

Key words: minor planets, asteroids: individual: PHA (297274) — techniques: photometric

1 INTRODUCTION

The main asteroid belt, located between the orbits of Mars and Jupiter, is composed of a population of small bodies with a primitive composition. The largest member, (1) Ceres, with a diameter of 914 km, will be visited by the DAWN spacecraft in 2015. In addition to (1) Ceres, the other asteroids, (2) Pallas (544 km), (4) Vesta (525 km) and (10) Hygiea (431 km) are the most massive examples, which might be classified as dwarf planets. Smaller objects, in the range down to km and sub-km, are mostly ejecta from impact cratering and/or catastrophic fragments via a collisional process (Bottke et al. 2002, 2005). Yoshida et al. (2004) discussed in detail the collisional evolution of asteroid families using the young Karin family as an example. They pointed out that photometric measurements of members of an asteroid family could provide important clues about the corresponding orbital evolution, internal composition and surface effects due to the process of space weathering (Clark et al. 2002; Sasaki et al. 2001). Because of the long-term gravitational perturbations of Jupiter and Saturn, some of the collisional fragments could be injected into orbits intercepting the orbits of terrestrial planets, which could potentially cause surface impact events. These scattered stray bodies are further classified as Amor asteroids if their perihelion distances (q) are between 1.3 AU and 1.017 AU, Apollo asteroids if their semi-major axis $a > 1.0$ AU and $q < 1.017$ AU, and Aten asteroids if $a < 1.0$ AU and the aphelion distance $Q > 0.983$ AU. As shown by Bottke et al. (2002),

the majority of these asteroids that cross the orbits of terrestrial planets come from the inner asteroid belt, even though some of them could have originated from the middle or outer asteroid belt, or from a comet.

Among the near-earth asteroids (NEAs), which are the general term for the Apollo and Aten asteroids, a number of them have non-zero probability of hitting Earth in the future. For example, it has been estimated that the total number of a subgroup of NEAs called potentially hazardous asteroids (PHAs) with $D > 100$ m is approximately 4700 ± 1450 (Mainzer et al. 2012). Close monitoring and in-depth investigations of the basic physical properties of PHAs, like sizes, shapes and compositions, are therefore important. In addition, PHAs could also represent a source of very valuable natural resources for space exploration and utilization because of their relatively easy access. With these key issues in mind, we have initiated a cooperative project at the Space Science Institute, Macau University of Science and Technology, together with the Astronomy Institute, National Central University, to produce a photometric survey of the taxonomical types of NEAs in low inclination orbits. In this work we report the results of an interesting object, (297274) 1996 SK, which is both an Apollo asteroid and PHA, based on observations taken on 2012 May 22 and 23, at Lulin Observatory, Taiwan. The observations are described in Section 2. The results of the data analysis are given in Section 3. In Section 4, a summary and discussion on the implications of the physical properties of the color variation will be given.

2 OBSERVATIONS

The criteria for selecting our first set of observational targets are (1) lack of prior measurements for the lightcurves and surface color, and (2) suitability of their optical brightness for time-series photometry. Asteroid (297274) 1996 SK has an absolute magnitude $H_v = 16.866$, with a semi-major axis $a = 2.434$ AU, eccentricity $e = 0.794$ and inclination $i = 1.962^\circ$. It was close to opposition and satisfied these conditions in May, 2012. With its perihelion distance of $q = 0.5$ AU and low inclination, (297274) 1996 SK is classified as a PHA. It was observed on 2012 May 22 and 23 by multi-filter photometry using the Lulin one-meter telescope (LOT). The CCD camera used for imaging was the PI-1300B, which has 1340×1300 pixels with an effective pixel scale of $0.516''$.

The observational log is given in Table 1. The filters used were broadband Bessel $BVRI$, which have central wavelengths of 442, 540, 647 and 786 nm, respectively. The R -band exposure time was 60 seconds per frame and the measurement sequence consisted of 20 continuous frames for each run. In total, seven runs were made. However, due to unstable weather on May 23, much fewer data were acquired. Three sets of B , V and I filter measurements were made in the first half night of May 22, and another set was made in the next night. The Landolt standard star fields used for color calibration were SA107 on May 22 and SA109 on May 23 (Landolt 1992). The calibrated absolute magnitudes and colors of each star are listed in Table 2. The photometric accuracy is 0.044 on average. All targets were observed with airmass between 1.2 and 2.0 during the nights.

The standard method of data processing was performed by using the IRAF program (Image Reduction and Analysis Facility, supplied by National Optical Astronomy Observatories) with the *ccdproc* package for image reduction, *apphot* for photometry and *photcal* for flux calibration with standard stars.

Table 1 Observation Log of (297274) 1996 SK

Instrument	Filter	Exposure	Date	r^*	Δ^*	$\Phi^*(^\circ)$	Airmass
LOT	B, V, R, I	60 s/frame	2012 May 22	1.454	0.443	4.218	1.28–1.97
		60 s/frame	2012 May 23	1.467	0.456	4.987	1.28–1.53

Notes: * The quantity on 16:00 UT of each date; r : Heliocentric distance (AU); Δ : Geocentric distance (AU); Φ : The phase angle of Sun-target-observer.

Table 2 Mean Calibrated Absolute V -band Magnitudes and Colors of Landolt Standard Stars Observed on 2012 May 22 and 23

Star	V^α	V^β	$(B - V)^\alpha$	$(B - V)^\beta$	$(V - R)^\alpha$	$(V - R)^\beta$	$(V - I)^\alpha$	$(V - I)^\beta$
107 459	12.284	12.252	0.900	0.915	0.525	0.370	1.045	0.940
107 457	14.910	14.887	0.792	0.830	0.494	0.507	0.964	0.971
107 456	12.919	12.875	0.921	0.918	0.537	0.549	1.015	1.035
107 592	11.847	11.895	1.318	1.204	0.709	0.389	1.357	1.050
107 599	14.675	14.671	0.698	0.727	0.433	0.463	0.869	0.898
107 600	14.884	14.863	0.503	0.540	0.339	0.358	0.700	0.715
107 601	14.646	14.632	1.412	1.441	0.923	0.949	1.761	1.787
107 602	12.116	12.116	0.991	0.934	0.545	0.367	1.074	0.962
109 949	12.828	12.829	0.806	0.805	0.500	0.503	1.020	1.024
109 954	12.436	12.435	1.296	1.305	0.764	0.756	1.496	1.491
109 956	14.639	14.644	1.283	1.269	0.779	0.788	1.525	1.533

α : Magnitudes and color indices from Landolt (1992); β : Mean values measured from this study.

3 RESULTS

Figure 1 shows the raw lightcurves of (297274) 1996 SK observed on May 22 and 23. Differential photometry was acquired from the reference stars, which do not show variability over time. The reference stars were chosen so that they have R -band magnitude brighter than 17.0 in the USNO-A2.0 catalog.

Using the Plavchan algorithm (Plavchan et al. 2008) to compute the periodogram, the spin period of (297274) 1996 SK was found to be 4.656 ± 0.122 hours. The uncertainty in the frequency was estimated based on the method of Horne & Baliunas (1986). The periodogram and the folded lightcurve from the R -band measurements along with the rotation phase are shown in Figure 2. The lightcurve shows that (297274) 1996 SK has a rather smooth configuration. For an asteroid that has an ellipsoidal shape, the peak-to-peak variation (Δm) of the lightcurve can be used to calculate the ratio of the long axis to short axis (a/b) according to the formula $\Delta m = 2.5 \log(a/b)$.

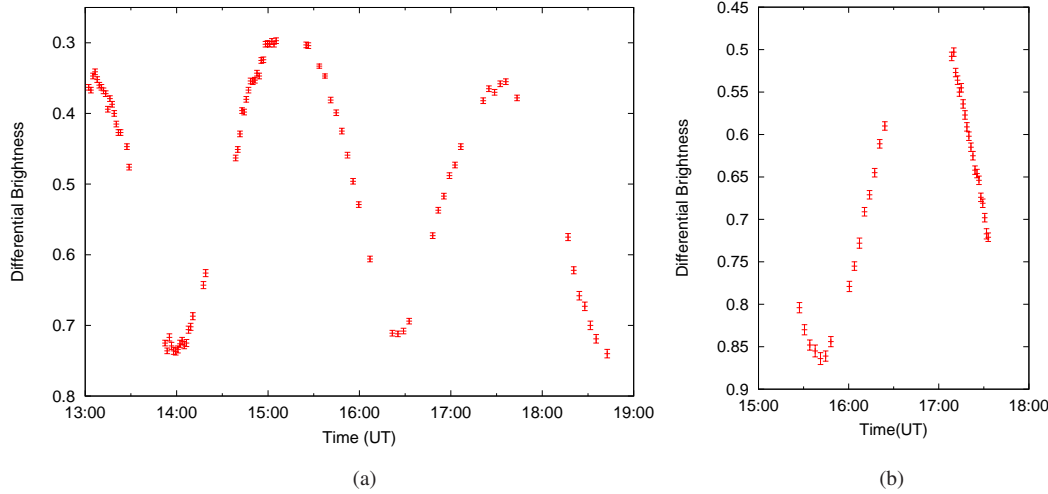


Fig. 1 The diagrams are the raw lightcurves of (297274) 1996 SK on (a) 2012 May 22 in terms of Universal Time (UT) and (b) 2012 May 23.

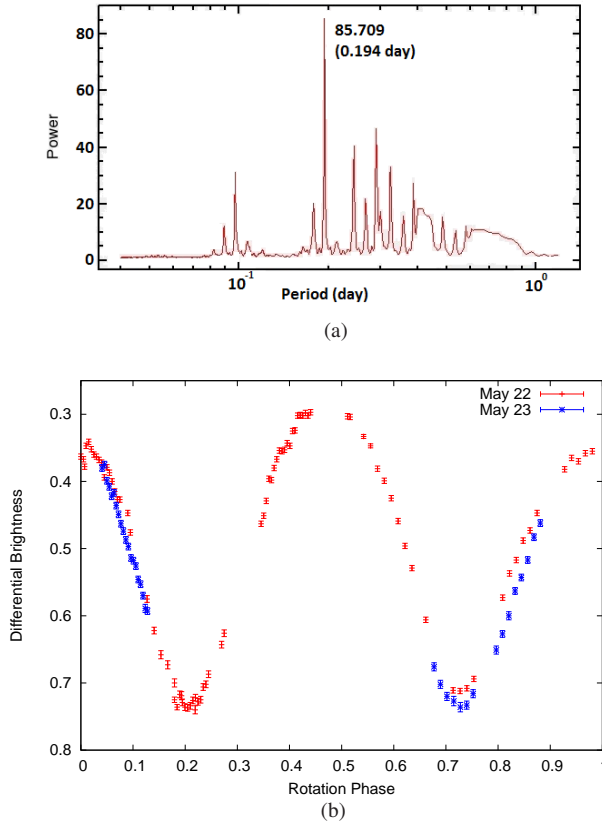


Fig. 2 The periodogram (a) and folded lightcurve (b) of (297274) 1996 SK consisting of both the data on 2012 May 22 and 23. The differential brightness is normalized to be consistent over two days.

From the lightcurve of (297274) 1996 SK, Δm was 0.44, which means that a/b is about 1.50. However, since the above a/b value is obtained by assuming that the asteroid was observed at an aspect angle (i.e., the angle between the line of sight and spin axis) of 90° , the actual axial ratio (a/b) may be more than that. The diameter of the asteroid (D) can be calculated by using the formula $\log D = 3.130 - 0.5 \log A - 0.2H$, where H is the absolute magnitude and A is the surface albedo (Yoshida et al. 2004). Assuming $A = 0.2$ (corresponding to the mean albedo of S-type asteroids) and $H = 16.866$ mag for (297274) 1996 SK, its diameter is 1.28 km. The long axis and the short axis can be computed to be 1.57 km and 1.05 km, respectively.

Table 3 summarizes the results of color measurements obtained on March 22 and 23. The multi-wavelength observations of (297274) 1996 SK at several different times allow us to estimate the color indices and to examine possible changes in its surface color during rotation.

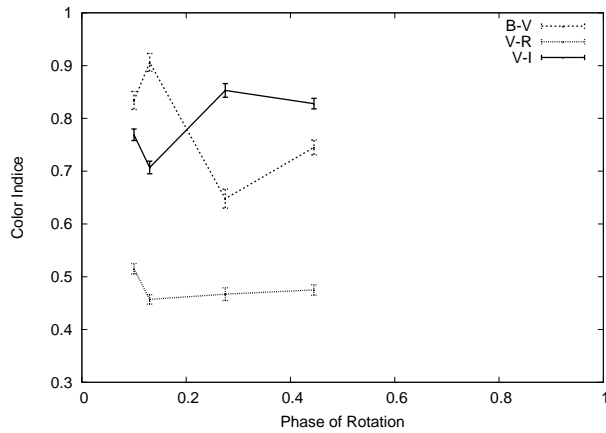
Figure 3 displays the color variations at four phases of rotation observed on the two days. It reveals that both $B - V$ and $V - I$ colors vary significantly, but the change in $V - R$ is comparatively small. The maximum changes between the phase 0 to 0.5 for $B - V$, $V - R$ and $V - I$ are 0.258, 0.058 and 0.146, respectively. Such a large range of color variation indicates the possible presence of surface heterogeneity on (297274) 1996 SK.

The brightness magnitudes of the B , V and I bands follow the general trend of the R -band lightcurve. The average values of $B - V = 0.767 \pm 0.016$, $V - R = 0.482 \pm 0.021$ and $V - I = 0.700 \pm 0.021$.

Table 3 A Summary of the Color Measurements of (297274) 1996 SK on 2012 May 22 and 23

UT_V	V	$B - V$	$V - R$	$V - I$	Airmass*
May 22					
13:30:36	16.259 ± 0.006	0.840 ± 0.012	0.520 ± 0.007	0.769 ± 0.008	1.553
13:31:58	16.270 ± 0.006	0.835 ± 0.012	0.511 ± 0.007	0.769 ± 0.008	1.546
14:20:46	16.390 ± 0.007	0.652 ± 0.013	0.459 ± 0.009	0.847 ± 0.009	1.373
14:22:10	16.386 ± 0.006	0.644 ± 0.012	0.475 ± 0.008	0.859 ± 0.008	1.370
15:07:03	16.063 ± 0.005	0.748 ± 0.010	0.472 ± 0.007	0.827 ± 0.007	1.297
15:08:26	16.065 ± 0.005	0.741 ± 0.010	0.478 ± 0.007	0.832 ± 0.007	1.296
May 23					
17:34:31	16.495 ± 0.007	0.906 ± 0.017	0.457 ± 0.009	0.707 ± 0.012	1.523
Mean	16.275 ± 0.016	0.767 ± 0.033	0.482 ± 0.021	0.801 ± 0.023	

Notes: * The airmass is displayed for the time when the V -band was observed because the $BVRJ$ observations in each color measurement were obtained in sequential order during a short time interval of 11 min.

**Fig. 3** Surface color variations of PHA (297274) 1996 SK over the phase of rotation.

$I = 0.801 \pm 0.025$ for (297274) 1996 SK can be compared with the known colors from different taxonomies of NEAs determined by previous observations archived in the “Data Base of Physical and Dynamical Properties of NEAs” published by the European Asteroid Research Node. These results are plotted in Figure 4, which shows the $B - V$ and $V - R$ terms that are generally classified into S-group (S, Q, R-types etc.), X-group (X, E-types etc.) and C-group (C, F, B-types etc.) of NEAs. This indicates that the surface color of (297274) 1996 SK is located on the boundary between S-group and X-group asteroids.

Figure 5 illustrates the average relative reflectance spectrum of (297274) 1996 SK obtained by subtracting the solar colors $B - V = 0.665$, $V - R = 0.367$ and $V - I = 0.705$ (Howell 1995) from its colors. It falls into the spectral region of S-type asteroids, so (297274) 1996 SK should be classified as a member of S-type objects. It is interesting to note that Rabinowitz (1998) reported color measurements of (297274) 1996 SK in October, 1996 with $V - R = 0.430 \pm 0.070$ and $V - I = 0.678 \pm 0.0587$. These values are close to the corresponding results obtained on May 23 (see Table 3 and Fig. 6), which are closer to the spectra of Q-type asteroids, but there are still significant differences from values taken at other times. The possible implication will be discussed later.

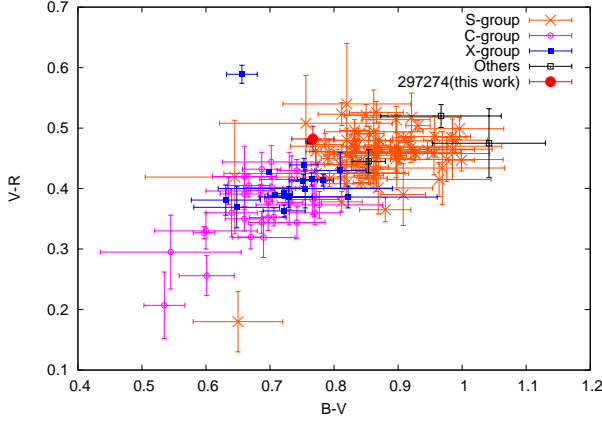


Fig. 4 The color-color diagram of NEAs with known color indices in different taxonomic types [α] and (297274) 1996 SK observed from this work. α means all references listed below (Betzler et al. 2010; Carbognani 2008; Dandy et al. 2003; Hapke 2000; Hergenrother et al. 2009; Hicks et al. 2011a,b, 2012a,b,c,d,e,f,g,h; Hicks & Dombroski 2012; Hicks et al. 2013a,b; Jewitt & Hsieh 2006; Jewitt 2013; Karashevich et al. 2012; Pieters et al. 2000; Ye 2011).

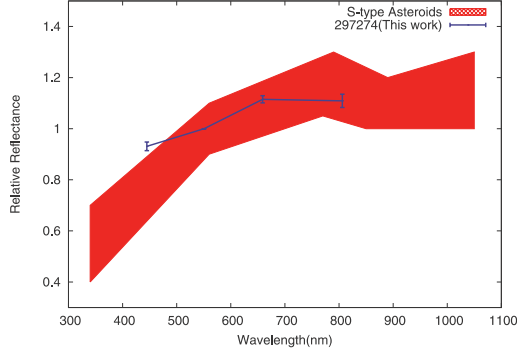


Fig. 5 Relative reflectance spectrum of (297472) 1996 SK from our data (thick line) in comparison with integrated spectra of S-type asteroids from data archived by the “Small Bodies Node.” The shaded area indicates the range of spectra from S-type asteroids.

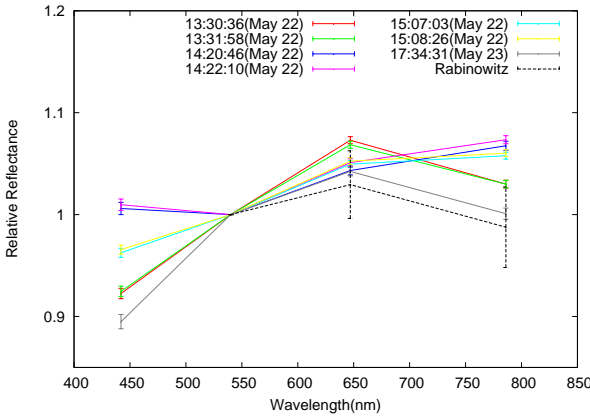


Fig. 6 A comparison of the relative reflectance spectra of (297274) 1996 SK taken at different times on March 22 and 23 with what was reported by Rabinowitz (1998).

4 SUMMARY AND DISCUSSION

Our observations of PHA (297274) 1996 SK at opposition in May, 2012 lead to the following conclusions:

- (1) The rotation period of this asteroid is found to be 4.656 ± 0.122 hours, i.e., well below the spin cutoff of 2.2 hours.
- (2) The amplitude of lightcurve variability is $\Delta m = 0.44$ indicating an elongated shape with the ratio of the long axis to the short axis (a/b) = 1.50, but this is possibly underestimated.
- (3) The average color indices of $B - V = 0.767 \pm 0.033$, $V - R = 0.482 \pm 0.021$, $V - I = 0.801 \pm 0.025$ and the corresponding surface reflectance means that (297274) 1996 SK belongs to the S-type taxonomic class. With the surface albedo assumed to be 0.2, which is a typical value of S-type asteroids, and $H_v = 16.866$, the projected long and short axes are 1.57 km and 1.05 km, respectively.
- (4) Over the rotation range of 133° , (297274) 1996 SK displays significant color changes which might imply the existence of a large change in mineralogical and/or compositional variation on its surface.

The detection of a large change in color is an important result of this work because it could mean that (297274) 1996 SK might contain various properties in its surface spectra. Because there is no information on the relation between the color measurements and the rotational phase in the work of Rabinowitz (1998), it is difficult to analyze the cause of these differences in color between our present results and his work. One thing is nearly certain; they could not be caused by a short-term effect of space weathering since the associated timescale is at least on the order of a million years (Vernazza et al. 2009). From this point of view, the existence of an inhomogeneous surface composition or the effect of differential space weathering would be the most viable explanation. The first scenario would mean that (297274) 1996 SK might contain the interface material from some differentiated region of its parent body after an impact disruption. The second scenario has been discussed by Yoshida et al. (2004) in the case of the color variation of (832) Karin – see also Sasaki et al. (2004, 2006a), Sasaki et al. (2006b) and Ito & Yoshida (2007). This could have come about by the process of micrometeoroid impact on young and older surface areas (Clark et al. 2002; Sasaki et al. 2004).

Figure 6 shows a comparison of relative reflectance spectra observed in different times, which vary from S-type to Q-type. It might be also related to the second scenario in that the asteroid has two parts, which are composed of weathered and un-weathered surfaces. It is a possibility that Rabinowitz (1998) measured the colors in the vicinity of the phase which we observed on May 23. Both possibilities mean that (297274) 1996 SK should not be covered by a homogeneous regolith layer of small particles. Could this surface cleansing be achieved by tidal breakup in previous close encounters with Earth or other terrestrial planets as proposed by Nesvorný et al. (2010)? These are issues we plan to investigate in the future.

Acknowledgements This work was partially supported by Project 019/2010/A2 of the Macau Science and Technology Development Fund: MSAR No. 0166 and Taiwan Ministry of Education under the Aim for Top University Program NCU. Lulin Observatory is operated by the Institute of Astronomy, National Central University, Taiwan, under grant NSC 96-2752-M-008-011-PAE.

References

- Betzler, A. S., Noaves, A. B., Santos, A. C. P., & Sobral, E. G. 2010, Minor Planet Bulletin, 37, 95
 Bottke, W. F., Morbidelli, A., Jedicke, R., et al. 2002, Icarus, 156, 399
 Bottke, W. F., Durda, D. D., Nesvorný, D., et al. 2005, Icarus, 175, 111

- Carbognani, A. 2008, Minor Planet Bulletin, 35, 109
- Clark, B. E., Hapke, B., Pieters, C., & Britt, D. 2002, Asteroids III, p.585, eds. W. F. Bottke, A. Cellino, P. Paolicchi, et al., The Univ. of Arizona Press
- Dandy, C. L., Fitzsimmons, A., & Collander-Brown, S. J. 2003, Icarus, 163, 363
- Hapke, B. 2000, in Lunar and Planetary Institute Science Conference Abstracts, 31, 1087
- Hergenrother, C. W., Whitley, R. J., & Christensen, E. J. 2009, Minor Planet Bulletin, 36, 16
- Hicks, M., Somers, J., Rhoades, H., et al. 2011a, The Astronomer's Telegram, 3460, 1
- Hicks, M., Truong, T., Gerhart, C., et al. 2011b, The Astronomer's Telegram, 3457, 1
- Hicks, M., Brewer, M., & Somers, J. 2012a, The Astronomer's Telegram, 4625, 1
- Hicks, M., Brewer, M., & Somers, J. 2012b, The Astronomer's Telegram, 4588, 1
- Hicks, M., Dombroski, D., & Brewer, M. 2012c, The Astronomer's Telegram, 4591, 1
- Hicks, M., Dombroski, D., Davtyan, T., Teague, S., & Strojia, C. 2012d, The Astronomer's Telegram, 4262, 1
- Hicks, M., Smythe, W., Davtyan, T., et al. 2012e, The Astronomer's Telegram, 4252, 1
- Hicks, M., Smythe, W., Dombroski, D., et al. 2012f, The Astronomer's Telegram, 4188, 1
- Hicks, M., Teague, S., & Strojia, C. 2012g, The Astronomer's Telegram, 4016, 1
- Hicks, M., Teague, S., Strojia, C., Dombroski, D., & Davtyan, T. 2012h, The Astronomer's Telegram, 4251, 1
- Hicks, M., & Dombroski, D. 2012, The Astronomer's Telegram, 4623, 1
- Hicks, M., Brewer, M., Carcione, A., Ebelhar, S., & Borlase, R. 2013a, The Astronomer's Telegram, 4969, 1
- Hicks, M., Buratt, B., & Dalba, P. 2013b, The Astronomer's Telegram, 5121, 1
- Horne, J. H., & Baliunas, S. L. 1986, ApJ, 302, 757
- Howell, E. S. 1995, Probing Asteroid Composition Using Visible and Near-Infrared Spectroscopy, Ph. D. Thesis, The University of Arizona
- Ito, T., & Yoshida, F. 2007, PASJ, 59, 269
- Jewitt, D., & Hsieh, H. 2006, AJ, 132, 1624
- Jewitt, D. 2013, AJ, 145, 133
- Karashevich, S. V., Devyatkin, A. V., Vereshchagina, I. A., L'vov, V. N., & Tsekmeister, S. D. 2012, Solar System Research, 46, 130
- Landolt, A. U. 1992, AJ, 104, 340
- Mainzer, A., Grav, T., Masiero, J., et al. 2012, ApJ, 752, 110
- Nesvorný, D., Bottke, W. F., Vokrouhlický, D., Chapman, C. R., & Rafkin, S. 2010, Icarus, 209, 510
- Pieters, C. M., Taylor, L. A., Noble, S. K., et al. 2000, Meteoritics and Planetary Science, 35, 1101
- Plavchan, P., Jura, M., Kirkpatrick, J. D., Cutri, R. M., & Gallagher, S. C. 2008, ApJS, 175, 191
- Rabinowitz, D. L. 1998, Icarus, 134, 342
- Sasaki, S., Nakamura, K., Hamabe, Y., Kurahashi, E., & Hiroi, T. 2001, Nature, 410, 555
- Sasaki, T., Sasaki, S., Watanabe, J.-I., et al. 2004, ApJ, 615, L161
- Sasaki, S., Sasaki, T., Watanabe, J.-I., et al. 2006a, Advances in Space Research, 38, 1995
- Sasaki, T., Sasaki, S., Watanabe, J.-I., et al. 2006b, Advances in Geosciences, 3: Planetary Science (PS), eds. A. Bhardwaj, & W.-H. Ip, 3, 331 (Singapore: World Sci. Publ.)
- Vernazza, P., Binzel, R. P., Rossi, A., Fulchignoni, M., & Birlan, M. 2009, Nature, 458, 993
- Ye, Q.-Z. 2011, AJ, 141, 32
- Yoshida, F., Dermawan, B., Ito, T., et al. 2004, PASJ, 56, 1105

Ground-based photometry for 42 Kepler-field RR Lyrae stars

Young-Beom Jeon¹, Chow-Choong Ngeow² and James M. Nemec³

¹Korea Astronomy and Space Science Institute (KASI), Daejeon 305-348, Korea
email: ybjeon@kasi.re.kr

²Graduate Institution of Astronomy, National Central University, Taiwan
email: cngeow@gmail.com

³Department of Physics & Astronomy, Camosun College, Victoria, British Columbia, Canada
email: jmn@isr.bc.ca

Abstract. Follow-up (*U*)BVRI photometric observations have been carried out for 42 RR Lyrae stars in the *Kepler* field. The new magnitude and color information will complement the available extensive high-precision *Kepler* photometry and recent spectroscopic results. The photometric observations were made with the following telescopes: 1-m and 41-cm telescopes of Lulin Observatory (Taiwan), 81-cm telescope of Tenagra Observatory (Arizona, USA), 1-m telescope at the Mt. Lemmon Optical Astronomy Observatory (LOAO, Arizona, USA), 1.8-m and 15-cm telescopes at the Bohyunsan Optical Astronomy Observatory (BOAO, Korea) and 61-cm telescope at the Sobaeksan Optical Astronomy Observatory (SOAO, Korea). The observations span from 2010 to 2013, with \sim 200 to \sim 600 data points per light curve. Preliminary results of the Korean observations were presented at the 5th KASC workshop in Hungary. In this work, we analyze all observations. These observations permit the construction of full light curves for these RR Lyrae stars and can be used to derive multi-filter Fourier parameters.

Keywords. stars: variable: RR Lyrae

We obtained ground-based (*U*)BVRI photometric observations for 42 RR Lyrae stars in the *Kepler* field. Figure 1 shows a phased light curve of KIC 3864443 and the correlation between $\phi_{31}(Kp)$ and $\phi_{31}(V)$ for all Blazhko and non-Blazhko RRab stars. Table 1 presents the total amplitudes, A_{tot} , and ϕ_{31} parameters from Fourier analysis of RRab

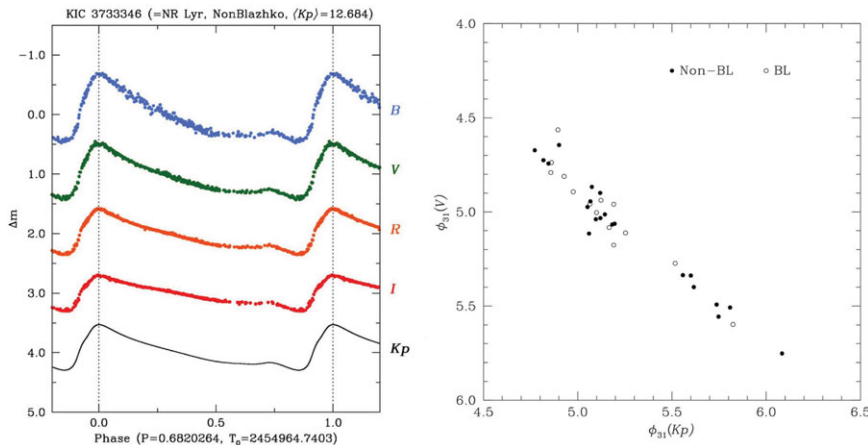


Figure 1. A sample phased light curve of KIC 3864443 (left) and the correlation between $\phi_{31}(Kp)$ and $\phi_{31}(V)$ for Blazhko and non-Blazhko RRab stars (right).

Table 1. Fourier parameters for RRab stars

KIC	GCVS	Period day	$A_{\text{tot}}(B)$ mag	$\phi_{31}(B)$ rad	$A_{\text{tot}}(V)$ mag	$\phi_{31}(V)$ rad	$A_{\text{tot}}(R)$ mag	$\phi_{31}(R)$ rad	$A_{\text{tot}}(I)$ mag	$\phi_{31}(I)$ rad
Blazhko:										
3864443	V2178 Cyg	0.48695	1.106	4.245	0.834	4.564	0.712	4.556	0.554	4.905
4484128	V808 Cyg	0.54786	1.398	4.856	1.115	5.055	0.922	5.254	0.707	5.621
5559631	V783 Cyg	0.6207	1.220	5.105	0.969	5.263	0.783	5.609	0.625	5.973
6183128	V354 Lyr	0.56169	1.028	4.942	0.821	5.168	0.639	5.496	0.490	6.082
6186029	V445 Lyr	0.51312	0.664	[6.514]	0.529	[6.964]	0.464	[7.106]	0.449	5.030
7257008	—	0.51178	1.252	4.632	0.997	4.769	0.739	5.149	0.594	5.057
7505345	V355 Lyr	0.4737	1.417	4.796	1.189	4.894	0.965	4.990	0.756	5.362
7671081	V450 Lyr	0.50461	1.122	4.519	0.873	4.919	0.736	4.884	0.614	5.381
9001926	V353 Lyr	0.5568	1.288	4.714	1.004	4.879	0.830	5.202	0.699	5.721
9578833	V366 Lyr	0.52703	1.344	4.935	1.067	5.090	0.869	5.385	0.662	5.576
9697825	V360 Lyr	0.55758	1.005	4.755	0.760	4.991	0.669	5.114	0.479	5.771
9973633	—	0.51075	1.506	5.240	1.315	5.107	0.909	5.206	0.732	5.526
10789273	V838 Cyg	0.48028	1.645	4.645	1.335	4.784	1.131	4.933	0.875	5.236
11125706	—	0.61322	0.706	5.302	0.540	5.614	0.452	5.970	0.352	[6.400]
12155928	V1104 Cyg	0.43639	1.603	4.657	1.295	4.689	1.062	4.851	0.891	5.242
Non-Blazhko:										
3733346	NR Lyr	0.68203	1.124	4.829	0.915	4.977	0.759	5.172	0.588	5.590
3866709	V715 Cyg	0.47071	1.525	4.702	1.226	4.643	1.015	4.929	0.841	5.269
5299596	V782 Cyg	0.52364	0.836	5.168	0.665	5.449	0.539	5.811	0.451	6.170
6070714	V784 Cyg	0.53409	1.055	5.477	0.830	5.839	0.616	6.191	0.482	[6.435]
6100702	—	0.48815	0.926	5.261	0.714	5.547	0.569	5.841	0.440	[6.357]
6763132	NQ Lyr	0.58779	1.185	4.811	0.954	4.958	0.770	5.105	0.606	5.628
6936115	FN Lyr	0.5274	1.482	4.622	1.226	4.758	0.996	4.857	0.813	5.204
7021124	—	0.62249	1.489	4.560	1.176	5.159	0.957	5.078	0.686	5.065
7030715	—	0.68361	0.944	5.162	0.732	5.437	0.605	5.639	0.473	6.202
7176080	V349 Lyr	0.50707	0.111	6.213	0.078	[8.054]	0.078	[6.859]	0.061	[7.009]
7742534	V368 Lyr	0.45649	1.666	4.551	1.327	4.705	1.104	4.932	0.976	5.174
7988343	V1510 Cyg	0.58114	1.496	4.850	1.247	4.963	0.970	5.122	0.759	5.427
8344381	V346 Lyr	0.57683	1.430	4.858	1.163	5.009	0.945	5.036	0.563	4.416
9508655	V350 Lyr	0.59424	1.452	4.809	1.189	4.955	0.974	5.130	0.758	5.523
9591503	V894 Cyg	0.57139	1.577	4.871	1.257	4.961	1.037	5.148	0.824	5.452
9658012	—	0.53321	1.402	4.811	1.125	5.012	0.943	5.103	0.719	5.489
9717032	—	0.55691	1.384	4.852	1.021	5.070	0.852	5.399	0.704	5.432
9947026	V2470 Cyg	0.54859	0.880	5.254	0.693	5.488	0.571	5.900	0.458	[6.344]
10136240	V1107 Cyg	0.56578	1.178	4.899	0.961	5.113	0.785	5.326	0.618	5.648
10136603	V1107 Cyg	0.43377	1.235	5.186	0.947	5.121	0.732	5.667	0.572	6.139
11802860	AW Dra	0.68722	1.321	5.240	1.045	5.431	0.848	5.639	0.652	6.045

Notes: [] denotes ϕ_{31} larger than 2π .

stars. RRc stars are expected to behave differently from the RRab stars and require special treatment, so they are not included. We used IRAF/digiphot/phot program to obtain the photometry. The periods in Table 1, as well as T_0 and K_p in Fig. 1, were taken from Nemec *et al.* (2011, 2013). The Fourier analysis was based on Géza Kovács' Fourier decomposition program.

From Table 1 we can calculate the mean differences between ϕ_{31} in *BVR*I bands and $\phi_{31}(K_p)$ and their standard deviations. They are the following: $\Delta\phi_{31}(B) = \langle\phi_{31}(B) - \phi_{31}(K_p)\rangle = 0.430 \pm 0.107$ rad from 34 stars, $\Delta\phi_{31}(V) = 0.174 \pm 0.085$ rad from 34 stars, $\Delta\phi_{31}(R) = -0.018 \pm 0.053$ rad from 34 stars and $\Delta\phi_{31}(I) = -0.192 \pm 0.063$ rad from 35 stars. Earlier, $\Delta\phi_{31}(V) = 0.151$ rad was derived by Nemec *et al.* (2011) based on only three RR Lyrae stars. These results can help to derive metal abundances using Fourier parameters if $\phi_{31}(B, V, R, I)$ vs. $\phi_{31}(K_p)$ relations will be used to translate the former to the latter and then the [Fe/H] vs. $\phi_{31}(K_p)$ relation of Nemec *et al.* (2013) will be used to derive [Fe/H].

Transformation to standard photometry is currently in progress.

References

- Nemec, J. M., Smolec, R., Benkő, J. M., *et al.* 2011, *MNRAS*, 417, 1022
 Nemec, J. M., Cohen, J. G., Ripepi, V., *et al.* 2013, *ApJ*, 773, 181

[SAO/NASA ADS](#) [Astronomy Abstract Service](#)

- [Find Similar Abstracts](#) (with [default settings below](#))
- [Table of Contents](#)
- [Reads History](#)
-
- [Translate This Page](#)

[Toggle Highlighting](#)

Title:	On the Activity of Comets
Authors:	Ma, Yuehua ; Shi, Jianchun
Publication:	40th COSPAR Scientific Assembly. Held 2-10 August 2014, in Moscow, Russia, Abstract B0.4-41-14.
Publication Date:	00/2014
Origin:	ADS
Bibliographic Code:	2014cosp...40E1927M

Abstract

Abstract: A comet at a large distance from the Sun is supposed to be inactive due to the low temperature and the absence of gas sublimation leading to coma formation. But it is found from observations that some comets are active in large heliocentric distance. We investigate three distant active comets 228P/LINEAR, C/2006 S3 (LONEOS) and 29P/Schwassmann-Wachmann 1 with the data obtained with the 1-m optical telescope at Lulin Observatory in Taiwan. By cometary morphological and photometric studies, the upper limits of the nuclei radii were derived. Also, the surface brightness profiles, (A_{frho}) parameters, mass production rates and the coma colors were measured. For the comet 103P/Hartley 2, the data were obtained with the NEO telescope at Purple Mountain Observatory, Chinese Academy of Sciences when it passed the perihelion in 2010. The result showed that its radius of the nucleus is <2.32 km (albedo 4%). What mechanisms could drive the activities is not very clear. We try to discuss in this aspect.

[Bibtex entry for this abstract](#)

工作報告

鹿林天文台觀測時數統計(2003-2014)

林宏欽、蕭翔耀、林啟生

鹿林天文台自 2002 年 9 月開始人員常駐，2003 年 LOT 一米望遠鏡上線，開始有正式觀測時數紀錄，可供瞭解鹿林長期的觀測狀況。依 2003-2014 共 12 年的統計結果，鹿林天文台年平均觀測時數約為 1450 小時。一年約可分為四個觀測季，

- 最佳觀測季：10-12 月。
- 次佳觀測季：1-3 月。
- 最差觀測季：4-6 月。4 月開始進入雨季，5-6 月受梅雨影響，天氣最差。
- 次差觀測季：7-9 月。主要受颱風及西南氣流影響，天氣變化大。此外夏季晝長夜短，每晚可觀測時間比冬季短得多。

詳細統計資料及統計圖如下，

表 1 每月觀測時數統計 (2003-2014)

Month	2003	2004	2005	2006	2007	2008	2009	2010	2011	2012	2013	2014	Average**
1	78.75	125	163.25	129	127.32	179	234.52	206.9	90.8	113.42	153.58	269.62	152.28
2	142.5	145.98	94.75	149	128.55	118.25	165.7	100.6	123.8	64.88	183.63	109.8	127.89
3	147.5	163	143	126.05	116.4	138.5	146.75	181.3	75.9	168.23	134.26	78.7	136.24
4	126.5	110.5	144.75	86.8	53.75	85.25	71.8	75.8	151.45	32.75	55.83	135.95	94.69
5	129.75	106.25	136.25	59.5	106.6	98.25	167.4	86.05	56.6	74.3	41.02	32.4	89.46
6	24	133	45	39.3	54	37	81.75	26.5	61.5	35.15	80.14	33.7	49.40
7	222.5	48	167.75	91.57	128.88	88.4	76.6	99.85	81.75	106.4	88.05	114.65	104.39
8	137.75	142	76	111.65	56.6	118.95	6.8	98.3	97.9	35.7	72.2	110.9	91.60
9	142	116	129.25	60.05	69.55	59.8	0	109.95	90.1	117.35	107.84	134.39	99.43
10	149.25	219.75	210.25	150.6	172.63	191.38	175.6	139.8	136.95	214.51	200.57	232.33	182.43
11	166.5	214.5	216.25	71.75	160.55	152.55	175.8	163.65	87.2	93.81	136.1	166.15	151.68
12	271.5	232.45	129	132	261.09	211.17	169.8	169.65	115.25	132.21	86	137.3	168.99
Total	1738.5	1756.43	1655.5	1207.27	1435.92	1478.5	1472.52	1458.35	1169.2	1188.71	1339.22	1555.89	1453.04

* 2009 年因受莫拉克颱風八八風災影響，自八月八日起至十月初約 2 個月期間道路中斷並停電，無法觀測。所以 2009 年之八、九月觀測時數偏低，甚至為 0。

**此 Average 值為扣除最高及最低值後取平均。

Lulin Yearly Observing Hours

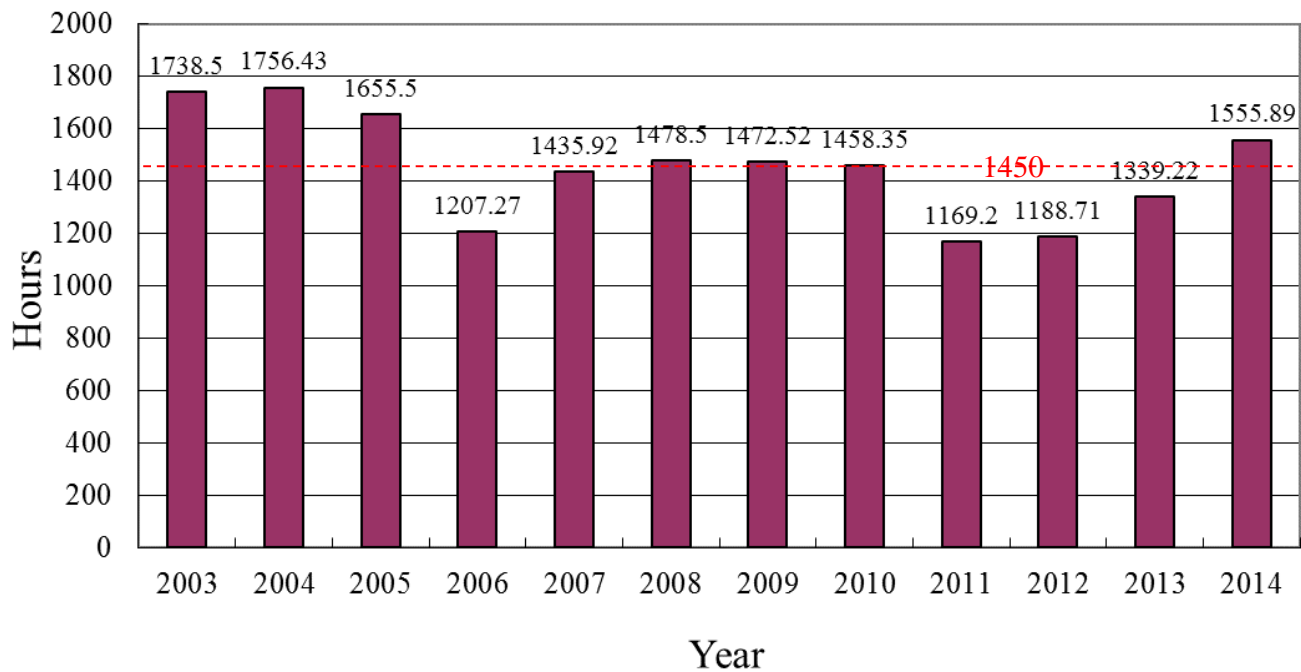


圖 1 鹿林天文台年平均觀測時數統計圖(2003-2014)

Lulin Monthly Average Observing Hours

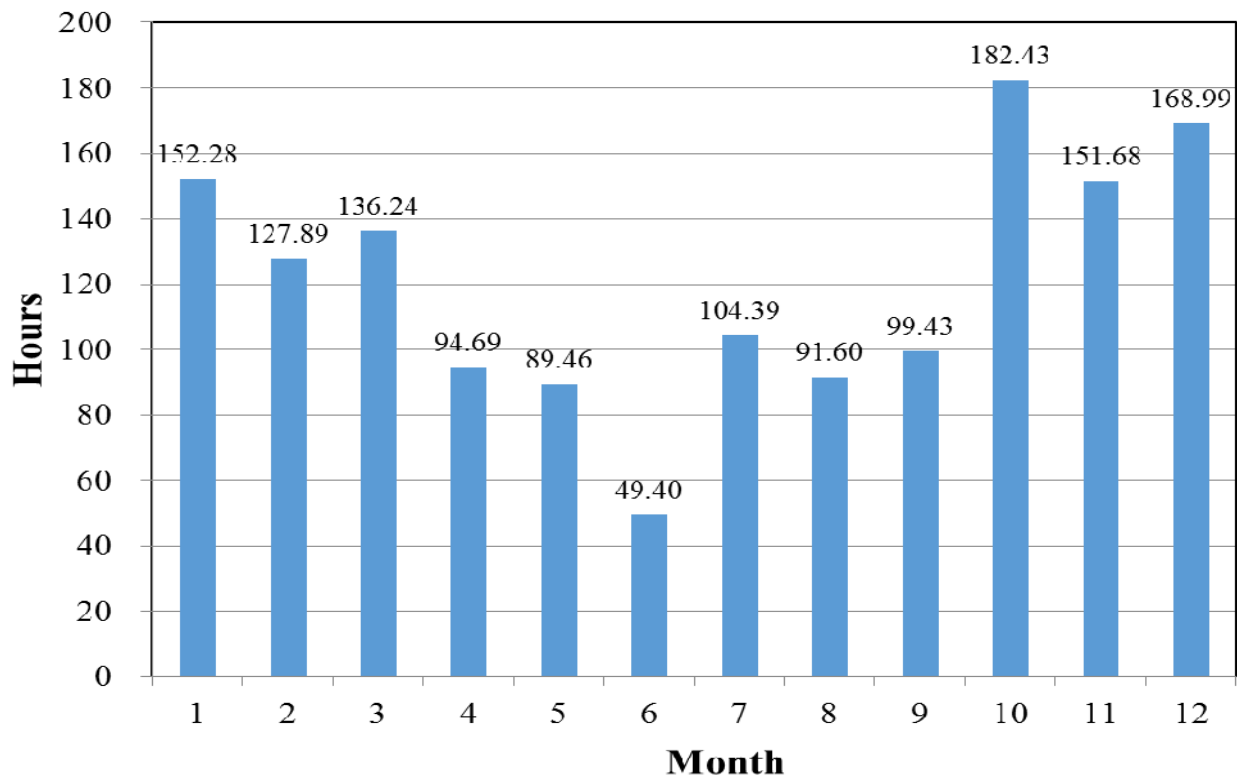


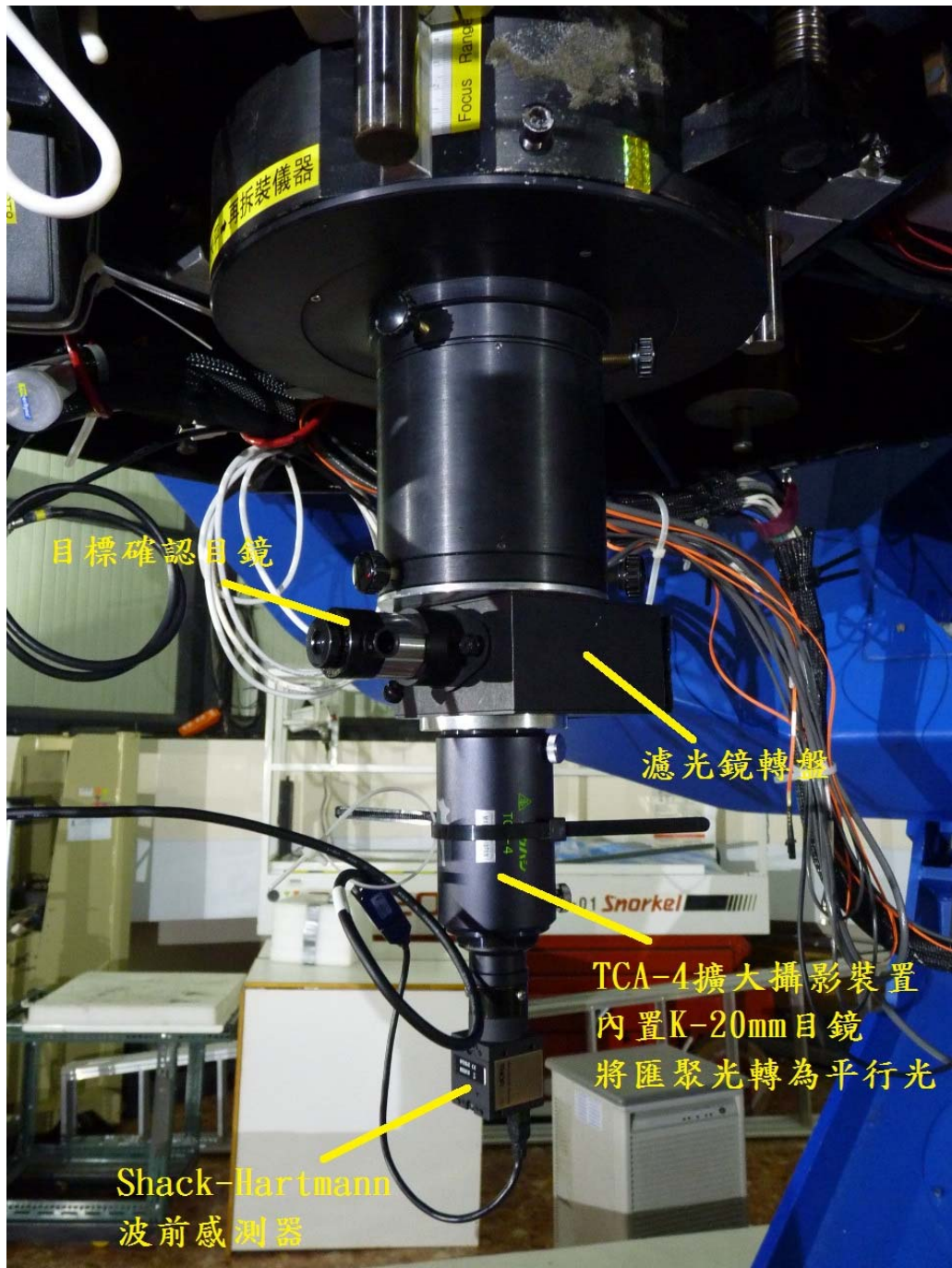
圖 2 鹿林天文台月平均觀測時數統計圖 (2003-2014)

AO 系統測試報告

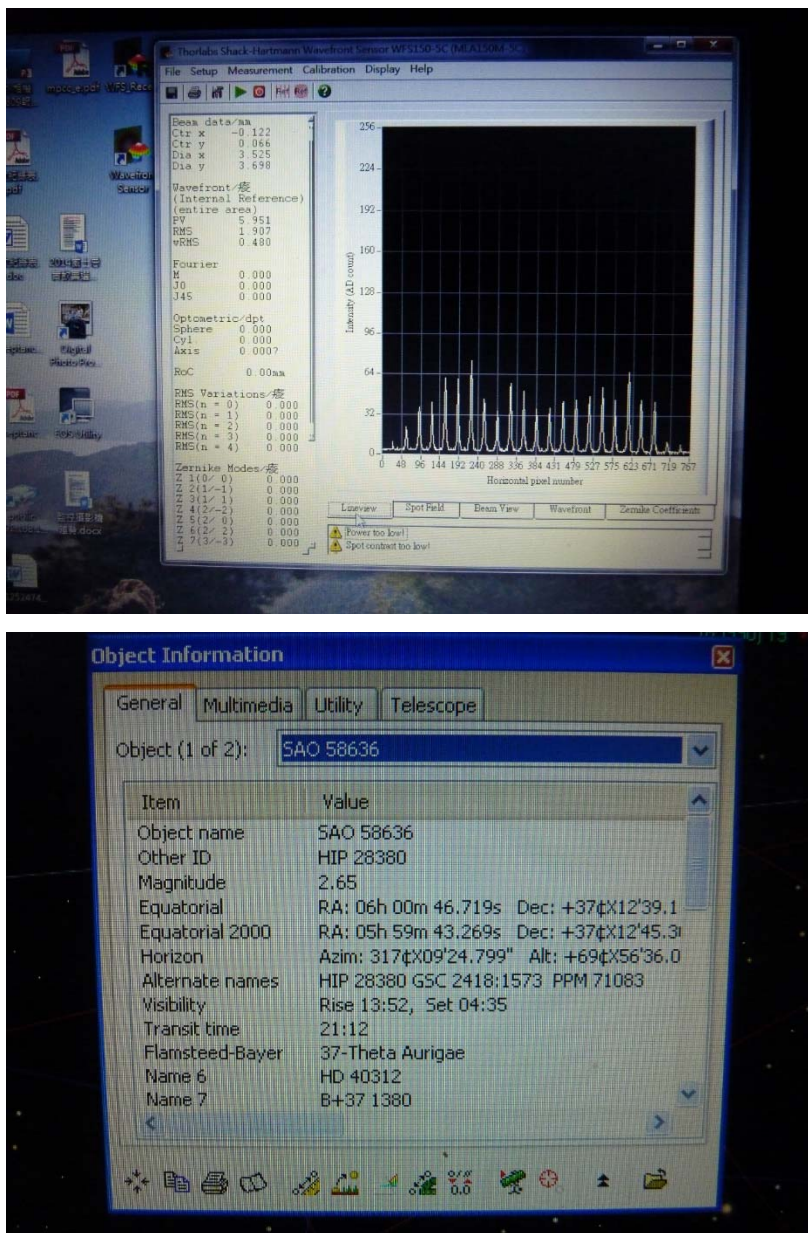
張永欣

AO 系統於校內 24 英吋望遠鏡觀測，修正效果不盡理想，所以安排 2015/02/01～02/03 前往大氣狀況較佳之鹿林天文台，利用 LOT 一米望遠鏡（以下簡稱 LOT）安裝波前感測器量測大氣擾動值，測試項目如下。

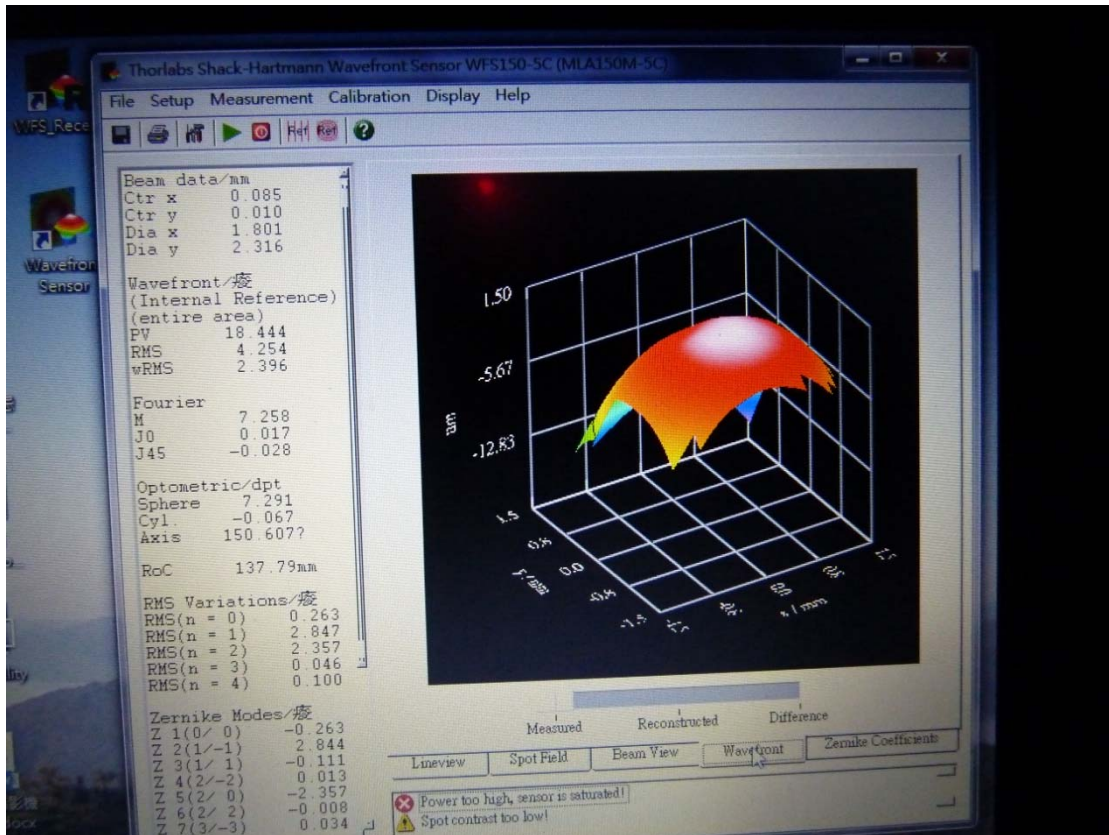
1. 不分光下波前感測器之極限星等
2. 焦點位置對於波前誤差之影響
3. 不同色光 R、G、B 三色波前誤差之差異
4. 不同目鏡焦距準直波形之差異
5. 大氣擾動之頻率



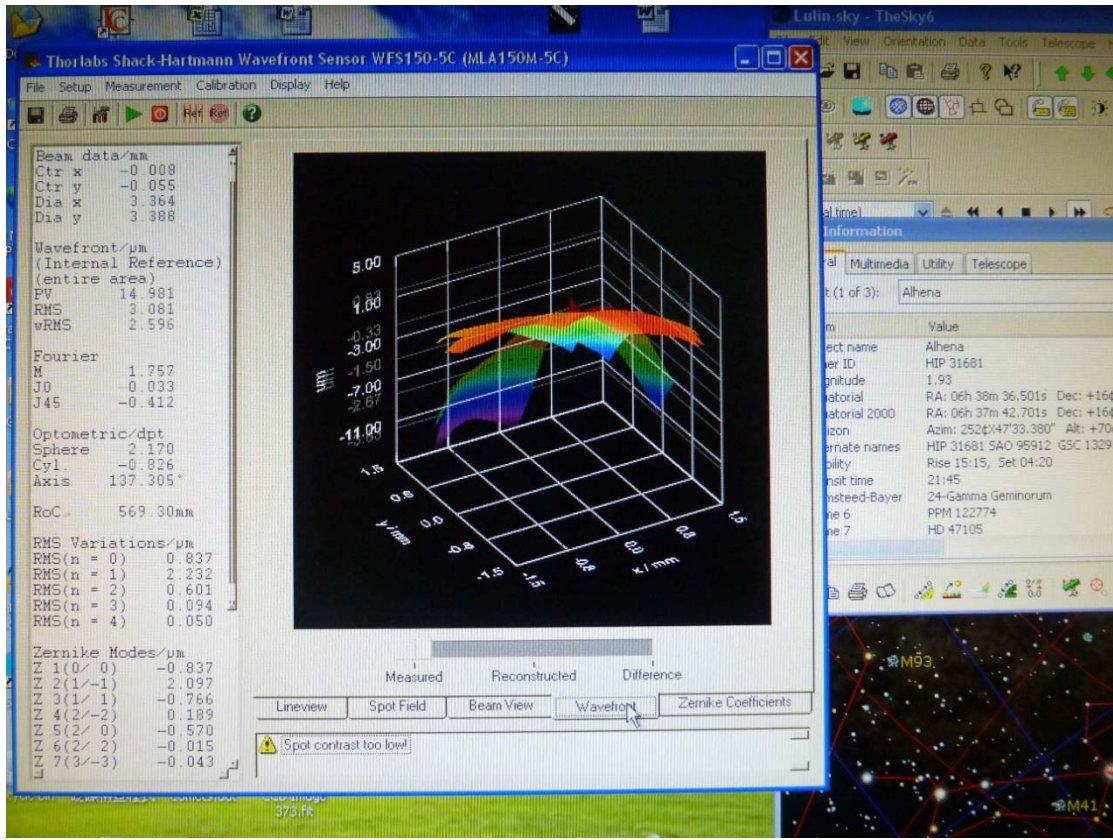
1. 無濾光且不分光下波前感測器之極限星等約在 2.65 等，低於此值，波前感測器解出值就不正常了，如下圖。



- 對於不同焦點位置，於焦點前、後，波前變形皆呈現單一方向之球面像差，研判是來自於 LOT 望遠鏡光軸誤差所致，必須進一步調整 LOT，才能量測，如下圖。



3. R、G、B 三色波前誤差之差異不大，均於 RMS 5~RMS 3 之間跳動，有可能為 LOT 像差太大所致，同樣需進一步調整 LOT，才能量測。
4. 原使用 k-20mm 焦距目鏡準直，像場恰為涵蓋全部波前感測器，量測誤差較為準確；更換 or-6mm 目鏡後，準直光束直徑明顯縮小，僅約 1/3 波前感測器偵測範圍，量測值無法使用。
5. 大氣擾動之頻率遠超過現有波前感測器之反應，波前感測器讀出張數極限為 15 張/秒，實際大氣擾動可能在 60Hz~120Hz 以上，如下圖 2 張畫面間刻度值瞬間差了 4 倍之多，所以 AO 系統於中壢校區內 24 英吋望遠鏡幾乎修正不了。



結論：

AO 光學設計架構是正確的，但由於沒有配置 Tip/Tilt 鏡修正波前傾斜值，
RMS 3~5um 誤差明顯超過 DM 可修正之 $\pm 1\mu\text{m}$ ，以至於 AO 修正不了。
大氣擾動之頻率遠超過現有波前感測器之反應，必須使用感度更高之 EM-CCD
增強訊號以高速輸出波前變化，才能讓 DM 完美修正波前形狀。
以上兩個關鍵都必須在投入高質量人才與大量軟體撰寫及測試，進一步之開
發成本非常昂貴。



中大鹿林天文臺

文/ 林宏欽

鹿林天文臺位於玉山國家公園塔塔加地區的鹿林前山，海拔2,862公尺，是臺灣最重要的光學天文基地。目前主要的研究設施有1米望遠鏡(LOT)、0.4米望遠鏡(SLT40)、0.35米望遠鏡(L35)以及中美掩星計畫(TAOS)四座0.5米自動望遠鏡。

沿革

國立中央大學天文研究所於民國81年(1992)設立，為國內最早成立之天文相關研究與教學單位，以培養高等人才為宗旨。提供學子接觸宇宙科學的管道，使其瞭解宇宙天體能量的本質、運行規律，以及演化的過程，藉以建立科學的宇宙觀。並藉由觀察宇宙的過程，了解自然並關懷自然。

本所發展策劃除了理論研究外，以光學與紅外天文為主，利用鹿林天文臺及國外大型望遠鏡進行課題研究，並參與多項國際合作研究計畫，讓卓越研究與教育並重為本所最大特色。在教育部與國科會支持下，以中央大學天文所為首的數

個大學單位，正共同合作將鹿林天文臺協力開發成可供全國天文學術機構合用的天文研究設施與觀測中心。

中央大學在苗栗時期(1958-1965)就已設有天文臺，1977年中央大學物理系成立「物理與天文研究所」。1981年在旅美華人天文學家呂克華的協助下，在科學一館頂樓設置了「科一館天文臺」(中大天文臺)，使用美國博精儀器公司(Perkin-Elmer)製造的24吋(60公分)蓋賽格林(Cassegrain)反射式望遠鏡進行天文研究，該望遠鏡在啓用後將近二十年的時間是臺灣最大的望遠鏡，肩負教育及研究的使命。中大天文臺為臺灣第一座具有天文研究用大型望遠鏡的天文臺，以現代觀測工具及技術研究天文現象。2013年在

李國鼎科技發展基金會的支持下中大天文臺進行全面整修，現作為開放參觀及教學用途。

由於中壢市區急遽發展，中大校內建設大幅增加，光害污染日趨嚴重，中大天文臺已不適合從事天文觀測研究，必須另覓理想的觀測地點。1990年在國科會支持下，蔡文祥教授開始進行臺灣天文臺選址計畫，於鹿林前山設置一個臨時觀測站進行選址研究及天文教學。歷經3年的視相(seeing)、氣候、夜天光背景等條件調查後，確定玉山國家公園的鹿林前山為優良的天文臺臺址。1997年獲得太空計畫室（今國家太空中心）補助，興建第一座天文臺-SLT，1999年完工，內設自行設計製造的76公分超輕型望遠鏡（SLT76），是鹿林天文臺初期最重要的觀測設備。在建造、校正與觀測過程中，培養了許多使用與維護望遠鏡的人才，對日後鹿林天文臺的運作提供了重要基礎。在教育部追求學術卓越發展計畫的挹注下，2002年建置臺灣首座口徑突破1公尺的鹿林一米望遠鏡（LOT），同年冬季開始觀測。目前正全力籌建二米望遠鏡，預定2018年完成。

鹿林天文臺

鹿林天文臺位於玉山國家公園塔塔加地區的鹿林前山，海拔2,862公尺，是臺灣最重要的光學天文基地。目前主要的研究設施有1米望遠鏡（LOT）、0.4米望遠鏡(SLT40)、0.35米望遠鏡(L35)以及中美掩星計畫(TAOS)四座0.5米自動望遠鏡。此外基地內還有成功大學的紅色精靈地面觀測與極低頻無線電波偵測系統、中央大學太空所的氣暉全天相機及環保署鹿林山大氣背景站(LABS)等



中大天文社在中大天文臺用24吋望遠鏡進行天文觀測教育訓練

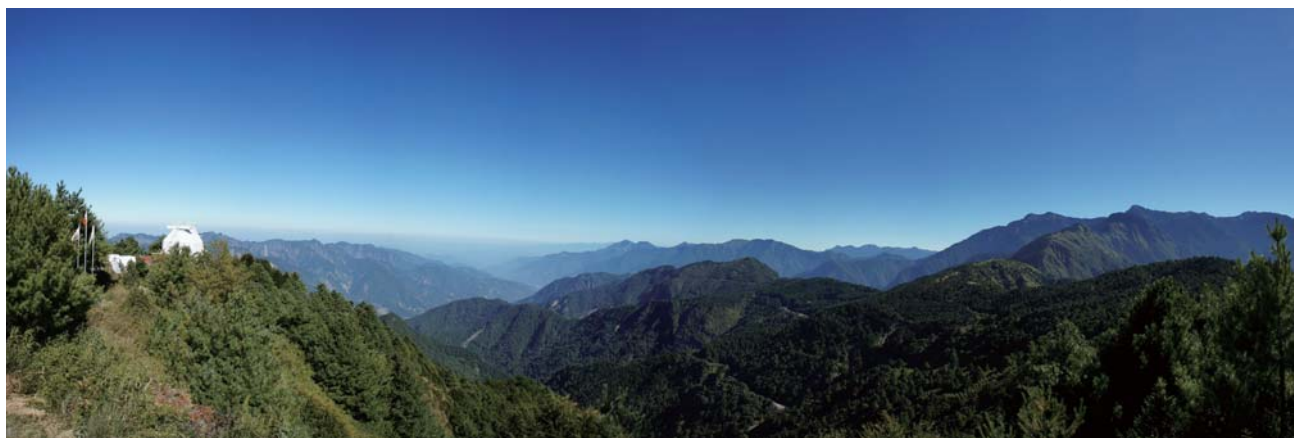
大氣、太空相關領域的研究設施。

鹿林天文臺位於臺灣中部，較不受東北季風、西南氣流及颱風的影響；加上位於高山，透明度及天空條件均相當理想。此臺址的天空背景極暗，幾無光害，可觀測天數約180天，較好的觀測季節是每年的秋季與冬季。

鹿林天文臺是應用小型望遠鏡和臺灣觀測條件優勢的典範。因為小型望遠鏡的運作及時間分配，比中大型望遠鏡更具彈性，而臺灣緯度接近赤道，地理經度上與世界各主要天文臺相輔，因此可以集中注意力在南天目標，也可以針對瞬間爆發的天文現象（如超新星及伽瑪射線爆），與各大天文臺合作協力觀測。

在臺灣近百年的天文發展史上，鹿林天文臺締造了許多首度紀錄：首度發現小行星、首度發現超新星、首度發現彗星、首度發現近地小行星及首度小行星命名。

鹿林天文臺全景（圖右為玉山群峰）

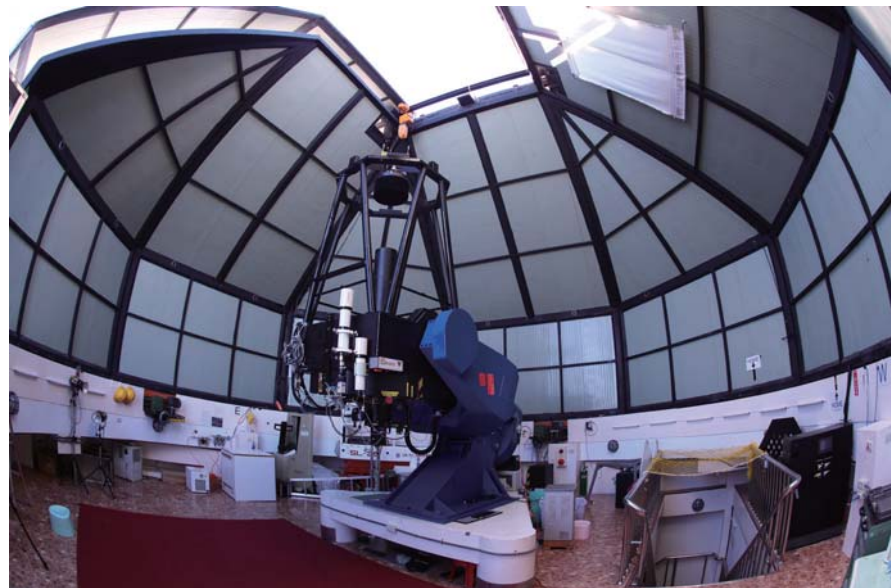


鹿林一米望遠鏡(LOT)

鹿林一米望遠鏡(LOT)是目前臺灣最大的望遠鏡，代表鹿林天文臺的基礎建設完成，標誌著臺灣本土的天文觀測設施可以提供國內天文研究的基本需求。鹿林一米望遠鏡為蓋賽格林反射式望遠鏡，具備全電腦控制的叉式赤道儀，高精度的驅動裝置及位置迴授系統，擁有極佳的指向精度及追蹤精度，加上高靈敏度的天文CCD相機，可以看到比裸眼觀測暗百萬倍的天體。

鹿林一米望遠鏡以多波段成像及測光為主，開展不同科學主題的研究。對彗星、小行星、恆星、星雲、星團、星際物質及星系等，進行多波段、不同周期、快速光變等觀測。同時更與國際接軌，積極參與國際天文聯測計畫，如全球望遠鏡聯合觀測（The Whole Earth Telescope, WET）、全球蠍虎BL類星體聯合觀測（The Whole Earth Blazar Telescope, WEBT）等。

2003年鹿林一米望遠鏡加入伽瑪射線爆（gamma ray bursts, GRB）光學餘暉觀測行列，並與日本、大陸以及韓國的天文臺合作成立東



鹿林一米望遠鏡(LOT)

亞伽瑪射線爆觀測網（East-Asia GRB Follow-up Observation Network, EAFON），三年內成功觀測15個光學餘暉。此外，臺灣超新星巡天計劃（Taiwan Supernovae Survey）利用LOT進行超新星巡天工作，2004-2007年共發現了15顆超新星。目前每年約有20幾個研究計畫在LOT上進行，十年來已發表上百篇研究論文。在研究之外更提供部分時間供大學及中學天文觀測教學實習，讓學生美夢成真，當一日天文學家擁有使用大望遠鏡的深刻體驗。



中美掩星計畫其中二部0.5米自動望遠鏡，圖後方為LOT一米望遠鏡

TAOS中美掩星計畫

(四部0.5米自動望遠鏡)

中美掩星計畫是中研院天文所、中央大學、美國哈佛史密松天文物理中心與韓國延世大學的合作計畫。本計畫藉由四部0.5米自動望遠鏡，每晚監測約1,000顆恆星來蒐尋位於古柏帶的太陽系天體對遠方背景恆星造成的掩星現象。2005年開始運轉，六年的觀測結果顯示太陽系外圍天體的數量，沒有某些理論估計來得多；對太陽系中直徑大於500公尺的古柏帶天體數量設下了非常嚴格的上限。

SLT40 (0.4米望遠鏡)

由於自製的76公分望遠鏡有許多問題。2005年將望遠鏡拆下後在既有的圓頂安裝了一具40公分望遠鏡，進行鹿林巡天計畫(LUSS)專門搜尋小天體，在2006-2009年間共發現800多顆小行星。其中有300多顆已獲得永久編號，小行星發現數排名世界第47。鹿林天文臺發現的小行星目前已有50多顆得到永久命名，小行星名遍全臺，逐一將臺灣的人物、團體、地理、山水及原住民族送上太空，神遊宇宙。2007年鹿林天文臺首度發現彗星(C/2007 N3)與近地小行星(2007 NL1)，該彗星後來命名為「鹿林彗星」(Comet Lulin)。2010年起回到一般觀測研究工作，主要進行長期的變星、彗星等監測工作。

L35 (0.35米望遠鏡)

2012年臺大鹿林發射線巡天觀測計畫(LELIS)計畫結束後，利用原有的圓頂安裝一具0.35米望遠鏡(C14)，2013年上線後開始進行長期的變星監測工作，未來目標是建成一座全自動天文臺。



未來計劃

鹿林兩米望遠鏡計畫為中央大學「發展國際一流大學及頂尖研究中心計畫」分項計畫之一，由教育部補助，預定2018年完成，將成為東亞最大望遠鏡之一。兩米望遠鏡集光能力為鹿林一米望遠鏡(LOT)的4倍，配合高效率、高感度的四色同步成像儀，觀測效率將是LOT的10倍，可觀測到遙遠的銀河系外天體。鹿林兩米望遠鏡的建置，將可提升臺灣本土的光學觀測能力、拓展國際合作網絡、促進天文儀器軟硬體開發以及專業天文人才的養成。

開放與交通資訊

中大天文臺(中壢中央大學校區)

參觀、教學活動與教育推廣課程採專案方式申請，詳情請洽中大天文所張光祥先生，聯絡電話：(03)427-8445，E-mail: khchang@astro.ncu.edu.tw。

交通資訊：中大天文臺位在中壢中央大學校區(桃園縣中壢市中大路300號/科學一館)，自行開車或搭乘公共交通運輸都很便利，詳細請參考：中央大學網站==>關於中大==>交通資訊==>如何到中大

http://www.ncu.edu.tw/ch/about_22.html



張光祥叔叔為小學生解說24吋望遠鏡



鹿林二米望遠鏡

鹿林天文臺

鹿林天文臺因位處高山(鹿林前山)，海拔2862 公尺，且車輛無法抵達，申請前請先慎重考慮，如有心臟病、高血壓、糖尿病、懼高症、孕婦或曾有高山症者及其他重大疾病或不適合高山活動者請勿參加。此外鹿林天文臺位於玉山林道管制區內，一般車輛無法進入，從上東埔停車場(臺18線公路108k處)往返天文臺需步行約4 小時(往返全程約9 公里)。

鹿林天文臺之參觀採預約申請方式，每個月以 3 團為限，一日限 1 團，採優先登記順序。同一單位申請以一年一次為限。

申請對象資格：以非營利目的，對天文有興趣的機關、學校或團體，每團人數至少 10 人，上限為 30 人。不受理「個人」名義申請！

申請參觀之時段：以下午 14:00~17:00 參觀時段為限，每一參觀案件，以不超過 2 小時為原則。晚上不開放！

其他注意事項詳見：鹿林天文臺網站==>申請書表==>鹿林天文臺參觀辦法

http://140.115.33.61/Lulin_Visitor_form_5.pdf



阿里山來吉國小學生參觀鹿林天文臺



參考資料

國立中央大學天文研究所網站

鹿林天文臺網站

中研院天文所-中美掩星計畫

鹿林天文臺- 維基百科

鹿林天文臺- 臺灣大百科全書

鹿林一米望遠鏡- 臺灣大百科全書

鹿林兩米望遠鏡計畫- 臺灣大百科全書

中大校區天文臺- 臺灣大百科全書

林宏欽：國立中央大學天文所-鹿林天文臺主任



因著國科會第二期高瞻計畫的資助、清華大學賴詩萍等諸位教授的輔導、以及中央大學與鹿林天文臺的協助，於2013年7月底，北一女中高瞻計畫團隊師生進行了鹿林天文臺的初次拜訪。從行前的觀測計畫擬定、實地進行觀測操作、以及最後的影像處理，一連串的訓練過程帶領喜愛星空的師生初探了天文研究的大門，更徘徊流連於玉山夜空的美。三天兩夜的過程，意外訪客SN 2013ej的現蹤更是驚奇的收穫。架構在此次的初訪經驗，於2013年10月中旬，北一女中地科社邀請建中天文社共同進行聯合觀測活動、再次拜訪了鹿林天文臺。

兩次的觀測行，同學們將觀測經驗分享與傳承，從規劃到執行，除了想分享感動、更想穩固一同追逐星夢的夥伴情誼。以下文章為同學們造訪鹿林天文臺的觀測心得與省思，期能分享給有志一同的天文愛好者們，也將我們的經驗提供給各友校師生作為參閱。～林郁梅老師



2013年7月份北一女中高瞻計畫團隊師生
鹿林天文臺觀測行。

文/ 陳心平、廖乙馨、許苡蘿、
蔡欣儒、許雅婷、王蕾婷、
沈庭、陳麒瑞

那一夜， 鹿林的星空 我們的心空



2013年10月份北一女中與建國中學師生鹿林天文臺觀測行。

啟 程

都 市的影子逐漸遠去，橫越新中橫的崎嶇山路，我們沿著臺二十一線前行，遠處的山峰在和我們捉迷藏。從臺北出發，五個多小時的車程、一個小時的漫長跋涉，對於習慣以車代步的都市小孩而言，這是一場體力與毅力的長跑戰。好不容易，我們來到了雲霧上頭的世界，海拔兩千八百六十二公尺的高度，我們前腳在嘉義、後腳在南投，左手邊的太陽一溜煙的躲到了山後，右手邊的玉山依然挺拔，看見白色矮房在鬱鬱蔥蔥的樹林綻放，那正是此趟旅程的目的地——鹿林天文臺。

等 待

夜幕低垂之時，總算要是履行這次行程的主要目的——星體觀測，只可惜起初雲霧沒有散去的意思，一次又一次的落空，無可奈何也只能耐心等待。到了午夜時分，天空終於揭開神祕的面紗，我們像個小小的冒險者來到天臺，探索著鹿林的夜景。我們觀賞著一頭的月明，與另一頭的星漢，曝曬一段月光浴，讓光芒照耀我們心空。以前的星空對我們而言，僅是一幅美麗的插畫，而這次的邂逅才使我們和星空逐漸有了共通的語言……仙后與北極星的微妙連結；夏季大三角勾勒夏季的清爽俐落；秋四邊的皇族宮廷盛狀；獵戶座陽剛的姿態傲視群雄；木星與天狼星在空中閃爍最明亮的色彩……突然間，這樣生澀的我們也變得專業了！而專業的是心情，不是智慧，也開始有了如同身為天文臺的家人一般的認同感，體會到一位天文學家在黑夜靜待時機成熟之際的殷勤盼望。

慌 亂

鹿林是我們與大型望遠鏡的第一次接觸，有些陌生。在天未開時，我們依循著操作流程，一步步進行，調焦距、確認目標、試拍秒數、調整曝光時間等，一一完成。等待天氣狀況穩定後，終得以開啟天文臺圓頂正式進行拍攝，聽著望遠鏡轉動的嗡嗡聲，坐在螢幕前，按按鍵盤，



天未開前，於鹿林天文臺觀測室內進行模擬觀測操作。



夜半天開後，忙碌地進行計算與操控望遠鏡進行觀測。

影像出爐，觀看示範時一切似乎如此容易，自己上陣又如登天難，忘了按某個鍵、無法攝出理想影像、甚至因天候曝光時間須重算等。我們體悟到，身為初學者，要帶著謙卑的心，多練習、多問、多嘗試，才能成長，機會是留給準備好的人！雲朵遮蔽了我們上半夜的觀測計畫，此時備案才顯得特別重要，我們開始聽星體呢喃、訴說它們的故事、存下一張張影像、寫下一行行觀測紀錄。

在實際拍攝星雲時，常有“流血”(過度曝光)的現象，是因在選擇觀測星體時，忽略了其內部的亮星，因此亮星已過曝而雲氣尚未露臉；亦或是理論所估算之曝光時間與實際情況的差距，而這就需要經驗的指點了。在數次拍攝、修正以及觀測員陪伴的指導下，終於漸入佳境。由於夜半才開始觀測，鹿林駐站人員更替我們多開了一臺口徑35公分的望遠鏡，操作方式與鹿林望遠

鏡1公尺相同，但換了望遠鏡一切數據需重來規劃計算。幸好上山前擬定觀測計劃時的練習，我們能不遲疑、迅速切換尋找新目標。來到清晨時分，我們開始捕捉ISON彗星那燦爛優雅卻短暫的身影，輸入事前預備的數據試拍，多次嘗試後總算測出適用數值卻已過最佳拍攝時間，此時才體悟須在出發前即做好一切資料查詢，以免錯過良時，這些事在在告訴我們萬全的準備是重要的。

反思

觀測計畫

拜訪鹿林山之前，為了善用夜晚的時光，把握老天給我們開天的機會，觀測計畫的重要性是不容小覷的，深深攸關到此趟行程的最終目的的成功與否。在安排計畫前，也必須清楚如何去選取觀測的目標物，因此，行前的集訓課程是不可



2013年10月中旬聯合觀測行前課程，學生們互相教學如何規劃觀測計畫。

或缺的，大約一至兩堂課的時間，需解說(1)關於展源星等的計算方式，並藉此由觀測星體估算最佳的所需拍攝時間；(2)目標物與月亮的距離及仰角必須大於30度，以確保在可觀測高度之上，並且不會被明亮的月光蓋過；(3)目標物大小是否符合望遠鏡視野範圍，初估可能的成像畫面……等多項因素。讓同學們有一定的先備知識，並對於拍攝星體的流程具有熟悉度，會使觀測活動更有目標與成就感。

食、衣

除了學術方面，上山前的準備事項也得注意。隨著海拔高度的變化，氣溫驟降，即使在夏季溫暖的七月，天文臺的溫度就如同冬季的臺北，更可與寒流來襲相作比擬。更遑論受到溼潤季風的吹拂，上山時車子便在霧裡鑽入鑽出，而此時眺望層巒群峰，更是雲霧繚繞，若隱若現。當高山的溼度創造了美景，卻也使原本微涼的氣溫因含了許多水氣而越發令人覺得冷冽了。而若在十月中旬、正值深秋之際的時刻前往，山上的氣溫在夜裡下降後總徘徊於5度左右，山風更是颼颼吹個不停，這時保暖的衣著便是十分重要。

建議的事前準備有：

- (1)行前數天可查詢當地的最高溫及最低溫才不會錯估衣物的準備。
- (2)溫差大的山頂上適合多件衣物的洋蔥式穿著。
- (3)需注意臉部、手部的保暖，外衣應以防風防潮的羽絨外套為佳，而下半身的穿著儘量避免

目標	座標	視星等	大小	展源星等	S/N	曝光時間(s)	曝光時間*3	分	s/張	張數*3	可觀測時段	濾鏡
19:00-21:00												
M57-NGC6720	18:53:35.07 +33:02:00	8.8	2.5	18.19	20	125	500	8.333333333	30	5*4	19:00-21:30	H B V R
環狀星雲	天琴座									20mins		
M71	19:54:24 +18:49:00	8.18	3.3	18.1691	30	186	558	9.3	30	8*3	19:00-22:00	B V R
球狀星團										12mins		
M27	19:59:36.34 +22:43:16.09	7.5	8*5.6	19.02	40	600	2400	40	60	10*4	19:00-22:30	H B V R
啞鈴星雲	狐狸座									40mins		
NGC659	01:44:00 +60:42	7.9	5	18.7914	40	473	1419	23.65	60	8*3	19:00-4:00	B V R
疏散星團										24mins		

行前的觀測計畫擬定。



2013年10月中旬的聯合觀測後，電腦處理後獲得的三色合成影像。

NGC2261/北一女中邱楚玉同學。(左圖)

M78/北一女中楊曉晴同學。(右圖)

牛仔褲，才不會因褲子吸水造成不舒服的感覺，必要時再加件衛生褲更能保持溫暖。此外，沒有登山經驗的同學容易忽略山上的低溫，準備的衣物不夠而感冒，甚至加重高山症症狀。

(4)而溼寒的天氣裡徹夜未眠讓人不知不覺就想補充熱量、進食，糧食方面需注意的是，充氣式包裝的食品可能會因為高山的低壓而出現膨脹甚至是爆破的情況，使這些食品不易存放，建議攜帶沖泡式的熱飲與泡麵會是為最佳的選擇。

住、行

上山時結伴同行，是避免落單且安全登山的好方法之一。進行戶外活動必須三人以上才可成行，以讓小組成員足以互相照應。另外，由於空氣稀薄再加上低氣溫，每個人會因體質異同或多或少有些不適的症狀，諸如頭痛、胸痛等，一有不適應需立即反應，以免耽誤自身生命安全。所以，行前身體的保養也十分重要，睡眠充足、飲食正常、衣著保暖，特別是調整好上山前一周的生理作息，讓自己有一副強健的身體以避免高山症乘虛而入，也別忘攜帶健保卡等重要證件。抱持健康愉快的心情和身體，即是觀測活動不可缺少的動力之一！

省思

而身為入山者的我們，是來到這座山的客人，應懷有對大自然的敬意；對天文臺、對當地應有的禮節；對老師長輩的尊重。隨手的簡易小事如整理垃圾和回收物、走路輕聲避免驚擾休息

的人、不浪費各種得來不易的資源、懂得讓位而不霸據一方，離去前把環境回歸適當。高山大地之美是大家共同維護的，讓鹿林永遠是逐星最美好的聖地。

夜未眠

雲雨擾亂，始終沒澆熄我們對於開天的一絲希望，一夜的觀測，雖然等待的時間稍顯漫長，但天文觀測偶爾必然掌握於運氣之間的。在這身處高山的夜晚之後，帶著熬了一晚的倦意，我們靜盼著曙光亮起的時刻、早晨的歸來。

莫約七點出頭，屋外的景致已換上不同的光彩，陽光散去微薄空氣中的寒意，灑落在一片山巒之中，山稜線因光影而勻稱，那遠在一方的玉山主峰格外撼動人心。站在天臺上，凝視雲海的遼闊，雲海之後的地平線上湛橙的金星帶交疊於暗藍地影之上，此時身在一片綠意中的鹿林顯得意外小巧。雖然待在這兒的時間短暫，但仍然很是高興能夠有如此難能可貴的機會來訪鹿林天文臺，擁有那全臺最接近天空的望遠鏡，在絕佳的視野靜觀天文景象。

超新星

照片裡的一個亮點，同世間成萬上億顆星靜止於此瞬間，安靜到我們沒有察覺，靜到星系的美將之覆蓋，我們起初歎為觀止的對象不是它，

→ 北一女中高瞻計畫師生團隊七月底於鹿林天文臺所拍攝的SN 2013ej影像。左下圖為該超新星的光度變化曲線，紅框處即為本團隊的貢獻成果。

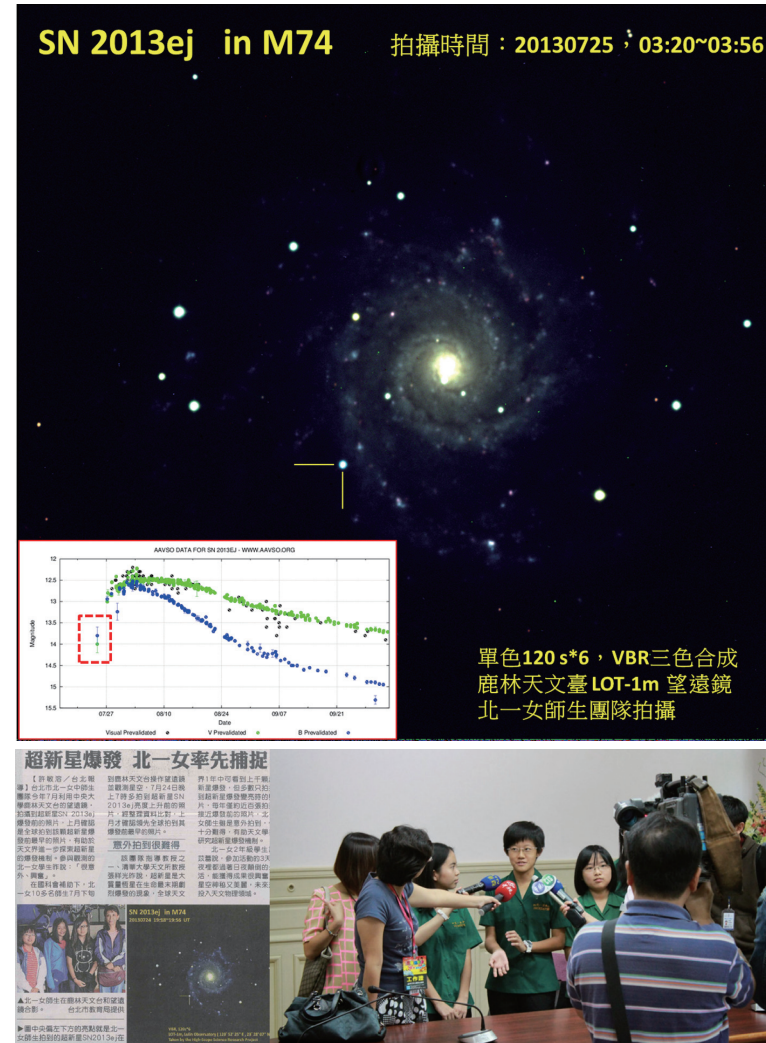
→ 2013年7月使用鹿林天文臺1公尺望遠鏡拍攝到SN 2013ej超新星身影的報紙新聞與媒體採訪。

直到其身份被發掘：那宇宙中最激烈的爆炸——邁向死亡的星。幾張照片將數萬年前的光芒限縮於幾個pixel，照片後的它並不如其貌優雅，是更加瘋狂、特殊，無意間我們留存下這份光線。無意間，只是循著觀測計劃的安排，我們抓到渺小的機會，是運氣，讓我們對鹿林與星空牽上更深一層的羈絆。

不如其名超新星並非新的星，而是一直存在於比它光彩的世界當中隱沒。然而星等銳減，亮度暴增，竭盡所能的閃耀，或許是最後掙扎但它做到了，讓世人看見，在資料庫上畫下深刻的一筆，這好像我們一樣，原本安靜的生活被打破，突然間接到來自各報記者的電話詢問、採訪，瞬時一躍上報，成了歷史紀錄其中的小小版面，發光發熱一時，連著激發周圍環境物質，儘管如今已黯淡，還是有殘骸、有遺跡，溫度並未褪去。餘溫尚存，因超新星而沸騰的心情伴著我們，繼續探索無際的天外，想要遇見更多可能性，益加堅定這條通往天文的未來之路。

懷 恩

回憶隨著流逝的時間被逐漸拉長，切割成細碎的片段，形成一種短暫卻深刻的駐留，記得那躍過天際的流星、獵戶排列的腰帶、如木壘板一樣棱角分明的御夫……。鹿林天文臺帶給我們



的感動很多，但感謝，更多。更要謝謝隨行的師長，以及天文臺全體的人員。當我們沉浸在星空之美時，他們在一旁默默的照看，不厭其煩的講解、不時提供協助，讓我們在觀測時能快速就上手。每個人都很熱情、都很有耐心，沒有因為我們只是一介年少輕狂的高中生，而有差別待遇。

我們都會記得，那天山上很是寒冷，但鹿林天文臺的氛圍是溫暖人心的。

林郁梅：臺北市立第一女子高級中學 地科老師
陳心平、廖乙馨、許苡蕾、蔡欣儒、許雅婷、
王蕾婷、沈庭：就讀於臺北市立第一女子高級
中學

陳麒瑞：就讀於臺北市立建國高級中學

臺灣流星觀測網 介紹

(Taiwan Elegant Meteor and TLE Network)

文/ 楊義清

當我們試著將整個地球看作一個系統來看，那麼這個系統會受到地球外的太陽系環境所產生之影響的情況並不多；除了來自太陽風暴的干擾外，另一種常見的現象就是流星體進入大氣層。

當研究者企圖藉由流星來瞭解太陽系的環境時，計算出流星體在太陽系中的軌道是一項在研究中很重要的資訊。然而想要準確地得到軌道資訊，便需要利用三角定位法來進行，因此對單一流星的多點觀測就成了唯一的途徑。多點觀測所獲得的資料再加上分析軟體，就可以得出流星體在太陽系裡運行的軌道，而且越多點的觀測資料會提高資料的精確度。

基於對流星體軌道的研究，2008年任職於中央大學天文所的阿部新助助理教授便著手在中央大學校區內及鹿林天文臺上架設自動觀測系統。筆者是在2009年透過任職於臺中科博館的林志隆副研究員介紹得知此一構想。鑑於流星自動觀測系統在技術與資金的門檻條件不高，所以2010年筆者與當時專題生曹俊傑便著手在臺東及高雄兩地分別規劃架設一套自動觀測系統。自動觀測系統的基本原理可參閱吳秉勳在本期中《流星自動觀測與分析軟體介紹》一文。2010年下半年先完成位於高雄的自動觀測系統，隔年暑假時接著臺東處的自動觀測系統。這兩處的系統架設完成後，便已具有定位流星體軌道的能力。但是流星自動觀測系統中的高感度光電耦合器都是固定方



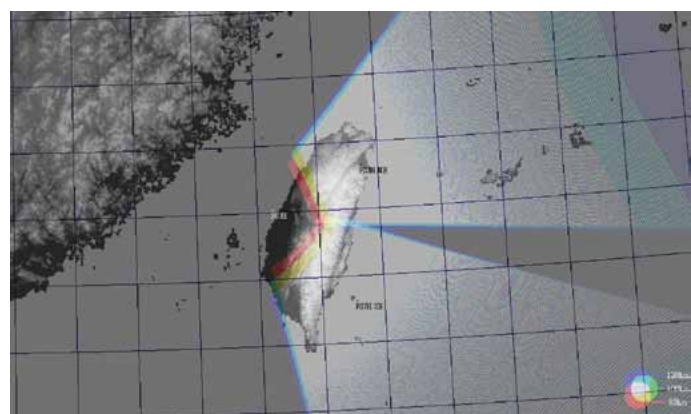
圖一、目前流星觀測網的觀測地點與監視器觀測方向

向的，因此可觀測範圍就變得有限。僅以上述四處的自動觀測系統所能涵蓋的範圍便顯得非常不足。

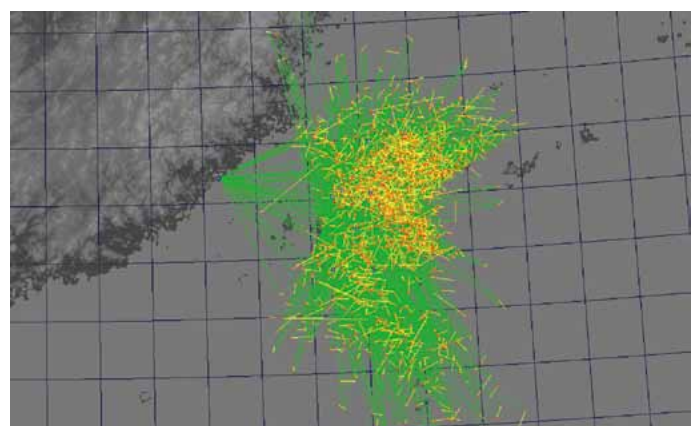
因此，2012年起，首先是林志隆副研究員與臺中大里高中的林土超老師於臺灣大學梅峰農場處架設一套自動觀測系統；阿部新助助理教授所指導的研究生，臺中惠文高中的吳秉勳老師也在惠文高中校內架設自動觀測系統。然後吳秉勳老師又尋得金門金城國中蔡松輝老師及彰化福興國中的吳炳連老師參與，在金城國中及福興國中內又分別架設自動觀測系統。最後，東華大學物理系的紀信昌也加入團隊，並於東華大學內架設自動觀測系統。至此，團隊雛型已成。所以大家覺得應該幫整個團隊取上一個容易上口又好記的名稱，最後大家一致同意採用由阿部新助助理教授所提議的英文名稱『Taiwan Elegant Meteor and TLE Network』，縮寫則為『TWEET』，中文名稱則用『臺灣流星觀測網』。

環觀世界各地，許多地區也多已有成立類似的組織。如最早於1911年成立的美國流星協會，該協會早期是以目視紀錄為主。另一個較大的觀測網絡為歐洲視頻流星觀測網絡 (European viDeo MeteOr Network Database, EDMOND)，這是有數個較小的觀測網絡所共同形成的，其中成員有法國業餘觀測網絡 (BOAM)，中歐流星網絡 (CEMeNt)、匈牙利業餘觀測 (HMN)、義大利流星和TLE 網絡 (IMTN)、波蘭火球網 (PFN)、斯洛伐克視頻流星網 (SVMN) 及若干幾位單獨的業餘觀察者。在日本則有成立於2004年的『SonotaCo Network』。而跨國之間的最大型組織則是成立於1988年的國際流星組織『IMO』，那是一個國際性的科學非營利組織。

由於流星自動觀測在技術與資金上的門檻條件都不高，因此在國外為許多天文業餘愛好者所青睞。在2013年5月31日，臺灣時間晚上10點28分全臺各地都有超亮火流星的目擊及視訊紀錄（特別的是大多數的視訊紀錄都是來自於汽車的行車紀錄器），而臺灣流星觀測網中的福興國中觀測點跟梅峰農場觀測點也都記錄到東南方有一顆超亮的流星。稍晚便由吳秉勳老師將這顆流星的軌跡給算出來（見圖四左），出現位置在綠島東方約100公里處的高空。不過很可惜這次的結果並沒有快速地利用管道向外界披露，為此臺灣流星觀測網的成員便商議成立臉書粉絲首頁（同年6月7日），作為科研成果快速呈現的管道。在阿部新



圖二、彰化福興國中觀測站所觀測涵蓋的天空區域，顯示的顏色代表為不同海拔高度所能觀測的涵蓋範圍。

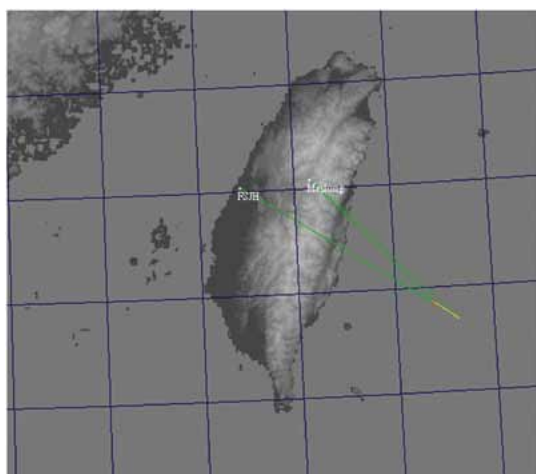


圖三、2010年至2013年經由兩個觀測站以上所記錄到的流星軌跡。

助助理教授回到日本任教後，為了加強成員間彼此的聯繫，因此大家決議設立召集人一名（2014年由筆者擔任）來召集討論有關臺灣流星觀測網的任何事宜。臺灣流星觀測網歡迎有興趣的業餘天文愛好者加入，任何有興趣者可以直接連絡筆者，或是就近聯繫上述文中提到的人員。

楊義清：臺東大學應用科學系 副教授

Email:icyang@nttu.edu.tw



圖四左、2013年5月31日晚上10點28分（臺灣時間）發生於臺灣附近高空的超亮火流星事件之軌跡圖。

圖四右、於梅峰所記錄下來的火流星影像，絕對星等推算小於-8等。

流星現象基礎原理

文/吳秉勳

彗星與小行星對於太陽系的形成過程提供了很重要的資訊，一般在地球上除了用望遠鏡觀測外，很難直接瞭解其成分，太空探測中，一些太空船帶著探測設備造訪彗星或小行星。

著名的美國NASA深擊號太空船（Deep Impact）於2005年9月釋放了一枚撞擊器，藉由撞擊週期彗星譚普一號（9P/Tempel 1）所噴發的灰塵，透過光譜得到成分組成；日本JAXA的隼鳥號（Hayabusa）則是在2005年11月接觸編號第25143糸川小行星（Itokawa），採集了小行星的樣本並返回地球。而流星和隕石則是直接將樣本帶到地球，提供我們分析，預估每天約有40公噸重的流星體掉落至地球，相當於一顆直徑1.4公尺的小行星（以球粒隕石的密度估算）。

名詞與分類

彗星（Comet）：主要由冰所組成的太陽系小天體，當它接近太陽時，受到太陽加熱而噴出它的氣體與塵埃形成彗髮與彗尾，這些噴出的物質會受到太陽輻射與太陽風的影響，研究彗星是瞭解太陽系形成的重要資訊來源，而大部分流星雨的來源往往是某顆彗星噴發的物質，該彗星就會稱為某流星雨的母彗星。

小行星（Asteroid）：小行星特別指是位於太陽系內側的小天體，通常沒有像彗星的活動特徵，但我們仍發現有一些小行星的表面散布了揮發性物質。通常定義其軌道在木星以內的稱為小行星，更遠的小天體則包含了半人馬小行星（Centaur）和海王星外天體（Trans-Neptunian

object, TNO）；編號3200的法厄同（Phaethon）小行星就是造成每年12月13-14日雙子座流星雨的來源。

流星體（Meteoroid）：散佈在太陽系中的流星體是小型岩石和金屬物質，明顯地小於小行星，介於細砂至1公尺寬的大小，通常來自彗星和小行星的碎片，也有部份來自受到撞擊的月球和火星碎片。當流星體以數十公里的秒速進入地球，會因為和地球大氣摩擦的熱而發光，此時我們就稱為流星，若是最後仍有殘餘物直撞擊地表，我們稱為隕石。



鹿林天文台北向的流星監視器在2012年12月13日當晚捕捉到超過500顆的流星。



一顆大小約五公分的鐵質隕石

微流星體（Micrometeorites）：質量約為 $10\text{-}12\text{-}10\text{-}6\text{g}$ ，直徑約為 $0.6\text{~}\sim\text{~}60\mu\text{m}$ ，此類微小的物質進入地球大氣時，通常無法經由可見光或是雷達觀測到類似流星的現象，但是可在分析平流層、冰芯、深海與內陸的沉積物中發現。

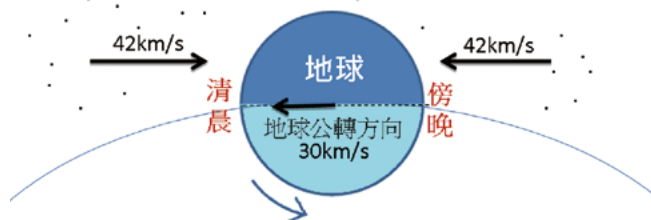
流星（Meteor）：當流星體進入地球大氣，摩擦生熱而發光的這段期間，我們稱此現象為流星，高度大多發生在 120km 到 80km 之間，直徑約為 0.01mm 到 20cm ，質量約為 $10^{-9}\text{~}\sim\text{~}10^4\text{g}$ ，我們通常可以在無光害的夜晚觀測到，也可以利用相機拍攝，雷達則能觀測到更暗、更高的流星，日本京都大學的中高層大氣雷達（MU Radar）每天可以觀測 $40,000\text{~}\sim\text{~}50,000$ 顆流星。雖然天文學界中無明確規定，通常亮度小於-3等的稱為火流星（Fireball），亮度小於-8等的稱為巨大火流星（Bolide）。國際流星組織（IMO）正開始建立全球火流星的觀測紀錄，歡迎有興趣的人在看到火流星之後，到<http://dev.imo.amsmeteors.org/>填寫簡單的觀測報告，越多人的參與便能讓流星的科學研究更完整。

流星雨（Meteor Shower）：在晴朗的夜晚常可以見到流星出現，若是這些流星從天空中一個所謂的輻射點發射出來（實際上不是一點，而是一個小區域，而且每天稍微改變），我們稱

之為流星雨，形成流星雨的流星和其母彗星的軌道有關，有類似的速度與運動方向，而彗星往往很難經常觀測，也幾乎沒有直接的樣本可以取得，也因此若能藉由研究流星，我們就能對母彗星有更深入的瞭解。另外沒有屬於任何流星雨的流星，我們在每天晚上都有機會看到，稱之為偶發流星（sporadic meteor）。

流星的速度

在計算流星的速度時我們先不考慮地球自轉的影響（影響約佔1%），我們要求出流星相對地心的速度（geocentric velocity）：

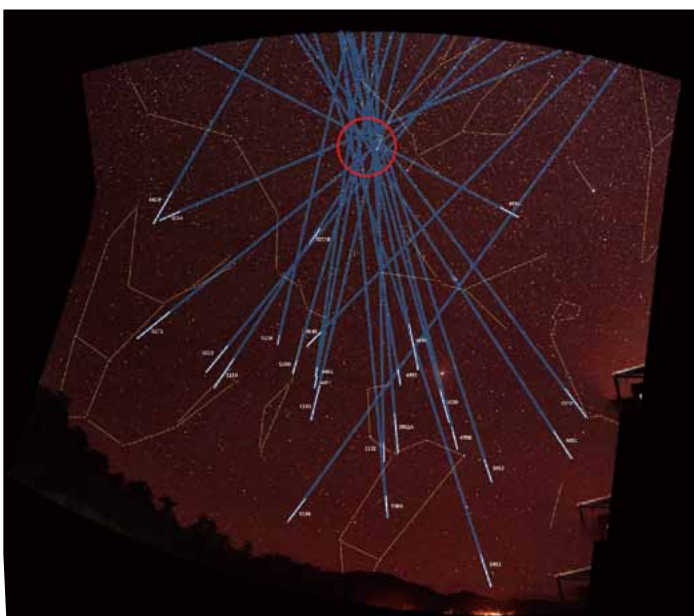


地球繞太陽的公轉速度約為 30km/s ，在 1AU 距離的太陽系逃逸速度（第三宇宙速度）約為 42km/s ，流星體自己的速度不可能大於 42km/s ，若是大於 42km/s 則速度大於太陽的重力吸引而離開太陽系；因此在地球清晨的那一面，流星會以較快的速度撞擊地球，速度最大為 72km/s （ $42+30=72$ ），而在地球傍晚的那一面流星則須追上地球，因此相對地心的速度會較慢，流星也會較少，那麼流星最小的速度是多少呢？

因此流星的地心速度為 $11\text{~}\sim\text{~}72\text{km/s}$ ，在過午夜後的地球那一側也較容易看到流星，速度也較快。

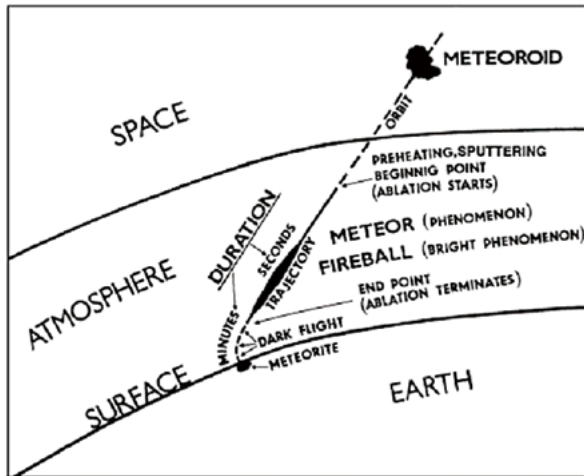
進入過程

流星在進入地球大氣層之後可以分為三段過程：預熱期（preheating）、消融期（ablation）、無光飛行期（dark flight）



將雙子座流星雨多幅拍攝照片合成並延伸軌跡後得到輻射點所在區域

在400~120km的地球高空，此時大氣的平均自由徑（mean free path）有150km，流星體和大氣很難碰撞，因此幾乎無法和流星體摩擦發光，僅有雷達觀測可以觀測到400km高微弱的流星現象。



資料來源：<http://www.asterism.org/tutorials/tut36%20Meteor%20Showers.pdf>

消融期是指當流星體抵達130~120km高的地球高空時，氣體分子已逐漸增加，會和流星體摩擦加熱至2000K，此時流星體就會開始消融而發光，同時周圍空氣分子也會受到能量激發也有發光現象，這段期間會大約發生在120到80km左右。

當流星受到大氣摩擦減慢到終端速度後（火流星約為3~4km/s），便不再能發光，一直到撞擊地面的這段時期稱為無光飛行期，10g左右的隕石

最後落下的速度為~10m/s，10 kg大的隕石速度為~100m/s；在此期之前的飛行約為直線，無光飛行期受到較大的阻力，速度也較慢因此行徑路線往地面彎曲，若要憑著流星軌跡尋找隕石，則須考慮此一因素。

發光現象

流星在天上劃過後，我們能觀察到是因為流星在消融期時所發出的光，而發光的種類其實也有很多種，在此介紹最常見到的：流星尾（meteor wake）、短暫的流星跡（Short duration meteor train）、短暫的流星餘暉（meteor afterglow）、持續的流星跡（Persistent Meteor Train）。

流星尾（meteor wake）是流星體本身的氣體和粒子受熱電子躍遷的發光現象，流星尾大約有數百公尺到數公里長，並只持續數十分之一秒。

短暫的流星跡（Short duration meteor train）最多可出現數秒，發光波長為557.7nm，和極光的綠色光芒一樣，也就是高層大氣中氧原子的禁線，像獵戶座流星雨、英仙座流星雨、獵戶座流星雨這種速度快（速度大於60km/s）的流星特別明顯有此類的發光現象。

短暫的流星餘暉（meteor afterglow）是要透過光譜分析而分辨出來，流星帶來的金屬元素，其電子受激發後回到基態時的光，最多可持續數秒。



NASA太空人Ron Garan在國際太空站上於2011年英仙座流星雨的期間拍攝了這幅照片。版權：NASA/Ron Garan。資料來源：<http://apod.nasa.gov/apod/ap110817.html>

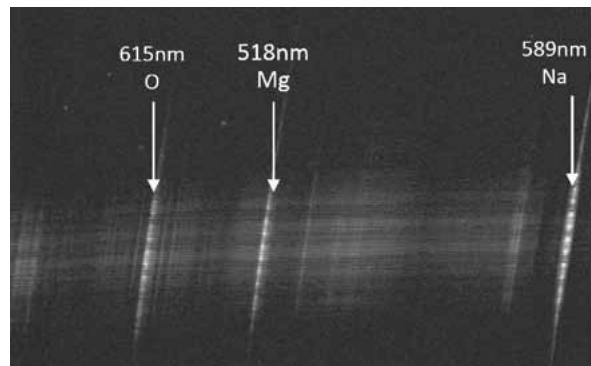


一顆流星在一秒內的發光變化情形。



流星尾端的綠色光芒是氧原子的禁線。

資料來源：http://en.wikipedia.org/wiki/Meteoroid#mediaviewer/File:Leonid_Meteor.jpg



透過光譜可以分析出流星最主要的三條光譜線，分別是鈉、鎂和氧，還有其他種元素譜線。



遊客於2012年6月28日在澳洲伯斯海邊所拍攝到的流星塵埃雲

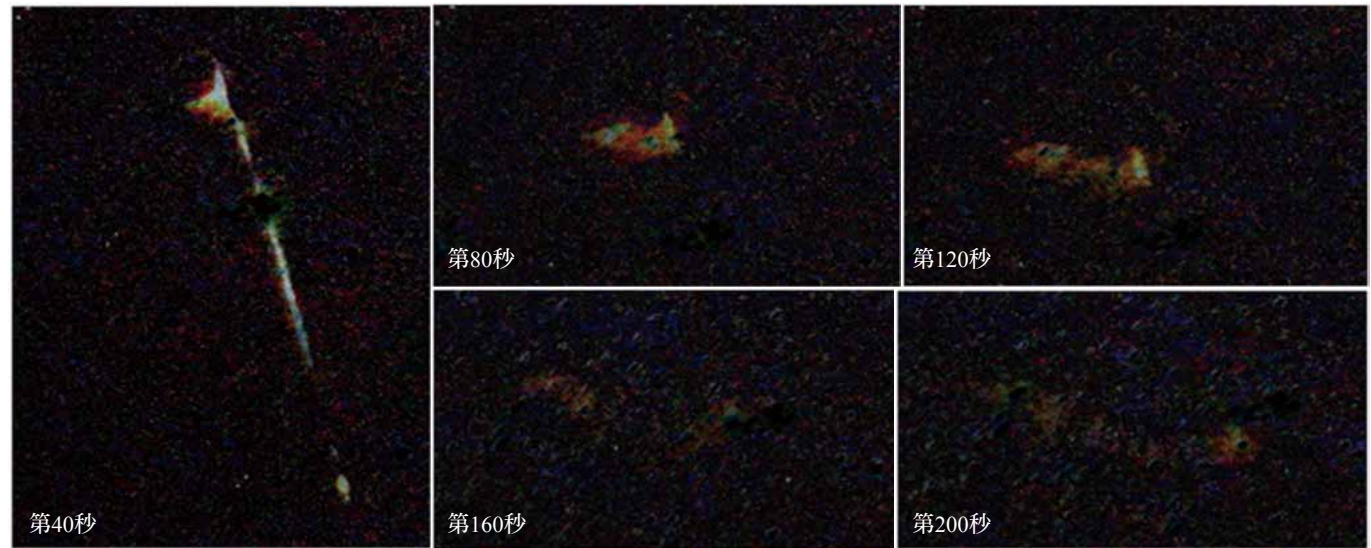
資料來源：<http://thewatchers.adorraeli.com/2012/07/01/meteor-plunges-into-ocean-lighting-up-perth-sky/>



2013年2月15日上午發生在俄羅斯Chelyabinsk市的隕石撞擊事件，空中留下巨大的雲

https://commons.wikimedia.org/wiki/File:Ekaterinburg_view_of_2zz013_meteor_event.jpg?uselang=ru

吳秉勳：任教於臺中市立惠文高中



2013年5月31日一顆超過-8等的火流星照亮台灣東部海岸，隨後留下4分鐘以上的流星跡。拍攝者：姜漿薑

鎏金歲月

流星體與母體軌道相關性研究

文/林士超、倪嘉晟、彭宣儒、廖彥朋

每年都有三大美麗流星雨分別是：一月的象限儀座流星雨、8月的英仙座流星雨、12月的雙子座流星雨。雖然每顆流星在劃過天際時有長有短，但同一星座的流星群都是從天空中某一區的輻射點(面)射出；雙子座流星雨是以雙子座附近為輻射點出現的流星雨。每年在12月7日至16日前後出現，於12月14日達到高潮。

流星是外太空的小碎片掉到地球大氣層內所產生的發光現象。而流星雨的成因常說是起源自特定的彗星小碎片。但是，流星雨的母體真的是彗星？若是如此，雙子座流星雨的母體是誰？是小行星3200厄法同(Phaethon)?因此臺灣的流星觀測網想要借由相當龐大的火流星數量，進行雙子座流星體及其輻射點回推的初步研究，並且若有一定數量的火流星可觀測到，我們更想對其流星母體進行驗證，是否為坊間流傳的小行星3200 Phaethon。

全文修改自中華民國第五十三屆(2013年)中小學科學展覽會(中三區)高中組地球科學科作品說明書。(關鍵詞：雙子座流星雨、流星體、母體軌道。)

源起

在2012年年底臺灣有幾位天文同好，包括了臺中科博館林志隆博士、臺中惠文高中吳秉勳老師、暨大附中曾世佑老師、興大附中（原為國立大里高中）林士超老師，以及臺中市天文學會簡明毅先生、金門的金城國中蔡松輝老師，還有鹿林天文臺的流星觀測團隊（阿部新助教授、林宏欽臺長、林啓生與蕭翔耀兩位研究助理），共同建置了臺灣流星觀測網雛型，進行火流星的觀

測，基本的概念就是以多點聯合觀測，由三角定位法來找出流星體的空間飛行軌跡。

恰巧2012年十二月雙子座流星雨期間，月相與天氣都難得的好。於是我們想試著了解2012年雙子座流星雨的每一顆流星體的軌道特性（空間位置與時間特性）；並依觀測資料來推知、歸納出雙子座流星雨母體的軌道特性。最後，引用文獻中的軌道參數相似度評估法（Dsh判定），進行小行星軌道是否會與流星雨的軌道相接近判定。

這一次使用的儀器包含：高敏感度CCD(WATEC-910HX或902H)、C型接環廣角鏡頭(3-15mm, F值1到2)、每個戶外測站皆需個人電腦一臺，及影像記錄電腦程式UFO Capture (Sonotaco Inc.)，另外需個人電腦一臺，含分析用電腦程式UFO Analyzer及UFO Orbit (Sonotaco Inc.)、MS-Excel軟體。(圖1)

我們藉由臺灣多站的流星觀測點架設，如圖2，包含北部的中央大學中壢校園、中部的臺大山地實驗農場梅峰本部、南部的中央大學鹿林天文臺及海峽西方的金城國中，南部也還有高雄師大與臺東大學校園，透過高敏感度感光元件CCD(Watec 902H或910 H)與軟體UFO Capture(<http://sonotaco.com/>)搭配，進行火球流星的觀測與記錄，再用人工以肉眼去判斷流星觀測記錄是否確實為流星事件。

以電腦軟體UFO Analyzer讀取所記錄的影像檔，如圖3所示，以做為判斷拍攝資料中是否有流星、閃電或車燈。

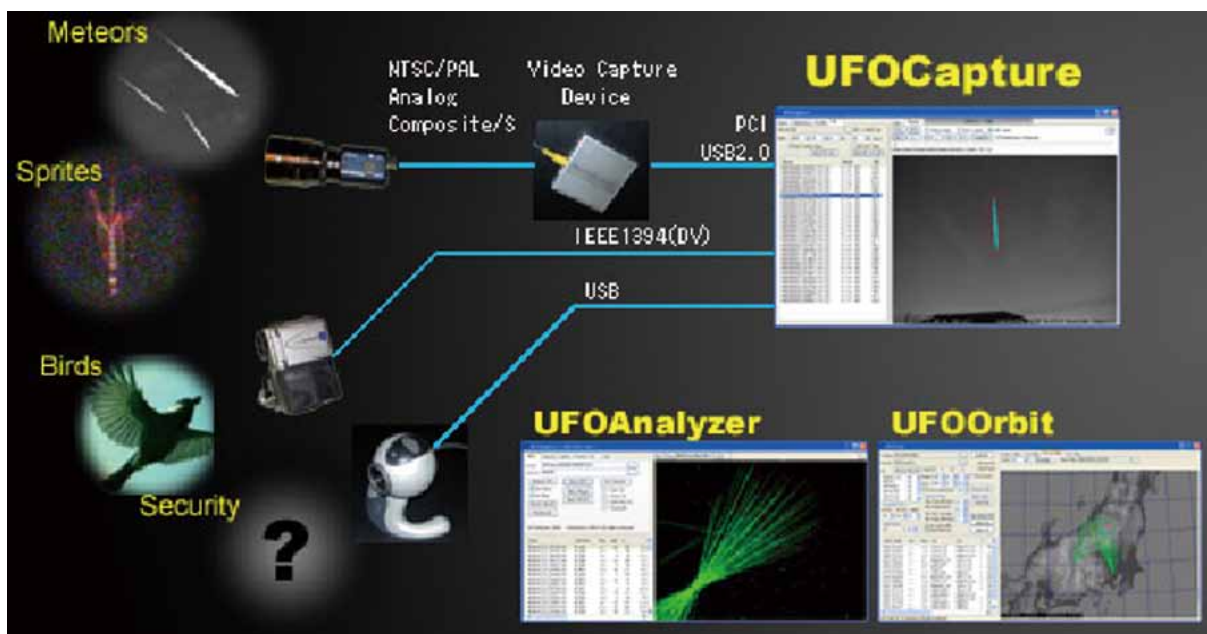


圖1. 流星觀測原理與設備需求，此一部份與影像監視系統相似。



圖2. 流星觀測點，有六個測站，十餘臺攝影機

觀測原理與工作流程

為了要確定流星在天空的正確位置，我們先在UFO Analyzer的協助下，進行每一個測站的影片判斷；再借由Analyzer程式畫面所面向的天空方位設定好，如圖.4，也就是攝影鏡頭可錄得的天空視野(FOV, Field of View)；最後，再以某時間的星空為觀測影片的天空為依據，調整軟體內預測的星圖，不斷的放大或縮小，直到星空所觀測

到的星點與星圖中的星點吻合。此等設定的數值即為錄影機面向的方位，再以此方位的數值套用到當天所有錄製的影片，進行每顆流星的分析。UFO Analyzer這套軟體就可以解出每個流星的出現時間、所在天球位置、亮度，還有各流星的基本參數（流星出現與消失的方位角及仰角、流星出現與消失的天球座標等），並將數據匯出存成純文字的M*.csv檔(是一種不含格式的純文字檔案的型態)，如圖.5。上一步驟是解出了單一測站的流星觀測事件的基本時空條件。

站與站的合作

接下來，再用UFO Orbit將UFO Analyzer分析所得的各測站M*.csv檔案的匯入進行交叉比對，操作畫面如圖.6，以三角測量的方法計算不同測站接觀察到的同一顆流星的真正位置（出現／消失的經緯度、高度）、流星速度（對地表或對地心的速度）與克卜勒軌道參數（ a 、 q 、 e 、 ω 、 Ω 及 i ，如圖.7所示），計算的概念如圖.8。如此一來可知火流星在夜空中的正確位置、流星軌跡回推的輻射點（如圖.9）及輻射點在天球座標的投影點（如圖.10）。最後，將交叉比對的結果匯出存成純文字的U*.csv檔。

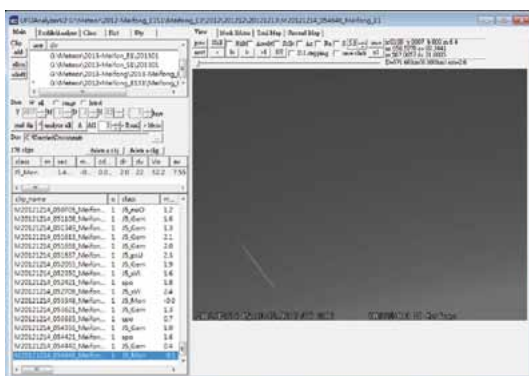


圖.3 UFO Analyzer畫面一（流星判定）

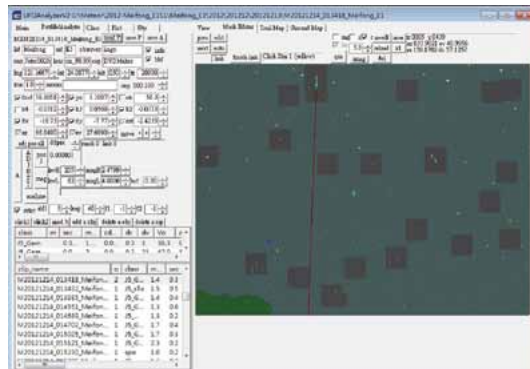


圖.4 Analyzer畫面二（星圖比對）

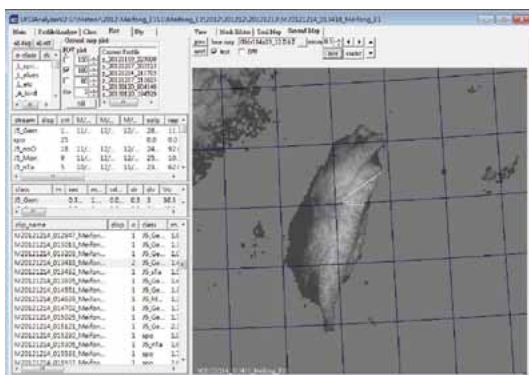


圖.5 Analyzer畫面三（地面資料）

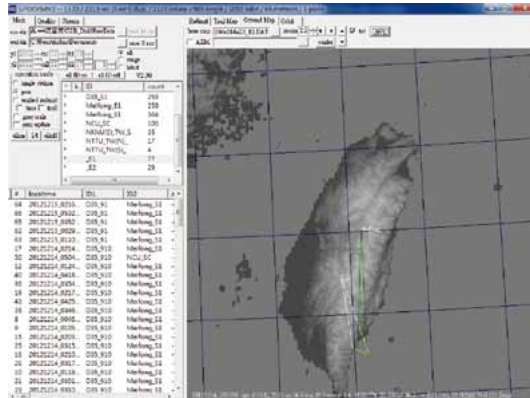
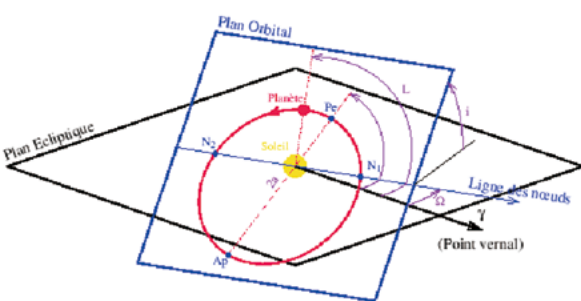


圖.6 UFO Orbit畫面三之一（比對地面二個站的資料，找出屬於同一顆流星的記錄）



Les 6 éléments orbitaux:

- i : Inclinaison du plan orbital.
- Ω : Longitude écliptique du nœud ascendant (N_1).
- ω : Longitude composite du périhélie.
- L : Longitude composite moyenne du corps à la date T .
- a : Demi-grand axe.
- e : Excentricité.

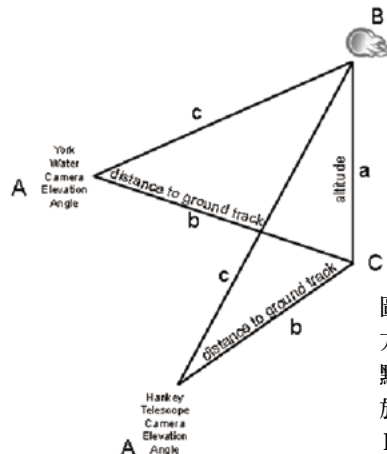
圖.7 流星體在空間軌跡的克卜勒軌道參數（a、e、L或 ω 、 Ω 及*i*）

圖.8 三角測量的方法（地面有二點A & A'相對於天上的流星B）

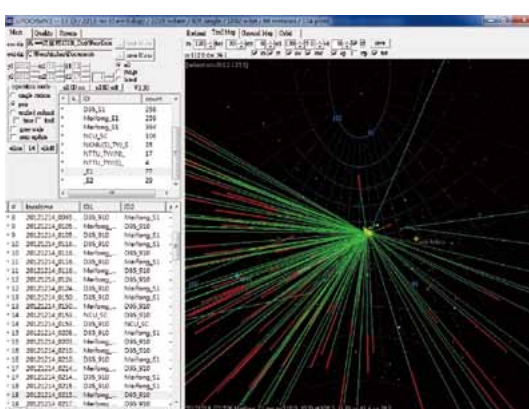


圖.9. UFO Orbit畫面三之二（火流星在夜空中的正確位置及回推的軌跡）

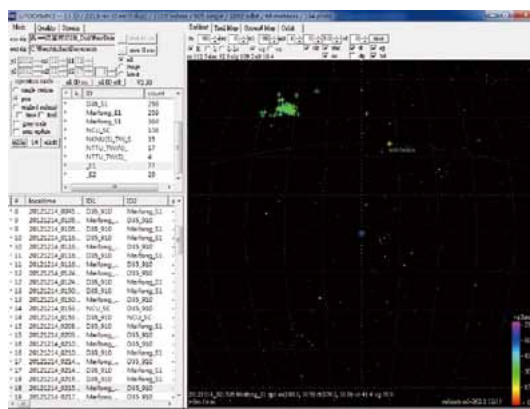


圖.10. UFO Orbit畫面三之三（輻射點在天球座標投影位置，及該顆流星的速度，以顏色表示）

交叉比對與軌道逆推

接下來的工作是利用EXCEL整理比對資料(U*.csv)來尋找各測站彼此之間在同一時間發現的流星，找出軌道較長、較短和較特別的流星，將其數值做進一步比較，猜測不同參數的性質。最後，以UFO Orbit所表列出來的火流星體的個別克卜勒軌道參數資料(a、e、ω、Ω及i)進行流星體的母體軌道回推，先是以國際天文聯合會IAU所公佈的3200 Phaethon小行星的克卜勒軌道參數資料為比較對象，進行Dsh的軌道相似度估算，來做為母體軌道的研判依據。Dsh是由克卜勒軌道參數所計算出來，計算式如下所列：

$$D_{\text{SH}}^2 = [e_2 - e_1]^2 + [q_2 - q_1]^2 + \left[2 \sin \frac{I_{21}}{2} \right]^2 + \left[\left(\frac{e_2 + e_1}{2} \right) \left(2 \sin \frac{\pi_{21}}{2} \right) \right]^2,$$

where

$$I_{21} = \arccos[\cos i_1 \cos i_2 + \sin i_1 \sin i_2 \cos(\Omega_2 - \Omega_1)]$$

and

$$\pi_{21} = \omega_2 - \omega_1 + 2 \arcsin \left[\cos \frac{i_2 + i_1}{2} \sin \frac{\Omega_2 - \Omega_1}{2} \sec \frac{I_{21}}{2} \right]$$

其中，e、q、I、π 分別是橢圓的扁平率、近日點距、小行星與流星體的軌道傾斜角差異值及某一個軌道特徵值；而 1 與 2 分別表示小行星與流星體。

觀測結果

除鹿林山與中央大學是較早架設觀測設備外，其他測站皆是在2012年才完成初步架設的流星觀測儀器，恰巧趕上了2012年12月的雙子座流星雨觀測。在天氣與月相的干擾因素下，只觀測了二個晚上（2012年12月13及14日，含15日凌晨），總計六個測站，有觀測到2219筆單站的火流星，各站資料詳閱表一。

上述的2219顆火流星中，由表二可得知：本次（2012年雙子座流星雨）觀測所得的火流星最大亮度可達 -5.3等、平均亮度在 -0.5等、火流星最早出現的高度是地表上的120公里高、但多數是90公里上下就出現流星的現象，火流星最晚結束高度是在60公里、但多數是75公里上下就結束流星的現象、相對地表的速度分佈在24.4~66.5 Km/s，火流星進入大氣時的平均速度在36 Km/s，相較於其他的流星雨，速度算來得慢一些。

最值得一提的是本次的雙子座火流星觀測特性之一為火流星出現時間算是比較長，平均達0.6秒，極可能是墜落入大氣層的顆粒比起其他次的流星雨是大的顆粒。簡而言之，2012年的雙子座流星雨具有：流星體速度較慢；亮流星很多，常有火流星出現。

代號	站名	地點	代號	相機型號	FOV 視野	Nights 觀測夜數	流星數
NCU	中央大學	桃園	NCU	WAT-910HX + 3.5-10.5mm/F1.0	~55	2	106
MeiFong	台大梅峰	南投	MF	Wattec 902 + 12mm/F1.4 Lens	~45	2	623
Lulin	鹿林山	嘉義	D35	WAT-910HX + 3.5-10.5mm/F1.0	~55	2	1328
Kimen	金城國中	金門	KM	Wattec 902 + 15mm/F1.4 Lens	~45	2	106
NKNU	高雄師大	高雄	KS	-	-	2	35
NTTU	臺東大學	台東	TT	-	-	2	21
				Overall	約120小時	2219	

表一：各測站基本資料與所觀測流星數

	亮度 (等)	出現高度 (Km)	結束高度 (Km)	速度 (相對地表,Km/s)	觀測時間 (sec.)
最大	-5.3	119.5	103.1	66.5	1.6
最小	1.6	75	59	24.4	0.2
最大瞬間	-5.8				
中位數	-0.5	92.7	78.2	36.6	0.5
平均	-0.6	92.9	77.1	36.6	0.6

表二：各測站基
本資料與所觀測
流星數

同時也可以發現：在二個晚上的2219顆火流星中，有66顆火流星是同時被二個測站觀測到的流星，交叉比較的資料參閱表三與圖.11。在表三中，ID1與ID2是分別代表不同的觀測站，由於鹿林山天文臺(D35)幾乎沒有光害，天光的背景值較低，再加上是架設三個方向各一支CCD；而臺大山地農場梅峰本部也有相似條件，二支CCD同時觀測。所以鹿林－梅峰這個組合，貢獻上52次，是66顆組火流星中最多的組合，接近六分之五，是本研究中品質較好的觀測站。至於，金門其他天數的流星數皆屬可以的條件，就2012年12月的

雙子座流星雨極大期間，天候不佳，斷斷續續的起霧。

終於，我們得到了二個晚上的2219顆火流星之中，有66顆火流星是同時被二個測站觀測到的流星，直接將它們推估的各別輻射點採平均值計算，參考圖.12，可得到2012年雙子座流星雨的輻射點位置赤經：7 h 35.6m，赤緯+31.8度，在雙子座Alpha星的附近，與文獻的差距都在1度以內，本研究的主要輻射點是參考2009年WGN37-2, The Journal Of IMO.

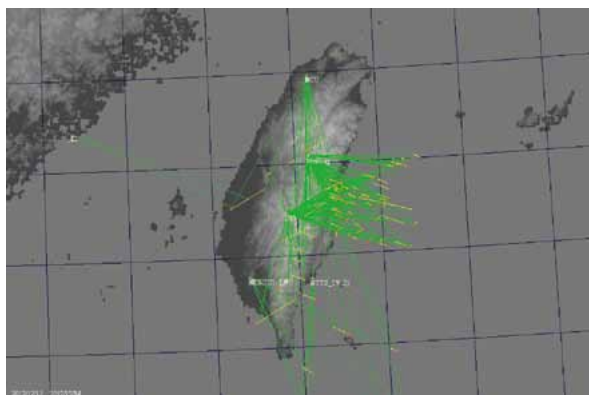


圖11. 自UFO Orbit畫面匯出的66顆火流星空間位置分佈

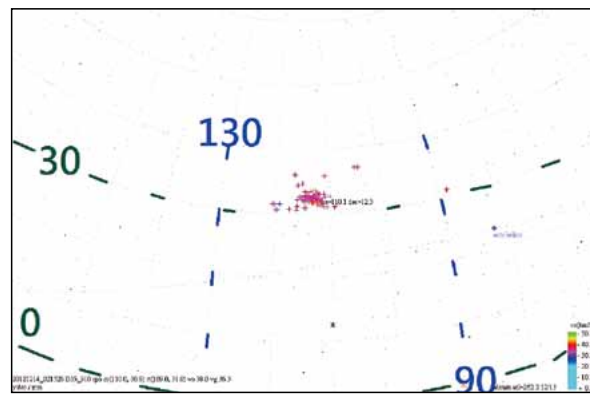


圖12. 自UFO Orbit畫面匯出的66顆火流星輻射點位置分佈，
圖中90與130是指天球赤經(度數)，0與30是指天球赤緯(度數)。

ID2 \ ID1	鹿林	梅峰	高師大	台東大學	中央大學	金城
鹿林	-	52			5	
梅峰	[52]	-	3		3	
高師大		[3]	-	2		
台東大學			[2]	-		
中央大學	[5]	[3]			-	1
金城					[1]	-

表三：66顆火流星
是同時被二個測站
觀測到的流星

Symbol	a	q	e	ω	Ω	i	Mag	Dsh
Theory	1.27	0.14	0.89	321.978	265.427	22.169		
Fireball-1	2.21	0.54	0.76	266.802	81.973	169.32	0.4	0.824
Fireball-2	2.9	0.57	0.8	272.775	81.973	169.546	-0.2	0.713
Fireball-3	1.18	0.18	0.84	321.008	261.975	19.841		0.564
Fireball-4	1.04	0.22	0.79	319.974	261.975	16.622	-0.5	0.47
Fireball-5	1.15	0.15	0.87	325.063	261.769	26.99	-2.1	0.282
Fireball-6	2.51	0.55	0.78	269.842	81.973	169.435	0.1	0.235
Fireball-7	0.95	0.24	0.74	320.029	261.958	13.708	0.1	0.063
Fireball-8	1.78	0.1	0.95	328.838	262.028	28.515	-1.1	0.047
Fireball-9	0.99	0.24	0.76	318.906	262.031	13.019	-1.7	0.037
Fireball-10	3.17	0.07	0.98	331.715	261.941	41.332	-0.6	0.036
Fireball-11	0.91	0.23	0.75	322.36	262.031	14.571	0.8	0.031
Fireball-12	1.14	0.24	0.79	315.774	262.026	19.874	-1.7	0.031
Fireball-13	1.03	0.23	0.77	318.504	261.968	13.331	0.4	0.03

表四：66顆火流星中，依Dsh的值由大至小取出前13名，Theory指的是Phaethon

軌道相不相似呢？

本研究是以UFO Orbit進行流星體的軌道回推，將每個流星體的位置變化以克卜勒行星運動方程式求出軌道參數，再佐以Dsh的軌道相似度做母體軌道的研判。此次計算的母體：採用小行星（3200）Phaethon，周期約1.4年，軌道很扁，近日距可達0.14天文單位，它的軌道參數取自JPL@NASA與WikiPedia.org。在表格四中，66顆的火流星中，只有6顆的火流星軌道相似度Dsh值是超過0.2（以粗體字表示），有可能是新的流星雨。其餘的火流星軌道相似度Dsh值皆小於0.2（Fireball-7以後的部份）。

累積成功的經驗

這一次我們藉由分散在臺灣的六個流星觀測站的架設，包含南部的中央大學鹿林天文臺、中部的臺大山地實驗農場梅峰本部、北部的中央大學中壢校園及西方的金門國中，先進行天空物體移動與否的判定進行記錄；再對照各站觀測影片的內容，判定火流星的出現與消失時間是否只有些許的差異（皆在零點零幾秒），做為判定是否

觀測到同一顆流星，是最先的想法。

但實際的做法是必需借由軟體先行計算流星體在天空的座標，若是有兩個測站皆觀測到位置相近的火流星（出現或消失），才會自動判定為同一顆火流星。所以才發現：從2012年12月13日晚上9點22分起至2012年12月15日凌晨5點32分，共有66顆流星是同時被兩個觀測站觀測到，更特別的是在2012年12月14日凌晨5點52分58秒有顆火流星是同時被三座觀測站觀測到。傳統以目視觀測流星有其辛苦之處，包含人員數目、交通、保暖、專注力及記錄等多方面限制。本研究已經改進為自動觀測，只要天氣條件與月相合宜，雖然只能觀測到較亮的火流星，而無法有星等小於2等的較暗流星，但事後的分析研究是有比較多事件可進行的，這方面歐美與日本皆已行之有年。例如，流星觀測之後都會將流星雨在單位時間通過天頂的數量ZHR值（如圖.12，是在IMO公佈的2012年雙子座流星雨的逐時ZHR）、輻射點、速度、顏色等數據做具體的描述。

在雙子座流星雨極大期的二個晚上，同時觀測的66顆流星，就各個觀測站所觀測到的流星數目

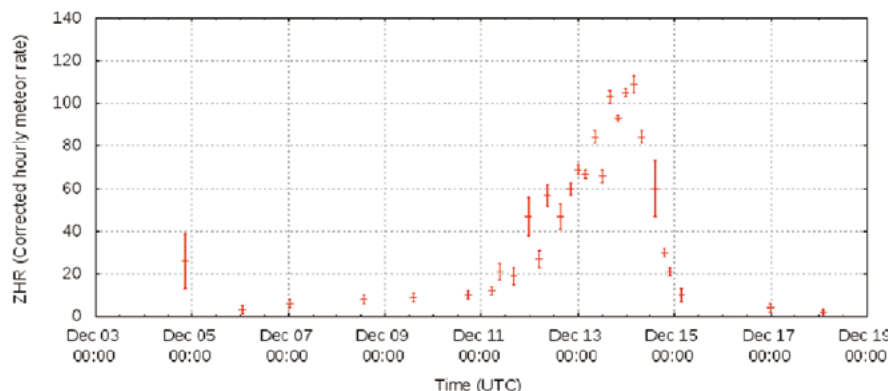


圖13. IMO公佈的2012年
雙子座流星雨的逐時ZHR
(<http://www.imo.net>)

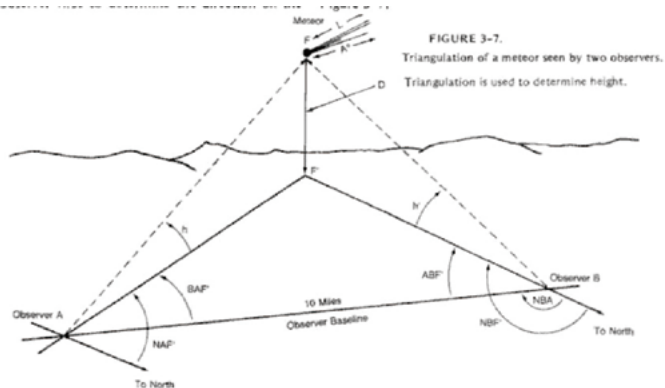
而言不算多，佔全部2219顆火流星的百分之3。在66顆火流星之中，臺大梅峰東與南向CCD觀測到最多對的流星，有58顆火流星，貢獻最多。其次，鹿林山向北與向南的CCD觀測到次多對的流星，有57顆火流星，有52顆是搭配臺大梅峰與鹿林山的組合。相反地66顆火流星之中，六個地點之一的金門僅與鹿林天文臺有一顆的火流星，或許需要進一步探討攝影機面對的方向、或選擇的站址、或環境天候不佳，方能更有效改善觀測的品質。

突破傳統

在傳統的目視或底片觀測流星，進行流星的三角定位，站與站之間通常是採取距離約50公里到70公里之間，最能適合進行三角計算求出確實的空間座標。本研究改以高敏感度CCD進行火流星觀測，事後用UFO Orbit軟體分析雙子座流星雨，我們所設的測點有比傳統方法的距離加大一些。

例如：中央大學距梅峰為98公里，梅峰距鹿林山為75公里，中央大學距鹿林山為170公里，梅峰距高師大為164公里，高師大距臺東大學為76公里；另外，金門到中央大學為297公里。此外，仍需考量地球圓弧外形、大氣的折射與短焦鏡頭的變型問題，所幸在UFO Orbit軟體分析過中已多有修正（真實星點與電子星圖比對）。總的來說，本研究大致能提供火流星定位與臺灣流星觀測網建置的初步參考依據。

本研究借由UFO Orbit所繪出的軌道空間分佈，加上Dsh的計算（計算式參見研究過程的步驟



From: A Complete Manual of Amateur Astronomy: Tools and Techniques for Astronomical Observations
P. Clay Sherrod, Thomas L. Koed (Prentice-Hall Press, 1981)

圖14. 三角定位示意圖（圖左右兩個測站A與B，決定了高度D）

），用來推估流星體是否來自同一母體。文獻中用Dsh公式將流星體及母體的六個軌道參數帶入，檢測兩者之間對太陽的繞行軌道面半長軸 a 、近日點距離 q 、偏心率 e 、近日點的輻角 ω 、(上)升交點經度 Ω 與傾(夾)角 i 相互之間的差異，據此作為判斷兩者是否就是同一天體的依據。

本研究也找一些彗星或小行星來當成判定的參考依據，如下表五，有哈雷彗星、週期彗星168P/Hergenrother（週期七年，上一次近日點時刻在2012年10月）、今（2012）年二月近距離飛馳過地球旁的2012 DA14小行星、及小行星中心（MPC）公佈的Phaethon（其軌道根數與JPL@NASA公佈的有些許不同）、我們自己胡亂編出的一組軌道根數以及2012年2月15日掉落在俄羅斯的大流星體Chelyabinsk的軌道參數。

（Theory指的是3200 Phaethon小行星，http://en.wikipedia.org/wiki/3200_Phaethon）

Symbol	a	q	e	ω	Ω	i	Dsh
Theory	1.271	0.14	0.89	321.978	265.427	22.169	
1P Halley	17.737	0.593	0.967	112.055	59.396	161.963	3.481
168P	3.581	1.359	0.621	14.991	355.472	21.612	2.045
2012 DA14	0.910	0.829	0.089	195.535	146.996	11.608	1.902
3200 Phaethon	1.271	0.14	0.89	321.978	265.427	22.169	0
胡亂編	1.2	0.2	0.95	300	265	23	0.131
MPC,IAU	1.271	0.14	0.890	322.148	265.267	22.241	0.000
Chelyabinsk	1.55	0.768	0.5	109.7	326.41	3.6	2.345

表五：用來當成Dsh的參考值判定依據的天體軌道參數表列

從表五的軌道參數計算出來的Dsh可看出1P哈雷彗星、週期彗星168P、小行星2012 DA14以及俄羅斯大流星體Chelyabinsk的Dsh計算結果，呈現出Dsh值都在2到3之間，明顯偏大，不是本研究雙子座流星雨的母體，至少今年不是。

有趣的是，取用同一組軌道參數（表五的3200 Phaethon）Dsh計算結果數值零，就是同一個天體；若是取用小行星中心的另一組軌道參數（表五的MPC,IAU）Dsh計算結果數值也幾乎等於零，也就是幾乎可說是同一個天體。讓我們回顧表格四，在66顆的火流星中，存在6顆的火流星軌道相似度Dsh值是超過0.2，我們有信心說它們可能是新的流星雨，值得後續的觀測分析。

註：MPC/IAU參數與維基百科/JPL@NASA有些許差異，應該是多年觀測值與大行星對軌道參數的長週期攝動perturbation造成的。

總結

研究發現2012年12月13及14日（含15日凌晨）雙子座流星雨，總計二個晚上，六個測站，觀測到2219筆單站的火流星；交叉比對火流星，有66顆火流星可以提供軌道參數，以計算軌道相似度Dsh。再者，2012年雙子座流星雨的火流星最大亮度可達-5.3等、平均亮度-0.5等、多數流星發生在地表90公里～75公里高；平均速度36 Km/s，輻射點赤經7 h 35.6m，赤緯+31.8度，具速度慢、亮流星多的特點。

若是以小行星3200 Phaethon為母體判定依據，66顆火流星中，有6顆的火流星軌道相似度Dsh值超過0.2，可能是新的流星雨；其餘火流星Dsh值小於0.2，表示Phaethon就是2012年雙子座流星雨的母體。

參考文獻

- (1) Davies, J. K., Are the IRAS-detected Apollo asteroids extinct comets?, Monthly Notices of the Royal Astronomical Society (ISSN 0035-8711), vol. 221, July 1, 1986, p. 19P-23P.
- (2) <http://www.astro.amu.edu.pl/~jopek/MDC2007/>, MDC@IAU
- (3) <http://sonotaco.com/>
- (4) J. D. Drummond, A test of comet and meteor shower associations, ICARUS 45, 545-553, 1981
- (5) A meteor shower catalog based on video observations in 2007–2008, SonotaCo, WGN37-2, 55-62, 2009, <http://www.imo.net/files/wgn/2009/WGN37-2.pdf>
- (6) <http://en.wikipedia.org/wiki/Triangulation>
- (7) 三角測量 (Trigonometric Measurements) , <http://case.ntu.edu.tw/hs/wordpress/?p=17379>
- (8) 3200 Phaethon軌道參數,<http://ssd.jpl.nasa.gov/sbdb.cgi?sstr=3200;orb=1>
- (9) http://blog.sina.com.tw/astro_calculator/article.php?pbgid=24388&entryid=307106, 天文計算實驗室_流星的軌跡

林士超：任教於國立興大附中

倪嘉晟、彭宣儒、廖彥朋：就讀於國立興大附中

Active brightness variation and polarization behavior of UXor type young star GM Cep

¹Po-Chieh Huang, ²Chang-Yao Chen, ³Chia-Ling Hu, ¹Chien-de Lee, ⁴Chi-Sheng Lin, ⁴Hsiang-Yao Hsiao, ⁵Shuhrat EHGAMBERDIEV, ⁵Otabek Burkhanov, ^{1,2}Wen-Ping Chen

¹ Graduate Institute of Astronomy, National Central University, Taiwan

² Departments of Physics, National Central University, Taiwan

³Taipei Astronomical Museum, Taiwan

⁴Lulin Observatory, National Central University, Taiwan

⁵Maidanak Astronomical Observatory, Ulugh Beg Astronomical Institute (UBAI), Uzbekistan Academy of Sciences, Uzbekistan

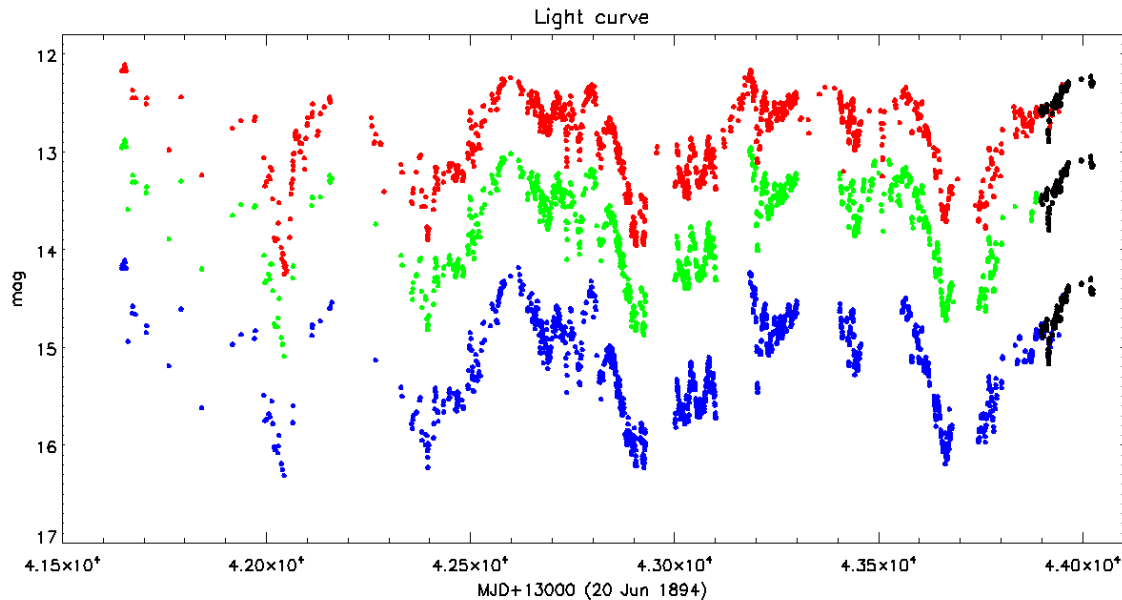


Fig. 1 Light curve of GM Cep. Red is R-band, green is V-band and blue is B-band.

GM Cephei (R.A. =21:38:17.32, Dec=57:31:22, J2000) is a solar-type pre-main-sequence star in the young (~4 Myr) open cluster Trumpler 37 (Sicilia-Aguilar et al. 2004, 2005), which is located at ~ 900 pc (Contreras et al. 2002). GM Cep shows prominent infrared excess, H-alpha emission, and flare activity. The star was classified as a UX Orionis (UXor) type star (Chen et al. 2012). UXor type stars are intermediate mass and mostly are a sub-type of Herbig Ae/Be or T-tauri exhibiting sporadic extinction of stellar light due to circumstellar dust obscuration. The intense multi-color photometric monitoring from 2009 to 2015 demonstrated the cyclic occultation events, but not strictly periodical, each lasting for a couple of months, with a probable recurrence time of about two years by the orbiting dust clump, as shown in figure 1. This signifies the onset of disk inhomogeneity from grain growth in the molecular cloud in transit to formation of planetesimals. In figure 1, blue is B-band, green is V-band and red is R-band, respectively. Black points represent the data came from Lulin SLT. SLT provided high coverage of light curve in 2014 and helped us very much.

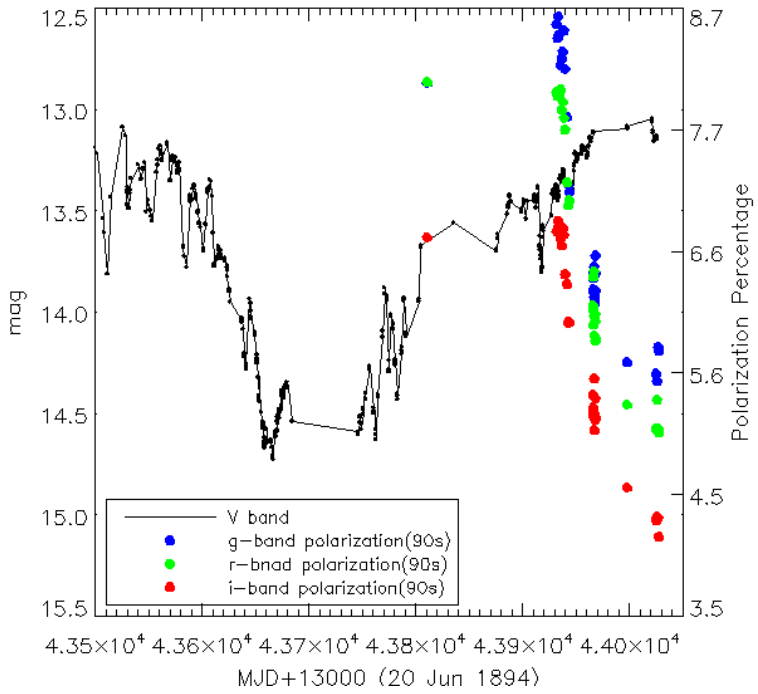


Figure 2 Polarization behavior of GM Cep. Red is i-band, green is r-band and blue is g-band.

Since the asymmetric disk distribution of the star system, the polarization phenomenon is unavoidable. The polarization measurements for the GM Cep have been processed a few times by TRIPOL. In order to cover long time variation of brightness of GM Cep, our strategy is doing regular observation per month. TRIPOL is a powerful instrument to observe the different filters simultaneously. But, we have to pay more attention for the maximum counts of each filter during the observations. In this case, the maximum counts were controlled in the range of 5000-35000 both in the g-, r- and i-band so that the counts of image keep in the linear region of CCD. After we make sure that the quality of all images are no problems, then we do the image reduction by combining darks and twilight flats. The twilight flats were observed before sunset and after sunrise, and the average counts were controlled in the range of 5000-30000 both in the SDSS g-, r- and i-band. Through our pipeline, the results of polarization and polarization angle were calculated by the fluxes of four different degree images (i.e. 0 deg, 45 deg, 22.5 deg and 67.5 deg), as shown in figure 2. In order to reduce the influences by the weather conditions (e.g. thin cloud pass through) during the long exposure time (90-120s), each data point is the mean value from 5-20 times continuous observations within one night. GM Cep shows the moderately polarization from about 4% to 9% in SDSS g-, r- and i-band. We found the evidence that polarization is anti-correlated with the brightness of star, during which the clump dust back scatter the stellar light. The polarization results are consistent with the linear polarization patterns. The results in this case demonstrate that TRIPOL is a good facility to do the polarimetric observations even if TRIPOL is a simple design instrument.

新聞報導

台灣驕傲！中央大學團隊助分析彗星照

中央大學天文所教授葉永烜（烜音同選），10 年前在德國馬克斯普朗克太陽系研究所服務期間，就參與歐洲太空總署（ESA）的羅賽塔號彗星探測船計劃，返台後他帶著中大天文所助理研究員林忠義和一些大學部學生一起加入，幫忙分析羅賽塔號的照片等資料。

原文轉載自【2014-11-14/中華民國 103 年 11 月 14 日 台視新聞】

相關連結 /

<http://www.ttv.com.tw/103/11/1031114/103111400040001.htm?from=568>

分析彗星組成 台助菲萊登陸

【記者陳奕如桃園報導】漫遊宇宙十年的羅賽塔太空船(Rosetta)12 日釋放探測器菲萊(Philae)，隔日凌晨成功登陸「67P/楚留莫夫－格拉希門克彗星」(67P/Churyumov- Gerasimenko)。中央大學天文所教授葉永烜及其團隊，協同各國研究小組，參與史上首度登陸彗星的計畫。

林忠義博士與地球科學系學生李睿綺從羅賽塔上的光學成像系統「OSIRIS」，分析其拍攝的 67P 彗核表面圖。他們研究彗核地表噴流的源處與岩石分布，屏除化學作用活躍之處及顛簸的地域，協助歐洲太空總署(ESA)尋找最適合菲萊著陸的地點。

OSIRIS 裝置的每個濾鏡都吸收不同的電磁波段，因而呈現相異的彩色地表圖像。不同顏色的區塊，反映出組成物質相異。林忠義與李睿綺根據每張圖片顏色代表的波段，推測 67P 的成分，再與他國團隊研究的結果進行比對，試圖分析彗星的組成。

李睿綺表示，因與地球距離甚遠，羅賽塔傳回來的照片經解壓縮後，常呈現錯誤訊息，需等待專業校正小組修復圖像，方能繼續研究。林忠義表示，彗核的組成物，光憑單一波段無從比較，要經過冗長驗證，過程充滿不確定的因素。

此外，菲萊因登陸時重力過小，著陸後經兩次大彈跳，偏離預定地，現今下落不明。而 17 日 OSIRIS 拍到菲萊第一次著陸碰撞的地表痕跡，可望藉由衝擊的方向找到它。

李睿綺說：「近距離觀察彗星的地貌，讓我們可以深入了解彗星，及太陽系形成時遺留下來的痕跡。」林忠義表示，彗星絕對不只是「髒雪球」，團隊將會持續研究 OSIRIS 回傳的圖片，直到羅賽塔不再運作。

原文轉載自【2014-11-21/第 1581 期 大學報 11/21-11/28 >> 新知】

相關連結 / http://www.uonline.nccu.edu.tw/index_content.asp?sn=6&an=19711

中央大學團隊 助分析彗星照

中央大學天文所教授葉永烜，協助分析羅賽塔號探測船的資料。壹週刊台灣之光

中央大學天文所教授葉永烜（烜音同選），10 年前在德國馬克斯普朗克太陽系研究所服務期間，就參與歐洲太空總署（ESA）的羅賽塔號彗星探測船計劃，返台後他帶著中大天文所助理研究員林忠義和一些大學部學生一起加入，幫忙分析羅賽塔號的照片等資料。

無線電波傳回母船

葉永烜昨表示，中大參與的是羅賽塔號上的紅外線可見光影像技術（OSIRIS）照相機，協助分析彗星照片，了解彗核（彗星中心固體的部分）表面軟硬、表面水和沙塵混合程度及化學成分，希望透過彩色照片分析彗核組成礦物種類等。至於菲萊無人登陸器，上有 10 種儀器，將在 67P 彗星表面鑽洞，研究溫度變化，最重要的儀器是無線電波透地雷達，訊號將穿透彗核傳回羅賽塔號，藉此推斷彗核構造、內部的水冰是分散還是塊狀，以解開彗星之謎。

未來永遠留在表面

葉永烜表示，加入計劃以來，看到 OSIRIS 照相機拍到的彗星照片最讓他感到驚奇，因為他之前也沒看過彗星的樣子。未來一個月將是菲萊的資料能否順利回傳的關鍵，隨著 67P 彗星逐漸接近太陽，彗星中的氣體可能會湧出，可能對菲萊及羅賽塔號造成傷害。

歐洲太空總署並無回收菲萊和羅賽塔號的計劃，菲萊在任務結束後將永遠留在 67P 彗星表面，至於羅賽塔號將待 2016 年再評估，如果可以，將繼續觀察彗星遠離太陽過程的變化，應該會很有趣。

記者陳怡妏

原文轉載自【2014-11-14/蘋果日報/A12/要聞】

相關連結 /

<http://www.appledaily.com.tw/appledaily/article/headline/20141114/36206962/>

台灣驕傲！中央大學團隊助分析彗星照

中央大學天文所教授葉永烜（烜音同選），10 年前在德國馬克斯普朗克太陽系研究所服務期間，就參與歐洲太空總署（ESA）的羅賽塔號彗星探測船計劃，返台後他帶著中大天文所助理研究員林忠義和一些大學部學生一起加入，幫忙分析羅賽塔號的照片等資料。

原文轉載自【2014-11-14 台視新聞/綜合新聞】

相關連結 /

<http://www.ttv.com.tw/103/11/1031114/103111400040001.htm?from=579>

參與首次登陸彗星行動 台研究團隊振奮 中央大學天文所 助分析探測器傳回資料 台學者參與計劃 影像分析解開彗星之謎

羅賽塔號彗星探測船計劃，台灣的研究團隊也參與其中！中央大學天文所教授葉永烜表示，10 年前即加入歐洲太空總署的羅賽塔號彗星探測船計劃，返台後他仍帶領中央大學團隊一起加入分析羅賽塔號的照片等資料。如今，首度目睹照相機拍到的彗星照片，感到既驚奇又興奮，未來透過這些影像分析，將有助進一步解開彗星之謎。

歐洲太空總署的彗星探測船「羅賽塔號」，經過長達 10 年的太空飛行後，終於在 11 月 12 日釋出小型登陸器，探測任務目標 67P 彗星。這對天文學研究者來說，別具意義。而這一刻，台灣也沒錯過，中央大學天文所教授葉永烜和助理研究員林忠義和一些大學部學生一起參與這項史無前例的彗星探測計劃，餘有榮焉。中央大學參與的是羅賽塔號上的紅外線可見光影像技術 (OSIRIS) 照相機，協助分析彗星照片，了解彗核（彗星中心固體的部分）表面軟硬、表面水和沙塵混合程度及化學成分，希望透過彩色照片分析彗核組成礦物種類等。葉永烜教授表示，加入計劃以來，看到彗星照片是最讓他感到驚奇的部份，因為他之前也沒看過彗星的樣子。未來一個月將是菲萊的資料能否順利回傳的關鍵

原文轉載自【2014-11-14 台視新聞/生活新聞】

相關連結 /

<http://www.ttv.com.tw/103/11/1031114/10311140018400V.htm?from=579>

中央大學團隊 助分析菲萊傳回資料

徐秀娥/綜合報導

羅賽塔號彗星探測船計劃，台灣的研究團隊也參與其中！中央大學天文所教授葉永烜表示，10 年前即加入歐洲太空總署 (ESA) 的羅賽塔號 (Rosetta) 彗星探測船計劃，返台後他仍帶領中央大學團隊一起加入分析羅賽塔號的照片等資料。如今，首度目睹 OSIRIS 照相機拍到的彗星照片，感到既驚奇又興奮，未來透過這些影像分析，將有助進一步解開彗星之謎。

根據蘋果日報報導，在中大天文所教授葉永烜領導下，助理研究員林忠義和一些大學部學生一起參與這項史無前例的彗星探測計劃。中大主要參與的項目是，協助分析從羅賽塔號上的紅外線可見光影像技術 (OSIRIS) 照相機拍得的彗星照片，從探測器菲萊 (Philae) 傳回的影像等資料，可了解彗核（彗星中心固體的部分）表面軟硬、表面水和沙塵混合程度及化學成分，希望透過彩色照片

分析彗核組成礦物種類等。

這次 ESA 將彗星探測船命名為羅賽塔號，其實別具歷史意義。根據維基百科解釋，羅賽塔是一石碑之名，現藏於大英博物館。公元前 196 年，一塊刻有古埃及法老托勒密五世詔書的大理石石碑，同時刻有三種不同語言版本的同段內容，使得近代得以解讀出已失傳千餘年的埃及象形文，而成為今日研究古埃及歷史的重要里程碑。彗星探測船以此為名，象徵希望解彗星之謎。

原文轉載自【2014-11-14 中時電子報/科技】

相關連結 / <http://www.chinatimes.com/realtimenews/20141114002030-260412>

台灣天文學家 參與規劃研發

蘋果日報 2014 年 11 月 13 日

台灣天文學家 參與規劃研發

這項重大的國際合作無人探測器登陸彗星計劃，也有台灣科學家參與！據中央大學天文研究所發布的訊息，該所教授葉永烜（音同選）是此計劃的科學團隊協同主持人，提供科學資訊、參與資料分析，將計劃從德國延續至台灣，並協同該所助理研究員林忠義投入研究工作。

林忠義昨向《蘋果》表示，葉永烜教授早在 10 年前於德國馬克斯普朗克太陽系研究所服務期間，就從頭參與規劃和 3 個任務的研發，其中紅外線可見光影像技術（OSIRIS），可透過精密影像了解彗核表面構造、氣體塵埃粒子的誕生，以及彗核顏色分析等。

林忠義表示，之前人類對於彗星的觀測都只是匆匆一瞥，只能從照片發現有冰和石頭，卻不能找到水。如登陸成功，可對彗星進行地下探測，如證明有水，就代表可能有生命存在。

可防彗星撞地球

台灣大學天文物理研究所教授孫維新指出，彗星表面有太陽系最原始物質，能幫助我們了解太陽系、彗星，包括地球等其他天體構成與起源。他說這項任務命運多舛，2004 年 ESA 錯過另一個彗星最佳發射窗口，天文界相當扼腕。中央大學天文所陳文屏教授說，因彗星有可能撞擊地球，了解彗星也有助人類防禦這個天體敵人。

◎記者韓政燕、吳貞儀

原文轉載自【2014-11-13/蘋果日報/A2/要聞】

相關連結 /

<http://www.appledaily.com.tw/appledaily/article/headline/20141113/36204973/>

鹿林天文台發現小行星 命名台北

客家電視台 CH 17

鹿林天文台發現小行星 命名台北

最近的天空變得不一樣，有顆小行星叫「台北」，國立中央大學「鹿林巡天計畫」，在 2006 年發現一顆編號 171381 的小行星，現在通過國際天文聯合會的命名，取名為「Taipei」，未來大家抬頭看天上的天星，有一顆星星的名字，就叫台北。

一顆位在火星與木星之間，繞太陽公轉一圈，需要 5.16 年的小行星，2006 年 7 月 22 日，被國立中央大學「鹿林巡天計畫」發現，發現者是他，中央大學天文所，鹿林天文台台長林宏欽，現在這顆，編號 171381 號的小行星，經過「國際天文聯合會」，小天體命名委員會，正式審核通過取名為台北。

中央大學鹿林天文台台長 林宏欽：「命名台北的原因，最重要的就是說，台北除了是台灣首善之都之外，他其實也是台灣天文的中心，台灣天文的發源，其實就是從台北開始的。」

這顆就是小行星「台北」的模型，這幾年的 3 月最接近地球，因此明年 3 月，民眾使用最高倍數的望遠鏡，就可觀測到「台北小行星」。

中央大學鹿林天文台台長 林宏欽：「發現之後就會給它一個編號，有點像監獄裡面，你給犯人一個編號，他們有名字的，但是我現在給它一個名字，就賦予它跟台北連結在一起。」

中央大學也表示，鹿林巡天計畫，已發現 800 多顆小行星，其中約 300 顆已取得永久編號，約 50 顆已命名「台北」是第 10 個，以台灣縣市名為名的小行星，第 1 個是「嘉義」，前 1 個是「澎湖」，除了慶祝「台北小行星」命名通過，台北市政府也希望，透過這顆台北小行星，讓世界看見台北。 (2014-10-24)

原文轉載自【2014-10-24/客家電視台 CH 17】

相關連結 / <http://web.pts.org.tw/hakka/news/detail.php?id=116192>

發現小行星，名字叫 Taipei

一年一度天文迷的年度盛會，獅子座流星雨即將展開，而且今年獅子座附近的一顆小行星，有了正式的新名字：Taipei。國立中央大學有鑑於台北市對天文研究與教育的長期貢獻，將 2006 年發現的編號 171381 小行星，命名為 Taipei，並且在 2014 年 9 月 9 日經國際天文聯合會（IAU/CSBN）正式審核通過。

40 公分望遠鏡 發現台北小行星

這個名叫台北的小行星，是中央大學鹿林天文台台長林宏欽，與當時就讀中國廣東中山大學的葉泉志，在 2006 年 7 月 22 日，利用 40 公分望遠鏡所發現。台北小行星的大小估計直徑約 2 到 5 公里，位在火星與木星之間，有著接近圓形的橢

圓軌道，軌道傾角約 11 度，繞太陽公轉一圈需時 5.16 年。2006 年發現當時位在摩羯座、人馬座與顯微鏡座之間的區域，目前則位在獅子座附近。

巡天計畫 找小行星

位在玉山國家公園內，海拔 2,862 公尺的鹿林天文台，工作環境不僅相當克難，科學家們為了各種天文觀測計畫，生活更是日夜顛倒。「鹿林巡天計畫」是一個 2006 年到 2009 年持續三年的尋找行星、慧星的計畫，這段期間天文科學家們就發現了 800 多顆小行星，其中有 300 多顆有永久編號，但只有 27 顆通過正式命名，今年定名的台北小行星就是其一。

要在宇宙千億個星系中辨認出新的星體且命名，並不容易。林宏欽表示，尚未被發現的行星亮度較低，不僅要有極佳的眼力、耐心，還要有專業的判斷力；再來要經過長時間的軌道資料累積，才能確認是新發現的小行星，給予永久編號，然後才能正式命名。台北小行星，從林宏欽發現到被定名就經過了 8 年，才躍上世界舞台，留下永恆之名。

最佳觀測期明年 3 月

林宏欽表示，由於台北小行星很小，只有 19 到 20 等的亮度，顯得較暗，要觀測實體和拍照都不容易。台北小行星一年中會有一段時間最接近地球而較易觀察，明年 2015 年的 3 月到 4 月會是最佳觀測期。

參考資料來源：國立中央大學

整理撰文：潘佳修

原文轉載自【2014-10-30/國家地理雜誌】

相關連結 /

http://www.ngtaiwan.com/9191?utm_source=edm0&utm_medium=mail&utm_campaign=ngtaiwan

台北小行星 國際留名

【聯合報／記者吳思萍／即時報導】 2014.10.24 12:31 pm

中央大學摘星人林宏欽自 2006 年起已發現 100 多顆小行星，今天他將 12 年前發現的直徑 2 至 5 公里小行星命名為台北小行星，紀念台北市是天文發展的重鎮。林宏欽說，這個小行星較黯淡，就像觀察「月亮上的一抹燭光」困難，千億個星體中，命名的不多，很可惜「台灣」這個名稱，已被大陸觀察的小行星命名，接下來希望要以全台縣市名稱為之後發現的小行星命名，增加國際能見度。

【2014/10/24 聯合報】@ <http://udn.com/>

原文轉載自【2014-10-24/聯合新聞網 要聞 即時新聞】

相關連結 /

<http://udn.com/NEWS/BREAKINGNEWS/BREAKINGNEWS1/9020384.shtml>

「台北」小行星 在宇宙發光

【本報台北訊】國立中央大學今表示，將把鹿林巡天計畫發現的第 171381 號小行星命名為「台北」。「台北」小行星繞太陽公轉 1 圈需 5.16 年，預測明年 3 月，民眾使用最高倍數的望遠鏡，就可觀測到「台北」小行星。

編號第 171381 的小行星是由中央大學天文研究所鹿林天文台台長林宏欽，與當時就讀大陸廣東中山大學的葉泉志，在 2006 年 7 月 22 日利用鹿林天文台 40 公分望遠鏡進行的鹿林巡天計畫發現，經過 12.55 年，共約 120 筆觀測記錄，進行軌道確認後，今年 9 月 9 日經國際天文聯合會小天體命名委員會審核通過，經國際小行星中心公告，以「台北」命名。

「台北」小行星是中央大學天文研究所自 2006 年開始，新發現的 800 多顆小行星中，第 27 個通過正式命名，也是繼嘉義、南投、中壢、桃園、苗栗、高雄、台南、台中與澎湖之後，第 10 個以台灣地區縣市為名的小行星。

原文轉載自【2014-10-24/人間福報 即時新聞】

相關連結 / <http://www.merit-times.com/NewsPage.aspx?Unid=375539>

中大發現小行星 取名台北

【記者吳思萍／台北報導】

中央大學鹿林天文台長林宏欽昨天將發現的一顆小行星命名為「台北小行星」，紀念台北市是天文發展的重鎮；未來再發現小行星，也會以全台縣市名稱命名，集滿全台縣市命名版圖，以增加國際能見度。

林宏欽說，2006 年利用鹿林天文台的 40 公分望遠鏡觀測發現這顆小行星，歷經 12 年，共 120 筆觀測紀錄，確認軌道是無人發現的小行星後，今年 9 月 9 日經國際天文聯合會小天體命名委員會正式審核通過，並經國際小行星中心公告。

林宏欽說，宇宙千億個星體中，命名的不多，但是「台灣」這個名稱，可惜已被大陸觀察的小行星命名；台北是台灣天文發展的重鎮，努力推廣天文研究，很有代表性。

林宏欽說，台北小行星直徑大小約 2 至 6 公里，要在幾億公里以外觀察到，就像觀察「月亮上的一抹燭光」困難，每年要把握它與地球交會最近的時刻才能觀察，明年 3 月是最佳觀察期。台北小行星位於火星與木星之間的主小行星帶內。

台北小行星是中央大學天文研究所發現的小行星中，第 27 個通過正式命名的，也是第 10 個以台灣縣市為名的，之前已有嘉義、南投、中壢、桃園、苗栗、高雄等。

原文轉載自【2014-10-25/聯合報/AA4 版/教育】

相關連結 /

http://mag.udn.com/mag/edu/storypage.jsp?f_MAIN_ID=13&f_SUB_ID=33&f_ART_ID=542176

台北小行星 在宇宙發光

浩瀚的宇宙中，一顆以「台北」為名的小行星正閃閃發亮。國立中央大學將鹿林巡天計畫發現的第 171381 號小行星，正式命名為台北。台北小行星繞太陽公轉一圈需 5.16 年，預測明年 3 月台灣民眾使用最高倍數的望遠鏡，就可觀測到台北小行星。

台北小行星是中央大學天文研究所自 2006 年開始，新發現的 800 多顆小行星中，第 27 個通過正式命名，也是繼嘉義、南投、中壢、桃園、苗栗、高雄、台南、台中與澎湖之後，第 10 個以台灣地區縣市為名的小行星。

編號第 171381 的小行星由中央大學天文研究所鹿林天文台台長林宏欽，與當時就讀大陸廣東中山大學的葉泉志，在 2006 年 7 月 22 日利用鹿林天文台 40 公分望遠鏡進行的鹿林巡天計畫發現，經過 12.55 年，共約 120 筆觀測記錄，進行軌道確認後，今年 9 月 9 日經國際天文聯合會小天體命名委員會審核通過，經國際小行星中心公告，以

原文轉載自【2014-10-29/世界新聞網-北美華文新聞、華商資訊】

相關連結 /

http://www.worldjournal.com/pages/full_aTaiwan/push?article-%E5%8F%B0%E5%8C%97%E5%B0%8F%E8%A1%8C%E6%98%9F+%E5%9C%A8%E5%AE%87%E5%AE%99%E7%99%BC%E5%85%89%20&id=26013384#comments_26013384

中大發現小行星 以臺北為名

記者黃進福／臺北報導

國立中央大學天文研究所「鹿林巡天計畫」二〇〇六年觀測到過去未被發現的小行星，有感於臺北市政府長期進行天文推廣與教育，決定將學校發現的第 171381 號小行星，命名為「臺北」。

中央大學與臺北市政府昨日舉行「臺北小行星命名通過發表會」，中大校長周景揚致贈臺北小行星的銘牌與模型給臺北市政府，由副市長丁庭宇代表接受。

正式命名為「臺北小行星」的這顆小行星，是中大天文研究所鹿林天文台台長林宏欽，與當時就讀中國大陸廣東中山大學的葉泉志，利用鹿林天文台四十公分望遠鏡觀測影像發現，經過十二年、共約一百二十筆觀測記錄進行軌道確認後，九月經國際天文聯合會（IAU）小天體命名委員會（CSBN）正式審核通過，以「臺北」作為這顆小行星的正式名稱。

「臺北小行星」位在火星與木星之間的主小行星帶內，有接近圓形的橢圓軌道，

繞太陽公轉一圈需時五點一六年，大小粗估約二至六公里，相當於一座山，由於亮度相當低，下一次最靠近地球、觀測最佳時機大約在明年三月。

「臺北小行星」是中大天文研究所發現的八百多顆小行星中，第二十七個通過正式命名者，也是第十個以臺灣地區縣市名稱為名的小行星（之前按順序分別為嘉義、南投、中壢、桃園、苗栗、高雄、臺南、臺中與澎湖）。

原文轉載自【2014-10-28/青年日報/6 版/新視界】

相關連結 /

<http://news.gpwb.gov.tw/news.aspx?ydn=026dTHGgTRNpmRFEgxcbfb0e%2b%2beJP7D3HGsxhDrckoWljPztnWxAK1ovDE9BUS5Tmsy8dG7FK%2f74RCaAMLWnCMti780lQnpKXxz01Sx%2b2FU%3d>

央大巡天計畫發現全新小行星 正式定名「台北」

時節進入冬天，獅子座流星雨即將展開，但今年的獅子座卻不太一樣，因為多了一顆台北小行星，國立中央大學特別將這顆，於鹿林巡天計畫中，所發現的小行星，命名為台北小行星，希望能讓天文學在台北市這塊土地上生根茁壯。

由中央大學校長將台北小行星的銘牌以及模型贈予台北市政府，象徵雙方合作推廣天文教育的一個里程碑。

這顆編號 171381 號的小行星，是中央大學鹿林天文台台長林宏欽與廣東中山大學葉泉志於 2006 年所發現，在 2014 年經國際天文聯合會正式審核通過，以台北市做為這顆小行星的命名，而這也是第 10 顆以台灣縣市為名的行星。

台北市政府也表示，很感謝中央大學能讓台北這個名字出現在繁星之中，勉勵市政府在天文推廣上的努力，並期許持續對天文的扎根再投入。

原文轉載自【2014-10-27/人間衛視】

相關連結 / <http://www.bltv.tv/news/?f=content&cid=24683>

央大發現台北小行星 國際留名

【本報台北訊】中央大學鹿林天文台長林宏欽昨天將發現的一顆小行星命名為「台北小行星」，紀念台北市是天文發展的重鎮。林宏欽說，這個小行星較黯淡，就像觀察「月亮上的一抹燭光」困難，未來再發現的小行星，會以全台縣市名稱命名，增加國際能見度。

林宏欽自二〇〇六年起已發現一百多顆小行星。他說，二〇〇六年利用鹿林天文台的四十公分望遠鏡觀測發現這顆小行星，當時暫時編號，歷經十二年，共一百

二十筆觀測紀錄，確認軌道是無人發現的小行星後，今年九月九日經國際天文聯合會小天體命名委員會正式審核通過，並經國際小行星中心公告。

「為什麼要命名為台北小行星？」林宏欽說，宇宙千億個星體中，命名的不多，但是「台灣」這個名稱，很可惜已被大陸搶先命名，台北是台灣天文發展的重鎮，努力推廣天文研究，很有代表性。

林宏欽說，台北小行星直徑大小約二至六公里，要在幾億公里以外觀察到，十分困難，常常只能看到黯淡的光點，因此每年要把握它與地球交會最近的時刻才能觀察，明年三月是最佳觀察期。

原文轉載自【2014/10/25 人間福報】

相關連結 / <http://www.merit-times.com.tw/NewsPage.aspx?Unid=375548>

臺北小行星 第10顆以臺灣縣市命名的小行星

楊惠芳／臺北報導

在浩瀚宇宙中，有一顆以「臺北」為名的小行星。中央大學將編號一七一三八一的小行星命名為「Taipei（臺北）」，並經國際天文聯合會審核通過，昨天發表。

臺北小行星目前位在獅子座中，預測明年三月時，使用最高倍數的望遠鏡，就可觀測到「臺北」小行星。

中央大學校長周景揚昨天頒授小行星銘板與模型給臺北市政府，由副市長丁庭宇代表接受。周景揚指出，臺北市是臺灣天文研究與推廣的重鎮，天文機構與研究人員數量都是全臺之冠，長期以來推動天文研究與教育不遺餘力，因此，中大將這顆小行星命名為「臺北」。

臺灣是相當熱中研究小行星的亞洲國家之一，中央大學已發現八百多顆，其中二十七顆通過正式命名，臺北是第十顆以臺灣縣市為名的小行星，其他依序為嘉義、南投、中壢、桃園、苗栗、高雄、臺南、臺中與澎湖。

臺北小行星發現者林宏欽說，臺北小行星位在火星與木星之間，繞太陽公轉一圈要五點一六年，目前還不清楚這顆小行星的大小、質量與密度。

小行星是目前唯一可由發現者命名，並得到世界公認的天體。早期，天文學者通常以羅馬或希臘眾神命名，後來，發現者開始取名自歷史人物、城市、地點、

童話人物等。

原文轉載自【2014/10/25 國語日報】

相關連結 / https://www.mdnkids.com/info/news/content.asp?Serial_NO=90664

〈台北都會〉台北小行星 明年3月觀測佳

〔記者謝佳君／台北報導〕中央大學天文研究所「鹿林巡天計畫」二〇〇六年觀測到過去未被發現的小行星，今年九月正式命名為「台北小行星」，是唯一以「台北」為名的小行星。這顆小行星位在火星與木星之間的主小行星帶內，大小粗估二至六公里，由於亮度相當低，下次最靠近地球的最佳觀測時機大約在明年三月。

中央大學天文研究所發現

中央大學天文研究所鹿林天文台台長林宏欽與當時就讀中國廣東中山大學的葉泉志，二〇〇六年七月時觀測到這顆小行星，當時暫時編號 2006OG17，經多年觀測確認其獨一無二的運行軌道，有了永久編號 171381，並在今年九月九月經國際天文聯合會小天體命名委員會審核通過、國際小行星中心公告，以「台北」為其正式名稱。

林宏欽說，台北小行星位在火星與木星之間的主小行星帶內，遠日點距離約三・二六六 AU（約四・八八億公里），近日點距離約二・七一〇AU（約四・〇五億公里），是接近圓形的橢圓軌道，軌道傾角約十一度，繞太陽公轉一圈需時五・一六年。

林宏欽說，由於台北小行星很小，距離太陽又遠，最大亮度約只有十九至二十等，相當黯淡，就像在觀測月亮上的燭光，觀測實體和拍照都很困難，也因為繞太陽一圈大約要五年，一年中只有一次最接近地球，近幾年大約都是三月為最佳觀測時期。

中央大學校長周景揚表示，該校天文研究所自二〇〇六年迄今新發現八百多顆小行星，其中三百多顆有永久編號，五十多顆已正式命名，其中二十七顆由中央大學命名；台北小行星是第二十七個通過正式命名，也是第十個以台灣縣市為名的小行星。昨北市府舉辦小行星命名發表會，中央大學致贈台北小行星名牌與模型給北市府，副市長丁庭宇代表接受。

原文轉載自【2014/10/25 自由時報】

相關連結 / <http://news.ltn.com.tw/news/local/paper/824565>

天空有顆星 名字就叫「台北」

最近的天空變得不一樣，有顆小行星叫「台北」。中央大學、北市府今合辦小行星的「命名發表會」，將中大「鹿林巡天計畫」於 2006 年 7 月 22 日發現、編號 171381 號小行星命名為「台北」，表揚北市府在天文教育和知識普及的貢獻。中大表示，「台北」是第 10 個以台灣縣市名為名的小行星，第 1 個是「嘉義」，前 1 個是「澎湖」。

「台北」由中大天文研究所鹿林天文台台長林宏欽、當時就讀中國廣東中山大學的學生葉泉志發現，今年 9 月 9 日經國際天文聯合會小天體命名委員會審核通過。林宏欽表示，這顆星位於火星與木星之間的主小行星帶內，繞太陽一圈要 5.16 年，這幾年的 3 月最接近地球，但因為距離太遠，從望遠鏡看來只是 1 個黯淡的光點，「有如看月亮上的燭光。」

中大鹿林巡天計畫已發現 800 多顆小行星，其中約 300 顆已取得永久編號，約 50 顆已命名，林宏欽參與發現的就有 100 顆左右。(蔡永彬／台北報導)

原文轉載自【2014-10-25/蘋果日報】

相關連結

<http://www.appledaily.com.tw/realtimenews/article/life/20141024/493774/%E5%A4%A9%E7%A9%BA%E6%9C%89%E9%A1%86%E6%98%9F%E3%80%80%E5%90%8D%E5%AD%97%E5%B0%B1%E5%8F%AB%E3%80%8C%E5%8F%B0%E5%8C%97%E3%80%8D>

台北滿天飛 新發現小行星 明年 3 月露面

【記者陳珮琦】

浩瀚的宇宙中，一顆以「台北」為名的小行星正閃閃發亮。國立中央大學將鹿林巡天計畫發現的第 171381 號小行星，命名為台北，昨天正式發表。台北小行星繞太陽公轉一圈需 5.16 年，預測明年 3 月民眾使用最高倍數的望遠鏡，就可觀測到台北小行星。

台北小行星是中央大學天文研究所自 2006 年開始，新發現的 800 多顆小行星中，第 27 個通過正式命名，也是第十個以台灣地區縣市為名的小行星。昨天的命名發表會，中央大學校長周景揚致贈台北小行星的銘牌與模型給北市府，由副市長丁庭宇代表接受。

編號第 171381 的小行星由中央大學天文研究所鹿林天文台台長林宏欽，與當

時就讀大陸廣東中山大學的葉泉志，在 2006 年 7 月 22 日利用鹿林天文台 40 公分望遠鏡進行的鹿林巡天計畫發現，經過 12.55 年，共約 120 筆觀測記錄，進行軌道確認後，今年 9 月 9 日經審核通過，由國際小行星中心公告，以台北命名。以台灣縣市為名的小行星

- 1.嘉義
- 2.南投
- 3.中壢
- 4.桃園
- 5.苗栗
- 6.高雄
- 7.台南
- 8.台中
- 9.澎湖
- 10.台北

製表／Upaper

●小行星怎命名？

【陳珮琦】

小行星是目前唯一可以由發現者命名，得到世界公認的天體。當觀測到一顆新小行星，但不能立刻確定時，可先給它一個臨時編號。當這顆小行星確認是新發現的小行星後，即可得到一個國際統一格式的暫定編號。

當小行星至少四次在回歸中心被觀測到，精確測定出其運行軌道參數後，就會得到國際小行星中心給予的永久編號，如台北小行星的永久編號為 171381。

發現者擁有對小行星的命名權，在十年內隨時可以行使，報經國際小行星中心和小行星命名委員會審議通過後，才公諸於世，並為世界公認。

原文轉載自【2014-10-25/Upaper/1 版/要聞】

位於火星與木星間 台北小行星 全世界都看見

【張潼／台北報導】

太陽系有顆小行星叫「台北」！2006 年 7 月 22 日中央大學執行「鹿林尋天計畫」時，觀測到位於火星與木星間的小行星，經多年觀測、確認軌道後，今年 9 月 9 日獲國際天文聯合會（IAU）審核通過，定名為「台北」。未來星圖上，「台北」不但能被世界看見，這也是央大第 10 個以台灣縣市來命名的小行星。

歷經 12 年記錄資料

台北小行星由央大天文研究所鹿林天文台長林宏欽、當時在中國廣東中山大學就讀的學生葉泉志一起發現，歷經 12 餘年記錄軌道資料、向國際組織申請正式編號，終在上個月獲得命名權。此次考量到台北市對天文教育的貢獻，決定以

「台北」為名。

這顆國際正式編號 171381 的台北小行星，位於火星與木星間主小行星帶內，直徑約 2 至 5 公里，繞太陽公轉一周需 5.16 年，軌道是接近圓形的橢圓軌道，地球可觀測到最亮的亮度則在 19 至 20 等間，從望遠鏡看起來只是「月亮上的燭光一般大小」。

林宏欽說，當年利用 40 公分望遠鏡觀測到台北小行星，且每年只能趁著它距離地球最近時的幾天，觀測其運行軌道。

林宏欽 摘星星的男人

中大校長周景揚表示，天文研究所自 2006 年起陸續發現 800 多顆小行星，林宏欽參與發現的就有 100 顆，有「摘星星的男人」之稱；在這些小行星中，其中 27 個由央大命名，也有「雲門」、「陳樹菊」等，這些來自台灣的名字都可以被國際看見。

原文轉載自【2014-10-25/中國時報/A9 版/生活新聞】

相關連結 / <http://www.chinatimes.com/newspapers/20141025000359-260114>

中央大學發現小行星 命名台北

發稿時間：2014/10/24 12:07 最新更新：2014/10/24 12:07

(中央社記者顧荃台北 24 日電) 國立中央大學今天表示，有感於台北市政府長期進行天文推廣與教育，決定將學校發現的第 171381 號小行星，命名為「台北」。

台北市教育局上午舉行「台北小行星命名通過發表會」，國立中央大學校長周景揚致贈台北小行星的銘牌與模型給台北市政府，由副市長丁庭宇代表接受。

中央大學表示，台北小行星 (171381 Taipei) 是中央大學天文研究所鹿林天文台台長林宏欽 (H.-C. Lin)，與當時就讀中國廣東中山大學的葉泉志 (Q.-z. Ye)，於 2006 年時利用鹿林天文台 40 公分望遠鏡觀測影像發現。

經過 12 年、共約 120 筆觀測記錄進行軌道確認後，於 9 月 9 日經國際天文聯合會 (IAU) 小天體命名委員會 (CSBN) 正式審核通過，以「台北」作為這顆小行星的正式名稱。

中央大學說，台北小行星位在火星與木星之間的主小行星帶內，有接近圓形的橢圓軌道，繞太陽公轉一圈需時 5.16 年。目前尚不清楚這顆小行星的大小、質量與密度等物理參數。2006 年發現當時位在摩羯座、人馬座與顯微鏡座之間的區域，目前則位在獅子座中。

台北小行星是中央大學天文研究所發現的 800 多顆小行星中，第 27 個通過正式命名者，也是第 10 個以台灣地區縣市名稱為名的小行星（之前按順序分別為嘉義、南投、中壢、桃園、苗栗、高雄、台南、台中與澎湖）。

台北市政府表示，從 1938 年公會堂設立天文台開始，台北市就是台灣地區的天文研究與推廣重鎮。現在台北市內天文機構與研究人員的數量為全台之冠，不

僅有國家級的天文與天文物理研究所、國立的天文高等教育機構，還有中小學的天文台、星象館或天文社團，並設立台北市立天文科學教育館作為天文社教機構。1031024

原文轉載自【2014-10-24 /中央社首頁 > 地方新聞】

相關連結 / <http://www.cna.com.tw/news/alloc/201410240125-1.aspx>

「台北小行星」一遊未盡 25 日起到天文館玩吧

2014 年 10 月 24 日 16:46

記者葉立斌／台北報導

國立中央大學特別將鹿林巡天計畫所發現的第 171381 號小行星定名為「台北小行星」，並於 10 月 24 日上午舉辦命名發表會，由中央大學校長周景揚致贈台北市政府「台北小行星」的銘牌與模型，由台北市副市長丁庭宇代表接受。期待台北小行星的命名，能夠作為國立中央大學與臺北市政府合作推廣天文教育的一個里程碑，共同攜手讓天文學繼續生根茁壯。

丁庭予表示，從 1938 年公會堂設立天文台就開始，北市積極投入天文研究與教育。如今，北市內不僅有國家級的天文與天文物理研究所及國立的天文高等教育機構，中小學的天文台、星象館或天文社團也蓬勃發展；1997 年更是設立台北市立天文科學教育館作為專責天文社會教育機構，希望能夠積極推展天文研究與教育。

台北小行星為中央大學鹿林天文台長林宏欽，與當時就讀中國廣東中山大學的葉泉志於 2006 年 7 月 22 日，用鹿林天文台 40 公分望遠鏡發現，並於 2014 年 9 月 9 日經國際天文聯合會小天體命名委員會(IAU CSBN)正式審核通過。台北小行星目前位在火星與木星之間的主小行星帶內，遠日點距離約 3.266AU (約 4.88 億公里)，近日點距離約 2.710AU (約 4.05 億公里)，離心率約 0.09312，是個接近圓形的橢圓軌道，軌道傾角約 11 度，繞太陽公轉一圈需時 5.16 年，初步估計大小約 2 至 6 公里。2006 年發現當時位在摩羯座、人馬座與顯微鏡座之間的區域，目前則位在獅子座中。

台北小行星有多大？看得見它嗎？會撞擊地球嗎？10 月 25 日起，台北市立天文科學教育館與中央大學天文研究所合作辦理「發現台北小行星」系列活動，其中包含特展，假日更推出主題導覽、演講等，民眾亦可以搭乘宇宙探險，參加前進台北小行星任務，凡完成任務者可獲得一張「完成任務證書」、神秘禮物。

原文轉載自【2014-10-25/nownews】

相關連結 / <http://www.nownews.com/n/2014/10/24/1473266>

以縣市為名 「台北」小行星命名通過

(中央社記者顧荃台北 24 日電) 台北市教育局上午舉行「台北小行星命名通過發表會」，國立中央大學校長周景揚致贈台北小行星的銘牌與模型給台北市政府，由副市長丁庭宇代表接受。

中央大學表示，台北小行星 (171381 Taipei) 是中央大學天文研究所鹿林天文台台長林宏欽 (H.-C. Lin)，與當時就讀中國廣東中山大學的葉泉志 (Q.-z. Ye)，於 2006 年時利用鹿林天文台 40 公分望遠鏡觀測影像發現。

經過 12 年、共約 120 筆觀測記錄進行軌道確認後，於 9 月 9 日經國際天文聯合會 (IAU) 小天體命名委員會 (CSBN) 正式審核通過，以「台北」作為這顆小行星的正式名稱。

中央大學說，台北小行星位在火星與木星之間的主小行星帶內，有接近圓形的橢圓軌道，繞太陽公轉一圈需時 5.16 年。目前尚不清楚這顆小行星的大小、質量與密度等物理參數。2006 年發現當時位在摩羯座、人馬座與顯微鏡座之間的區域，目前則位在獅子座中。

台北小行星是中央大學天文研究所發現的 800 多顆小行星中，第 27 個通過正式命名者，也是第 10 個以台灣地區縣市名稱為名的小行星（之前按順序分別為嘉義、南投、中壢、桃園、苗栗、高雄、台南、台中與澎湖）。

台北市政府表示，從 1938 年公會堂設立天文台開始，台北市就是台灣地區的天文研究與推廣重鎮。現在台北市內天文機構與研究人員的數量為全台之冠，不僅有國家級的天文與天文物理研究所、國立的天文高等教育機構，還有中小學的天文台、星象館或天文社團，並設立台北市立天文科學教育館作為天文社教機構。

原文轉載自【2014-10-25/蕃新聞】

相關連結 / <http://n.yam.com/cna/life/20141024/20141024638480.html>

台北小行星正式命名發表

【聯合晚報／記者陳珮琦／即時報導】 2014.10.24 12:24 pm

浩翰的宇宙中，一顆以「台北」為名的小行星正閃閃發亮！國立中央大學因

感於北市府在天文的推廣與教育上的貢獻，特別將鹿林巡天計畫所發現的第 171381 號小行星，命名為「台北」，今天正式發表；「台北小行星」繞太陽公轉一圈需 5.16 年，因此預測要到明年 3 月，民眾使用最高倍數的望遠鏡就可觀測到「台北小行星」。

台北小行星是中央大學天文研究所自 2006 年開始新發現的 800 多顆小行星中，第 27 個通過正式命名，也是繼嘉義、南投、中壢、桃園、苗栗、高雄、台南、台中與澎湖之後，第 10 個以台灣地區縣市為名的小行星。

上午的台北小行星命名發表會上，國立中央大學校長周景揚致贈台北小行星的銘牌與模型給北市府，由副市長丁庭宇代表接受。周景揚表示，期待這一次台北小行星的命名，能夠作為國立中央大學與北市府合作推廣天文教育的一個里程碑，讓天文學能夠在北市生根茁壯。

原文轉載自【2014-10-25/聯合晚報】

相關連結 /

<http://udn.com/NEWS/BREAKINGNEWS/BREAKINGNEWS3/9020394.shtml>

首顆以台北為名小行星 命名通過

2014 年 10 月 24 日 11:57

張潼報導

中央大學天文研究所鹿林天文台長林宏欽，2006 年與當時在中國廣東中山大學就讀的學生葉泉志，一起觀測到 1 顆小行星，經過約 120 筆觀測記錄確認軌道後，今年 9 月 9 日正式獲國際天文聯合會（IAU）審核通過，以台灣天文重鎮「台北」替它命名。

「台北小行星」位於火星與木星間主小行星帶內，估計直徑約 2 到 5 公里，繞太陽公轉一周需 5.16 年，其軌道是接近圓形的橢圓軌道，地球可觀測到最亮的亮度則在 19 至 20 等間。

發現者林宏欽表示，2006 年 7 月 22 日進行「鹿林巡天計畫（Lulin Sky Survey）」時，利用 40 公分望遠鏡觀測到當時暫時編號為 2006 OG17 的小行星，並利用每年幾天內它距離地球最近時，觀測其運行軌道，以確定它是獨一無二、還未被發現的小行星。

林宏欽說，台北小行星與地球相隔幾億公里，觀測時就像看一個小光點，除非衛星飛到附近，否則現在還很難確認其形狀、質量、密度等物理參數。

中央大學校長周景揚表示，天文研究所自 2006 年起陸續發現 800 多顆小行星，林宏欽掛名發現者的就有 100 顆；此外，在這些被發現的小行星中，現已有 50 餘顆有命名，其中 27 個則是中央大學自己所名命，除以台灣各縣市為名，也有「雲門」、「陳樹菊」等，在星圖上，這些來自台灣的名字可以被國際看見。

台北市副市長丁庭宇則表示，台北市一向是台灣天文研究的重鎮，機構與人員數量都是全台之冠。此次小行星正式定名，是首次以台北為名，格外具象徵意義。

原文轉載自【2014-10-25/中時電子報/生活】

相關連結 / <http://www.chinatimes.com/realtimenews/20141024002822-260405>

中大巡天計畫發現全新小行星 正式定名「台北」

2014 年 10 月 24 日 11:25

記者葉立斌／台北報導

未來孩子們觀測星空，會知道有一顆小行星，名叫台北！

小行星發現人林宏欽表示，台北小行星，編號第 171381，為國立中央大學天文研究所鹿林天文台長林宏欽(H.-C. Lin)與當時就讀中國廣東中山大學的葉泉志(Q.-z. Ye)，於 2006 年 7 月 22 日利用鹿林天文台 40 公分望遠鏡進行的中央大學鹿林巡天計畫(Lulin Sky Survey, LUSS)觀測影像發現的，當時的暫時編號為 2006 OG17。經過 12 餘年、約 120 筆觀測記錄進行軌道確認後，於 2014 年 9 月 9 日經國際天文聯合會(IAU)小天體命名委員會(CSBN)正式審核通過，並經國際小行星中心(Minor Planet Center, MPC)公告，以台北市作為這顆小行星的正式名稱。

這顆小行星位在火星與木星之間的主小行星帶內，遠日點距離約 3.266AU (約 4.88 億公里)，近日點距離約 2.710AU (約 4.05 億公里)，離心率約 0.09312，是個接近圓形的橢圓軌道，軌道傾角約 11 度，繞太陽公轉一圈需時 5.16 年。目前尚不清楚這顆小行星的大小、質量與密度等物理參數。2006 年發現當時位在摩羯座、人馬座與顯微鏡座之間的區域，目前（9 月 19 日）則位在獅子座中。

台北小行星是中央大學天文研究所自 2006 年開始新發現的 800 多顆小行星中，第 27 個通過正式命名者，也是第 10 個以台灣地區縣市名稱為名的小行星，前十個按順序分別為嘉義、南投、中壢、桃園、苗栗、高雄、台南、台中與澎湖；其中除澎湖外，均與中央大學、中央大學鹿林天文台及小行星發現者有淵源。

原文轉載自【2014-10-25/nownews/生活】

相關連結 / <http://wwwnownews.com/n/2014/10/24/1472822>

台北小行星命名通過 明年3月來觀察

[記者謝佳君／台北報導]國立中央大學天文研究所「鹿林巡天計畫」2006年觀測到過去未被發現的小行星，今年9月正式命名為「台北小行星」。這顆小行星位在火星與木星之間的主小行星帶內，大小粗估約2至6公里，相當於一座山，由於亮度相當低，下一次最靠近地球、觀測最佳時機大約在明年3月。

中央大學天文研究所鹿林天文台台長林宏欽說，經過多年的觀測紀錄確認這顆小行星獨一無二的運行軌道後，小行星有了永久編號171381，並在今年9月9月經國際天文聯合會小天體命名委員會審核通過、國際小行星中心公告，以「台北」作為其正式名稱。

林宏欽介紹，台北小行星位在火星與木星之間的主小行星帶內，遠日點距離約3.266AU（約4.88億公里），近日點距離約2.710AU（約4.05公里），是接近圓形的橢圓軌道，軌道傾角約11度，繞太陽公轉一圈需時5.16年。

林宏欽說，台北小行星最大亮度大約只有19至20等，相當黯淡，就像在觀測月亮上的燭光，一年中只有一次最接近地球，錯過又要再等一年，近幾年大約都是三月為最佳觀測時期。

中央大學校長周景揚表示，該校天文研究所自2006年迄今已新發現800多顆小行星，其中300多顆有永久編號，50多顆已正式命名，其中27顆由中央大學命名；台北小行星是第27個通過正式命名，也是第10個以台灣縣市名稱為名的小行星。今天上午北市府舉辦小行星命名發表會，中央大學致贈台北小行星銘牌與模型給台北市府，副市長丁庭宇代表接受。

原文轉載自【2014-10-25/自由時報/生活】

相關連結 / <http://news.ltn.com.tw/news/life/breakingnews/1139530>

首顆以"台北"為名 小行星命名通過 小行星名為"台北" 近火星.木星之間

最近的天空變得不太一樣，因為有一顆小行星被命名叫做「台北」。它也是第10個以台灣縣市名為名的小行星這是為了表揚北市府在天文教育和知識普及的貢獻，所以才命名為台北。根據中央大學表示，這一顆星位於火星和木星之間的

主小行星帶內，繞太陽一圈要 5.16 年，這幾年的 3 月，最接近地球，不過因為距離太遠，如果從望遠鏡看起來，只是 1 個黯淡的光點，這是從 2006 年開始新發現的 800 多顆小行星中，第 27 個通過正式命名的，也是第 10 個以台灣地區縣市名稱為名的小行星。

原文轉載自【2014/10/24 台視新聞】

相關連結 /

<http://www.ttv.com.tw/103/10/1031024/10310240020900V.htm?from=579>

「臺北」小行星命名通過

現今太空探索日漸蓬勃，天文學扎根成為各國競相發展的課題，也是教育學程中重要的一環。國立中央大學感於臺北市政府在天文的推廣與教育上之貢獻，特別將鹿林巡天計畫所發現的第 171381 號小行星，命名為「臺北」，並將於今天(24)早上舉辦命名發表會。

臺北小行星是國立中央大學天文研究所鹿林天文臺臺長林宏欽於 2006 年 7 月 22 日所發現，在今年(103)通過國際天文聯合會審核，以「臺北」作為這顆小行星的正式名稱。林宏欽表示，命名為「臺北」是為了感謝臺北對於天文研究與教育的貢獻。

中央大學天文研究所自 2006 年開始，新發現的小行星有 800 多顆，有 27 顆通過正式命名。中央大學校長周景揚指出，要發現小行星非常不容易，很感謝同仁對於天文的付出。

會中周景揚致贈臺北小行星銘牌與模型給臺北市政府，期待這次臺北小行星的命名能夠作為中央大學與臺北市政府合作推廣天文的里程碑，共同攜手讓天文學在台灣生根茁壯。

臺北小行星資料：

臺北小行星，小行星編號第 171381，於 2006 年 7 月 22 日利用鹿林天文台 40 公分望遠鏡進行的中央大學鹿林巡天計畫 (Lulin Sky Survey, LUSS) 觀測影像發現的，當時的暫時編號為 2006 OG17。經過 12.55 年、共約 120 筆觀測記錄進行軌道確認後，於 2014 年 9 月 9 日經國際天文聯合會 (IAU) 小天體命名委員會 (CSBN) 正式審核通過，並經國際小行星中心 (Minor Planet Center, MPC) 公告 (MPC 89389- 89838)，以臺北市作為這顆小行星的正式名稱。

這顆小行星位在火星與木星之間的主小行星帶內，遠日點距離約 3.266AU（約 4.88 億公里），近日點距離約 2.710AU（約 4.05 億公里），離心率約 0.09312，是個接近圓形的橢圓軌道，軌道傾角約 11 度，繞太陽公轉一圈需時 5.16 年。目前尚不清楚這顆小行星的大小、質量與密度等物理參數。2006 年發現當時位在摩羯座、人馬座與顯微鏡座之間的區域，目前（2014/9/19）則位在獅子座中。

原文轉載自【2014/10/24 國立教育廣播電台】

相關連結 / <http://news.ner.gov.tw/index.php?act=culnews&code=view&ids=169578>

以縣市為名 「臺北」小行星閃耀星空

由國立中央大學鹿林天文台台長林宏欽與中國大陸廣東中山大學學生葉泉志，所發現的一顆小行星，今天(24 日)正式命名為「臺北」小行星，這也是第 10 個以台灣縣市命名的小行星。

林宏欽與葉泉志 2 人在 2006 年利用中央大學鹿林天文台 40 公分望遠鏡，觀測到一顆小行星，這顆小行星後來在今年 9 月 9 日，經過國際天文聯合會正式審核通過。

中央大學有感於台北市政府長期推廣天文教育，於是將這顆小行星命名為「臺北」，24 日在台北市政府，中央大學校長周景揚親自致贈「臺北」小行星的模型，由台北市副市長丁庭宇代表接受。丁庭宇說：『(原音)行星發現不是那麼容易，中央大學願意跟我們分享這個名稱，我們覺得非常榮幸。台北市自己有天文台，主要是科學教育館，以後我們希望把臺北小行星當作我們一個參觀的重點。』

中央大學從 2006 年起，共發現了 800 多顆小行星；其中「臺北」小行星是第 27 個通過正式命名者，也是第 10 個以台灣縣市命名的小行星。

鹿林天文台台長林宏欽表示，臺北小行星 2006 年發現時，在摩羯座、人馬座與顯微鏡座之間的區域，目前位在獅子座。臺北小行星相較其他小行星，亮度不是很亮，預估最近一次最接近地球的時間在明年 3 月，星等亮度大約 19 等，平時大約在 20 幾等。

原文轉載自【2014/10/24 中央廣播電台】

相關連結 / <http://news.rti.org.tw/news/detail/?recordId=145894>

叫「台北」的小行星 明年看得見

【聯合晚報／記者陳珮琦／台北報導】

浩瀚的宇宙中，有一顆以「台北」為名的小行星。國立中央大學將鹿林巡天計畫發現的第 171381 號小行星，命名為台北，今天正式發表。台北小行星繞太陽公轉一圈需 5.16 年，預測明年 3 月民眾使用最高倍數的望遠鏡，就可觀測到台北小行星。

台北小行星是中央大學天文研究所自 2006 年開始，新發現的 800 多顆小行星中，第 27 個通過正式命名，也是繼嘉義、南投、中壢、桃園、苗栗、高雄、台南、台中與澎湖之後，第 10 個以台灣地區縣市為名的小行星。

上午的命名發表會，中央大學校長周景揚致贈台北小行星的銘牌與模型給北市府，由副市長丁庭宇代表接受。周景揚表示，期待這一次台北小行星的命名，能夠作為中央大學與北市府合作推廣天文教育的一個里程碑，讓天文學能夠在北市生根茁壯。

編號第 171381 的小行星由中央大學天文研究所鹿林天文台台長林宏欽，與當時就讀大陸廣東中山大學的葉泉志，在 2006 年 7 月 22 日利用鹿林天文台 40 公分望遠鏡進行的鹿林巡天計畫發現，經過 12.55 年，共約 120 筆觀測記錄，進行軌道確認後，今年 9 月 9 日經國際天文聯合會小天體命名委員會審核通過，經國際小行星中心公告，以台北命名。

小行星怎命名？

小行星是目前唯一可以由發現者命名，得到世界公認的天體。觀測到一顆小行星後，不能立刻確定是否為一顆新發現的小行星，可以先給它一個臨時編號。當這顆小行星在不同的夜晚被觀測到，並報告國際小行星中心，確認是新發現的小行星之後，即可得到一個國際統一格式的暫定編號，「台北小行星」的暫時編號為 2006 OG17。

當小行星至少四次在回歸中心被觀測到，精確測定出其運行軌道參數後，就會得到國際小行星中心給予的永久編號，如台北小行星的永久編號為 171381。

發現者擁有對小行星的命名權，在 10 年內隨時可以行使。所有小行星命名，須報經國際小行星中心和小行星命名委員會審議通過後，才公諸於世，並為世界各國公認。

原文轉載自【2014-10-24/聯合晚報/A15 版/都會生活】

相關連結 /

<http://www.udn.com/2014/10/24/NEWS/NATIONAL/NAT5/9020637.shtml>

台北小行星正式命名發表

浩瀚的宇宙中，一顆以「台北」為名的小行星正閃閃發亮！國立中央大學因感於北市府在天文的推廣與教育上的貢獻，特別將鹿林巡天計畫所發現的第 171381 號小行星，命名為「台北」，今天正式發表；「台北小行星」繞太陽公轉一圈需 5.16 年，因此預測要到明年 3 月，民眾使用最高倍數的望遠鏡就可觀測到「台北小行星」。

台北小行星是中央大學天文研究所自 2006 年開始新發現的 800 多顆小行星中，第 27 個通過正式命名，也是繼嘉義、南投、中壢、桃園、苗栗、高雄、台南、台中與澎湖之後，第 10 個以台灣地區縣市為名的小行星。

上午的台北小行星命名發表會上，國立中央大學校長周景揚致贈台北小行星的銘牌與模型給北市府，由副市長丁庭宇代表接受。周景揚表示，期待這一次台北小行星的命名，能夠作為國立中央大學與北市府合作推廣天文教育的一個里程碑，讓天文學能夠在北市生根茁壯。

原文轉載自【2014/10/24 聯合晚報】

相關連結 /

<http://udn.com/NEWS/BREAKINGNEWS/BREAKINGNEWS3/9020394.shtml>

睽違 3 年紅月亮現身 天文館孩子們專心欣賞

NOWnews 今日新聞

睽違 3 年紅月亮現身 天文館孩子們專心欣賞

2014 年 10 月 09 日 00:19

記者葉立斌／台北報導

現在在外面的朋友，有看到紅色的月亮嗎？紅色月亮在今(8)晚現身。這次是台灣自 2011 年 12 月 10 日以來再次可見完整的月面全食過程；這次月食發生時，全食的過程發生在晚間 6 時 25 分到晚間 7 時 25 分之間。氣象局說，月食時月面的仰角不高，喜好攝影的民眾，容易搭配合適的地景，拍攝美麗的月食影像。

台北地區受到雲層遮蔽影響，在整個月全食過程中只能驚鴻一瞥看到紅色月亮，有看到的民眾運氣很好喔！

台北天文館對此舉辦活動，現場參加月全食活動的近 1300 位民眾，看到紅月亮時一陣驚呼。天文館大廳則透過網路轉播畫面觀看國內外的月食即時影像，民眾在天文館工作同仁的解說下，更深入地瞭解月食發生的原因和其他種種與月食

相關的知識和故事。

台北天文館的員工周紹孔特別前往新竹南寮地區進行觀測，透過偶爾飄過的雲朵搶拍。天文台將這個與台灣睽違了 3 年之久的紅色月全食記錄下來並做成組圖，與全台民眾一起分享。

▲食甚時的月全食與天王星。(圖／國立中央大學鹿林天文台提供)

月全食/中大天文台邀民眾一睹全食紅月

<http://www.cdnews.com.tw> 2014-10-08 23:13:54

李漢揚/整理

為了讓民眾一睹全食紅月風采，中央大學 8 日晚開放天文台，吸引民眾大排長龍，並邀請專家分享科普演講，讓民眾對月亮有更深層的認識。

中央社 8 日報導，中央大學天文所長高仲明表示，這次月全食是繼 2011 年 12 月 10 日後，台灣地區再見到月全食，預估全部過程將歷經 5 小時又 21 分鐘，其中本影食將歷時 3 小時又 20 分鐘，最大本影食分為 1.172。

為了讓民眾一睹罕見的「紅月」全食丰采，中央大學今晚也開放科學一館的天文台，吸引民眾大排長龍參觀，現場提供高倍數、大口徑的天文望遠鏡，滿足大小朋友對月亮的好奇與科學的探索。

高仲明說，中大科一館天文台開放，要感謝台達電創辦人暨榮譽董事長鄭崇華的慷慨捐助，讓已有 32 年歷史的科一館天文台得以重整並以嶄新的面貌與大家見面，發揮天文科普教育與推廣的功能。

中央大學表示，天文所教授葉永烜也在現場分享「在月亮的兔子」科普演講，從歷史傳說到人類對月球的探測，帶領民眾對月亮有更深層的認識。

【中央網路報】

原文轉載自【2014-10-16/中央日報網路報-臺灣聚焦】

相關連結 /

http://www.cdnews.com.tw/cdnews_site/docDetail.jsp?coluid=108&docid=10294510

3

中央大學天文台開放 「在月亮的兔子」細說天文史

2014 年 10 月 09 日 18:34

記者葉立斌／台北報導

國立中央大學長時間耕耘天文教育與研究，中部的民眾想了解月全食，怎能不快點找他們！為一睹難得一見的「紅月」全食丰采，中央大學科學一館天文台在 10 月 8 日晚間開放，吸引民眾大排長龍參觀。高倍數、大口徑的天文望遠鏡，滿足大小朋友對月亮的好奇與科學的探索。

由中央大學天文所葉永烜教授主講的「在月亮的兔子」科普演講，也吸引滿場的聽眾。從歷史的傳說到人類對月球的探測，帶領民眾對月亮有更深層的認識。許多民眾好奇此次演講的題目，葉永烜教授也不失其幽默的口吻說，兔子往月裏奔，原來是月球藏有許多「地洞」，讓大小朋友不禁會心一笑！

中央大學天文所長高仲明表示，這次月全食是繼 2011 年 12 月 10 日之後，台灣地區再見到月全食，預估全部過程將歷經 5 小時又 21 分鐘，其中本影食將歷時 3 小時又 20 分鐘。最大本影食分為 1.172。台灣時間下午 4 時 14 分半影食始，預計 5 時 15 分初虧，18 時 25 分食既，19 時 25 分生光，20 時 35 分復圓，21 時 35 分半影食終。中壢地區的民眾，可自 17 時 29 分月亮自方位 83 度升起後，觀測月出帶食及整個月全食後段變化。下次要等到 2015 年 4 月 4 日，台灣地區民眾才可望再見月全食。

高仲明特別感謝企業家台達創辦人暨榮譽董事長鄭崇華先生等的慷慨捐助，讓已有 32 年歷史的科一館天文台得以重整並以嶄新的面貌與大家見面，再次發揮天文科普教育與推廣之功能。科一館天文台於民國 70 年啟用，配備口徑 60 公分的望遠鏡是當時全國最大的光學望遠鏡，由中央大學開國內天文教育先河，於民國 66 年成立的物理與天文研究所籌建，前後花了 5 年的時間建立了當時國內天文研究的重要基地，服務期間也為國內培育多位天文研究人才。

原文轉載自【2014-10-09/NOWnews 今日新聞】

相關連結 / <http://www.nownews.com/n/2014/10/09/1449130>

一睹“紅月”全食丰采 桃園高校天文台擠爆

中國評論新聞：一睹“紅月”全食丰采 桃園高校天文台擠爆

一睹“紅月”全食丰采 桃園高校天文台擠爆

<http://www.CRNTT.com> 2014-10-09 00:54:57

中評社桃園 10 月 9 日電(記者 黃文杰)為一睹罕見的“紅月”全食丰采，桃園包括中原及中央大學 8 日均開放天文台，吸引民眾大排長龍參觀，高倍數、大口徑的天文望遠鏡，滿足大小朋友對月亮的好奇與科學的探索。

這次的月全食台灣時間 8 日下午 16 時 14 分半影食始，17 時 15 分初虧，18 時 25 分食既，19 時 25 分生光，20 時 35 分復圓，21 時 35 分半影食終。

另外，由台灣中央大學天文所葉永烜教授主講的“在月亮的兔子”科普演講，也吸引滿場的聽眾。從歷史的傳說到人類對月球的探測，帶領民眾對月亮有更深層的認識。

許多民眾好奇此次演講的題目，葉永烜教授也不失其幽默的口吻說，兔子往月球奔去，原來是月球藏有許多“地洞”，讓大小朋友不禁會心一笑。

位於桃園中壢的中原大學，晚間也開放科學館 9 樓天文台，透過各種高倍率的望遠鏡，由天文社學生陪民眾一起觀測難得的天文景象。

中原大學天文台配備圓頂觀測台、寬闊天台。圓頂設有高倍率的折反射式望遠鏡，可以清楚觀測月球表面。

天台設有反射式、折射式、折反射式望遠鏡，供民眾觀測使用。天文社學生於科學館 1 樓接待處，也提供明信片、書籤等小紀念品免費索取。

台灣中大天文所高仲明所長表示，這次月全食是繼 2011 年 12 月 10 日之後，台灣地區再見到月全食，預估全部過程將歷經 5 小時又 21 分鐘，其中本影食將歷時 3 小時又 20 分鐘。

中壢地區的民眾，從 17 時 29 分月亮自方位 83 度升起後，觀測月出帶食及整個月全食後段變化。錯過這次，下次台灣地區再見月全食，要等到明年 4 月 4 日。

月全食發生時，月球呈現暗紅色，又稱為“血月”，因此引發不少穿鑿附會傳說。

中原大學天文社同學解釋，由於月食過程中，地球大地層將其他光線吸收，只剩下紅色光穿透折射到月球表面，月亮看起來就變成暗紅色。

台灣上次可見的月全食發生於 2011 年 12 月 10 日，如果錯過這次機會，就得等明年 4 月 4 日。

中原大學天文社表示，月全食當天還可一併觀測天王星衝，也就是遙遠的天王星在視角上剛好移到月亮附近，利用望遠鏡就可以隱約看見青綠色的小圓點。

中原天文社創社已 44 年，曾舉辦過火星觀測、金星凌日、中秋賞月、日食觀測等活動。

原文轉載自【2014-10-09/中國評論新聞】

相關連結 /

<http://hk.crntt.com/doc/1034/1/9/3/103419319.html?coluid=93&kindid=8110&docid=103419319&mdate=1009005457>

一窺月全食現象 中大、中原開放天文台

自由時報電子報 首頁 > 生活

一窺月全食現象 中大、中原開放天文台

2014-10-08 21:57

〔記者李容萍／桃園報導〕為一睹罕見的「紅月」全食丰采，桃園縣的中央大學、

中原大學今晚同步開放科學館天文台供民眾一起觀測難得的天文景象，傍晚吸引民眾大排長龍等候參觀；經統計，兩校計有超過 1000 人透過高倍數、大口徑的天文望遠鏡，滿足對月亮的好奇與科學的探索。

中央大學天文所長高仲明表示，這次月全食是繼 2011 年 12 月 10 日之後，台灣地區再見到月全食，全程歷經 5 小時又 21 分鐘，其中本影食歷時 3 小時 20 鐘，最大本影食分為 1.172。

高仲明說，今天下午 5 時 29 分月亮自方位 83 度升起後，原本從晚上 6 時 25 分至 7 時 25 分整整 1 個小時，將出現全食紅月面現象，但因北部雲層稍厚蓋住，一直到晚上 7 時許雲層漸散去，7 時 25 分生光，8 時 35 分復圓，以及 9 時 35 分半影食終。

中大校長周景揚就說，中壢地區的民眾，中後半段可以清楚觀測月出帶食及整個月全食後段變化，算是運氣還不錯。

中原大學天文社也說，月全食發生時，月球呈現暗紅色，又稱為「血月」，因此引發不少穿鑿附會傳說；由於月食過程中，地球大地層將其他光線吸收，只剩下紅色光穿透折射到月球表面，月亮看起來就變成暗紅色。錯過這次，下次台灣地區再見月全食，要等到明年 4 月 4 日。

原文轉載自【2014-10-08/自由時報電子報 首頁 > 生活】

相關連結 / <http://news.ltn.com.tw/news/life/breakingnews/1126297>

中大天文台邀民眾一睹全食紅月

中央社首頁 > 教育文化

中大天文台邀民眾一睹全食紅月

發稿時間：2014/10/08 20:52 最新更新：2014/10/08 20:52

(中央社記者許秩維台北 8 日電)為了讓民眾一睹全食紅月風采，中央大學今天晚開放天文台，吸引民眾大排長龍，並邀請專家分享科普演講，讓民眾對月亮有更深層的認識。

中央大學天文所長高仲明表示，這次月全食是繼 2011 年 12 月 10 日後，台灣地區再見到月全食，預估全部過程將歷經 5 小時又 21 分鐘，其中本影食將歷時 3 小時又 20 分鐘，最大本影食分為 1.172。

為了讓民眾一睹罕見的「紅月」全食丰采，中央大學今晚也開放科學一館的天文台，吸引民眾大排長龍參觀，現場提供高倍數、大口徑的天文望遠鏡，滿足大小朋友對月亮的好奇與科學的探索。

高仲明說，中大科一館天文台開放，要感謝台達電創辦人暨榮譽董事長鄭崇華的慷慨捐助，讓已有 32 年歷史的科一館天文台得以重整並以嶄新的面貌與大家見面，發揮天文科普教育與推廣的功能。

中央大學表示，天文所教授葉永烜也在現場分享「在月亮的兔子」科普演講，從歷史傳說到人類對月球的探測，帶領民眾對月亮有更深層的認識。1031008
原文轉載自【2014-10-08/中央社首頁 > 教育文化】
相關連結 / <http://www.cna.com.tw/news/aedu/201410080462-1.aspx>

全球瘋血月 台灣搶先看

發稿時間：2014/10/08 23:20 最新更新：2014/10/08 23:28
月全食血月（記者裴禛 合成示意圖）
(中央社台北 8 日電) 月全食，全球瘋血月，台灣搶先看。8 日賞血月，台東上空在晚上 6 時 25 分搶先看到血月。

天文奇觀月全食賞血月 台東搶先看（記者盧太城攝）
「哇，我看到了」，一場親子共賞月全食活動晚間在高雄科工館登場，雖時有多雲擾局，但仍不減民眾觀賞天文奇觀興緻，小朋友看到血月的驚喜聲劃破夜空。

小朋友專注觀看天文奇觀「血月」（記者程啟峰攝）
全球許多地方，包括台灣在內，8日晚間可看到月全食景象，還可見到月球全部隱沒在地球影子區內的全食紅月面現象，即所謂的「血月」。

月全食登場 攝影迷興奮（游凱翔攝）
為了讓民眾一睹全食紅月風采，中央大學 8 日晚開放天文台，吸引民眾大排長龍，並邀請專家分享科普演講，讓民眾對月亮有更深層的認識。

親子共賞月全食（記者程啟峰攝）
中央大學天文所長高仲明表示，這次月全食是繼 2011 年 12 月 10 日後，台灣地區再見到月全食，全部過程歷經 5 小時又 21 分鐘，其中本影食將歷時 3 小時又 20 分鐘，最大本影食分為 1.172。

港都月全食（記者程啟峰攝）
在高雄，華燈初上，科工館南館廣場前也停滿汽機車，不少親子參加天文科教活動，現場架滿各式天文望遠鏡，還有專家以模型解說月全食原理。雖然時有多雲擾局，但月全食過程仍依稀可見，不少路過民眾也紛紛停下車拿起手機拍下這難得一見的天文奇景，並拿起手機奔相走告，要家裡親人探頭觀賞窗外的這場天文秀。

嘉義月全食 時隱時現（記者江俊亮攝）
一名婦人邊觀賞，邊以手機打電話回家告訴孩子說，「趕快出去看月亮，月全食

還有一點點可看，錯過還要等很久」。

雲縫中看月食（記者裴禛攝）

中央氣象局表示，今晚的月全食是屬於四重月全食組合中的第 2 個，連續 4 次的四重月全食，21 世紀共會出現 8 次。

台北市民眾賞血月（記者徐肇昌攝）

月球繞地球公轉，當月球移到地球的影子區內時，造成月面有缺角或隱沒時，稱為月食。

月全食 攝影愛好者搶拍（記者廖王楷攝）

今晚的月全食，是 2014 年至 2015 年四重月全食組合中的第 2 個，第 1 個是今年 4 月 15 日，明年 4 月 4 日及 9 月 28 日還各 1 個。

天文站說，當發生月全食時，很難看到原本滿月的月面，但照射包圍在地球周邊大氣層的太陽光，其中藍色光等波長較短的光線，會被地球大氣散射，較長波的紅色光則被折射到地球影子區內的月面上，形成所見的全食月面呈紅銅色。

不過，月全食紅銅色月面的明暗度是會隨著地球大氣的成分而不同，若地球大氣較清澈，較偏橙紅；若大氣中灰塵較多導致大氣較混濁，使紅色光的穿透量較少，呈現的紅銅色月面會較暗淡。今晚在台灣看到的月全食可謂「紅透透」，讓全台民眾見識到了「血月」的天文奇觀。

月全食 台灣各地賞血月（記者裴禛攝）

原文轉載自【2014-10-08/中央社首頁 > 重點新聞】

相關連結 / <http://www.cna.com.tw/news/firstnews/201410085007-1.aspx>

[台灣/看月全食 中原中央開放天文台](#)

<http://www.cdnews.com.tw> 2014-10-08 13:15:14

李漢揚/整理

月全食將在今晚出現，中原、中央大學也將開放天文台，讓民眾一窺天文現象，另外也提供書籤、並安排專家舉行科普演講。

中央社桃園 8 日電，中原大學天文社表示，下午 5 時 30 分到 10 時開放科學館天文台，帶領觀測並解說月食過程，讓民眾透過不同口徑的天文望遠鏡，高倍率觀察月球的整個月食過程。

中原大學指出，校內的天文台配備圓頂觀測台、寬闊天台。圓頂設有高倍率的折反射式望遠鏡，可以清楚觀測月球表面；天台設有反射式、折射式、折反射式

望遠鏡，供民眾觀測使用，科學館 1 樓接待處，也提供明信片、書籤等小紀念品免費索取。

中央大學也表示，學校內的科學一館天文台將於下午 5 時到 10 時開放民眾觀賞；晚間 7 時 30 分也將由天文所教授葉永烜進行一場「在月亮的兔子」的科普演講，歡迎民眾參與。

中央大學天文所長高仲明說，這次月全食是繼 2011 年 12 月 10 日之後，台灣地區再見到月全食，預估全部過程將歷經 5 小時 21 分鐘，其中本影食將歷時 3 小時 20 分鐘。

如果錯過這次，下次台灣地區再見月全食，要等到明年 4 月 4 日，對天文有興趣的民眾可以把握機會。

【中央網路報】

原文轉載自【2014-10-08/中央日報網路報-教育藝文】

相關連結 /

http://www.cdnews.com.tw/cdnews_site/docDetail.jsp?coluid=121&docid=10294379

1

看月全食 中原中央開放天文台

發稿時間：2014/10/08 10:41 最新更新：2014/10/08 10:41

(中央社記者邱俊欽桃園 8 日電) 月全食將在今晚出現，中原、中央大學也將開放天文台，讓民眾一窺天文現象，另外也提供書籤、並安排專家舉行科普演講。

中原大學天文社表示，下午 5 時 30 分到 10 時開放科學館天文台，帶領觀測並解說月食過程，讓民眾透過不同口徑的天文望遠鏡，高倍率觀察月球的整個月食過程。

中原大學指出，校內的天文台配備圓頂觀測台、寬闊天台。圓頂設有高倍率的折反射式望遠鏡，可以清楚觀測月球表面；天台設有反射式、折射式、折反射式望遠鏡，供民眾觀測使用，科學館 1 樓接待處，也提供明信片、書籤等小紀念品免費索取。

中央大學也表示，學校內的科學一館天文台將於下午 5 時到 10 時開放民眾觀賞；晚間 7 時 30 分也將由天文所教授葉永烜進行一場「在月亮的兔子」的科普演講，歡迎民眾參與。

中央大學天文所長高仲明說，這次月全食是繼 2011 年 12 月 10 日之後，台灣地區再見到月全食，預估全部過程將歷經 5 小時 21 分鐘，其中本影食將歷時 3 小時 20 分鐘。

如果錯過這次，下次台灣地區再見月全食，要等到明年 4 月 4 日，對天文有興趣的民眾可以把握機會。1031008

原文轉載自【2014-10-08/中央社首頁 > 教育文化】

相關連結 /

[http://www.cna.com.tw/news/aedu/201410080078-1.aspx?utm_source=feedburner&utm_medium=feed&utm_campaign=Feed%3A+cnaToday+\(Central+News+Agency+%7C+RealTime+News\)](http://www.cna.com.tw/news/aedu/201410080078-1.aspx?utm_source=feedburner&utm_medium=feed&utm_campaign=Feed%3A+cnaToday+(Central+News+Agency+%7C+RealTime+News))

明晚月全食 中大天文台開放

記者李容萍/中壢報導

迎接睽違三年的「月全食」，中央大學科學一館天文台將於明天下午五點至晚上十點開放民眾免費賞月，明晚七點半邀請天文所教授葉永烜主講「在月亮的兔子」，讓民眾一窺月球的奧秘。

中央大學天文所所長高仲明指出，這次月全食，預計台灣時間從明天下午四點十四分的「半影食」，五點十五分「初虧」，晚上九點卅五分「半影食」終。建議民眾可從下午五點廿九分，月亮自方位八十三度升起後，觀測「月出帶食」及整個「月全食」後段變化。

原文轉載自【2014-10-07/自由時報/A12 版/桃園焦點】

8 日觀賞月全食 台灣中央大學開放天文台

中評社桃園 10 月 7 日電（記者 黃文杰）為了迎接睽違三年的月全食現象，台灣中央大學 8 日將開放科一館天文台供民眾觀賞，中大天文所還加開“在月亮的兔子”的科普演講。

這次月全食現象，預計台灣時間 10 月 8 日下午 16 時 14 分半影食始，預計 17 時 15 分初虧，18 時 25 分食既，19 時 25 分生光，20 時 35 分復圓，21 時 35 分半影食終。中大天文所所長高仲明指出，這次月全食，是繼 2011 年 12 月 10 日之後，台灣地區再見到月全食，預估全部過程，將歷經 5 小時又 21 分鐘。

有趣的是，不論演講的名稱，或是海報上頭圖樣設計，可以看到，月球表面有隻兔子的陰影，不禁聯想，日前在桃園展出的霍夫曼“月兔”不幸遭燒毀，是否已經羽化升天，飛向月亮。

其中本影食將歷時 3 小時又 20 分鐘。最大本影食分為 1.172。

高仲明說，中大科一館天文台開放，要特別感謝企業家台達電創辦人暨榮譽董事長鄭崇華的慷慨捐助，讓已有 32 年歷史的科一館天文台，得以重整並以嶄新的面貌與大家見面，再次發揮天文科普教育與推廣之功能。

科一館天文台，於 1981 年啟用，配備口徑 60 公分的望遠鏡，是當時全台最大的光學望遠鏡。

校方從下午 5 點至 10 點開放天文台供民眾觀賞，並在健雄館 2 樓，由本校天文所葉永烜教授進行一場“在月亮的兔子”的科普演講，內容到底是否與霍夫

曼“月兔”裝置藝術，最後拆除遭燒毀有關？校方先賣關子，拭目以待。

原文轉載自【2014-10-07/中國評論新聞】

相關連結 /

<http://hk.crntt.com/doc/1034/1/6/4/103416484.html?coluid=93&kindid=8110&docid=103416484&mdate=1007004533>

迎接 10/8 月全食 中大科一館天文台開放

2014-10-03 經濟日報 曹松清

中央大學科學一館天文台配備口徑 60 公分的望遠鏡，作天文科普教育與推廣之用。中大／提供

迎接睽違三年的月全食現象，中央大學科學一館天文台將於 10 月 8 日下午五點至十點開放民眾觀賞。另於當晚 7:30-8:30 於健雄館 2 樓由該校天文所教授葉永烜進行一場「在月亮的兔子」的科普演講。

中央大學天文所所長高仲明表示，這次月全食是繼 2011 年 12 月 10 日之後，台灣地區再見到月全食，預估全部過程將歷經 5 小時又 21 分鐘，其中本影食將歷時 3 小時又 20 分鐘。最大本影食分為 1.172。

高仲明說，中大科一館天文台開放，要特別感謝企業家台達創辦人暨榮譽董事長鄭崇華等的慷慨捐助，讓已有 32 年歷史的科一館天文台得以重整並以嶄新的面貌與大家見面，再次發揮天文科普教育與推廣的功能。

科一館天文台於民國 70 年啟用，配備口徑 60 公分的望遠鏡是當時全國最大的光學望遠鏡，由中央大學開國內天文教育先河，於民國 66 年成立的物理與天文研究所籌建，前後花了 5 年的時間建立了當時國內天文研究的重要基地，服務期間也為國內培育多位天文研究人才。

這次月全食現象，預計台灣時間下午 16 時 14 分半影食始，預計 17 時 15 分初虧，18 時 25 分食既，19 時 25 分生光，20 時 35 分復圓，21 時 35 分半影食終。中壢地區的民眾，可自 17 時 29 分月亮自方位 83 度升起後，觀測月出帶食及整個月全食後段變化。錯過這次，下次台灣地區再見月全食，要等到明年 4 月 4 日。

原文轉載自【2014-10-03/聯合財經網 商情】

相關連結 / http://money.udn.com/storypage.php?sub_id=5723&art_id=399986

睽違 3 年 賞月全食 中大天文台 8 日開放

記者成志平／桃園報導

迎接睽違三年的月全食現象，中央大學科學一館天文台將於 8 日下午 5 時至 10 時開放民眾觀賞。另於當晚 7 時 30 分至 8 時 30 分於健雄館 2 樓由天文所葉

永烜教授進行一場「在月亮的兔子」的科普演講，歡迎民眾參與。

中央大學天文所所長高仲明表示，這次月全食是繼 2011 年 12 月 10 日之後，臺灣地區再見到月全食，預估全部過程將歷經 5 小時又 21 分鐘，其中本影食將歷時 3 小時又 20 分鐘。

高仲明說，中大科一館天文台開放，要特別感謝企業家台達創辦人暨榮譽董事長鄭崇華等人的慷慨捐助，讓已有 32 年歷史的科一館天文台得以重整並以嶄新的面貌與大家見面，再次發揮天文科普教育與推廣之功能。

此次月全食現象，預計臺灣時間 8 日下午 16 時 14 分半影食始，預計 17 時 15 分初虧，18 時 25 分食既，19 時 25 分生光，20 時 35 分復圓，21 時 35 分半影食終。中壢地區的民眾，可自 17 時 29 分月亮自方位 83 度升起後，觀測月出帶食及整個月全食後段變化。

原文轉載自【2014-10-03/青年日報首頁 > 桃竹苗】

相關連結 /

<http://news.gpwb.gov.tw/news.aspx?ydn=026dTHGgTRNpmRFEgxcbfWIQrJWsAo05toS0aglp%2bn8lHjBaW4BvSAz%2b4UMK7V1ojCPkWVSF2QouT3XUf7AAySuqsu%2fb0fOULGZRWALG2Sk%3d>

迎接月全食中大科一館天文台開放

【大紀元 2014 年 10 月 02 日訊】(大紀元記者陳建霖台灣桃園報導)迎接睽違三年的月全食現象，中央大學科學一館天文台將於 8 日下午五點至十點開放民眾觀賞。錯過這次，下次台灣地區再見月全食，要等到明年 4 月 4 日。

科一館天文台於民國 70 年啟用，配備口徑 60 公分的望遠鏡是當時全國最大的光學望遠鏡，由中央大學開國內天文教育先河，於民國 66 年成立的物理與天文研究所籌建，前後花了 5 年的時間建立了當時國內天文研究的重要基地，服務期間也為國內培育多位天文研究人才。

中央大學天文所高仲明所長表示，這次月全食是繼 2011 年 12 月 10 日之後，臺灣地區再見到月全食，預估全部過程將歷經 5 小時又 21 分鐘，其中本影食將歷時 3 小時又 20 分鐘。最大本影食分為 1.172。

高仲明說，中大科一館天文台開放，要特別感謝企業家台達創辦人暨榮譽董事長鄭崇華先生等的慷慨捐助，讓已有 32 年歷史的科一館天文台得以重整並以嶄新的面貌與大家見面，再次發揮天文科普教育與推廣之功能。

高仲明也說，本次月全食現象，預計臺灣時間下午 16 時 14 分半影食始，預計 17 時 15 分初虧，18 時 25 分食既，19 時 25 分生光，20 時 35 分復圓，21 時

35 分半影食終。中壢地區的民眾，可自 17 時 29 分月亮自方位 83 度升起後，觀測月出帶食及整個月全食後段變化。◇

責任編輯：陳真

原文轉載自【2014-10-03/大紀元】

相關連結

<http://www.epochtimes.com/b5/14/10/2/n4262809.htm>

中大開放天文台 可賞月全食

（中央社記者邱俊欽桃園 2 日電）10 月 8 日將發生月全食，中央大學當天將開放天文台，讓民眾瞭解月亮奧秘，另外安排專家進行「在月亮的兔子」科普演講。

中央大學今天表示，學校內的科學一館天文台將於 8 日下午 5 時到 10 時開放民眾觀賞；晚間 7 時 30 分也將由天文所教授葉永烜進行一場「在月亮的兔子」的科普演講，歡迎民眾參與。

中央大學天文所長高仲明說，這次月全食是繼 2011 年 12 月 10 日之後，台灣地區再見到月全食，預估全部過程將歷經 5 小時 21 分鐘，其中本影食將歷時 3 小時 20 分鐘。

中大表示，如果錯過這次，下次台灣地區再見月全食，要等到明年 4 月 4 日，對天文有興趣的民眾可以把握機會。1031002

原文轉載自【2014-10-03/中央社】

相關連結 / <http://www.cna.com.tw/news/aedu/201410020308-1.aspx>

觀賞月全食 中大開放天文台

中廣新聞網 (2014-10-03 05:32)

睽違三年的月全食現象，十月八日將再次出現。為了讓民眾可以欣賞過程，中央大學科學一館天文台，十月八日當天下午五點到十點開放供民眾觀賞；中大表示，錯過這次，下次台灣地區再見到月全食，要等到明年 4 月 4 日，有興趣民

眾要把握良機。(李明朝報導)

中央大學天文所高仲明所長表示，這次月全食是繼 2011 年 12 月 10 日之後，台灣地區再見到月全食，預估這次全部過程，將歷經 5 小時又 21 分鐘，其中本影食將歷時 3 小時又 20 分鐘。

中大校方人員表示這次月全食現象，預計台灣時間是在十月八日下午 16 時 14 分半影食始，預計 17 時 15 分初虧，18 時 25 分食既，19 時 25 分生光，20 時 35 分復圓，21 時 35 分半影食終。中壢地區的民眾，可自 17 時 29 分月亮自方位 83 度升起後，觀測月出帶食及整個月全食後段變化。

中大表示，科一館天文台於民國 70 年啟用，配備口徑 60 公分的望遠鏡，是當時全國最大的光學望遠鏡，由中央大學開國內天文教育先河，民國 66 年成立的物理與天文研究所籌建，前後花了 5 年的時間建立了當時國內天文研究的重要基地，服務期間也為國內培育多位天文研究人才。

中大表示，錯過這次，下次台灣地區再見月全食，要等到明年 4 月 4 日，歡迎民眾把握良機。若想更進一步了解相關訊息，可電洽中央大學天文所 (03)4227151 分機 65977 。

原文轉載自【2014-10-03/新浪新聞中心/生活消費新聞】

相關連結 / <http://news.sina.com.tw/article/20141003/13423366.html>

台灣/中大開放天文台 可賞月全食

李漢揚/整理

10 月 8 日將發生月全食，中央大學當天將開放天文台，讓民眾瞭解月亮奧秘，另外安排專家進行「在月亮的兔子」科普演講。

根據中央社 2 日報導指出，中央大學今天表示，學校內的科學一館天文台將於 8 日下午 5 時到 10 時開放民眾觀賞；晚間 7 時 30 分也將由天文所教授葉永烜進行一場「在月亮的兔子」的科普演講，歡迎民眾參與。

中央大學天文所長高仲明說，這次月全食是繼 2011 年 12 月 10 日之後，台灣地區再見到月全食，預估全部過程將歷經 5 小時 21 分鐘，其中本影食將歷時 3 小時 20 分鐘。

中大表示，如果錯過這次，下次台灣地區再見月全食，要等到明年4月4日，對天文有興趣的民眾可以把握機會。

原文轉載自【2014-10-03/中央網路報】

相關連結 /

http://www.cdnews.com.tw/cdnews_site/docDetail.jsp?coluid=121&docid=102937514

年輕天文學者講座 德國葛伊娃教授獲獎

由國立中央大學與台達電子文教基金會共同頒發的「年輕天文學者講座」，今天（22）由中央大學校長周景揚頒獎給獲獎者德國海德堡大學物理研究中心主任葛伊娃教授（Professor Eva Grebel）。

中央大學表示，這個獎座是表彰45歲以下，在研究領域有卓越表現的國際天文學者，葛伊娃教授專長為星系演化與宇宙學，是這個講座成立以來第四位獲獎者。獲獎的葛伊娃教授9月23號起將分別在臺北、桃園和臺中，展開三場天文演講，希望能啟發年輕學子與社會大眾對宇宙天文的探索，有關年輕天文學者講座可上網。（http://www.astro.ncu.edu.tw/ncu_delta/index.php）查詢。

（2014-09-22 18:05:34 徐詠絮）

原文轉載自【2014-09-22/教育廣播電台/校園】

相關連結 / <http://news.ner.gov.tw/index.php?act=culnews&code=view&ids=168338>

近距離拍攝 「雙彗核」現形

2014/8/7 上午 09:33:31

／編輯／謝俊峰

歐洲太空總署太空船「羅塞塔號」在7月中下旬捕捉到彗星「雙彗核」影像，是人類首次以太空船近距離拍攝到雙彗核；8月3日距離彗星僅300公里，拍攝到的畫面更可依稀看出彗星的地形和地貌，是人類首次如此「近距離」接近彗星。

彗星是太陽系形成後留下的遺跡之一，主要由髒冰塊與泥塊組成，是太陽系中改變最少的天體，可藉由研究彗星結構的物理特性，還原當時原始太陽系形成區域的環境。參與這項計畫的協同主持人中央大學天文所教授葉永烜昨指出，透過兩台拍攝彗星的可見光攝影機精密儀器，可進一步了解彗核表面構造、氣體塵埃粒子。

中大團隊參與計畫

中央大學天文所助理研究學者林忠義則表示，過去觀測彗星以地面望遠鏡為主，這次藉由太空船近距離觀測，除發現 67P 彗核可能是由兩個緊密個體組成，顛覆原以為是一個個體的模擬；「雙彗核」代表可能是兩個個體，也可能是一個、但中間的揮發物很多，都需進一步分析。

原文轉載自【2014-08-07/中國網路電子報】

相關連結 / http://www.echinanews.com.tw/shownews.asp?news_id=194163

羅塞塔號攝得“雙彗核” 台灣研究團隊振奮

中國評論新聞：羅塞塔號攝得“雙彗核” 台灣研究團隊振奮

<http://www.CRNTT.com> 2014-08-07 01:18:37

中評社桃園 8 月 7 日電(記者 黃文杰)歐洲太空總署發射的太空船“羅塞塔號”，經過長達 10 年的飛行與等待，在台北時間 6 日下午 5 時，正式進入長期追蹤的 67P/Churyumov-Gerasimenko 彗星軌道，全球矚目，太空船也捕捉到預期之外的彗星“雙彗核”影像，讓參與計劃的台灣中央大學天文所團隊相當振奮。

台灣中大天文所教授葉永烜，是這項計劃的科學團隊之協同主持人，提供科學資訊和參與資料分析，將計劃從德國延續至台灣，並協同該校天文所助理研究員林忠義，投入這項研究工作，一接受到罕見的“雙彗核”影像，興奮難以筆墨形容。

葉永烜教授指出，羅賽塔號太空船在 8 月 3 日距彗星 300 公里時，成功拍攝罕見的“雙彗核”影像，依稀可看出彗星的地形和地貌，這是人類首次如此“近距離”接近彗星，看到彗星最真實影像。

另外，歐洲太空總署計劃在 11 月初釋放登彗小艇“菲萊”(Philae)，如果順利的話，也將是人類史上第一次登入彗核的探測器。

早在 10 年前，中大天文所教授葉永烜在德國馬克斯普朗克太陽系研究所服務期間，參與這項歐空局所領導的科學任務，經過十年的醞釀與等待，終於能圓一個夢。

葉永烜教授同時也是土星探測計劃—卡西尼計劃主要發起人之一，卡西尼計劃的太空船飛行任務更長達 20 年，顯見其視野和遠見。

他解釋，這項歐空局所領導的科學任務(OSIRIS)，有兩台拍攝彗星的可見光攝影機，其中一架負責大視場拍攝(WAC)，另一架雖視野小，但有較高的解析度(NAC)。透過此精密儀器，可進一步了解彗核表面構造、氣體塵埃粒子的誕生，以及彗核顏色分析等，對於彗星探索更進一步。

協同計劃的中大天文所助理研究員林忠義表示，彗星總是來去匆匆，驚鴻一瞥，以往人類對彗星的觀測，主要來自地面望遠鏡，此次藉由太空船近距離觀測，除發現 67P 彗核可能是由兩個緊密的個體相接組成(contact binaries)之外，更令天

文學家意外的是，“顛覆原先模擬”，因為在此之前，由地面上的觀測，並未發現 67P “雙彗核”的存在，這也顯示羅賽達號科學任務的重要性。

林忠義說，彗星是太陽系形成後所留下來的遺跡之一，主要由髒冰塊與泥塊組成，是太陽系中改變最少的天體，因此可藉由研究彗星結構中的物理特性，來還原當時原始太陽系形成區域的環境，並且得知太陽系形成的一些線索。

令人好奇的是，“雙彗核”的成因？林忠義解釋，有可能是兩個彗星碰撞，也可能原始生成，經過長久天文演化造成，但都需進一步分析。

目前 67P 繞太陽一圈的軌道週期為 6.45 年，自轉一週 12.4 小時，預計明（2015）年 8 月 13 日為其近日點（最接近太陽時），屆時也將引發另一波天文迷關注。

原文轉載自【2014-08-07/中國評論新聞】

相關連結 /

<http://hk.crntt.com/doc/1033/2/6/1/103326119.html?coluid=93&kindid=8110&docid=103326119&mdate=0807011837>

罕見「雙彗核」 太空船近距離捕捉

【湯雅雯／台北報導】

歐洲太空總署 10 年前發射的太空船—羅塞塔號，經過長達 10 年的飛行與等待，昨正式進入長期追蹤的 67P／楚留莫夫・格拉稀門克（Churyumov-Gerasimenko）彗星軌道，日前意外捕捉到彗星罕見「雙彗核」影像，令天文迷相當振奮。

中央大學天文所教授葉永烜是這項計畫的科學團隊的協同主持人，他和天文所助理研究員林忠義一起提供科學資訊和參與資料分析，將計畫從德國延續至台灣。

林忠義表示，罕見的「雙彗核」影像，是羅賽塔號太空船日前在距彗星 300 公里時所拍攝，依稀可看出彗星的地形和地貌，這是人類首次如此「近距離」接近彗星，並捕捉到彗星最真實的影像。

林忠義說，歐洲太空總署計畫在 11 月初釋放登彗小艇「菲萊」，如果順利的話，也將是人類史上第一次登入彗核的探測器。

他指出，彗星總是來去匆匆，驚鴻一瞥，以往人類對彗星的觀測，主要來自地面望遠鏡，此次藉由太空船近距離觀測，除發現 67P 彗核可能是由 2 個緊密的個體相接組成外，更顛覆天文學家的原先模擬，因為在此之前由地面上的觀測，並未發現 67P 「雙彗核」的存在，這也顯示太空船科學任務的重要性。

他說，過去少有機會長期觀測、探索彗星演化，藉由太空船科學任務，釋放探

測器到彗星上，未來可進一步分析彗星表面構造、氣體塵埃粒子的誕生及彗核顏色分析等，甚至防止彗星撞地球。

林忠義說，「雙彗核」的成因，有可能是 2 個彗星碰撞，也可能是經過長久天文演化造成，需進一步分析。目前 67P 繞太陽一圈的軌道周期為 6.45 年，自轉一周 12.4 小時，預計明年 8 月 13 日最接近太陽，屆時也將引發另一波天文迷關注。

原文轉載自【2014-08-07/中國時報/A8 版/生活新聞】

相關連結 / <http://www.chinatimes.com/newspapers/20140807000493-260114>

羅賽塔號 接軌 黃色小鴨
人類首次 近距接觸「雙彗核」

【記者陳皓嫵／台北報導】

歐洲太空總署十年前發射的太空船羅賽塔，昨天傍晚成功進入 67P 彗星的軌道中，人類首次以一百公里的近距離接觸、觀測彗星。羅賽塔並拍攝到科學家們預期外、罕見的「雙彗核」影像，令科學家們非常興奮，直說：「羅賽塔讓我們最近天天過耶誕節！」

這項國際計畫也有台灣學者參與，中央大學天文所教授葉永烜是該計畫的協同主持人，和另一位助理研究學者林忠義皆投入其中，提供並分析相關資料；因時差關係，他們每天可比歐美的科學家早幾個小時取得彗星第一影像，並著手解讀。

林忠義表示，過去人類只在地球上觀測衛星，以幾千公里之遙看著彗星來去匆匆；因觀測限制多，對彗星了解有限。

藉由羅賽塔長期追蹤、細看彗星，讓科學家終於得以解開彗星的成分、結構之謎。林忠義說，就好像羅賽塔石碑讓考古學家得以解讀埃及象形文字的意義一樣。

「一般觀測到的彗星多只有一個核，過去看 67P 也認為它是單核彗星。」林忠義指出，羅賽塔拍到的彗星形狀卻像一隻鴨子，由兩個緊密的個體相接組成，顛覆天文學家之前推測雙核心可能是兩個彗星相撞而成的看法，「雙彗核」可能原本生成時就是這樣，但仍須進一步研究。

歐洲太空總署將在今年十一月初釋放「登彗小艇菲萊」，如果它順利登陸，就是人類史上第一次登陸彗星的探測器。67P 彗星繞太陽一周約要六年半，預計明年八月十三日最接近地球，將引發天文迷另一波關注熱潮。

原文轉載自【2014-08-07/聯合報/A5 版/話題】

相關連結 / <http://www.udn.com/2014/8/7/NEWS/WORLD/WOR4/8854994.shtml>

300 公里近距離拍攝 「雙彗核」現形

〔記者湯佳玲／台北報導〕歐洲太空總署太空船「羅塞塔號」在7月中下旬捕捉到彗星「雙彗核」影像，是人類首次以太空船近距離拍攝到雙彗核；8月3日距離彗星僅300公里，拍攝到的畫面更可依稀看出彗星的地形和地貌，是人類首次如此「近距離」接近彗星。

彗星是太陽系形成後留下的遺跡之一，主要由髒冰塊與泥塊組成，是太陽系中改變最少的天體，可藉由研究彗星結構的物理特性，還原當時原始太陽系形成區域的環境。參與這項計畫的協同主持人中央大學天文所教授葉永烜指出，透過兩台拍攝彗星的可見光攝影機精密儀器，可進一步了解彗核表面構造、氣體塵埃粒子。

中大團隊參與計畫

中央大學天文所助理研究學者林忠義則表示，過去觀測彗星以地面望遠鏡為主，這次藉由太空船近距離觀測，除發現67P彗核可能是由兩個緊密個體組成，顛覆原以為是一個個體的模擬；「雙彗核」代表可能是兩個個體，也可能是一個、但中間的揮發物很多，都需進一步分析。

原文轉載自【2014-08-07/自由時報/A10版/國際萬象】

相關連結 / <http://news.ltn.com.tw/news/world/paper/802431>

中大捕捉到彗星雙彗核 人類首次近距離觀測

2014-08-06 18:56

〔記者湯佳玲／台北報導〕歐洲太空總署10年前發射的太空船-羅塞塔號，經過長達10年的飛行與等待，預計在今天（台北時間8月6日下午五時）正式進入長期追蹤的67P/Churyumov-Gerasimenko彗星軌道，全球矚目。最近更傳來令人振奮消息，捕捉到預期之外的彗星「雙彗核」影像。

「雙彗核」影像是羅賽塔號太空船在8月3日距彗星300公里時所拍攝，依稀可看出彗星的地形和地貌，是人類首次如此「近距離」接近彗星。歐洲太空總署計畫在11月初釋放登彗小艇「菲萊」（Philae），如果順利的話，也將是人類史上第一次登陸彗核的探測器。

參與這項計劃的協同主持人中央大學天文所教授葉永烜，10年前在德國馬克斯普朗克太陽系研究所服務期間即已投入，並將計劃從德國延續至台灣，歷經10年醞釀與等待終有成果。他說，透過兩台拍攝彗星的可見光攝影機精密儀器，可進一步了解彗核表面構造、氣體塵埃粒子的誕生，以及彗核顏色分析等，對於彗星探索更進一步。

中央大學天文所助理研究學者林忠義表示，過去觀測彗星以地面望遠鏡為主，這次藉由太空船近距離觀測，除發現67P彗核可能是由兩個緊密的個體相接組成之外，更令天文學家意外的是「雙彗核」的存在，顛覆原先模擬。

林忠義說，彗星是太陽系形成後所留下來的遺跡之一，主要由髒冰塊與泥塊組成，是太陽系中改變最少的天體，因此可藉由研究彗星結構中的物理特性，來還

原當時原始太陽系形成區域的環境，並且得知太陽系形成的一些線索。「雙彗核」的成因，有可能是兩個彗星碰撞，也可能原始生成，經過長久天文演化造成，但都需進一步分析。

原文轉載自【2014-08-06/自由時報電子報 - 生活】

相關連結 / <http://news.ltn.com.tw/news/life/breakingnews/1074615>

中大捕捉 首次近看雙核彗星

【本報綜合外電報導】歐洲太空總署宣布，彗星探測器「羅賽塔號」經過十年，航行六十億公里，昨天進入長期追蹤的 67P 楚留莫夫・格拉稀門克 (Churyumov-Gerasimenko) 彗星軌道，成為人類史上首個進入彗星軌道的太空飛行器。日前意外捕捉到彗星罕見「雙彗核」影像，令天文迷非常興奮。

這項計畫科學團隊協同主持人、中央大學天文所教授葉永烜，和天文所助理研究員林忠義一起提供科學資訊並參與分析，將計畫從德國延續至台灣。

林忠義說，罕見「雙彗核」影像，是羅賽塔號日前在距彗星三百公里時所拍攝，依稀可看出彗星地形和地貌，這是人類首次如此近距離接近彗星，並捕捉到彗星最真實影像。

林忠義說，歐洲太空總署計畫在十一月初釋放登彗小艇「菲萊」，如果順利的話，將是人類史上第一次登入彗核的探測器。

他指出，彗星總是來去匆匆，以往人類對彗星的觀測主要來自地面望遠鏡，此次藉由太空船近距離觀測，除發現 67P 彗核可能是由二個緊密的個體相接組成，更顛覆天文學家的原先模擬，因為在此之前由地面上的觀測，並未發現 67P 「雙彗核」的存在，這也顯示太空船科學任務的重要性。

他說，過去很少有機會長期觀測、探索彗星演化，藉由太空船科學任務，釋放探測器到彗星上，未來可以進一步分析彗星表面構造、氣體塵埃粒子的誕生及彗核顏色分析等，甚至防止彗星撞地球。

林忠義說，「雙彗核」的成因，有可能是二個彗星碰撞，也可能是經過長久天文演化造成，需進一步分析。目前 67P 繞太陽一圈的軌道周期為六點四五年，自轉一周十二點四小時，預計明年八月十三日最接近太陽，屆時也將引發天文迷關注。

原文轉載自【2014-08-07/人間福報 綜合／社區】

相關連結 / <http://www.merit-times.com.tw/NewsPage.aspx?Unid=364800>

韓劇“星星”爆紅 中央大學天文台沾光

中評社桃園 4 月 15 日電(記者 黃文杰)韓劇“來自星星的你”掀起一股熱潮，連帶也使得台灣中央大學校區天文台，全台灣第一座具有天文研究用大型望遠鏡的天文台，跟著沾光，經常有團體預約導覽，連遠方的蒙古國也來參觀。

台灣中大天文研究所專業技術士張光祥替中評社導覽解說，聊起“一窩風”探索天文宇宙熱潮，最愛舉“流星雨”的冷笑話，1998 年獅子座流星雨超級轟動，引領大家觀測星空的風潮，結果竟然有人問：“看流星雨，要穿雨衣，還是打雨傘比較好？”

這部韓劇“來自星星的你”，最終一回演到，大家都看流星，男女情侶相互許願，欣賞“流星雨”，不再會鬧穿雨衣或打雨傘的笑話，但真正啟蒙天文知識，還是要到天文台。

台灣中央大學於 1977 年，成立物理與天文研究所時，開始籌建天文台，1981 年啟用，算算已經邁入 33 年，相當“老字號”。

在天文所技士張光祥的陪同，進入中大校區天文台，這裡有 61 公分望遠鏡，是當時台灣最大的天文望遠鏡，身負教育及研究的使命。

張光祥熱心介紹，並示範如何啟動天文台原弧形的密閉遮棚，年代雖久，但齒輪帶動開闔，幾乎是“天文觀測的傳統工藝之美”，相當有味道。

這套蓋賽格林(Cassegrain)反射式望遠鏡，為美國著名的 Perkin-Elmer 公司製造，早期使用的儀器為天文照相機及光電管光度計，1990 年始使用天文研究用的 CCD (Charge Coupled Device, 電荷耦合元件) 相機，主要從事變星、星團及雙星的天文成像及光度測量等觀測研究工作。

(原文來源網址：

<http://hk.cntt.com/doc/1031/3/0/0/103130049.html?coluid=93&kindid=8110&docid=103130049&mdate=0415004504>)

台天文學者追尋神秘行星 探索來自星星的你

中評社桃園 4 月 15 日電(記者 黃文杰)以台灣中央大學天文所葉永烜教授為主的研究團隊，長期追蹤宇宙星河新的行星，他們透過“泛星計劃”

(Pan-STARRS) 超廣角望遠鏡，加上行星軌道擾動推算，比海王星還遠 8 倍的距離，也就是太陽到地球的距離 250 倍，可能會有比地球重 5 倍的行星。

台灣中央大學天文所教授葉永烜將在四月底，受邀演講題目是“星星與你(妳)”，海報一貼出來，愛看韓劇的人，難免想到最夯的“來自星星的你”，認識葉教授的人直呼“怎麼這麼浪漫”

事實上，以葉永烜為主的研究團隊，他們對於外星人都敏俊教授、韓流明星千頌伊的偶像劇情，恐怕不清楚，但研究團隊天天在討論推算，行星軌道運行，

到底有沒有“超級地球”存在？

本身也是台灣聯合大學系統副校長葉永烜，他的研究團隊，分成好幾組投入宇宙天文不同的研究計劃。

博士後研究林省文首先解釋，所謂泛星計劃(Panoramic Survey Telescope And Rapid Response System，Pan-STARRS)直譯為全景巡天望遠鏡和快速回應系統。

林省文說，這是一個正在進行中的巡天計劃，該計劃將對全天空天體進行天文測量和光度測定，該計劃將比較同一天區不同時間的變化以期能發現彗星、小行星、變星等天體；尤其是有撞擊地球威脅性的近地天體。泛星計劃將建立一個所有在夏威夷能觀測到，視星等最暗可達24等的天體資料庫，總共可觀測全天四分之三的區域。

天文觀測儀器發展日新月異——望遠鏡口徑增變大，偵測器靈敏度提升，焦平面覆蓋面積增加。

(原文來源網址：

<http://hk.cntt.com/doc/1031/2/9/5/103129515.html?coluid=93&kindid=8110&docid=103129515&mdate=0415003857>)

解世紀之謎 大爆炸 不再只是「理論」

【記者郭政芬、呂筱蟬／連線報導】

「為宇宙瞬間暴脹找到直接證據！」清華大學天文所教授張祥光指出，科學家認為宇宙大爆炸後，有段暴脹期讓宇宙快速變大，這次觀測到宇宙「微波背景輻射」中的微小偏極化波紋，是宇宙論發展上的重要里程碑。

中央大學天文研究所教授黃崇源表示，這次美國研究團隊的成就，是讓大爆炸不再停留在「理論」階段，解開宇宙產生之謎。重力波現象是過去沒有人能發現和證實，所以郭兆林和團隊的發現才令人驚訝與震撼。

張祥光表示，宇宙大爆炸被認為是宇宙的開始，宇宙最先是由一個密度極大且高溫的狀態演變而來，因大爆炸而膨脹、溫度下降。

一九六七年科學家無意中發現「宇宙微波背景輻射」，為大霹靂理論提供最重要的證據，一九八四年有科學家認為大霹靂後，應該有經歷更快速的劇烈膨脹，這被稱為「暴脹理論」，但這始終都停留在理論，缺乏強有力的證據。

張祥光解釋，這次科學家靠著測量宇宙微波背景輻射的偏極化，得到宇宙暴脹所造成重力波留在微波背景輻射裡的痕跡，支持宇宙暴脹理論，是相當重要的發

現。

原文轉載自【2014-03-19/聯合報/A3 版/焦點】

相關連結 / <http://www.udn.com/2014/3/19/NEWS/WORLD/WORS4/8556836.shtml>

大爆炸產生星體 宇宙仍在膨脹

大爆炸（Big Bang）是宇宙誕生的理論，不少學者認為，宇宙萬物之初是一個很小而高密度、高溫的結構，約一百三十八億年前快速擴充（也就是所謂的大爆炸），產生原子的型態，導致星體和星系的誕生，宇宙至今仍不斷長大。

英國天文學者霍伊爾（Fred Hoyle）最早用「大爆炸」來形容此一理論，在大爆炸下產生的物質，應會有很大的密度變化，但宇宙初期密度變化非常小，美國學者古斯（Alan Guth）在一九八〇年代提出「暴脹」說法，解釋宇宙快速膨脹的過程。

重力波印證暴脹

中央大學天文所教授葉永烜比喻，宇宙暴脹過程就像先把一張紙搓成一團，如要把紙攤平而沒有皺褶，就需要用很大的力氣把紙張快速拉大攤開。

在大爆炸時，量子擾動隨即產生原始重力波，而重力波在宇宙暴脹後，放大成可以偵測的訊號，這些重力波在宇宙微波背景輻射中留下痕跡，而郭兆林等學者發現重力波的印記，證明宇宙暴脹的理論。

葉永烜指出，很多重要理論只要欠缺證據，就有可能是錯的，因此郭兆林發現重力波印記，是極為重大的進展。英國物理學者希格斯一九六四年就提出「上帝粒子」理論，近五十年後才獲證實存在，科學的發展就是如此，提出假設後還要去證實，才能繼續向前走。國際中心

原文轉載自【2014-03-19/蘋果日報/A6 版/要聞】

相關連結

<http://www.appledaily.com.tw/appledaily/article/headline/20140319/35709910/%E5%A4%A7%E7%88%86%E7%82%B8%E7%94%A2%E7%94%9F%E6%98%9F%E9%AB%94%E5%AE%87%E5%AE%99%E4%BB%8D%E5%9C%A8%E8%86%A8%E8%84%B9>

為何是在南極發現？

【記者嚴文廷/台北報導】

科學家在南極利用望遠鏡發現宇宙大爆炸後宇宙瞬間膨脹的直接證據，中央大學天文所教授黃崇源指出，宇宙大爆炸有很多證據可證實，但應該有個暴漲（Inflation）才會讓宇宙變得這麼大，這次觀測到宇宙「微波背景輻射」中的微弱極化光，證實確有暴漲的存在。

中研院天文及天文物理所副研究員王為豪指出，過去只能證明有宇宙大爆炸存在，但爆炸後有個瞬間膨脹的過程，且膨脹速度比光速還要快，但過去只能用各式各樣的理論去解釋，始終無法找到直接證據。這次科學家從「微波背景輻射」分析出「暴漲」的極微小波紋，是首次找到直接證據。

王為豪解釋，「微波背景輻射」大概跟微波爐的輻射差不多，人類的肉眼無法辨識，就像把石頭拿進微波爐加熱，加熱後皮膚透過空氣會感受到石頭的溫度，但肉眼是無法辨識，這次的發現就是從微波輻射中，分析出暴漲的波紋。

至於為什麼會在南極發現，王為豪說明，微波會被水分子干擾，南極因為地處高原，加上空氣中的水分子幾乎都因為低溫凝結，是地球上觀測宇宙微波的最好地點。加上儀器不斷精進下，才終於有這個天文學上相當重要的發現。

原文轉載自【2014-03-18/聯合晚報/A3 版/話題】

相關連結 / <http://udn.com/NEWS/WORLD/WORS4/8555066.shtml>

台灣學者說《星星》：教授“母星”至少上萬個

2014 年 02 月 28 日 13:18 來源：<http://internal.dbw.cn/>

原標題：台灣學者說《星星》：韓劇的天文觀念是錯的

據台灣《中國時報》報道，近來韓劇《來自星星的你》在台掀起一股天文熱。台灣“中研院”天文所研究助理陳英同笑說，星星是燙的，溫度常高達 4000 到 6000 摄氏度，根本不可能住人；依照目前的天文學理，沒有一顆彗星 400 年後會接近地球，所以韓劇的天文觀念都是錯的；民眾觀賞電視劇，看看就好，別認真。

由台灣“中央大學”參與的國際團隊在太陽系外圍找到 1 顆直徑約 300 公裡跟台灣差不多大的星球，未來有助於更清楚了解太陽系形成過程，或找到另一個太陽系。

“中央大學”天文所教授葉永烜表示，陳英同在就讀博士班時參與國際團隊到加拿大研究觀測時，意外發現這顆星球，編號為 2010GB174，再比對過去研究資料，發現有更多類似的星球，經推算估計，類似這樣星球至少上萬個，比之前估計量上修 10 倍。

原文轉載自【2014-02-28/人民網--人民網娛樂頻道】

相關連結 / <http://ent.people.com.cn/BIG5/n/2014/0228/c1012-24494167.html>

臺灣學者說《星星》：教授母星至少上萬個

2014年02月28日 14:40:42 來源：人民網

原標題：臺灣學者說《星星》：韓劇的天文觀念是錯的

據臺灣《中國時報》報道，近來韓劇《來自星星的你》在臺掀起一股天文熱。臺灣“中研院”天文所研究助理陳英同笑說，星星是燙的，溫度常高達4000到6000攝氏度，根本不可能住人；依照目前的天文學理，沒有一顆彗星400年後會接近地球，所以韓劇的天文觀念都是錯的；民眾觀賞電視劇，看看就好，別認真。

由臺灣“中央大學”參與的國際團隊在太陽係外圍找到1顆直徑約300公里跟臺灣差不多大的星球，未來有助于更清楚了解太陽係形成過程，或找到另一個太陽係。

“中央大學”天文所教授葉永烜表示，陳英同在就讀博士班時參與國際團隊到加拿大研究觀測時，意外發現這顆星球，編號為2010GB174，再比對過去研究資料，發現有更多類似的星球，經推算估計，類似這樣星球至少上萬個，比之前估計量上修10倍。

原文轉載自【2014-02-28/新華網-臺灣頻道】

相關連結 /

http://big5.xinhuanet.com/gate/big5/news.xinhuanet.com/tw/2014-02/28/c_126205528.htm

解密太陽系形成的關鍵 存在大量類冥王星天體

〔新網記者徐慧君台北特稿〕 太陽系外圍到底還有多少像冥王星的天體，向來是天文學家的未解之謎。由國科會補助的國際合作計畫，日前在太陽系外圍找到1顆直徑約300公里天體，加上先前觀測結果，推估該區至少有上萬個天體，將有助解密太陽系形成關鍵。

中研院研究助理陳英同博士在中央大學天文所修讀期間，得到國科會台加合作計劃的資助出國進修，與加拿大國家天文台 Herzberg 天文物理研究所 J.J. 卡法勒爾斯(J.J. Kavelaars)博士組成的合作團隊，利用在夏威夷的加法夏3.6米望遠鏡(CFHT)的觀察資料，作出詳細影像分析工作，除了90多個新發現的海王星外物體外，還找到一個編號為2010GB174的內奧特雲物體，其大小與距離僅次於賽特那矮行星。

第一個內奧特雲物體是在 2002 年發現，接著美國加州理工學院的一個大型巡天計劃在 2003 年發現一個名為賽特那(SeDna)的矮行星，其最接近太陽的距離為 76 天文單位，由此確立內奧特雲的存在，但在整個太陽系架構的瞭解中有一個盲點，即便是在海王星軌道外側到奧特雲之間，可能存在大量小物體，因距離太遠，直接用望遠鏡觀察相當有難度，且又缺乏恆星或其它行星擾動機制，使它們進入內太陽系變成彗星而被偵察，因此內奧特雲一直是個謎團，全部數目是個未知數。

陳應同表示，從艾松彗星的軌道參數來看，它應該是來自太陽系最外圍的奧特雲。這個離太陽距離逾 2 萬天文單位（一個天文單位是從地球到太陽的距離）並且成圓殼狀的空間，其中藏有數千億小物體。它們都是在太陽系初期，當天王星和海王星尚在形成的時候，給外行星彈射到遠處的太陽系原始物質，再經銀河的潮汐作用和恆星的重力擾動而演變成奧特雲，也是外界熟知彗星形成的區域。

有趣的是這個過程的一個重要結果，便是引起天王星和海王星從原來的位置外移到現在的軌道，同時造成木星的軌道略為內移。

中央大學天文所教授葉永烜說，研究團隊在觀察過程中除了新發現 90 多個海王星外物體外，4 年觀測中還找到一個編號為 2010GB174 的內奧特雲物體，其大小與距離僅次於賽特那矮行星。由上述新發現的天體，加上過去國際所觀測結果，由此推測這類位於內奧特雲天體至少有上萬個，比過去估計的數千個上修 10 倍。

葉永烜表示，這類的研究將有助於瞭解太陽系的形成過程，冥王星於 2006 年被降級為矮行星，原因在於其大小與軌道特性接與太陽系其他 8 大行星相異，這項研究對冥王星、土星、木星、海王星組成的原因帶來新的探究方向，並有助推論系外行星的來源以及演化。

頻道:捐贈贊助 分類:天文地理

專題:徐慧君 發稿日期:2014/2/26 下午 05:16:09

關鍵字:太陽系,冥王星,天文學,夏威夷,望遠鏡,國科會,海王星,矮行星,奧特雲,土星,木星

原文轉載自【2014-02-26/新網新聞網】

相關連結 / <http://newnet.tw/Newsletter/Comment.aspx?Info=5&iNumber=10487>

中大:太陽系外圍天體 上修 10 倍 星星是燙的 韓劇天文觀念錯了

【湯雅雯／台北報導】

太陽系外圍到底還有多少像冥王星的天體，一直是天文學家的未解之謎。中央大學參與的國際團隊，在太陽系外圍找到 1 顆直徑約 300 公里跟台灣差不多大的星球，估計這樣星球至少上萬個，比之前估計上修 10 倍，未來有助於更清楚了解太陽系形成過程，或找到另一個太陽系。

至於近來韓劇《來自星星的你》掀起一股天文熱，陳英同笑說，星星是燙的，溫度常高達 4000 到 6000°C，根本不可能住人，依照目前的天文學理，沒有一顆彗星 400 年後會接近地球，所以韓劇的天文觀念都是錯的，民眾觀賞電視劇，看看就好，別認真。

中央大學天文所教授葉永烜表示，陳英同在就讀博士班時參與國際團隊到加拿大研究觀測時，意外發現這顆星球，編號為 2010GB174，再比對過去研究資料，發現有更多類似的星球，經推算估計，類似這樣的星球至少上萬個，比之前估計量上修 10 倍。

原文轉載自【2014-02-27/中國時報/A6 版/生活新聞】

相關連結 / <http://life.chinatimes.com/LifeContent/1401/20140227000423.html>

發現新類冥王星 有助太陽系解密

賴義中 2014/02/26 19:49

【台灣醒報記者賴義中台北報導】2008 年，國際天文聯合會將冥王星由行星中除名，並將其與海王星外的矮行星歸為一類，並稱為「類冥王星」(plutoid) 天體，太陽系遂只剩下八大行星。像這樣的小行星究竟存在多少顆？中央大學天文所陳英同博士最近在太陽系外圍發現一顆直徑約 3 百公里的小型天體，將此結果與過去統計比較驗證後，推估類似大小的天體，至少有上萬個。

太陽系究竟如何形成？天文學家認為，太陽系在 46 億年前由巨大星雲盤中形成，內部原子經激烈碰撞後形成原始太陽，在太陽週遭形成由石質天體聚合而成的地球等類地行星，較遠的距離外，由水、甲烷等易揮發物質凝結，形成木星等氣體巨星。

行星盤中數千億未結合的微小碎片，則受週遭大行星重力影響，被拋射出太陽系外，在外形成一假想球殼狀地帶，稱作「奧特雲」(Oort Cloud)。

【奧特雲是什麼？】

中央大學天文所教授葉永烜說，去年底掀起熱潮的艾松彗星多半來自奧特雲，天文學家企圖藉由理解奧特雲的狀況，來解開太陽系演化的奧秘。奧特雲中的天

體多半極小，但仍以極緩速繞太陽公轉，而在海王星外側的「柯柏帶」(Kuiper Belt)和奧特雲之間約 50 至 1 萬天文單位處(1 天文單位為太陽到地球的距離)，有一個特殊的「內奧特雲」，其中可能存有大量類冥王星天體。

第一個內奧特雲物體發現於 2002 年，隔年科學家發現一顆直徑 700 公里的矮行星，命名為「賽特那」(Sedna)，距太陽約 76 天文單位。陳英同攻讀博士期間，獲國科會資助出國進修並加入加拿大的天文研究團隊，除在柯柏帶新發現 90 多個海王星外物體，還找到一個編號為 2010GB174 的內奧特雲物體，直徑 300 公里，近日點為 67 天文單位，皆僅次於賽特那。

【有助理解太陽系】

陳英同說，根據目前的發現及假設，天文學家估計內奧特雲存在數千顆類冥王星天體，但此次關鍵發現，再綜合過去觀察統計結果，可估計出類似大小的天體在內奧特雲中，至少存在上萬個，上修近 10 倍，與部分理論符合，是相當重要的結果。

葉永烜說，內奧特雲代表太陽系中最後的未知之地，受限於望遠鏡的觀測性能，人類對此處瞭解有限，但以這次發現為基礎，未來只要持續進一步觀察研究，將有助於天文學家瞭解太陽系的形成過程，及推論系外行星的來源及演化。陳英同更說，「有機會改寫太陽系理論。」

國科會 26 日召開記者會公布此次研究成果。

原文轉載自【2014-02-26/台灣醒報 Awakening News Networks】
相關連結 / <http://anntw.com/articles/20140226-M84B>

專家看《星星》指天文觀念錯了

2014-02-27 16:12 (中國 27 日訊) 紅遍亞洲的韓劇《來自星星的你》，因劇中金秀賢飾演的“都教授”來自 404 年前的星球而掀起一股天文熱，但有台灣專家卻直指韓劇的天文觀念是錯的，有待修正，民眾看看就好。

“都教授”自 404 年前的星球來到地球，與人類“千頌伊”的愛情讓大伙看得欲罷不能，將於今晚在韓國播出的完結篇，更是令星迷既期待又怕受傷害，擔心都教授離開千頌伊回到自己的星球。對於這股熱潮，台灣中央大學天文所研究助理陳英同表示，星星是燙的，溫度常高達 4000 到 6000°C，根本不可能住人，依照目前的天文學理，沒有一顆彗星 400 年後會接近地球，所以韓劇的天文觀念都是

錯的，民眾觀賞電視劇，看看就好，別認真。

原文轉載自【2014-02-27/星洲網首頁 > 娛樂 > 話國外】

相關連結 / <http://ent.sinchew.com.my/node/47410?tid=15>

我與國際合作新發現 可望改寫天文教科書 類冥王星達上萬顆 有助太陽系解密

(2014/2/27)

楊惠芳／臺北報導

太陽系外圍到底還有多少顆像冥王星的星球，一直是天文學家未解之謎。

國科會補助中央大學與中央研究院研究團隊參與跨國研究計畫，在太陽系外圍找到一顆直徑約三百公里的星球，估計這樣的星球至少有上萬顆，數量比之前估計上修十倍，未來可望改寫太陽系和天文教科書。

中央大學天文所教授葉永烜表示，這項計畫是和美國、法國及加拿大的國際團隊合作，針對距地球約五十到一萬天文單位（地球到太陽距離為天文單位）的內奧特雲觀測研究。過去由於科技等因素，較少進行相關研究，沒想到有意外發現。

中研院天文所研究助理陳英同博士指出，過去研究發現，冥王星不只有水，還有大氣，環境與地球類似，而眾多類冥王星的發現，不但可以更了解太陽系形成的過程，也讓天文學家相信，未來可能會發現更多「地球」。

不過，對近來很多民眾愛看的南韓電視連續劇《來自星星的你》，陳英同說，戲劇看看就好，劇中的天文理論都是沒有根據，且不可相信，因為戲裡的男主角來地球住了四百年，他的星球正巧會繞到地球，理論上沒有這樣的星球。

原文轉載自【2014-02-27/國語日報】

相關連結 / http://www.mdnkids.com/info/news/content.asp?Serial_NO=87609

上萬顆類冥王星 有助理解太陽系演化

時間：2014/2/26 19:12 撰稿・編輯：李憶璇 新聞引據：採訪

人類生存的地球位在太陽系中，但在太陽系之外還可能存在其他有生物體的星球。國科會補助的一項國際合作天文計畫，去年在太陽系外的「內奧特雲」找到一顆類冥王星星球，重新推算，類星球數量將超過上萬顆，是過去認知的十倍，學者認為此發現有助了解星系演化。

冥王星被剔除行星行列後，其他外面類似的星球都稱為「類冥王星」，目前還無法知道還有多少顆類冥王星；但中央大學參與的國際團隊去年用望遠鏡觀測

發現，在太陽系外圍找到 1 顆直徑約 300 公里的星球，依運行資料重新估算，預計這樣的星球大約有上萬顆，比以前的估計量上修 10 倍。

中央大學天文所教授葉永烜表示，地球到太陽的距離是一個天文單位，「內奧特雲」則是 50 到 1 萬天文單位遠的地方，是天文未知之地，因此多發現一顆星球，等於對它有更多了解，他說：『(原音)第一顆是在幾年前找到，現在陳英同博士用資料找到第二顆大的，在統計上就有意義，因為找到兩個不一樣大小，根據統計可以知道數目有多少，就可以估計太陽系外類似的東西有多少，他的結果是很驚訝發覺，新的結果比以前估算多了十倍。』

此研究修正過去天文理論，並有機會知道太陽系的形成過程，進一步找到另一個太陽系。

此則報導的來源網址：http://news.rti.org.tw/index_newsContent.aspx?nid=487084

原文轉載自【2014-02-26/中央廣播電臺新聞頻道】

相關連結 /

http://news.rti.org.tw/index_newsContent.aspx?nid=487084&id=3&id2=1

[專家：《星星》天文觀念都是錯的](#)

中時即時 湯雅雯

2014 年 02 月 26 日 14:30

太陽系外圍到底還有多少像冥王星的天體，一直是天文學家的未解之謎。國科會和中央大學天文所，包括探高計畫與台家合作計畫，日前在太陽系外圍找到一顆直徑約 300 公里的星球，跟台灣差不多大，這個關鍵結果加上至今有觀察統計比較，過去估計這樣大小的天體至少有上千個，如今發現至少有上萬個，比以前估計上修 10 倍，有機會改寫天文教科書的歷史。

至於近來韓劇《來自星星的你》掀起一股天文熱，中研院天文所研究助理陳英同表示，星星是燙的，溫度常高達 4000 到 6000°C，根本不可能住人，依照目前的天文學理，沒有一顆彗星 400 年後會接近地球，所以韓劇的天文觀念都是錯的，有待修正，民眾看看就好。

原文轉載自【2014-02-26/中時電子報 CTnews】

相關連結 / <http://www.chinatimes.com/realtimenews/20140226003470-260405>

[發現上萬顆冥王星天體 太陽系形成恐改寫](#)

2014-2-26 21:43 作者：本報訊

【記者劉仲書台北報導】人們已知距離太陽 40 到 50AU（1AU 等於地球到太陽的距離）之間的「古柏帶」（Kuiper belt）擁有大量的小型天體，這裡被視為太陽系的盡頭；但太陽系外圍有多少類似冥王星的天體，是天文學界的未解之謎。這個區域被稱為「內奧特雲」，距離太陽 50 到 1 萬 AU，屬於奧特雲（Oort cloud，50 到 10 萬 AU 的範圍）的內側，因距離太遠，難以透過望遠鏡觀測。

一項由行政院國科會補助的國際合作計畫，日前在太陽系外圍找到一顆直徑約 300 公里的天體，根據持續新觀測到的資料，發現太陽系外圍並非過去所認為的那樣。此次參與研究的博士陳英同說：「根據這次觀測計畫，在太陽系外圍大於 300 公里的天體大約有上萬個，這跟之前估計的數千個相差 10 倍。」這個發現可能改寫太陽系的形成理論。

冥王星於 2006 年被降級為矮行星，原因在於其大小與軌道特性接與太陽系其他八大行星相異，冥王星比月球小，尤其特別的是其繞太陽公轉的平面傾斜於八大行星的平面，並呈現橢圓狀，天文學家過去也發現有很多小行星的軌道與冥王星類似，甚至找到了比冥王星還大的類似星體，包含冥王星在內，這些星體都位於海王星外圍的古柏帶與內奧特雲。

海王星自此成為太陽系的界線，而太陽系週圍的探索，成了天文界近年來的新課題。

教授葉永烜表示，受到海王星影響、繞著太陽轉的系外小星體，有些軌道會拉到很遠，例如 2010GB174 小行星就遠到 700AU，它與太陽系的行星運行機制是分開的，這在太陽系力學上是很奇怪的事。

葉永烜說，在海王星軌道外可能有一團東西，它們質量多大、分佈多廣？這與太陽系的形成有很大的關係，過去估計的質量比現在少 10 倍，一個可能的理論是過去太陽系形成並不是單獨產生，而是有好幾個星系中心一起形成，互相影響、彈射之後變成現在的樣子；另一個可能的理論是其他地方還有大型行星，它干擾了這些星體與海王星之間拔河產生了這樣的軌道。他說，未來還要收集更多資料才能確定哪個理論正確。

過去的太陽系架構來自於距離 2 萬 AU 的圓殼狀奧特雲空間，其中有數千億的小物體，是天王星與海王星形成時被外行星彈射出去的太陽系原始物質，過程中也引起天王星與海王星發生軌道移動，這個架構長期被用來解釋奧特雲與系外物

體的結構。而內奧特雲是太陽系議題最後的未知之地，從這次發現開始能做定量的科學勘察，太陽系的形成理論可能會因此改寫。

原文轉載自【2014-02-26/台灣立報 > 科學 > 正文】

相關連結 / <http://www.lihpao.com/?action=viewnews-itemid-137993>

新發現天體 助解密太陽系

記者黃進福／臺北報導

太陽系外圍到底還有多少像冥王星的天體，一直是天文學家的未解之謎，中央大學天文所參與國際團隊進行探高計畫與臺加合作計畫，在太陽系外圍找到一顆直徑約三百公里的星球，這個關鍵結果加上觀察統計比較，估計這樣大小的天體至少有上萬個，比以前估計上修十倍，有助解密太陽系形成關鍵，並改寫天文教科書的歷史。

天文學家一直在探索海王星軌道外側，一個自成一格的「內奧特雲」，當中存在大量的物體，但因為距離太遠，很難直接用望遠鏡觀察到，因此內奧特雲一直是個謎團，第一個內奧特雲物體是在二〇〇二年發現，接著美國加州理工學院的一個大型巡天計畫在二〇〇三年，發現一個名為賽特那的矮行星，最接近太陽的距離為七十六天文單位，由此確立內奧特雲的存在，但全部數目則是未知數，國科會經費支持中央大學天文所與加拿大研究機構合作，利用夏威夷三點六米望遠鏡，新發現一個直徑約三百公里的物體。

中央大學天文所教授葉永烜表示，過去對太陽系已知的範圍只有六十個天文單位（一個天文單位等於地球到太陽的距離），如今發現一個新物體，並編號為2010GB174，未來只要持續觀測，有機會讓已知的太陽系，擴增到幾百甚至幾千個天文單位。

中研院研究助理陳英同說，過去國際曾發現類似星球，這次發現更多類行星，更可證實奧特雲存在，消除過去科學界對奧特雲是否存在的疑慮，經推算估計類似這樣星球至少上萬個，這類研究有助了解太陽系的形成過程，以及冥王星、土星、木星、海王星組成的原因，有助推論系外行星來源及演化。

原文轉載自【2014-02-27/青年日報/6 版/新視界】

相關連結 /

<http://news.gpwb.gov.tw/news.aspx?ydn=026dTHGgTRNpmRFEgxcbfb0e%2b%2beJP7D3HGsxhDrckoVorRhJNJDGY1uJbGcYwPlTDh726Lb0PMbhM8nw4ZzcDgRD>

類似天體恐逾萬 可能改寫太陽系理論

台灣中央大學天文團隊，最近發現了太陽系外的內奧特雲系有新的天體，研究團隊推論，類似的天體可能至少有上萬個，數量比預估的要多上十倍，有可能改寫太陽系理論。

人類身處的地球，不定時就會有彗星造訪行經，這些彗星多數來自太陽系外的遙遠外圍，稱之為奧特雲系，當他們行經地球，透過觀測記錄，科學家們能有所了解，反到是在離太陽系較近的內奧特雲系，到底有多少天體，對天文學家來說，一直是個謎。

==中央大學天文所教授 葉永烜==

我們估計

是很可能有些東西藏在那邊

繞著太陽在公轉

可是這些恆星它們很少有機會

會經過 100 到 1000 天文單位的地方

所以變成我們總是

沒有辦法去看到他們

2003 年美國加州理工學院，在內奧特雲區，發現了一個名為賽特那的矮行星，距離太陽約 76 個天文單位，最近中央大學再度在距離太陽 67 天文單位，發現了一個新天體。

==中央大學天文所博士 陳英同==

我們找到的就是一個距離太陽系

非常遠的天體 對我們之前的理解

就是有非常大的出入

之前覺得大概

只有數千個天體在那個位置

但這次我們的研究結果

發現就是說

在那個位置應該有上萬顆

甚至更多的天體在那個地方存在

以往因為受限於望遠鏡的性能，人類對內奧特雲系了解有限，隨著觀測技術的發展，陳英同興奮的說，雖然相隔了十多年才再度驗證內奧特雲系確實有天體存在，但相信不久的未來，類似的發現將愈來愈多，有機會重寫太陽系理論。

記者 陳姝君 陳保羅 林國煌 台北報導

(2014-02-27 12:00) 中畫新聞

原文轉載自【2014-02-27/公視新聞網 / 科技】
相關連結 / <http://news.pts.org.tw/detail.php?NEENO=263037>

天文大發現 類冥王星天體太陽系有上萬個

【記者嚴文廷/台北報導】

冥王星屬於矮行星，除了繞太陽運行，也受海王星的擾動。到底在太陽系的遙遠外圍，還有多少類似冥王星的天體，一直是天文學家一直想解開的謎題。國科會經費支持中央大學天文所與加拿大研究機構合作，利用夏威夷 3.6 米望遠鏡新發現一個直徑約 300 公里的物體，推論這樣大小的天體沖還有上萬個，打破過去的推估，而且一次就讓數字上修十倍。

天文學家一直在探索海王星軌道外側，一個自成一格的「內奧特雲」，當中存在大量的物體，但因為距離太遠，很難直接用望遠鏡觀察到，因此一直是太陽系中最未知的部分。

其中有一顆名為「賽特那」的矮行星，直徑有 700 公里，因為夠大，在 2003 年時被發現。中央大學天文所教授葉永烜表示，這次跨國合作新發現另一個在內奧特雲裡的物體，可證實裡頭可能還有很多物體存在。

葉永烜說，天文可以用各種理論來推論，但更重視眼見為憑。這次由中央大學天文所博士陳英同，與加拿大國家天文台合組團隊，一起觀測發現一顆直徑 300 公里的物體，驗證過去理論。

太陽系天文單位可能增加到千

葉永烜表示，過去對太陽系已知的範圍只有 60 個天文單位（一個天文單位等於地球到太陽的距離），如今發現一個新物體，並編號為 2010GB174，未來只要持續觀測，有機會讓已知的太陽系，擴增到幾百甚至幾千個天文單位。

葉永烜指出，內奧特雲代表我們對太陽系最後未知之地，發現新物體 2010GB174 可以開始展開定量的科學勘查，並進一步觀測研究，可以更清楚瞭解太陽系的形成過程，有助於推論行星的來源及演化等過程，逐步改寫現有的天文研究。

原文轉載自【2014-02-26/聯合晚報/A7 版/焦點】

相關連結 / <http://www.udn.com/2014/2/26/NEWS/WORLD/WOR4/8511662.shtml>

太陽系恐有上萬類冥王星天體

【聯合晚報／記者嚴文廷／即時報導】 2014.02.26 12:45 pm

冥王星屬於矮行星，除了繞著太陽運行，也受到海王星擾動。但到底在太陽系

的遙遠外圍，還有多少類似冥王星的天體，是天文學家一直想解開的謎題。國科會經費支持中央大學天文所與加拿大研究機構合，作利用夏威夷 3.6 米望遠鏡，新發現一個直徑約 300 公里的物體，並可推論類似大小的天體有上萬個，打破過去推估，一次就讓數字上修 10 倍。

過去認為太陽系範圍只有 60 個天文單位（一個天文單位等於地球到太陽的距離），如今發現一個新物體，並編號為 2010GB174。研究團隊認為，只要持續觀測，有機會讓已知的太陽系擴增到數百甚至數千個天文單位。

【2014/02/26 聯合晚報】@ <http://udn.com/>

原文轉載自【2014-02-26/聯合新聞網 生活 即時新聞】

相關連結 /

<http://udn.com/NEWS/BREAKINGNEWS/BREAKINGNEWS9/8511470.shtml>

類星球數量上修 可能有另個太陽系

2014 年 02 月 26 日 15:28 太陽系外圍到底還有多少顆像冥王星的星球，一直是天文學家未解之謎，中央大學參與的國際團隊，在太陽系外圍找到 1 顆直徑約 300 公里的星球（約台灣總長度），估計這樣星球至少上萬個，比之前估計上修 10 倍，未來有助於更清楚了解太陽系形成過程，或找到另一個太陽系。

現為中研院天文所研究助理的陳英同博士，在就讀中央大學天文所博士班期間，參與台、美、加、法的國際團隊，在加拿大到研究期間，針對距離地球約 50 至 1 萬天文單位（地球到太陽距離為 1 天文單位）的內奧特雲進行觀測研究。

陳英同說，觀測發現一個星球，經過影像及軌道分析，確認該星球存在，編號為 2010GB174，加上過去國際曾發現類似星球，本次發現更多類行星，更可證實奧特雲存在，消除過去科學界對奧特雲是否存在的疑慮，經推算估計類似這樣星球至少上萬個，比之前估計數量上修 10 倍，更多類星球存在，代表可能星球是繞著某一個恆星運轉，機率更高能找到類太陽系，或有助於科學家更清楚了解太陽系形成過程。（許敏溶／台北報導）

原文轉載自【2014-02-26/蘋果日報 即時新聞】

相關連結 /

<http://www.appledaily.com.tw/realtimenews/article/life/20140226/351466/>

象限儀座流星雨如期發生 監測照片數數有幾顆？

生活中心／台北報導

年度三大流星雨的「象限儀座流星雨」如期發生了！這群來自於彗星的小灰

塵，以高達每小時 14 萬公里的速度衝入大氣層，撞擊產生的光芒形成燦爛的流星雨。其中一張照片是 1 月 1 日至 5 日之間，由台灣流星觀測網在合歡山梅峰的自動監測設備所拍測，裡面出現 70 幾顆流星，台北市立天文館表示，您都找到了嗎？

台灣流星觀測網是國立中央大學、國立自然科學博物館與多所中學合作的計畫，在合歡山、鹿林山等多處高山設立監測攝影機，以高感光度的攝影捕捉流星與高空閃電的影像，藉以測量流星的位置與軌道，並探索高空閃電的發生原因。

原文網址：象限儀座流星雨如期發生 監測照片數數有幾顆？ | ETtoday 新奇新聞 | ETtoday 新聞雲

<http://www.ettoday.net/news/20140118/317608.htm#ixzz2r0qN1v3K>

Follow us: @ETtodaynet on Twitter | ETtoday on Facebook

原文轉載自【2014-01-18/ETtoday 新聞雲 ETtoday 新奇新聞】
相關連結 / <http://www.ettoday.net/news/20140118/317608.htm>

蘋果特寫：鹿林滿天星 多到溢出來
海拔 3 千米最高天文台 發現台灣首顆彗星

【許敏溶／嘉義報導】黑夜降臨，大地靜謐，位於嘉義縣阿里山鄉、海拔近 3000 公尺高的鹿林天文台內，一群男人才正要上工。這裡是國內天文研究重鎮，2007 年台灣首顆發現的彗星即由該研究團隊發現、並命名為「鹿林」。為體驗這些夜夜觀星人的生活，《蘋果》記者上月申請到該天文台過夜採訪，感受在攝氏零度的冷冽夜晚，既孤獨辛苦、卻也能眼見滿天星斗「多到快溢出來」的浪漫與震撼。

鹿林天文台位在海拔 2862 公尺的高山，是全國最高的天文台，隸屬中央大學天文研究所，擁有台灣口徑（鏡面直徑）最大的天文研究用望遠鏡，可觀測更細微的星象。現由台長林宏欽帶領林啟生、蕭翔耀 2 位觀測助理及 4 位原住民助理專員進行天文研究；編制分屬於國科會研究計劃助理、中大教職員。

團隊成員全是男性

要到天文台上班很吃力，開車只能停在 600 公尺外的停車場，之後得走山路，約須半小時才能抵達，因此他們採取「上 7 天、休 7 天」的輪班方式。林宏欽說，可能因體能負擔因素和安全考量，此團隊現全是男性，無女性加入。

林啟生、蕭翔耀負責觀測天象，每天日落後開始工作。記者抵達當天約下午 4

時，林已忙進忙出，要趁日落前架好戶外的小型觀測儀望遠鏡；5時許工作人員吃晚飯，至夜晚來臨，即展開觀測研究工作。

49 歲的林啟生是台灣第一顆彗星「鹿林」的發現者。他說，觀星須在晚上，觀測員作息都因此日夜顛倒；而夏天晝長夜短，觀測員「工時」約 10 小時；現已入冬，工時最長會達 14 小時。至今仍是單身的他說，有人問他是否已娶了星星為妻，他都笑說，星星會跟你不停眨眼睛示愛，且忠心不二。

在國際上小有名氣

各國天文研究單位都需收集多種天文資料，也需要其它國家協助觀測；鹿林天文台因天文望遠鏡口徑達一公尺、在國際上小有名氣，吸引不少學術單位以合作名義申請研究觀測計劃。美國夏威夷大學就曾提出觀測小行星尾巴成分計劃，觀測計劃至少需在半年前送中大天文所審查，通過後才能排定時間觀測。每晚，觀測員主要工作就是依各項觀測計劃，在控制室內透過電腦操控、記錄天文望遠鏡的觀測資料。

蕭翔耀說，天文望遠鏡是由精密電子儀器組成，晚間得隨時注意電腦上的氣象預報資料，見苗頭不對、恐下雨就得關上天文台的天窗、以免儀器故障，工作單調忙碌。林啟生說，他們多透過天文望遠鏡拍下星象變化，事後再比對，非用肉眼觀察，因此「發現彗星時當下並無特別興奮感」。

冬天深夜，鹿林天文台低溫僅攝氏零度；記者在室內穿著大外套仍感覺冷與睏，林啟生卻精神奕奕，十分適應。據觀測員們說，天亮前最後 2、3 個小時最難熬，會猛打瞌睡，只好吃泡麵等東西補充體力。

工作 12 年仍然感動

但觀測員對能在此「夜夜觀星」都很滿意。蕭翔耀說，2003 年初次造訪鹿林天文台時，看到夜空的星星又多又亮，非以往能想像；到此工作後，他仍常在晚上觀星，夏天有漂亮銀河、冬天的星星很亮，望著浩瀚夜空，「內心很平靜，也感到自己渺小」。

林宏欽說，1990 年還是碩士生時首次造訪鹿林，就被「多到快溢出來」的滿天星斗景象所震撼。而他 2002 年接任鹿林台長至今，每次看到滿天繁星仍然十分感動、覺得浪漫，「這可是『夜夜觀星的男人們』才能享有的 VIP 待遇」，他說。

鹿林天文台小檔案

★地址：嘉義縣阿里山鄉中山村自忠 78 號

★高度：海拔 2862 公尺

★網址：www.lulin.ncu.edu.tw/

★主要成員：

- 台長：林宏欽
- 觀測助理：林啟生、蕭翔耀
- 助理專員：石俊雄、石皓偉、汪榮進、杜進全

★特色：為台灣最重要光學天文基地、天文研究與觀測中心，裝有口徑（鏡面直徑）1 公尺的光學望遠鏡、為台灣口徑最大

★特殊紀錄：台灣首度發現小行星、首度發現彗星（「鹿林」）、首度發現近地小行星，是台灣發現小行星最多的天文台

資料來源：中央大學、《蘋果》採訪整理

鹿林天文台大事記

★1990 年：設置臨時觀測站

★1997 年：興建第一座天文台

★1999 年：裝設自行設計製造口徑 76 公分超輕型望遠鏡

★2002 年：建置台灣首座口徑 1 公尺望遠鏡

★2007 年：發現鹿林彗星、小行星「鹿林」和「中大」

★2017 年：將裝置口徑 2 公尺望遠鏡

資料來源：《蘋果》採訪整理

原文轉載自【2014-01-09/蘋果日報】

相關連結

<http://www.appledaily.com.tw/appledaily/article/headline/20140109/35566783/%E8%98%8B%E6%9E%9C%E7%89%B9%E5%AF%AB%EF%BC%9A%E9%B9%BF%E6%9E%97%E6%BB%BF%E5%A4%A9%E6%98%9F%E5%A4%9A%E5%88%B0%E6%BA%A2%E5%87%BA%E4%BE%86>

[蘋果特寫：鄒族原民助補給 揣百公斤上下山](#)

鹿林天文台是台灣天文研究與觀測中心，因遠離有光害的市區，交通不便，山上人員的民生問題全由 4 位鄒族原住民包辦；他們要買菜、煮飯、洗衣服、維修器材，還需上下山運補物資，每次負重數十公斤到上百公斤上下山、挑戰體能，對該天文台研究人員來說，不可或缺。

這 4 位鄒族原住民分別是石俊雄、石皓偉、汪榮進、杜進全，現屬中央大學聘

任的工友，也是該天文台助理專員；因得負重上下山運補，4人都是男性。46歲的石俊雄在此工作14年，在4人中年資最久，他說，最累的是常得用揹籃揹數十公斤到近百公斤物品上下山，從蔬果、汽油、瓦斯桶到發電機都有，最近還扛了一位到天文台參觀卻高山症發作的女學生下山。

為煮飯去學廚藝

他們也要輪流張羅三餐。台長林宏欽說，起初這4位同事的手藝不夠好，還送去學廚藝，後來果然大為進步，石俊雄更被稱為應可擁有丙級廚師證照，但石俊雄說好手藝反而讓太太有偷懶藉口，現在每次回家都是由他掌廚。石皓偉則說，招牌菜是「鹹蛋炒苦瓜」，最喜歡冬天下廚煮菜，「因為廚房很溫暖」。

林宏欽說，他上下山不需背負重物都已感覺吃力，上山爬坡累、下山要小心地面結霜滑倒，每次要負重上下山的4位工友，真是天文台不可或缺的人物。記者許敏溶

原文轉載自【2014-01-09/蘋果日報】

相關連結 /

<http://www.appledaily.com.tw/appledaily/article/headline/20140109/35566796/>

蘋果特寫：高山低溫0°C 冷風吹臉如針刺

採訪側記

鹿林天文台平常僅供學術研究使用，不受理個人名義申請參觀。《蘋果》記者為探訪觀星人員的生活，上月向中央大學申請過夜採訪，早上7時半從台北出發，開了6小時的車到鹿林天文台停車場，再徒步30分鐘才真正抵達天文台。走上山呼吸急促

採訪前台長林宏欽就提醒記者，從停車場到天文台，須爬600公尺、坡度平均20至30度的山路。記者原不以為意，但當自己揹著約20公斤的行李與攝影器材往上爬，高山稀薄空氣馬上令人呼吸急促。

此外，天文台海拔高，白天太陽下不到攝氏10度；夜間溫度只剩下約攝氏0度，若未戴口罩，冷風像細針般迎面刺來，讓人頭痛。即使在室內，寒意依舊在。

想想天文台的人員都得忍受低溫與生活不便，不禁佩服其奉獻。但山上空氣清新，白天可遠眺玉山，夜間可目睹繁星，甚至肉眼可見銀河，也讓記者留下深刻

印象。記者許敏溶、余志偉

原文轉載自【2014-01-09/蘋果日報】

相關連結 /

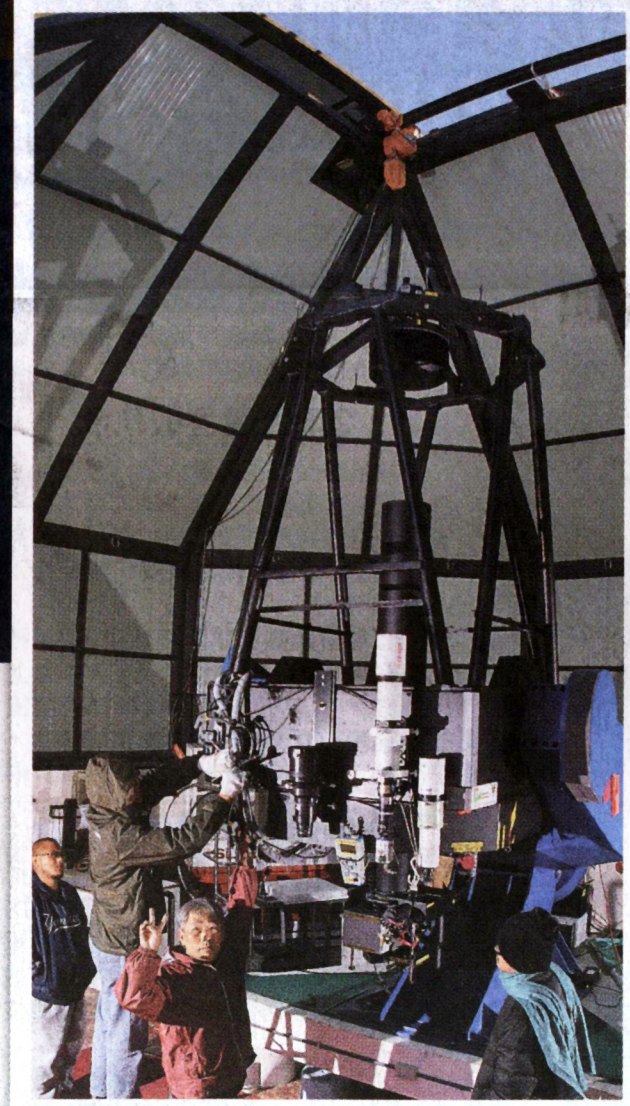
<http://www.appledaily.com.tw/appledaily/article/headline/20140109/35566799/>

鹿林滿天星 多到溢出來

海拔3千米最高天文台 發現台灣首顆彗星



■鹿林天文台的主要成員，右至左依序為觀測助理林啟生、台長林宏欽及助理專員石俊雄、石皓偉。余志偉攝



■林啟生（紅上衣者）等人正在調整台灣口徑最大的天文望遠鏡。



■林啟生是「鹿林」彗星
發現者。

**高山低溫0°C
冷風吹臉如針刺**

採訪側記

鹿林天文台平常僅供學術研究使用，不受理個人名義申請參觀。《蘋果》記者為探訪觀星人員的生活，上月向中央大學申請過夜採訪，早上7時半從台北出發，開了6小時的車到鹿林天文台停車場，再徒步30分鐘才真正抵達天文台。約20公斤的行李與攝影器材往上爬，高山稀薄空氣馬上令人呼吸急促。

此外，天文台海拔高，白天太陽下不到攝氏10度；夜間溫度只剩下約攝氏0度，若未戴口罩，冷風像細針般迎面刺來，讓人頭痛。即使在室內，寒意依舊在。

走上山呼吸急促

採訪前台長林宏欽就提醒記者，從停車場到天文台，須爬600公尺、坡度平均20至30度的山路。記者原不以為意，但當自己揹著



浪漫——這可是享有的VIP待遇」

他說。

- | | |
|----------|------------------------|
| 鹿林天文台大事記 | 資料來源：
《蘋果》採訪整理 |
| 1990年 | ► 設置臨時觀測站 |
| 1997年 | ► 興建第一座天文台 |
| 1999年 | ► 裝設自行設計製造口徑76公分超輕型望遠鏡 |
| 2002年 | ► 建置台灣首座口徑1公尺望遠鏡 |
| 2007年 | ► 發現鹿林彗星、小行星「鹿林」和「中大」 |
| 2017年 | ► 將裝置口徑2公尺望遠鏡 |



■石皓偉正在為天文台的人員做飯。

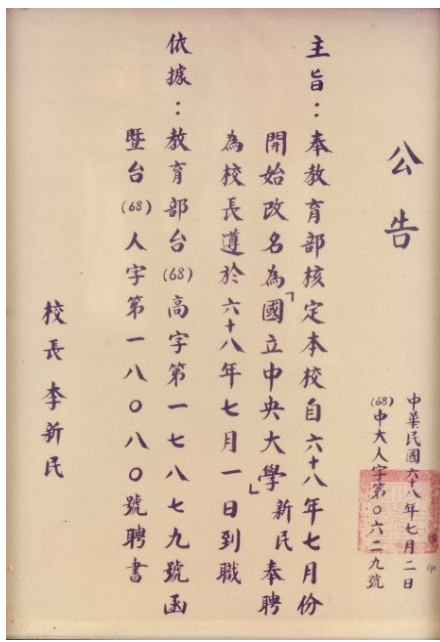
0809-013-666 爆料投訴e-mail : news@appledaily.com.tw 蔬果日報網址:<http://www.appledaily.com.tw>



恢復完全大學時期：1979年-1982年

文 / 編輯部

中大理學院成立後，陸續增設系所，李新民接任院長時，中大已具備恢復完全大學的規模。自1973年起，陸續有民意代表、校友會數次陳情恢復中大為完全大學，然政府單位均以「備存參考」回應。直至1978年6月，校友朱匯森接任教育部長後，改制之事始見轉機。適逢交通大學工學院也申請改制為大學，於是教育部決議同時審查兩校改制之申請。1979年7月，教育部審核通過，正式恢復中大「國立中央大學」校名，並聘請李新民為中大首任校長。



本校恢復國立中央大學校名，李新民為首任校長。（來源／本校校史館館藏）
(校史館館藏，年代：1968)

設備經費倍增 學術成果卓著

在中大恢復完全大學後，校內系所分隸於理、工、文三學院，設置三名院長。圖書館自教務處中獨立出來，成為一級單位，原講義組改為出版組，並新增共同科和電子計算中心。總務處另增營繕

組。訓導處新增畢業生就業輔導室與僑生輔導室（中大於一九七九年接受僑生入學）。組織系統擴大後，權責劃分亦更加明確。

因應一九七九年中美斷交與第二次石油危機後之國家政策，行政院於同年發布「科學技術發展方案」，積極推動資訊工業發展，相關系所以增設，教育經費亦從一九八〇年起大幅成長。由於政府當局的政策，使中大得以陸續新增實驗室與儀器，包含國內其他大學所沒有的貴重儀器，同時於中大校區內建造新天文臺，內設當時全國最大的望遠鏡（六十一公分）。

表：中大1979～1982年院系成立一覽表

年份	系所 / 單位	成立背景
1979年	統計研究所	為政府培養統計應用方面人才。
	地球物理研究所博士班	培養師資。
1980年	電機工程學系	1979年行政院推行「科學技術發展方案」，成立資訊工業策進會及新竹科學園區，全力發展電機及資訊工業，以促進工業升級，增強我國產品的國際競爭力。
	土木工程研究所	1978年，政府為擴大內需，推動「十二項建設」，需要大量土木工程師。
	法國語文學系	1. 因應1979年中美斷交，對外實質外交與貿易，急需語言人才。 2. 法國駐臺人員向教育部建議，可於國立大學設立法文系，法國可提供師資、設備、圖書、獎學金等協助。
	辦理在職科技人員進修招生（分修讀學位與修讀學分兩種）	配合行政院推行「科學技術發展方案」。招生對象為實施科學技術發展方案有直接相關之政府機關學校、公民營企業、或與中大有建教合作之單位為範圍。
	資訊及電子工程研究所	配合行政院推行「科學技術發展方案」。
1982年	機械工程研究所,光電科學研究所	配合行政院推行「科學技術發展方案」。

資料來源：國立中央大學數位校史網（1966-1968）



中大天文台於1981年正式啟用，天文台的61公分口徑望遠鏡為當時國內最大之望遠鏡。過去我國一直沒有供天文研究用的望遠鏡，中大天文台的建立，遂成為我國使用現代觀測工具及技術，來研究天文的一個開始。（來源／本校校史館館藏）

一九八二年，中大設有數學與統計研究圖書室、物理研究圖書室、工程研究圖書室及文學研究圖書室等，總藏書量逾十七萬冊（中文期刊七百零九種，西文期刊九百零二種）。在圖書儀器完善的狀況下，中大備受相關研究單位的重視，也因而催生出豐碩的研究成果，大幅提升學術地位，吸引更多建教合作的機會。

李氏辦學之道 首重研究環境

1973年李新民接任理學院院長，銳意革新，重視學生生活及其受教權，致力建構下列環境：

1、改善學生生活環境：例如整修學生宿舍、加鋪道路、增設籃球場、闢建腳踏車棚、曬衣場、增設水塔抽水機、改善餐廳衛生條件等。

2、改善學習及研究環境：他利用教育部所設置的「擴大延攬師資辦法」，增聘多位專任教師，健全師資結構；他強調行政人員應以支援教授研究、輔導學生為其主職，致力打造更好的研究與學習環境。

3、積極美化校園：李氏十分重視校園美化，在任期間大量植樹，1975年植樹節於正門圓環內種植黃榕編成「中央大學」四個大字。同時廣植松樹、闢建苗圃，以栽培花木。利用校友捐贈之涼亭、花廊、曲橋建構園林景致，整建「玄武湖」。

在李氏的經營下，中大由理學院正名為中央大學，校園美化亦奠立今日中大的幽美環境，為師生們所津津樂道。



李新民校長致力於提升師資素質，由簡報左側數字可知，中大具博士學位教授從61學年度的20人，增長到64學年度的56人，成長了2.8倍。（來源／本校校史館館藏）



66學年度，李新民校長（握手右者）頒獎時留影。當時中大學生必須穿著制服，並定期在中正圖書館（今舊圖）前司令台（現已不存，平台處目前置放公共藝術品）進行朝會。（來源／本校校史館館藏）

參考資料：

- (1) 國立中央大學，《中大校訊》，1976年編印。
- (2) 校史館館藏文物。
- (3) 中大數位校史網<http://sec.ncu.edu.tw/ncudhis/>

[>>回前頁](#)

發行單位：國立中央大學秘書室

發行人：周景揚

指導委員：徐國鎧、陳介豪

主編：邱燕淇（第15期開始）

版型設計：謝怡君、戴伯誠

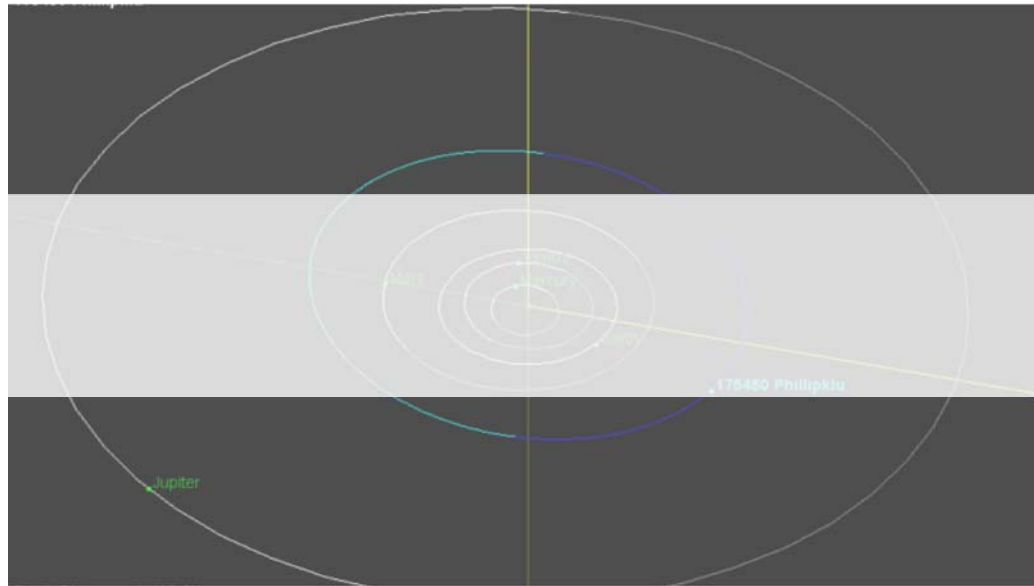
網頁編輯：洪舶凱

聯絡電話：(03)4227151 # 57045

E-mail：kelly@ncu.edu.tw

[訂閱本報](#) | [查詢舊報](#)

Asteroid Named After Retired Western Connecticut Professor



By Kathleen Megan

NOVEMBER 7, 2014,
8:49 PM

A newly-discovered asteroid has been named after retired WCSU professor Dr. Phillip Lu.

Dr. Phillip Lu is characteristically self-deprecating about the news that a newly discovered asteroid has been named after him.

"My younger daughter asked, 'Dad, what's this supposed to mean?'" said Lu, 82, a retired astronomy professor from Western Connecticut State University. "I said it means absolutely nothing."

But when pressed, Lu admits that it is a "tribute" that the astronomer who discovered the asteroid and charted its orbit — one of Lu's student's students — opted to name it 175450 Phillipklu in his honor.

"It's kind of a surprise. I didn't really expect this," Lu said from his home in Bethel. "It means somebody didn't forget me, that's all!"

The asteroid was observed in 2006 by Dr. H.C. Lin, the director of the National Lulin Observatory in Taiwan, and it has been seen 106 times since then — enough to have its orbit charted. Once an asteroid's orbit is established, it is considered a minor planet. As the discoverer of the object, Lin was entitled to recommend its name to the International Astronomical Union.

The connection between Lu and Lin began decades ago when Lin was a student in Taiwan. Lu, a native of China who went to college in Taiwan, moved to the United States in 1962, but returned to Taiwan in 1979 to help develop an astronomy program at the National Central University. While in Taiwan, Lu met W.S. Tsay and became his doctoral thesis adviser.

Lu began making annual trips to Taiwan and assisted in the design and construction of the National Lulin Observatory. Eventually, Tsay became Lin's teacher and Lu got to know him.

Lu said that Lin kept his choice of a name for the asteroid a secret so that Lu would be surprised about the time of his 82nd birthday. Lu's birthday was Oct. 11, and the minor planet was officially named on Oct. 9.

The minor planet, which is made of rock and is about 2 or 3 kilometers in diameter, travels in an elliptical orbit that averages about 238 million miles from the sun. It orbits the sun almost every four years between Mars and

Jupiter and is almost 60,000 times dimmer than the sun.

Lu's love of the stars began when he was an apprentice on a cargo ship that traveled around the world in the late 1950s and early '60s. Lu had joined the Chinese military at 15 before the Communist takeover and traveled to Taiwan. He was trained in ship navigation at a maritime college in Taiwan.

"In the middle of the ocean in the night time, there was nothing to see but the stars because there's no light," Lu said. "So I was curious, especially in such a dark place. The stars seemed brighter and closer. I became fascinated by the stars. I wanted to learn more about their motions, the structures and the chemical composition."

There were no astronomy majors or classes available in Taiwan, so in 1962 he went to Wesleyan University in Middletown to earn his master's degree in astronomy.

From there, he went to Columbia University to get his Ph.D. and then on to Yale for post-doctoral work. In 1970, he was hired by Western, where he taught for 29 years from 1970 to 1999. In 1992 he was honored by the Connecticut State University system as the "CSU Professor of Astronomy."

Since he retired, Lu has devoted much of his time to writing poetry in English and in Chinese.

When a friend congratulated him on "achieving a little immortality" through his namesake planet, Lu responded in verse:

"One tiny speck moves around our sun,
Carrying my name among planets,
The name, perhaps, is a bit immortal,
But never stops the erosion of my mortal body."

Lu has yet to see his namesake in the heavens, but hopes to when he returns to Taiwan sometime soon. It will take a 40-inch telescope — larger than he has at home — to do so.

"You aren't missing anything if you don't see it," Lu said.

Copyright © 2014, Hartford Courant

FROM AROUND THE WEB

Sponsored Links by Taboola

We're Smarter Than 36th In The World: Using Data Analytics to Empower U.S. Teachers and Students
Bloomberg by Xerox

Slavery Rife in Global Seafood Supply Chain
Walk Free

'Warren Buffett Indicator' Signals Collapse in Stock Market
Newsmax

15 Actresses of World Most Big Budget Movies
RaveBin

Past Stories

6/18/2014

Keyword

Search

Subscription

ROC students spot Kuiper belt object



The high school team that discovered Kuiper belt object 2014GE45 poses with professor Chen Wen-ping (front, second left) of Taoyuan County-based National Central University. (Courtesy of NCU)

Publication Date : 06/04/2014

Source : [Taiwan Today](#)

A five-member high school team from Taichung City discovered a Kuiper belt object in the outer reaches of the solar system beyond Neptune, project leader National Central University said June 3.

It is believed to be the first Kuiper belt object ever spotted by high school students.

According to project instructor NCU professor Chen Wen-ping, preliminary orbit calculations put trans-Neptunian object 2014GE45 at an average distance of 65 astronomical units from the sun. It takes 562 years for the object to complete its orbit.

The stargazers behind the discovery are A. Hoyle, H. C. Hsieh, C. C. Hsueh, J. J. Ji and Y. H. Lin, all first-year students from Affiliated Senior High School of National Chung Hsing University.

The project was carried out under the Taiwan chapter of the International Astronomical Search Collaboration, an educational outreach program in partnership with U.S.-based Panoramic Survey Telescope and Rapid Response System.

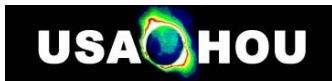
Pan-STARRS uses two Hawaii-based telescopes to detect near-Earth objects that threaten impact events.

Other Taiwan schools participating in the survey include National Changhua Senior High School, National Lo-Tung Senior High School, Taichung Municipal Hui-Wen High School and Taipei First Girls' High School, which also discovered an asteroid this time.

The Kuiper belt extends from the orbit of Neptune, at 30 AU, to about 50 AU from the Sun. Similar to the asteroid belt, it consists mainly of small bodies, but is far larger. The belt's best-known body is Pluto, which was formerly classed as a planet. (YHC-SDH)

Write to Taiwan Today at ttonline@mofa.gov.tw

[Top](#) [Back](#)



USA Hands-On Universe

IASC's First Trans-Neptunian object (TNO) Discovery

IASC's First Trans-Neptunian object (TNO) Discovery

2014/05/19 usa-hou No Comments

The International Astronomical Search Collaboration (IASC) made its first TNO discovery today!! Congratulations go to C.-C.Hsueh, J.-J. Ji, Y.-H. Lin, H.-C. Hsieh & A. Hoyle from the National Dali Senior High School in Taiwan. These students discovered 2014 GE45. Their observation was reported to IASC as NDL0020 from their April 4th Pan-STARRS image sets.

This object is not a Main Belt asteroid. It is a trans-Neptunian object (TNO). Preliminary orbit calculations put it at an average distance of 65 AU from the Sun. At that distance an object takes 562 years to go once around its orbit. To give a comparison, Pluto sits at an average distance of 40 AU from the Sun. At 65 AU, 2014 GE45 would be half-again further out into the Solar System than Pluto.

Congratulations to these 5 students!!

[announced by Dr. Patrick Miller, Department of Mathematics & Astronomy, Holland School of Science & Mathematics, Hardin-Simmons University, Abilene, TX 79698, iascsearch@hsutx.edu]

IASC ("Isaac") is a collaboration of Hardin-Simmons University (Abilene, TX), Lawrence Hall of Science (University of California at Berkeley), Astronomical Research Institute (Westfield, IL), Global Hands-On Universe Association (Portugal), Sierra Stars Observatory Network (Markleeville, CA), Tarleton State University (Stephenville, TX), The Faulkes Telescope Project (Wales), Yerkes Observatory (Williams Bay, WI), Western Kentucky University (Bowling Green, KY), Las Cumbras Observatory (Santa Barbara, CA), G.V. Schiaparelli Astronomical Observatory (Italy), Mt. Lemmon SkyCenter (Tucson, AZ), and Astrometrica (Austria). Special project collaborations include the Panoramic Survey Telescope & Rapid Response System (University of Hawaii), National Astronomical Observatories of China (Beijing), Astronomers Without Borders (United States), Space Generation Advisory Council (Vienna, Austria), Haus der Astronomie (Heidelberg, Germany), IceCube Neutrino Detector (University of Wisconsin, Madison), and Target Asteroids! (University of Arizona, Tucson).

[Uncategorized](#)

Author



Usa-Hou

Search

Recent Posts

[IASC reaches 1,000 Provisional Discoveries!](#)
[GHOU Conference 2015 August 3-5, 8 & 9.](#)
[IASC's First Trans-Neptunian object \(TNO\) Discovery](#)
[HOU Founder Carl Pennypacker helps design a fire detection satellite](#)
[USA-HOU since 1997](#)

Recent Comments

[Alan Gould on USA-HOU website now a subsite of GHOU](#)

Archives

[March 2015](#)
[February 2015](#)
[May 2014](#)
[October 2013](#)
[August 2013](#)

Categories

[Activities](#)
[Research](#)
[Resources](#)
[Uncategorized](#)



首頁新聞

新聞剪報

重要回顧

關鍵字搜尋



2014
2013
2012
2011
2010
2009
2008
2007
2006
2005
2004

【首頁新聞】

2014.06.04

「泛星計畫」最新成果 發現半人馬小行星

文／陳文屏教授

我要分享



中央大學天文所陳文屏教授（前排左二）共同主持的「泛星計畫」，帶領興大附中學生發現了古柏帶新天體。照片天文所提供

由中央大學天文所陳文屏教授所共同主持的「泛星計畫」(Pan-STARRS)，帶領我國高中生參與全球搜尋小行星活動，再度獲得重大成果！這回七個國家，共發現六顆暫時編號的小行星，其中兩顆屬於台灣學生，分別由北一女及興大附中團隊發現，其中興大附中發現了稀有的半人馬小行星，非常難得可貴。陳文屏教授說，「這應該是史上首次由高中生發現古柏帶天體。」

「國際天文搜尋聯盟」(International Astronomical Search Collaboration, IASC) 主辦之泛星計畫小行星搜尋活動，從三月十四日到四月十八日，共有來自七個國家將近四十所學校參與。除了我國以外，還有保加利亞、德國、波蘭、葡萄牙、蘇丹以及美國。我國參與的五所高中包括羅東高中、北一女中、彰化高中、惠文高中，以及國立大里高中（現改名中興大學附屬中學）。

在活動期間，泛星計畫釋出尚未經過科學家分析的影像，學生利用軟體找出移動天體，經過比對若非已知天體，便算初步發現。初步找到的疑似小行星經過後續觀測，驗證其軌道，便取得暫時編號。此次活動全球共發現六顆暫時編號的小行星，其中兩顆屬於台灣學生，分別由北一女及興大附中團隊發現，表現亮眼。尤其興大附中發現了稀有的半人馬小行星，非常難得。

太陽系當中的小行星絕大多數位於小行星帶當中，以圓形軌道繞行在木星與火星間，數量達數十萬顆。其他極少數小行星有特殊軌道，例如可能行經地球附近的「近地小行星」，以及軌道跨越木星與海王星區域的「半人馬小行星」。

這次興大附中發現的小行星，編號2014GE45，便屬於半人馬小行星，擁有狹長的橢圓軌道，遊走於內、外太陽系，性質介於小行星與彗星之間，動力學上不穩定。以地球到太陽之間距離一個天文單位，2014GE45 距離太陽平均65個天文單位，繞行太陽一圈需時562年。相比之下，太陽系最遠的行星海王星離太陽約30天文單位，而矮行星冥王星則為40天文單位。以距離來說2014GE45比海王星還遙遠，位於太陽系外圍，屬於古柏帶天體。

興大附中團隊全為高一學生，包括薛竹珺、紀政杰、林筠皓、謝昕蘊、何艾玲等，由林士超老師指導。林老師長期推動天文教育，多次帶領學生參與小行星搜尋活動，都有優秀成果。「這應該是史上首次由高中生發現古柏帶天體。」中央大學教授陳文屏說，大家原來要找小行星，結果有了意外發現，這需要技術、耐心，還有一點運氣。「如西方諺語所說，當老天把好運降下，你還得伸出雙手接住才行，好運發生在準備好的人身上。」

IASC安排每個學校與另一所其他國家的學校配對，給予相同影像。臺灣時間每週日晚上影像公布後，一方面自己學校的隊友彼此需要分工協調，在課餘找時間分析數據，以取得最佳結果，另方面與國外學校競爭，搶先取得成果。學生除了學習太空知識與分析數據的技術，也體會團隊「既合作又競爭」的工作態度。

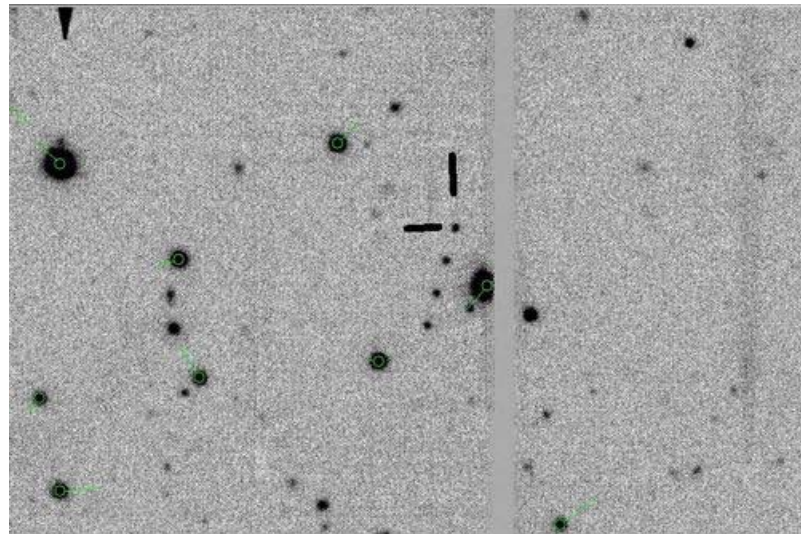
帶領興大附中成功發現半人馬天體的林士超老師回想學生利用午休或是下課時間，以生硬的英文與天文知識，找尋著電腦螢幕上移動的微弱光點。「技術上從生澀到熟練，引發學生開始思索小行星有多大？什麼形狀？是否會與地球相遇？並試圖研讀相關資訊，尋求答案。這個過程是參加這個活動最大的收穫。」

臺灣聯合大學系統副校長，也是中央大學天文所葉永烜教授專門研究太陽系天體，他也是泛星計畫主持人，針對這個發現說：「太陽系當中還隱藏著很多秘密，等待破解，這次高中生發現的半人馬天體就是個例子。希望年輕學子保持好奇心，爭取更多成績。」

太空中存在大量小行星，它們是形成太陽、行星與衛星之後剩下的小天體，遊走在廣大太空中。若與地球相碰撞，小如細沙者劃過夜空，留下讓人驚嘆的流星痕跡，軌道在地球附近的小行星，若是體積比較大，便可能威脅到地球，甚至危害人類文明。泛星計畫 (Pan-STARRS) 使用口徑1.8公尺的望遠鏡，位於美國夏威夷，配備最先進的電子相機，以高效率每個月巡視天空數次，以指認亮度改變的天體（例如恆星死亡爆發的超新星），或位置改變的天體（例如太陽系中的小行星）。因為儀器靈敏，泛星計畫可以偵測到數億公里外，直徑只有一公里的小行星，還不到一般高中校園的大小。



中興大學附屬中學學生在成果發表會上，報告發現編號2014GE45 半人馬小行星經過。照片
天文所提供



編號2014GE45 半人馬小行星影像。照片天文所提供

瀏覽人數：186

國立中央大學秘書室新聞組 版權所有 Copyright © 2011 National Central University
Tel : (03)422-7151轉57011-57013 [✉ 聯絡我們 : ncunews@ncu.edu.tw](mailto:ncunews@ncu.edu.tw) 瀏覽人數，since 2011.09 : 84509

Preferred
HOTEL GROUP

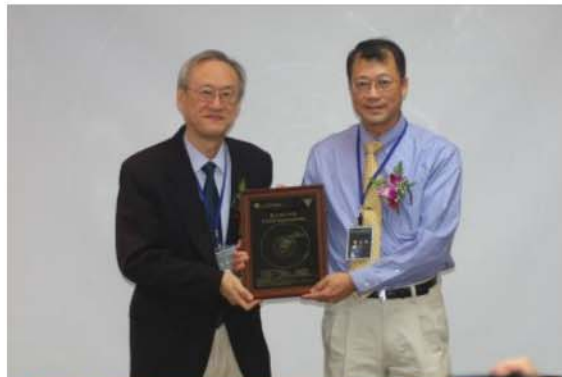
LEARN MORE

要聞 美國 中國 台灣 香港 國際 影藝 藝文 北美華人 世足 論壇 醫藥 法律 安居 周刊 旅遊 美食 English News 財經 教育 科技
 紐約 舊金山 洛杉磯 溫哥華 多倫多 新澤西 寶州 波士頓 芝加哥 大華府 亞特蘭大 佛州 休士頓/達拉斯 賭城 聖地牙哥 西雅圖/夏威夷

蔡文祥迷觀星 自建後院天文台

記者葉國超／亞特蘭大報導

July 01, 2014 06:00 AM | 55 次 | 0 回 | 0 留言 | 0 品



台灣可見光天文學研究的先驅蔡文祥（右），獲得當時中央大學代理校長李光華頒發的「蔡文祥小行星」紀念牌。（圖：蔡文祥提供）

小行星」。

目前旅居亞特蘭大的蔡文祥，早在1985年就拿到耶魯大學天文碩士學位，當時他希望從理論轉入觀測的天文學，剛好喬治亞州立大學正在發展他非常感興趣的先進光學干涉儀計畫(CHARA)，隔年他進入該校博士班，並實際參與協助喬治亞州立大學的天文台選址工作。

接著在因緣際會下，在蔡文祥取得博士學位的同一年，中央大學正好因為校內光害日趨嚴重，想將校園內的24吋天文望遠鏡覓地搬遷，蔡文祥於是抱著回報母校的心願回台任教，後任該校天文研究所所長。

2000年，44歲的蔡文祥為了與居住在美國的家人有更多團聚時間，毅然放棄在台灣天文學界的發展，他說，當初決定來亞特蘭大的時候，特別徵求家人支持，讓他買望遠鏡，繼續對天文的愛好。

美國人工貴，凡事可以自己動手做，他異想天開地在自家後院，蓋了一座命名為「伊卡美後院天文台(E-COMBO)」，並配備業餘天文界最高光學品質的12吋望遠鏡。

蔡文祥說，他在中央大學的十幾年，參與不少座天文台的建造，但都是「動口不動手」的統籌指揮，在亞特蘭大，不但要捲起袖子做苦工，而且還要很多智慧。

[繼續閱讀 >>](#)

分享 |

Like { 0 } SHARE



新聞總覽

更多...

51萬港人遊行 捍衛自主	07/02 港人與北京 恐一拍兩散	07/02
門神締造紀錄 美國飲恨出局	07/02 下一個是誰？巡視組可越級向習匯報	07/02
「伸手必被捉」人民日報：反腐無禁區	07/02 這邊遊行 那邊歡慶香港回歸	07/02
港民主自治 美表態支持	07/02 極危險暴風雨 中西部至少3死	07/02
蘋果日報網站 再遭駁	07/02 通宵佔中 港警凌晨強勢清場	07/02
與權貴決裂 習近平贏民心	07/02 热帶風暴北移 美東國慶「泡湯」	07/02
愛州雨急 少年捲洩洪道亡	07/02 信任危機 激出示威人潮	07/02
黃之鋒 做好被捕打算	07/02 梁國雄 篤信切格瓦拉	07/02





新聞網

電子報

分類

黃頁

社群

購物

行動

活動

播fun室

命理

廣告價目

註冊/登入 簡體 繁體



新竹寶山美地-晴山農園

ezfarm.com.tw

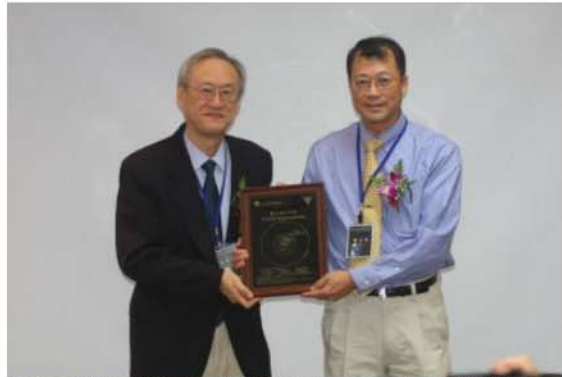
距交流道、市區、便利商店只要5分鐘 下班後最舒服自在的溫馨小屋

要聞 美國 中國 台灣 香港 國際 影藝 藝文 北美華人 世足 論壇 醫藥 法律 安居 周刊 旅遊 美食 English News 財經 教育 科技
 紐約 舊金山 洛杉磯 溫哥華 多倫多 新澤西 寧波 波士頓 芝加哥 大華府 亞特蘭大 佛州 休士頓/達拉斯 賭城 聖地牙哥 西雅圖/夏威夷

蔡文祥迷觀星 自建後院天文台

記者葉國超／亞特蘭大報導

July 01, 2014 06:00 AM | 56 次 | 0 回應 | 0 顯示 | 0 品味



台灣可見光天文學研究的先驅蔡文祥（右），獲得當時中央大學代理校長李光華頒發的「蔡文祥小行星」紀念牌。（圖：蔡文祥提供）

聲，最後通過新居不漏水的考驗。

有了硬體後，蔡文祥在經費考量下，做了長程的研究，完成採購包括光學望遠鏡、赤道儀、主要觀測儀器，這一路走來，蔡文祥希望的就是利用美國與台灣兩地間的日夜顛倒時差優勢，參與台灣國科會所推動的天文科學遠距教學計畫。

蔡文祥說，他的業餘天文台蓋好後，無數個夜晚，他都把精神放在他的天文台中，就這樣在八年時間中，他與台灣同步觀測彗星與流星等，嘉惠許多年輕天文後進。自家這套家庭後院天文台，也吸引中央大學阿拉斯加北極光觀測研究人員，特別跑到亞特蘭大來看他的「天文寵物」。

蔡文祥說，想觀星賞月的天文愛好者，可以從獵戶星座的鳥狀大雲星（M42）下手，因這個星座在冬季很容易辨認，M42就在獵人寶劍上，他建議配備七倍到十倍的雙筒望遠鏡、綠光雷射筆，以及購買智慧型手機或平板電腦的2.99元的Skysafari4軟體後，可以輕易上路觀星。

[《《回上一頁閱讀前文](#)

分享 |

Like 0 SHARE

新聞總覽

51萬港人遊行 捍衛自主	07/02	港人與北京 恐一拍兩散	07/02
門神締造紀錄 美國飲恨出局	07/02	下一個是誰？巡視組可越級向習匯報	07/02
「伸手必被捉」人民日報：反腐無禁區	07/02	這邊遊行 那邊歡慶香港回歸	07/02
港民主自治 美表態支持	07/02	極危險暴風雨 中西部至少3死	07/02
蘋果日報網站 再遭駁	07/02	通宵佔中 港警凌晨強勢清場	07/02
與權貴決裂 習近平贏民心	07/02	熱帶風暴北移 美東國慶「泡湯」	07/02
愛州雨急 少年捲洩洪道亡	07/02	信任危機 激出示威人潮	07/02
黃之鋒 做好被捕打算	07/02	梁國雄 篤信切格瓦拉	07/02

Usitrip华人旅游-华人推荐

[usitrip.com](#)

专业的华人旅行社，带您畅游美加 省钱省心，好服务。

本報徵才



•所有留言為網友自行上載發布，不代表本網站立場，並適用於本網站服務條款，本網站保留刪除權。

台灣高中生 發現古柏帶天體

2014年06月04日 04:10

溫雅雲／台北報導



8498 點閱 | 8/10 | 我要評比

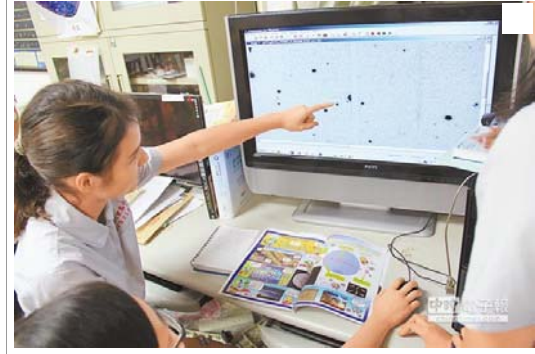
讚 299

8+1

1

①

299



1 中興大學附屬中學高一學生發現編號2014GE45的半人馬小行星，是天文史上頭一遭。（林士超提供）

1 台灣5所高中參加國際「泛星計畫」，這次7個國家，共發現6顆暫時編號的小行星，其中2顆分別由北一女及興大附中學生發現，值得一提的是，興大附中發現了稀有的半人馬小行星，這也是天文史上首次由高中生發現的古柏帶天體，表現相當亮眼。

興大附中 表現出色

「泛星計畫」由中央大學天文所教授陳文屏主持，帶領台灣高中學生參與全球搜尋小行星，今年除了台灣以外，還有來自美國、德國、波蘭、葡萄牙、蘇丹及保加利亞，共40所學校參與，台灣參與的5所高中包括羅東高中、北一女中、彰化高中、惠文高中，以及國立大里高中（現改名中興大學附屬中學）。

興大附中老師林士超說，這次參與計畫的學生多達14人，主要團隊成員包括高一學生薛竹珺、紀政杰、林筠皓、謝昕、何艾玲等，學生知道發現半人馬小行星，大家都很驚喜，直說「真的嗎？老師有沒有開玩笑？」

做足功課 運氣又好

他說，學生這次發現除了運氣好，他們事前也做了很多準備功課，提高敏感度，每天利用午休或放學後時間，到地球教室觀測，分析尚未經過科學家分析的影像，利用軟體找出移動天體，經過比對若非已知天體，便算初步發現，再驗證其軌道，便取得暫時編號。

「這應該是史上首次由高中生發現古柏帶天體！」中央大學教授陳文屏說，大家原來要找小行星，結果有了意外發現，這需要技術、耐心，還有一點運氣。

宇宙深處 發現不易

林士超表示，在火星外側及木星內側，擁有幾10萬小行星，但海王星外側的天體，因為很遠很暗，比較難發現，小行星也比較少，在此發現的天體稱為古柏帶天體。

陳文屏說，這次興大附中發現的小行星，編號2014GE45，便屬於半人馬小行星，擁有狹長的橢圓軌道，遊走於內、外太陽系，性質介於小行星與彗星之間，以地球到太陽之間距離一個天文單位，2014GE45距離太陽平均65個天文單位，繞行太陽一圈需時562年。